CLIMATE & MAYA CULTURAL CHANGE:

DETECTING CONNECTIONS USING BELIZEAN STALAGMITES

By

PETE DOUGLAS AKERS

(Under the Direction of George A. Brook)

ABSTRACT

A high-resolution paleoclimate record spanning 695 years (495-1190 cal yr BP [760-1455 AD]) was created from BZBT1, a 92 mm stalagmite from the Cayo District, Belize. A novel method of dating organic material trapped within the stalagmite was used to determine the chronology of stalagmite growth. Multiple proxies from BZBT1 provided evidence for climate changes during the growth period, with the best records obtained from stable isotopes and petrographic analysis. The region experienced a generalized climate pattern of dry-wet-dry conditions beginning around 1080 cal yr BP (870 AD) and extending through the final growth of BZBT1. The initial dry period corresponds to times of decline and abandonment for the Classic Maya civilization. The findings of this study match well with other regional and world climate records and contribute more evidence suggesting adverse climate played a role in the decline of Classical Maya civilization.

INDEX WORDS: Stalagmites, Maya, Belize, Droughts, Stable isotopes, Petrography, Paleoclimate

CLIMATE & MAYA CULTURAL CHANGE:

DETECTING CONNECTIONS USING BELIZEAN STALAGMITES

By

PETE DOUGLAS AKERS

B.S., Purdue University, 2009

A Thesis Submitted to the Graduate Faculty of The University of Georgia in Partial

Fulfillment of the Requirements of the Degree

MASTER OF SCIENCE

ATHENS, GEORGIA

2011

CLIMATE & MAYA CULTURAL CHANGE:

DETECTING CONNECTIONS USING BELIZEAN STALAGMITES

by

PETE DOUGLAS AKERS

Major Professor: George A. Brook

Committee: L. Bruce Railsback
Stephen A. Kowalewski

Electronic Version Approved:

Maureen Grasso
Dean of the Graduate School
The University of Georgia
December 2011

DEDICATION

To my parents, Doug & Marilyn Akers, and my sister, Suzanne Akers, whose unconditional love and support over all the years has enabled me to achieve my dreams to reach for ever greater ones.

ACKNOWLEDGEMENTS

This research was funded by the Alphawood Foundation.

I would like to thank first and foremost the members of my thesis committee: my major professor Dr. George A. Brook for the immense amount of support, freedom, and guidance over the past two years (particularly for providing a plethora of alternative options and solutions for when the standard research procedure invariably failed), Dr. L. Bruce Railsback for his encouragement and use of his laboratory tools and space along with a unique perspective on stalagmites through the tools of petrography, and Dr. Stephan A. Kowalewski for providing an anthropologist's insight and viewpoint concerning my research.

I would also like to thank the fellow members and associates of the Vaca Plateau project I have had the pleasure of meeting and working with while on field work in Belize: Dr. Phil Reeder, Dr. Jason Polk, Dr. Jim Webster, Dr. Gyles Iannone, Ben Miller, and Bill and Madeline Reynolds. Though I only spent a week in the field with them, I gained an enormous amount of knowledge on the techniques, skills, and mindset it takes for successful field work. I would also like to thank Alan Holder for allowing me the usage of his camera for petrographic imaging.

Finally, I would like to thank the faculty, staff, and fellow graduate students at the University of Georgia for assistance with everything from class work to working through the bureaucracy of forms and travel. I would in particular like to thank a group of present and former graduate students who provided a great deal of advice and support in my first months as a graduate student: Michele Flippo Bolduc, Amber Ignatius, Jordan Lieberman, Matt Miller, Jake McDonald, and Chris Ploetz.

TABLE OF CONTENTS

LIST OF TABLES

Page

LIST OF FIGURES

Page

CHAPTER 1
INTRODUCTION

The first millennium AD witnessed the rise and fall of the spectacular Maya civilization in the lowlands of southern Mexico and northern Central America (Figure 1.1). During the Classic Period (~250-900 AD) Maya populations organized into several major city centers, with hundreds of secondary centers (Houston and Inomata, 2009). Far from the early romantic view of a peaceful scholastic culture, Maya records and steles tell of large regional wars and conflicts involving dozens of cities (Marcus, 2003). The Maya developed earlier Mesoamerican influences into distinctive architecture, writing, and customs. By ~800 AD, cities and regional population centers were being abandoned and the Classic Period came to an end a century and a half later (Houston and Inomata, 2009).

In recent decades, paleoenvironmental work has offered evidence of climate changes coinciding with the end of the Classic Period. Cultural declines have increasingly been linked to climate degradations and shifts, ranging worldwide from Mesopotamia to the Andes (deMenocal, 2001). Most of the paleoclimate records from Mesoamerica are gleaned from sediment studies and point to exceptional droughts in the Maya region during the terminal abandonment (Curtis et al., 1996; Haug et al., 2003; Hodell et al., 2005; Neff et al., 2006; Polk et al., 2007). Other evidence pulled from pollen and historical records illustrates that drought is a recurring phenomenon in the Maya region (Acuna-Soto et al., 2005; Domínguez-Vázquez and Islebe, 2008). While sediment records are useful for determining long-term climate shifts, a lack of resolution in such records can hamper efforts to match arid events with specific cultural

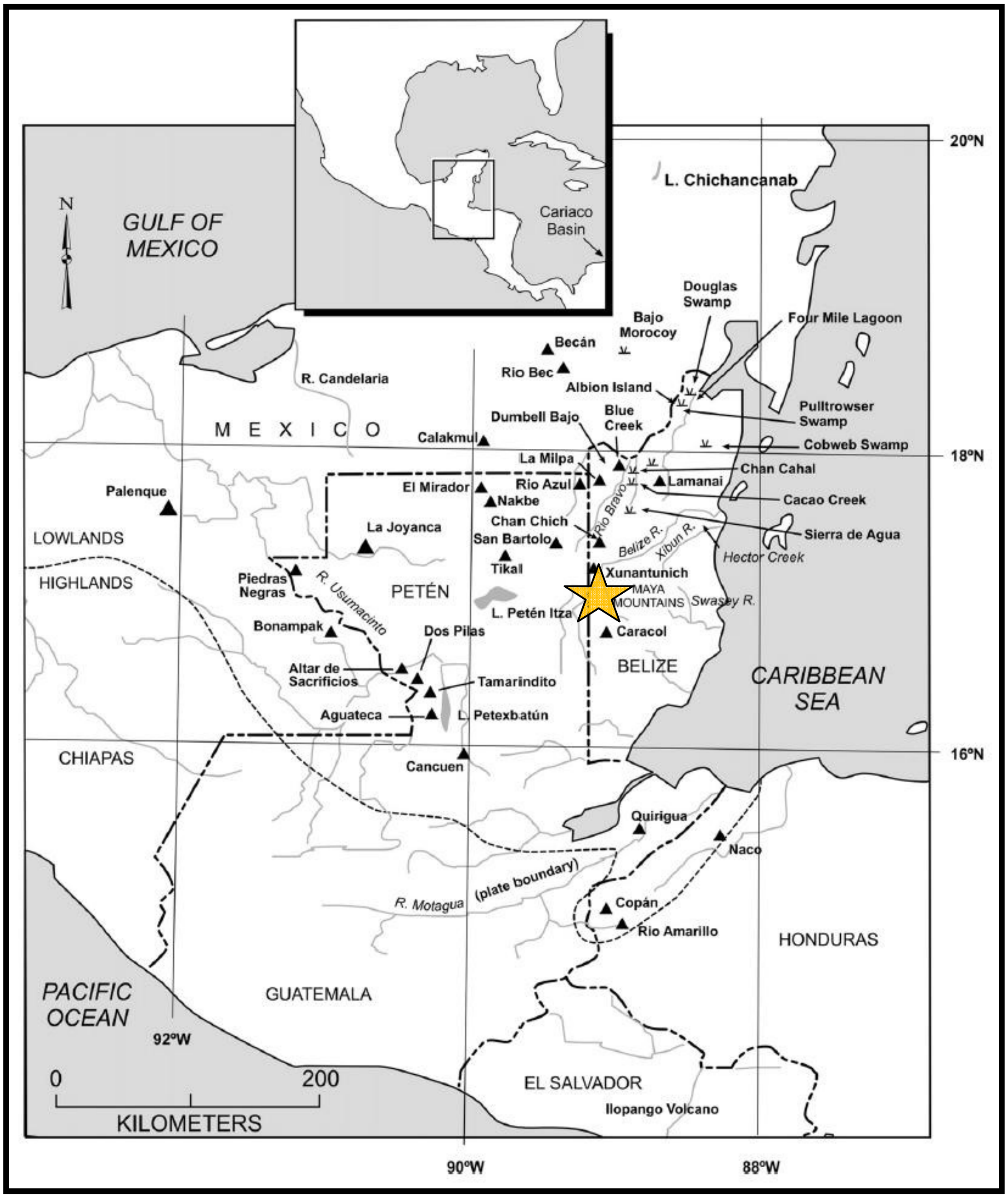

Figure 1.1. Map of the Maya Lowlands and major sites (Beach et al., 2008). Orange star added to show approximate location of Vaca Plateau.

declines. Speleothem research can offer a high-resolution look into the short-term paleoclimate events of regions with limestone geology.

Prior to the start of this research only one detailed speleothem study dedicated to the environment during Maya times had been performed. While this study provided unprecedented resolution of the proposed droughts, it presented the record from only a single stalagmite (Webster et al., 2007). Since then, more research based upon Mesoamerican stalagmites has been published (Medina-Elizalde et al., 2010; Pablo Bernal et al., 2011), but a need still exists for additional local records. More speleothems need to be sought out and analyzed in order to verify these findings. To this end, the following study was proposed in order to collect more paleoclimate evidence from speleothems in the Vaca Plateau of Belize. With more high-resolution paleoclimate data, a greater understanding of the range of climatic conditions during the collapse of Classic Maya society hopefully would be gained.

Objectives

The objectives of this thesis were as follows:

- Collect speleothems from the Vaca Plateau and surrounding regions in Belize
- Develop proficiency in a multi-proxy approach to speleothem data collection
- Successfully construct a chronology and paleoenvironmental record for one or more collected speleothems
- Examine how this paleoclimate record correlates with local and regional records of Maya cultural changes
- Examine this paleoclimate record correlates with regional and global climate records

Although this thesis addresses many of the same questions already examined in previous studies, several reasons exist to replicate and improve on these earlier studies. Most of paleoclimate records are reports from a single location and sometimes from a single sediment core or speleothem. In order to construct a comprehensive regional paleoclimate record, multiple records from spatially diverse locations must be collected and reported. This thesis is also part of a larger project focused on the Vaca Plateau with the goal of examining both its cultural and environmental histories in order to greater understand their interconnections.

CHAPTER 2

BACKGROUND RESEARCH

Study Location

The region focused upon for this thesis is the Vaca Plateau of Belize. The Vaca Plateau is a large karst region consisting of uplifted Campur Formation limestone found in the western half of Belize, along the border with Guatemala. The Vaca Plateau is bordered on the east by the Maya Mountains (Figure 2.1) and by the coastal plain beyond (Reeder, 1996). Elevation ranges from 450 to 600 m above sea level and running water on much of the plateau is nonexistent (Chase et al., 2011). Most of the Vaca Plateau vegetation is characterized as deciduous or seasonal broadleaved forest. The karst terrain exacerbates the water stress of the dry season and results in leaf drop for many of the plant species, with the steepest terrains producing the most water stress (Penn et al., 2004).

The climate of the Vaca plateau is tropical with clear wet and dry seasons. Accurate and lengthy rainfall records are difficult to obtain in Belize, so average rainfall for the Vaca Plateau was determined using satellite estimates via the NASA Giovanni tool (http://disc.sci.gsfc.nasa.gov/giovanni) and TRMM data (Huffman et al., 2007; Kummerow et al., 1998). Yearly rainfall averaged 2360 mm over the period from 1997-2008, ranging from 1950-3000 mm year to year (Figure 2.2). The dry season lasts from December through May (Furley and Newey, 1979) with a 30-day average of 98 mm, in contrast to the wet season's 30-day average of 283 mm. June, July, and August all average greater than 310 mm rainfall per month (Figure 2.3). Rainfall often decreases slightly around August before returning to previous intensity, resulting in a variable 'little dry' season termed a *canicula* (Magaña et al., 1999) or

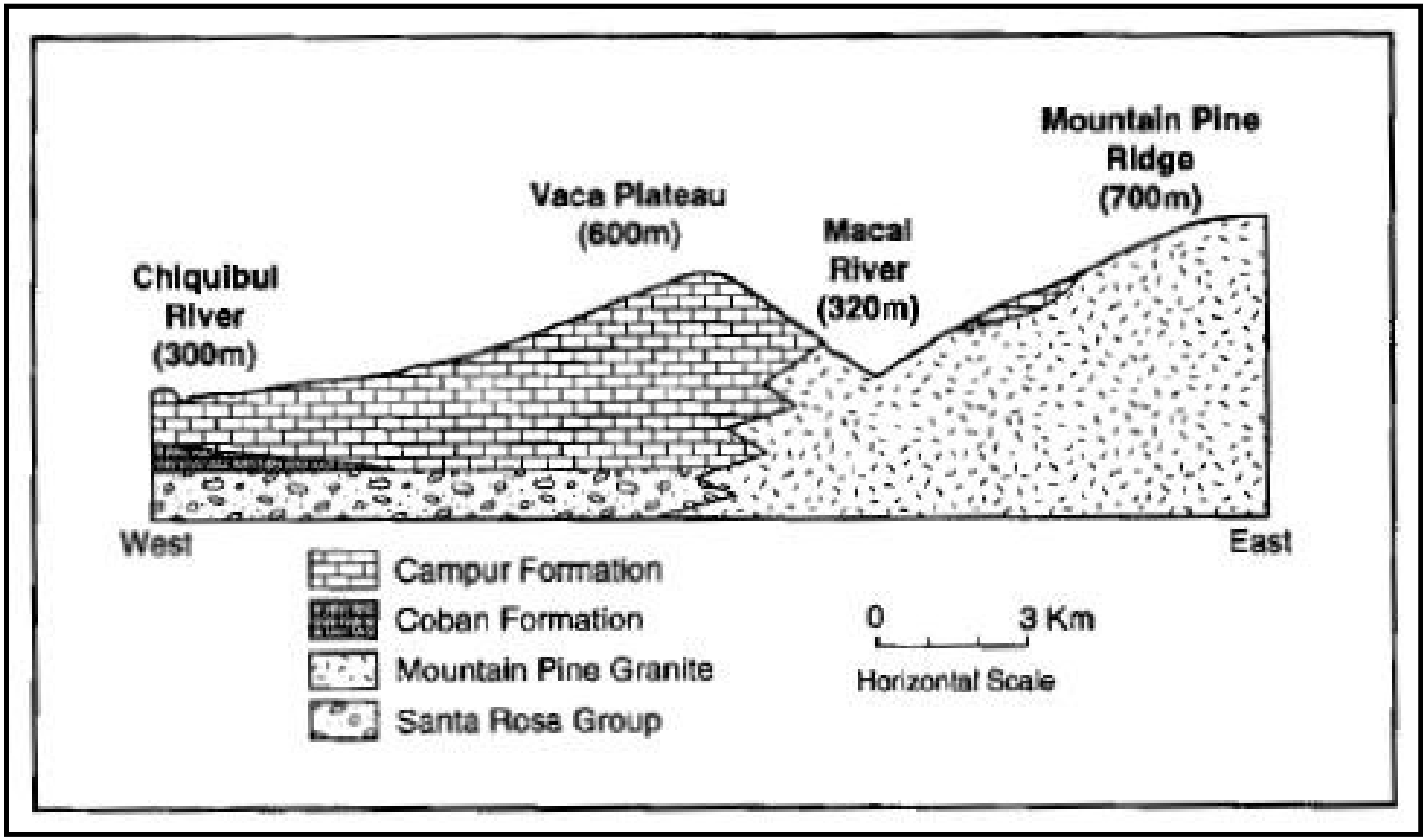

Figure 2.1. A generalized geologic cross section of the Vaca Plateau region (Reeder, 1996)

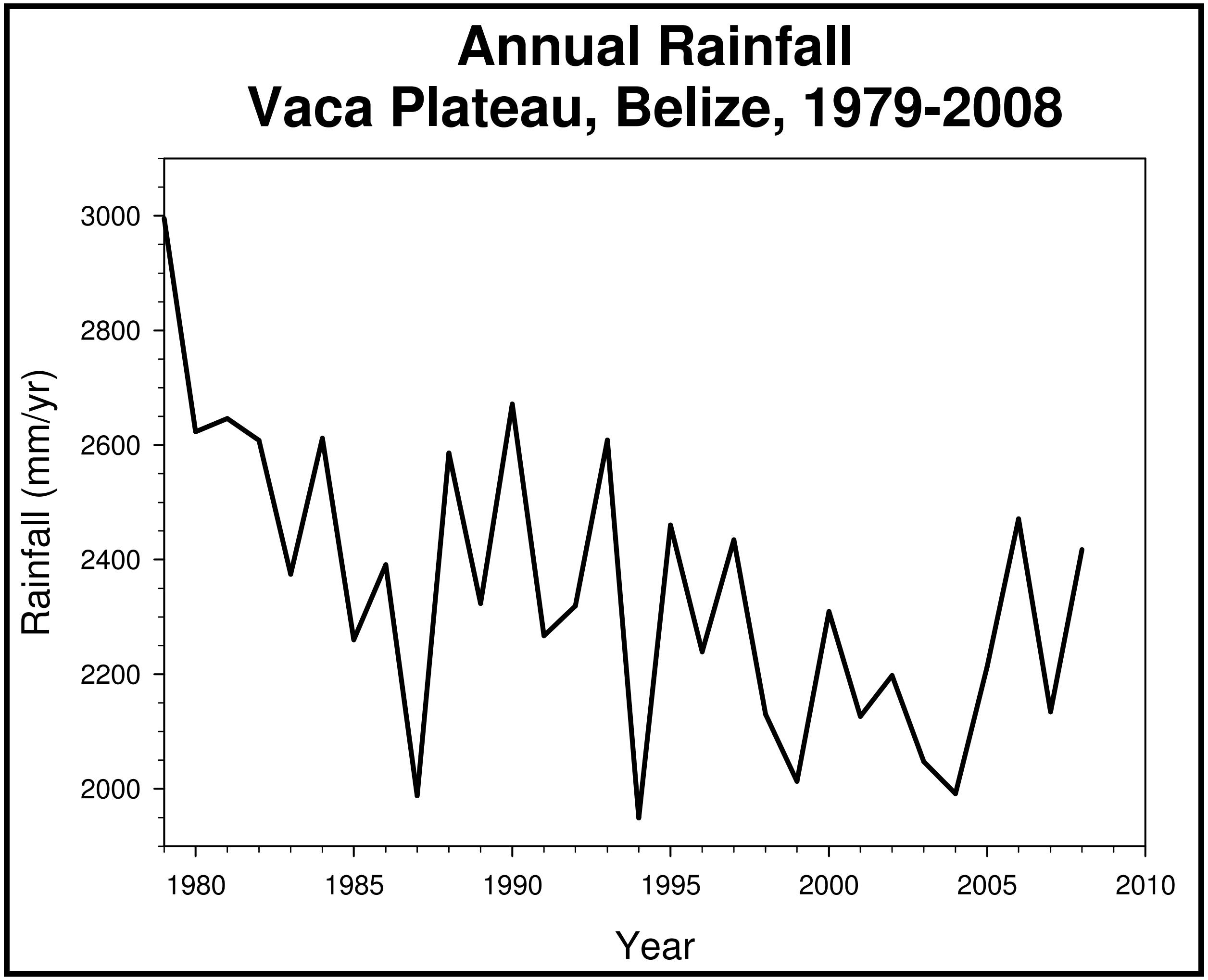

Figure 2.2. Annual rainfall variation over the period 1979-2008. Note that differences of 400 mm or more are common between adjacent years. Derived from TRMM data via NASA Giovanni tool (http://disc.sci.gsfc.nasa.gov/giovanni)

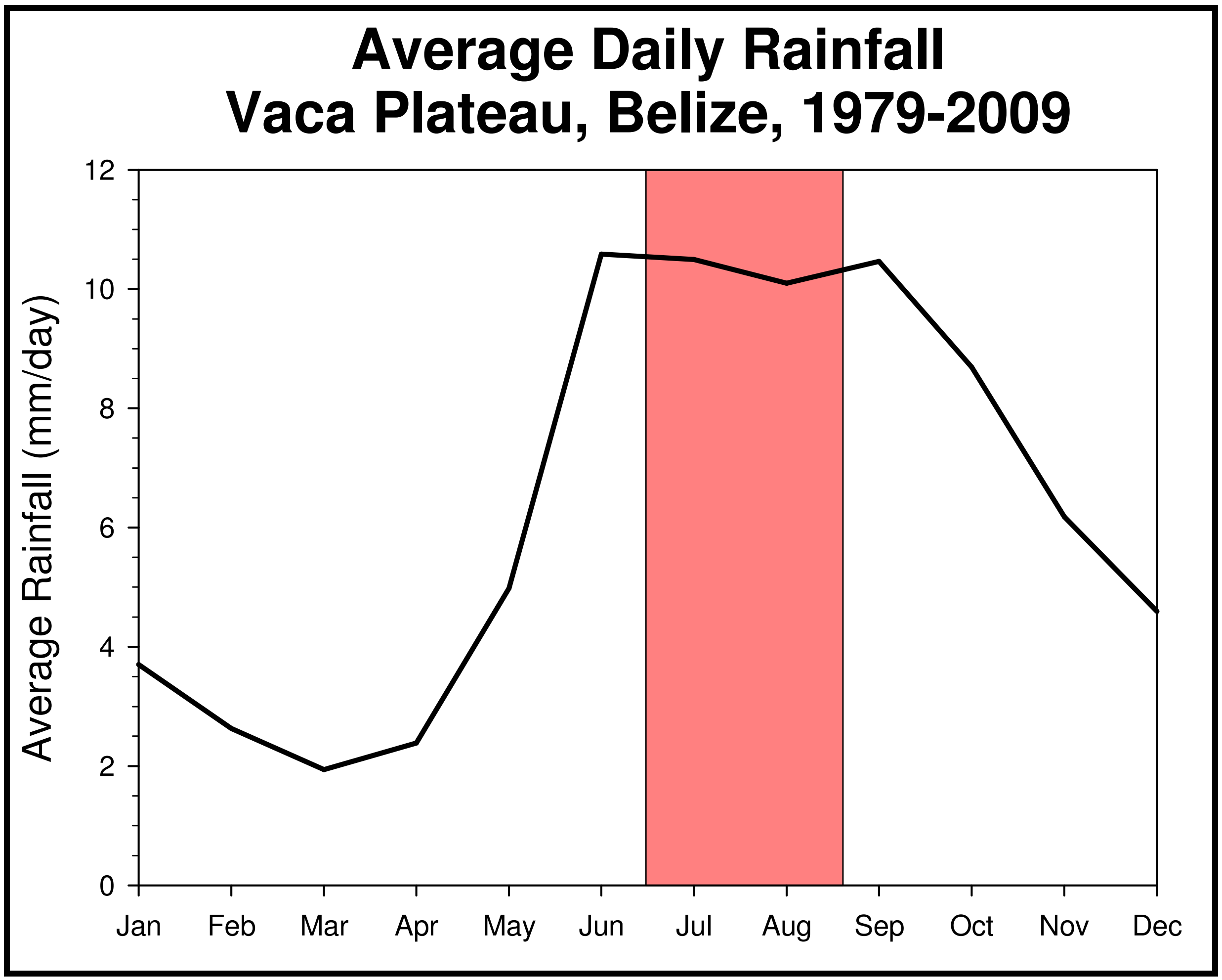

Figure 2.3. Daily rainfall accumulations averaged monthly for the period 1979-2009. The wet season begins with the large increase in daily rainfall in June. The slight decrease in precipitation highlighted in red is known as the midsummer dry spell and is highly variable in magnitude from year to year. Derived from TRMM data via NASA Giovanni tool (http://disc.sci.gsfc.nasa.gov/giovanni)

midsummer dry spell. Belize is also vulnerable to tropical storms and hurricanes. Generally, rainfall increases in a gradient from north to south; however, annual variation in rainfall is quite large. Unfortunately, detailed climate records are very limited in Belize, especially for the lesser populated western regions (Penn et al., 2004). Temperatures range from ~10 to 35°C (Webster et al., 2007) with a mean annual temperature of 25°C and maximum temperatures occurring in May (Polk et al., 2007). Much of the climate is controlled by the Atlantic weather system, with easterly trade winds bringing most of the precipitation (Gill et al., 2007).

Global Climate Variations

Global temperature and precipitation have varied substantially over the length of the Holocene. Temperature records have been created for much of the Holocene from many proxy data sets. The majority of these proxy data sets used in reconstructions of climate histories are from the Northern Hemisphere. Although researchers debate how truly global some climate shifts were, the general record is fairly well-agreed upon. Numerous and often rapid instances of climate change have been identified worldwide (Arz et al., 2006; Bar-Matthews et al., 1999; Cullen et al., 2000; Kaniewski et al., 2008; Lachniet et al., 2004a; Magny et al., 2009). Specific climatic changes in one location are not necessarily universal; often a sort of counter-balance oscillation is evident. Increased rainfall in eastern Africa often coincides with decreased rainfall in southern Africa, and vice versa (Brook, personal communication).

The past 1000 years have shown well-recognized temperature trends, with a peak around 1000-1100 AD (the “Medieval Climate Anomaly”) followed by a long period of cooler than average temperatures (the “Little Ice Age”) before returning to the warmer-than average present (Figure 2.4). Such natural fluctuations are now believed to be a common component of the global climate (Moberg et al., 2005). The late Holocene has been suggested to have three

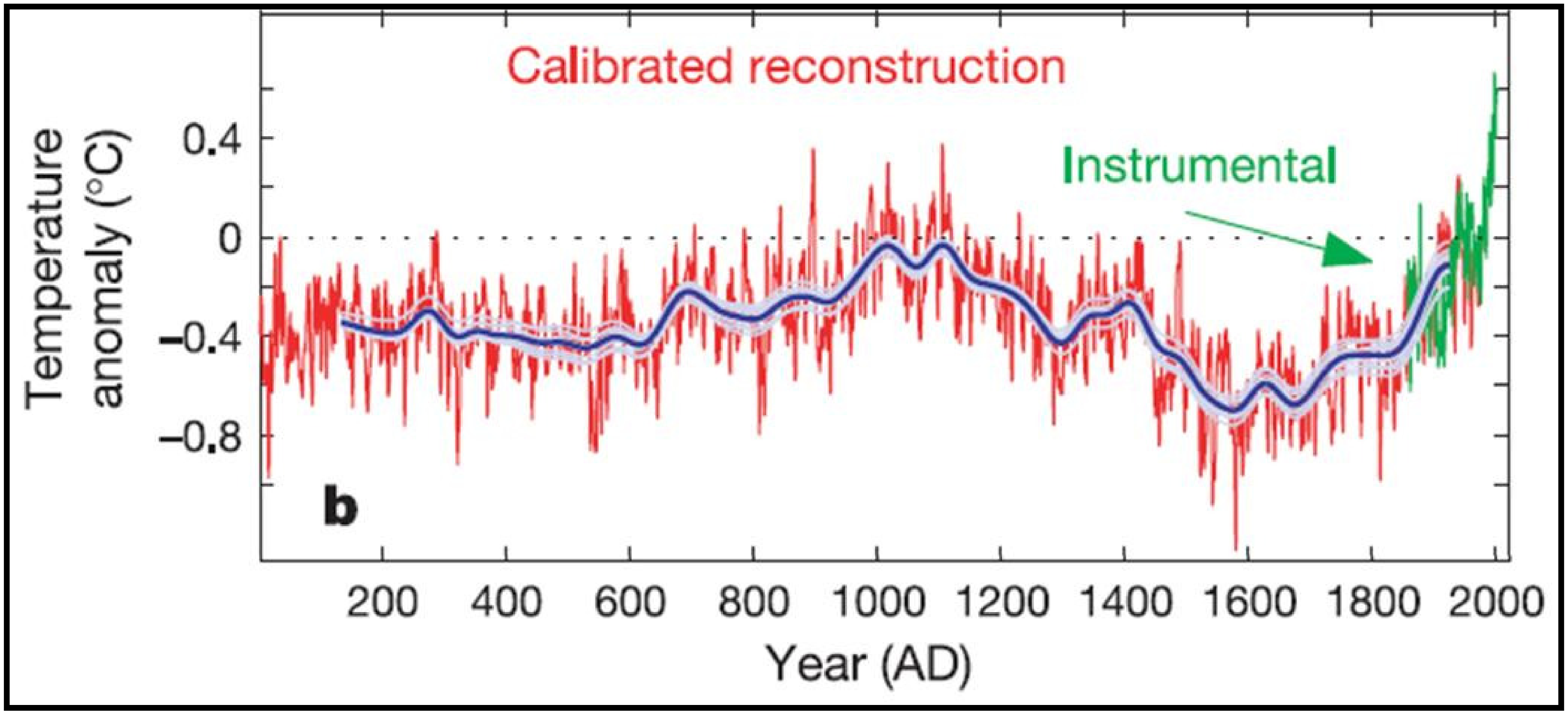

Figure 2.4. Temperature variation reconstruction over the past 2000 years. The peak around 1100 AD followed by the trough around 1650 AD illustrates the shift from the Medieval Optimum to the Little Ice Age (Moberg et al., 2005)

cool periods: the Sub-Atlantic (975-250 BC), Dark Ages (450-950 AD), and Little Ice Age (1400-1850 AD). These cooler times were separated by the Roman Warm Period (250 BC – 450 AD) and the Medieval Warm Period (950-1400 AD) (Baker et al., 1998). Exactly how global these climate shifts were is still a matter of debate; long-term climate records worldwide are needed to help determine if the effects of these cool-warm cycles truly were global.

Maya Region History

Although people have likely inhabited the Maya lowlands for much of the Holocene, the beginnings of agriculture in the region date back only to 3400 BC. At this time, maize and manioc pollen can be found in Belize, although significant deforestation does not appear for another millennium. Pottery appears in the region from 1200-900 BC. This formative cultural period lasting until approximately 250 AD is known as the Preclassic. The Preclassic Period was originally thought of as an archaic time leading up to a cultural explosion that produced a splendid Classic Period. Similar lines of thinking conjured up the retrogressive Postclassic Period that began around 900 AD after the collapse of the Classic societies. Modern research has now revealed that many "Classic" concepts and technologies actually began in the Preclassic while several centers continued to prosper well after the Classic collapse; however, the utilization of these time periods as a reference is still widespread and useful (Houston and Inomata, 2009). The exact timing and duration of each period varies among researchers; in this thesis, the following chronology is utilized (Table 2.1).

Populations in the Maya lowlands appear to have stayed low until after 1000 BC and began growing only after advances in maize allowed for greater agricultural productivity. Cultural homogeneity was beginning to emerge from 700-600 BC in the form of Mamom ceramics and monumental architecture. By the Late Preclassic, truly gigantic structures were being erected, most notably at El Mirador in the Mirador Basin of northern Guatemala. Two pyramids at El Mirador were constructed in excess of 50 meters in height, with the base of one (La Danta complex) covering an area of 175 000 m^2 (Figure 2.5). Murals and sculpture dating to the Late Preclassic have been found at several cities across the Maya lowlands, while defensive structures at El Mirador and Cerros hint at violence and war. Around 200 AD, El Mirador and other Preclassic centers were abandoned. This so-called Preclassic Abandonment signifies the end of the Preclassic and the beginning of the Classic Period. At least one palace was destroyed violently and other signs of rapid abandonment have been found; however, some cities, including Tikal, survived the Preclassic Abandonment en route to flourishing in the Classic Period (Houston and Inomata, 2009).

Table 2.1. Date ranges for periods mentioned in this thesis. The exact date range of these periods varies among researchers, but the different ranges never stray far from the dates listed above.

Period	**Date Range**
Preclassic	2500 BC – 250 AD
Early Classic	250 – 600 AD
Late Classic	600 – 800 AD
Terminal Classic	800 – 900 AD
Postclassic	900 – 1519 AD

A common misconception of the Maya is the concept of a single Maya political entity. On the contrary, much of the Classic Period is the story of rival superpower city-states competing and warring among themselves. While the Maya certainly shared a common

Figure 2.5. Modern remains of the La Danta complex at El Mirador (Photograph taken by and used with permission from Dennis Jarvis)

heritage and culture, regional differences were prevalent and little evidence exists that the Maya saw themselves as a single polity or culture (Houston and Inomata, 2009). In several ways, the ancient politics of the Classic Maya are comparable to that of Classical Greece. Rather like Athens and Sparta trading victories, Tikal and Calakmul battled for centuries. Contrary to early 20th century depictions of the Maya as almost pacifist in nature, the Classic Maya were extremely warlike. A large portion of their written records concern battle results and other war captions (Webster, 2000). Tikal appears to be the earliest Classic Maya city to rise to large-scale political power, with a stele dating back to 292 AD. Other major cities, such as Calakmul and Palenque, appear as players from 300-500 AD.

Tikal suffered a major defeat by Caracol in 562 AD (Houston and Inomata, 2009) and did not produce stelae for decades afterwards (Proskouriakoff, 1993). This cultural decline is termed the Maya Hiatus, though scholars seem to lack agreement on how widespread this "hiatus" was. Calakmul and its ally Caracol are listed as prospering during this time by some (Houston and Inomata, 2009) but halting in stele erection and cultural constructs by others (Proskouriakoff, 1993). Population declines are found at other sites, including some in Belize, during this time (Demarest et al., 2004). Regardless, the defeat of Tikal is commonly taken as the point of transition from the Early Classic to the Late Classic.

What is agreed upon is that the 8th century brought about the height of Classic Maya civilization. The well-known pyramids of Tikal were constructed in their final form during this time, along with the Hieroglyphic Stairway at Copan (Houston and Inomata, 2009) and the stucco facades at Xunantunich (LeCount and Yaeger, 2010) (Figure 2.6). The northern Yucatán cities rapidly developed after centuries of limited or delayed growth. Combined with sustained growth in the Maya lowlands, population and monument creation in the Maya regions were at their peak (Houston and Inomata, 2009). Cities like Minanha and Xunantunich in Belize

Figure 2.6. Classic Maya constructs. Left: Pyramid IV at Tikal, Guatemala; Right: Stucco facade on El Castillo, Xunantunich, Belize

experienced rapid urban development and expansion (Iannone, 2005). Caracol constructed over 75 km of causeways to create a quasi-metropolitan area of 177 sq km that reached a peak population of 115 000 people (Chase et al., 2011).

This height would not last for long, however, as a large number of centers stopped erecting monuments around 800-820 AD. This apparent desertion of cities afflicted a wide geographical area, ranging from Palenque in the southwest through Tikal and Calakmul in the central lowlands to Copan in the southeast. Two discoveries reveal how serious and expansive the Late Classic decline was. First, very few sites record the end of a *bak'tun* cycle (a major calendar turnover) at 830 AD. Second, both Tikal and Calakmul fall victim to the political collapse. In the Maya Hiatus and the resurrection of Tikal around 700 AD, misfortune for one of the archrivals would typically be balanced by prosperity by the other (Houston and Inomata, 2009). Some of these abandonments appear to be accompanied by violence (such as Aguateca in 810 AD (Inomata et al., 2004)), but many other cities appear to have simply been deserted (Aimers, 2007; Iannone, 2005).

The Late Classic Maya "Collapse" is not a single, short-term event. Rather, events related to the "Collapse" extended over 300 years and varied greatly both spatially and temporally. The Petén region has been a focus of archaeological research from the beginning, and much of the commonly accepted chronology of the Late Classic decline is derived from studies here. Population declined at major centers in the Petén and southernmost Yucatán peninsula from 830-850 AD, and most sites appear to have been largely deserted by the Postclassic (Aimers, 2007).

The initial Late Classic decline in the Southern Lowlands was followed by a brief revival of more stable society during the Terminal Classic and early Postclassic. Some centers that suffered during the Late Classic collapse showed a brief revival, while other centers made it through the collapse relatively unscathed. Tikal and Calakmul both dedicated steles late in the 9th century, but the cities did not gain much of their former power back. The city Seibal became the dominant power in the southern lowlands after the decline of Caracol and other former leading cities. Interestingly, Seibal's layout in the Terminal Classic does not contain defensive features to the degree common in the Late Classic. However, even this city was abandoned by 950 AD (Houston and Inomata, 2009).

The Terminal Classic Period in the northern lowlands of the Yucatán Peninsula offers a stark contrast from the southern lowlands. The Maya cities of the northern Yucatán peninsula did not decline during the 9th century, and many (Uxmal, Sayil, Chichén Itzá) flourished, possibly in part by taking in Maya fleeing other regions (Aimers, 2007). Little sign of the decline from 800-820 AD has been detected, and several cities prospered well into the 10th century. The magnificent city of Chichén Itzá was perhaps the last of the Classic cities to fall. Chichén Itzá rose to prominence in the late 9th century and expanded its influence and power throughout the 10th century. The city still provokes a great deal of debate about its rise to power due to styles of architecture that some have described as Mexicanized. While some scholars propose that a Toltec ruler from central Mexico took over the city sometime in the Terminal Classic, others believe that changes in the architecture can be explained by cultural evolution alone. At any rate, Chichén Itzá prospered long after other Maya centers in the south had been abandoned and apparently spread militarily at the expense of other northern cities. Chichén Itzá abandoned the Maya tradition of erecting dated monuments sometime towards the end of the 10th century, but appears to have finally declined as a power sometime between 1000 and 1200 AD. Other city-states would rise and fall in the centuries leading to the Spanish conquest, but the culture and politics of these centers had changed significantly from the Classic Maya Period (Houston and Inomata, 2009).

Many northern Belize cities did not decline in the Terminal Classic to the degree experienced in the Southern Lowlands. These cities are located within major river valleys and close proximity to the Caribbean Sea (Figure 2.7). Some sites (e.g., Lamanai) did not show major interruptions, but others (Colha) appear to have been attacked violently. As time progressed into the Postclassic, signs of influence from the Yucatán cities grow more apparent. Trade and contact with the successful Yucatán cities and access to river and marine resources may have enabled some cities to survive longer. By 900-1250 AD, population around the Three Rivers region of Belize is estimated to have dropped to 10% of the Classic Period peak. The major Belizean city of Caracol was located far from the stable water resources of the Three Rivers region (Aimers, 2007). Caracol erected a stele as late as 859 AD and was occupied in some fashion until 895 AD, although the final days of the city appear to have been violent (Aimers, 2007; Houston and Inomata, 2009). Other Belizean sites located in the karst uplands, such as Minanha and Xunantunich, were abandoned early in the Terminal Classic, although their abandonment appears much more orderly and planned than Caracol (Iannone, 2005).

Maya Collapse Theories

Violence

The 1950s brought about several theories promoting the idea that the Maya peasants revolted against the elite to explain the sudden end of high culture and monument erection. These theories focused intensely upon weakness within the supposed two-class society. Recently, these ideas have lost favor in many circles as new archaeological findings undermine several of the original theory's assumptions. The two-class model is believed to be too simplistic and does not examine the true complexity of Maya social structures (Houston and Inomata, 2009). These peasant revolt views may have been influenced by the strong Marxist presence in

Figure 2.7. The Belize River near Unitedville, Belize. The Maya settlement of Lower Dover is located within 500 m of the river at this location.

the world at that time. Why these peasant revolutions would not lead to new forms of governance and instead to abandonment has not been answered; neither has the question as to how so many independent city-states would revolt nearly simultaneously.

Unusual archaeological findings at sites along the Pasíon River led some researchers to propose foreign invasion had occurred towards the end of the Classic Period. Under this premise, southern lowland Maya cities were invaded by Mexicanized-Maya or other non-Maya people, upsetting the local governance and society. This theory was fairly short lived, as later researchers modified it to propose that the invasions followed a prior collapse of the Maya cities. Many current researchers doubt that any foreign invasion actually occurred in the Southern Lowlands (Houston and Inomata, 2009).

Strife has been brought up again recently under a new theory promoting internal warfare as a cause for the Maya declines. Warfare has been documented throughout Maya history, and the destructive nature of war no doubt led to several sites' endings. The strongest argument against the warfare theory is that war leads both to destruction but also to social development. Ancient cultures such as Rome and the Mexica engaged in long-term periods of war while creating political unity. Warfare is also often seen as occurring due to social decline rather than creating it (Houston and Inomata, 2009).

Disease

Some researchers have argued that a severe drop in population followed by a lack of recovery is symptomatic of a disease epidemic. Epidemics are well-documented in Mexico following the Spanish conquest. Typically these epidemics were caused by imported Old World diseases such as smallpox and measles, to which the native population had no immunity. A Mexican population of around 20 million in 1518 was reduced to fewer than one million a century later, mostly due to disease (Marr and Kiracofe, 2000). An epidemic from 1576-1580 was particularly severe and brought about the loss of 50% of the population (Acuna-Soto et al., 2005). The few records dating from the epidemic appear to show that the disease was unknown to both the Spanish and Aztecs, who invented a new term for the sickness: *hueycocoliztli*, or great pestilence. Modern scholars often assume that the disease was smallpox or typhus, but more in-depth research into historical records cast some doubt on this assumption. Namely, the symptoms of the disease (bleeding from the nose and other bodily openings, destruction of red blood cells and platelets, and internal hemorrhaging) do not match the standard symptoms of any of the common European diseases. Also unusual is that Spanish doctors well-versed in smallpox and typhus do not use the Spanish terms for this epidemic (Marr and Kiracofe, 2000).

One newer theory proposes that the *hueycocoliztli* was a hemorrhagic fever virus native to the New World that is still unknown. Native hemorrhagic fever viruses typically reside in rodent reservoirs and can remain unknown for centuries (as noted with the Hantavirus outbreak in the southwestern United States in 1993). Other hemorrhagic fever viruses have been known to emerge during times of radical changes in agricultural practice that force interaction between humans and infected rodents (Marr and Kiracofe, 2000). The 1576 epidemic also happened to occur during one of the most severe droughts of the past 1000 years. More specifically, the epidemic (and a similar previous, but smaller, epidemic) occurred during a brief wet-phase in the longer-term drought. The Hantavirus outbreak in 1993 began during a similar wet phase (Acuna-Soto et al., 2005). Interestingly, the climate record for the Late Classic also contains alternations between severe drought and a return to wet conditions, as will be described in detail later (Hodell et al., 2007). The similar environmental and demographic parallels of the Late Classic decline have led some to speculate that a similar disease outbreak may have afflicted the Classic Maya (Acuna-Soto et al., 2005), though such speculation is typically tempered with the acknowledgement that little to no physical evidence for this theory exists presently (Marr and Kiracofe, 2000).

Environmental Degradation

One of the most popular theories is that the Maya outstripped the capacity of their environment to sustain them. According to this view, as populations and number of elites grew during the Classic Period, the Maya cleared more and more forest for food production (Emery, 2008). As urban expansion took over agricultural land, the Maya shortened fallow periods and exhausted the soils. Deforestation and intensified agriculture then brought about catastrophic soil erosion (McNeil et al., 2010). Luxury and trade goods grew in demand, leading to extreme stress placed upon the natural ecosystems. Eventually, the environment's ability to sustain the Maya civilization collapsed, leading to famine, disease, and the eventual destruction of the Classic Maya (Emery, 2008). With this viewpoint, the Maya are presented to the modern world as a lesson in living sustainably within the limits of the environment or face total annihilation. This lesson has rapidly gained favor among teachers (Fedick, 2010), environmentalists, and authors (Diamond, 2005) as an aid to support the call of sustainability. As noble as the mission of modern sustainability is, recent research is beginning to question the theory that the Maya ruined their environment to their own demise.

Kitty Emery has published many papers on reconstructing Maya meat diets from zooarchaeological examinations (Emery, 2007, 2008; Emery and Thornton, 2008). The environmental degradation theory would predict that during the Late Classic and Terminal Classic periods few wild animals would be available for food. As the Maya's only domestic animal was the dog, meat was largely gathered from hunting wild animals. Foraging ecology proposes that predators (in this case, Maya hunters) aim for the most efficient method of gaining food. Large animals such as white-tailed deer (*Odocoileus virginianus*) are hence more prized than rodents and other small game (Emery, 2007). Emery produced large-game/small-game ratios for several sites, dating from the Preclassic up through colonial times. Some findings support changes in hunting tactics towards the end of the Classic; non-food species valued for feathers and specimens show up more often and large game proportions drop during the Terminal Classic/Postclassic periods (Emery, 2007). Little evidence exists, however, that wild game availability dropped to critical levels afflicting nutrition in either the Petexbatun polity (Emery, 2008) or in the general Classic Maya world (Emery, 2007; Emery and Thornton, 2008). White-tailed deer never appeared to suffer a lack of normal, non-maize browse, and the greatest impacts on the environment actually appear to have occurred in the Preclassic (Emery and Thornton, 2008).

Recent pollen studies are also concluding that deforestation was not rampant throughout the Late Classic. Early sediment cores taken near the city of Copan, Honduras, were presented as evidence of massive deforestation, in agreement with the environmental collapse theory. These studies are now believed to have several flawed assumptions about the pollen analysis and timing of the Maya decline. Recent sediment core samples contain a record dating back nearly 3000 years and present a more complete view of environmental changes. Several periods of deforestation are noted, but none occur during the Late Classic. In fact the most severe deforestation appears to have occurred in the Preclassic (McNeil et al., 2010), in agreement with zooarchaeological evidence that the Preclassic may have harbored the greatest environmental changes (Emery and Thornton, 2008). A higher arboreal-herb pollen ratio is found in the Late Classic compared with even the Early Classic. Increases in pine and tree pollen signifies that the Maya near Copan were not denuding their landscape, but appear to have been managing it quite well given the population pressures (McNeil et al., 2010). Many species noted to increase in this pollen record are from trees and plants known to be used as food by later Maya populations (Fedick, 2010). Early Spanish accounts of Maya villages describe cities with large numbers of useful trees, creating a so-called *forest-garden*. The current species composition of forests around the Classic Maya site of El Pilar is still artificially enriched in these economically useful trees (Ross, 2011).

Droughts

Recently, the idea that a series of droughts may have led to the decline of the Classic Maya has gained prominence due to several studies finding physical evidence for a shift in climate coinciding with the Late Classic Period. Currently, researchers are debating to what degree these droughts may have affected the Maya. To that end, an explanation of common paleoenvironmental proxies and examination of select similar situations worldwide will be discussed, followed by research that was undertaken in the Maya region.

CHAPTER 3
PALEOENVIRONMENTAL EVIDENCE

Stable Isotopes

Much previously discovered paleoclimate information comes from stable isotope studies of ^{18}O. Early research hoped to link land-based $\delta^{18}O$ records to paleotemperatures. While this was later determined to be quite complex and difficult to tease out from terrestrial records, changes in $\delta^{18}O$ values are providing valuable insights into other aspects of paleoclimate. ^{16}O is evaporated preferentially over ^{18}O; high amounts of evaporation, therefore, will lead to greater $\delta^{18}O$ values in the remaining water. Similarly, ^{18}O is preferentially condensed from water vapor, leading to depleted remaining water vapor (Lachniet, 2009). Values of $\delta^{18}O$ also vary spatially and seasonally with atmospheric weather changes and moisture sources. The $\delta^{18}O$ values can be altered by changes in mean annual temperature; however, it is believed that tropical temperatures have not varied greatly enough in the Holocene for temperature to add much to the $\delta^{18}O$ signal (Hodell et al., 2007). Of particular value to studies is the 'amount effect': here, an increase in rainfall results in a decrease in $\delta^{18}O$ values (Figure 3.1). Values of $\delta^{18}O$ for Middle America are greatest in March-April and lowest in June and September-October (Figure 3.2), ranging on average from 0.5‰ during the dry season to -5.2‰ or -7.9‰ (depending on the location) in the wet season (Figure 3.3). The decrease of rainfall during the midsummer dry spell is reflected with an increase in $\delta^{18}O$ values (IAEA/WMO, 2006).

Another stable isotope commonly used for paleoclimate research is ^{13}C. As rainwater percolates through the soil, it will acquire calcium carbonate from its surroundings.

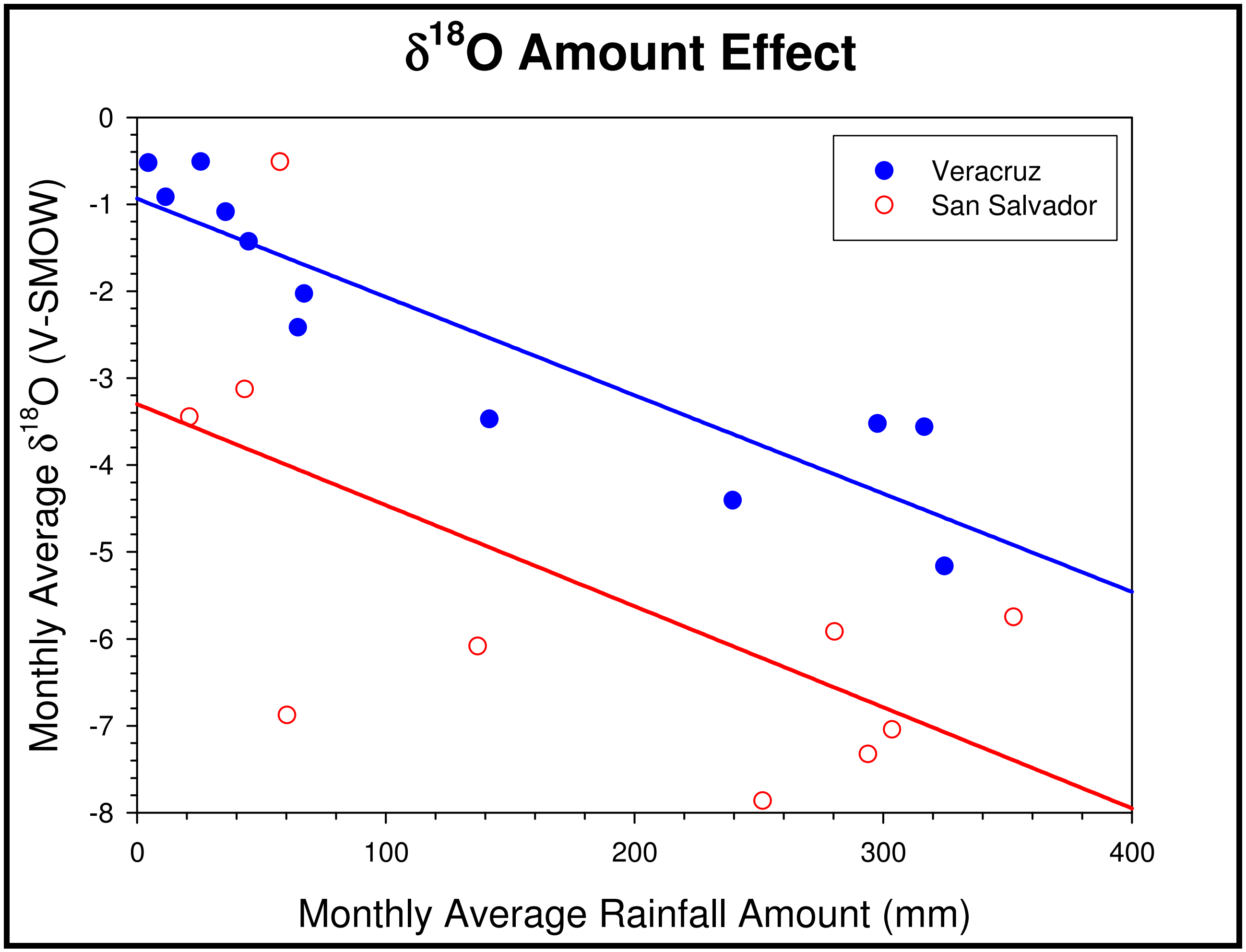

Figure 3.1. Negative correlation between monthly average rainfall $\delta^{18}O$ values and amount for the two GNIP stations closest to Belize (Veracruz, Mexico {blue, closed}, and San Salvador, El Salvador {red, open}), illustrating the 'amount effect'. Although values for San Salvador are 2-3‰ lower than those from Veracruz, the slope of the regression lines are remarkably similar. Derived from GNIP data (IAEA/WMO, 2006).

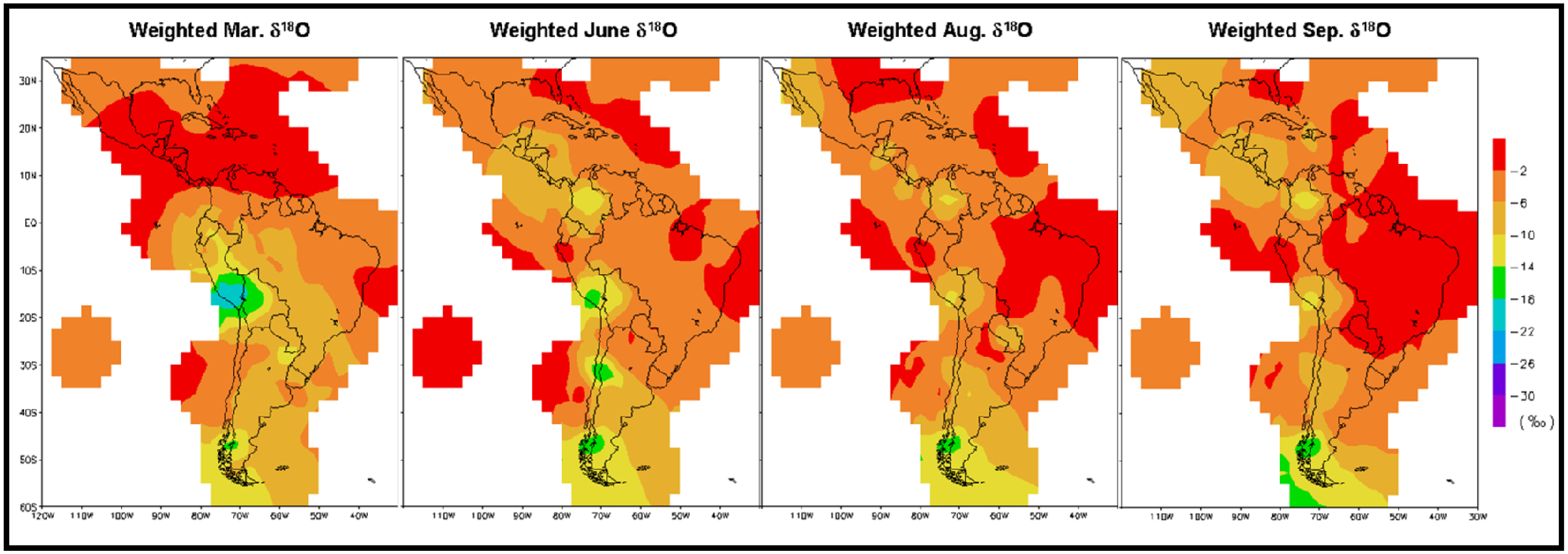

Figure 3.2. Select monthly changes in rainfall $\delta^{18}O$. The greatest values for Belize (> -2‰) are found during March, while the lowest values for Belize (< -6‰) are found in June and September (IAEA/WMO, 2006). An increase in $\delta^{18}O$ values occurs between June and September due to the midsummer dry spell.

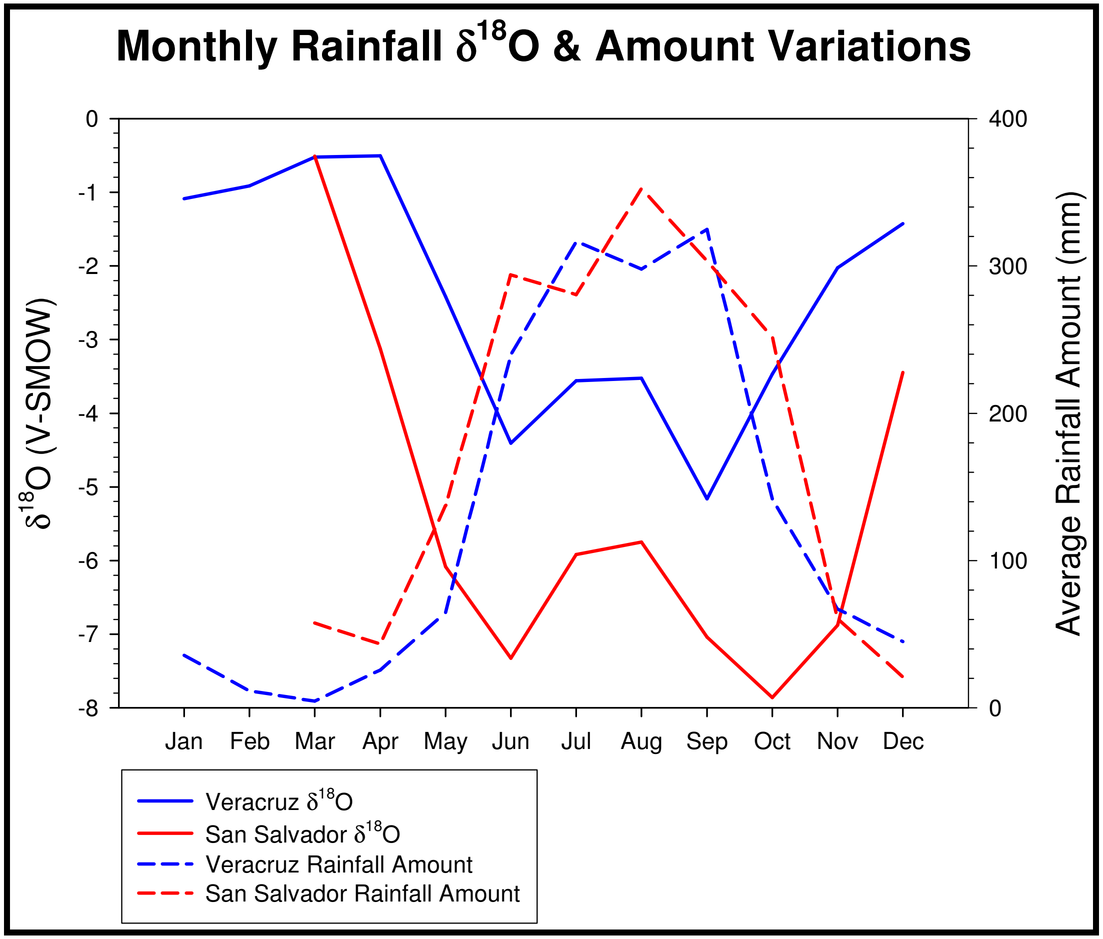

Figure 3.3. Monthly variations in both rainfall amount and $\delta^{18}O$ for the two GNIP stations closest to Belize (Veracruz, Mexico {blue}, and San Salvador, El Salvador (Stahle et al.)). San Salvador lacked data for January and February. A strong inverse relationship between rainfall $\delta^{18}O$ and amount is evident at both stations. The increase in $\delta^{18}O$ values in July and August due to the midsummer dry spell is proportionally greater than the decrease in rainfall amount during the same period. Minimum $\delta^{18}O$ values for San Salvador are ~3‰ lower than for Veracruz, possibly due to greater Pacific Ocean influence at San Salvador. Derived from GNIP data (IAEA/WMO, 2006).

The CO_2 present in the soil will react with the dissolved carbonate to form bicarbonate. Assuming that a continuous equilibration exists between the rainwater and an infinite reserve of soil CO_2, this water will have a $\delta^{13}C$ identical to the $\delta^{13}C$ of the soil CO_2 (McDermott, 2004). In a tropical location such as Belize, changes in precipitation are reflected in vegetation photosynthesis strategies. Abundant precipitation will result in vegetation dominated by plants utilizing the C3 photosynthesis pathway. Drier conditions tend to favor grasses and other plants that utilize the C4 photosynthesis pathway (Faust and Ashkenazy, 2007). Although the atmosphere maintains an average $\delta^{13}C$ of -7.8‰, plants alter this value during photosynthesis by favoring ^{12}C (Bender, 1971). The two different photosynthesis pathways favor ^{12}C to different degrees and thus result in unique soil CO_2 $\delta^{13}C$ values: C3 plant values range from -26‰ to -20‰, whereas C4 plant values range from -16‰ to -10‰. Although several other environmental variables can alter the $\delta^{13}C$ in plants, these changes are typically overshadowed by the C4-C3 dichotomy (Vogel, 1980; Webster, 2007). Maize, an extremely important crop in Mesoamerica, is a C4 plant, and the expansion of maize production can be traced through changes in $\delta^{13}C$ values (Webb et al., 2004). Changes in soil aridity and evaporation rates can also be reflected in the $\delta^{13}C$ values (Baldini et al., 2005; Hesterberg and Siegenthaler, 1991).

In order to reconstruct the paleoclimate for a region through stable isotopes, a preserved record of the isotopes must be found. Closed-basin lakes are especially sensitive to aridity and are preferentially sought out for sediment cores (Brenner et al., 2003). A common source for paleoecologically useful oxygen isotope data is freshwater calcium carbonate shells of small aquatic creatures. These creatures (typically ostracods and gastropods) produce their calcium carbonate shells partly with oxygen from the surrounding water; hence, the carbonate $\delta^{18}O$ will reflect that of the lake $\delta^{18}O$ while the organism was growing. After a short life, a creature will die and settle on the lakebed along with sediments, preserving the $\delta^{18}O$ values present during its life (Hodell et al., 2007). Carbon isotope ratios can be determined from organic materials or carbonates. Inorganic calcium carbonate can be precipitated from supersaturated water in the form of either calcite or aragonite (Railsback, 1999).

Climate-Human Culture Interactions

The idea that climate changes can affect human cultural development has been met with hostility and scrutiny in the past. In the past few decades, however, researchers have discovered that several eras of decline or changes in human history can be linked with climatic changes. These studies have helped to change the image of civilized man from one living above his natural environment into one who was often deeply affected by changes in the natural world.

One of the best documented instances where a climate change has been implicated in the decline of a human culture is during what is known as the 4.2 ka event. Around 4200 yr BP, significant drying is believed to have occurred over much of the Mediterranean, Middle East, and Africa. A selection of evidence for the 4.2 ka event was discussed by Magney et al. (2009) (Figure 3.4). Among the evidence cited were moisture minima indicated by flowstone in Italy (Drysdale et al., 2006), reduced soil formation in Tunisia (Zielhofer and Faust, 2008), and reduced flooding in Spain (Carrion, 2002). Much of their paper was dedicated to their investigation of sediments in two European lakes where the researchers found the signal of a drop in water level, corresponding to the 4.2 ka event known from the African tropics (Magny et al., 2009).

Cores from the Gulf of Oman have revealed a large increase in aeolian dolomite and calcite deposition at the approximate time of the Akkadian Empire collapse. The dolomite is believed to have a Mesopotamian origin, suggesting that a large area of Mesopotamia had

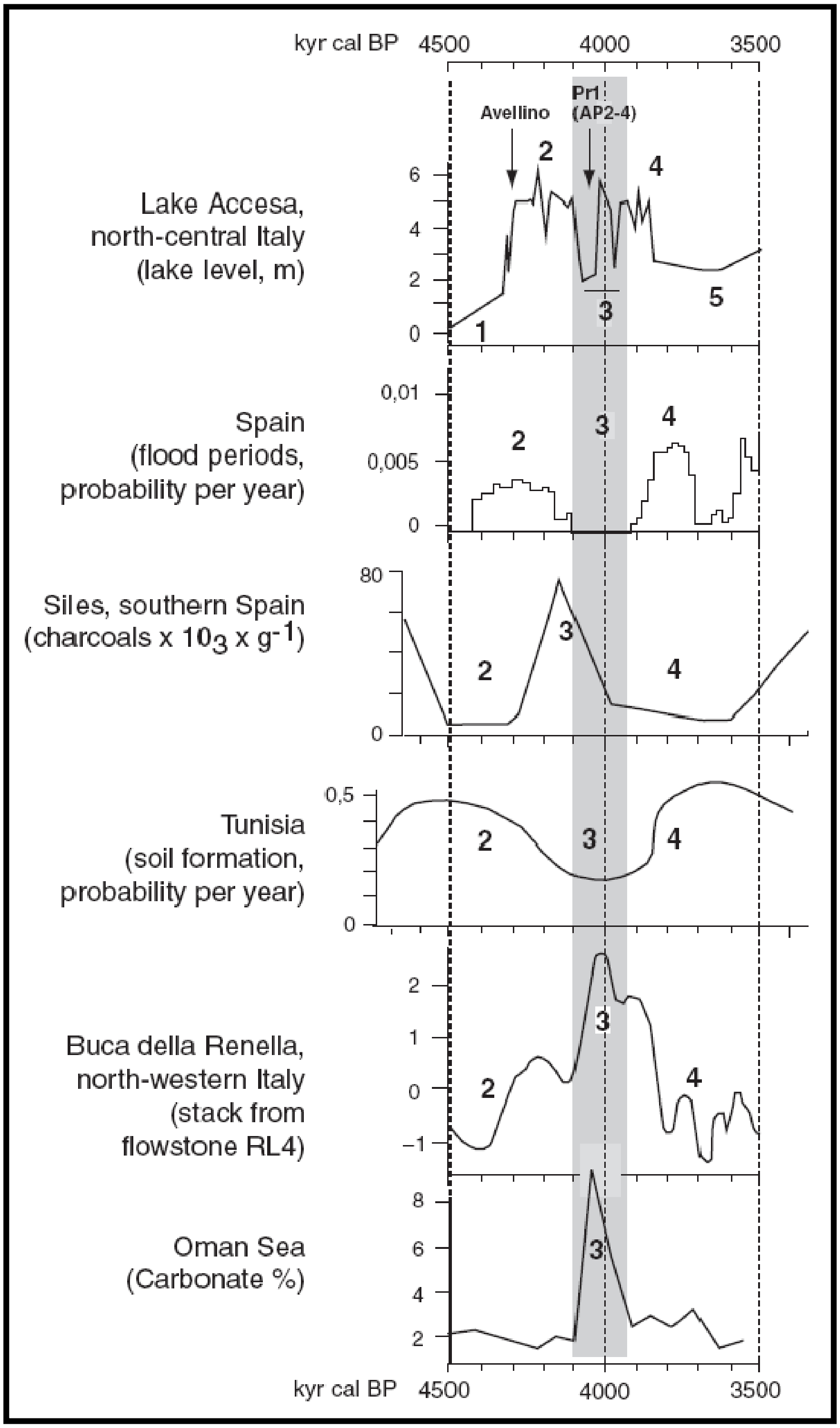

Figure 3.4. Evidence for the arid 4.2 ka event from sites around the Mediterranean (Magny et al., 2009)

rapidly increased in aridity (Cullen et al., 2000). For a culture highly dependent upon predictable rainfall and located in a semi-arid region, any drop in precipitation would have calamitous effects on food production. Finally, two sediment cores taken from the Nile Delta had iron oxide layers dating from 4250 cal yr BP and 4050 cal yr BP and found nowhere else in the mid-Holocene records. Since sediments allowed to dry out will form these oxides when exposed to air, this has been interpreted as more evidence of an unprecedented and short-term shift to extreme aridity and coincides with the collapse of the Egyptian Old Kingdom (Stanley et al., 2003).

Typically the focus on climate abnormalities in semiarid regions is on sudden drying events, whereas humid intervals are assumed to be beneficial to and supportive of human cultural growth. A paper by Faust and Ashkenazy analyzed an occasion when the Israeli coastal plain suffered population declines during a humid interval. They concluded that an *excess* of precipitation was the root cause of this decline. In most of the Near East, the period prior to the 4.2 ka event was a time of urban development and cultural growth corresponding with a well-recognized humid period. The number of minor Israeli coastal plain settlements during this time dropped, however, from 17 to 4. The researchers mention that although this oddity was noticed previously, no one had yet attempted to explain it (Faust and Ashkenazy, 2007).

An examination of the geology of the coastal plain reveals parallel coastal ridges that impede water drainage. Most agriculture and cities are located in river valleys. Faust and Ashkenazy argue that an increase in precipitation would have resulted in severe drainage problems, turning once fertile river valleys into swamps. Coupled with a loss of farmland, swamps would provide ideal breeding grounds for diseases such as malaria and bilharzias. Some excavations in the area have provided evidence of clay sediment layers and increases in marsh vegetation (Faust and Ashkenazy, 2007). While no one is suggesting that increased rainfall caused the Maya decline, researchers must be prepared to think creatively when odd or conflicting climate data are found rather than simply ignoring it.

Previous Research into Climate-Maya Culture Link

Archaeological surveys of Maya cities have shown the citizens and rulers to be well-aware of the need to mitigate dry periods. Much of the Maya homeland suffers under water stress from the combination of an unconfined water table lacking springs, large seasonal rainfall variations, the possibility of midsummer dry spells (*caniculas*), and a general lack of surface waters due to the permeable bedrock (Silverstein et al., 2009). The architecture in the city of Tikal in the riverless Petén region of Guatemala appears to help funnel rainwater into reservoirs (Figure 3.5**)**. Catchment areas ranged up to 62 ha, leading to three major reservoir types: central precinct, residential, and bajo-margin. The central precinct reservoir is estimated to have collected more than 900 000 m^3 of water every year (Scarborough and Gallopin, 1991). The Maya used several techniques to support their agriculture in the marginal landscape, including terracing, canal building, and possible conversion of wetlands. Recently, some researchers have put forth the idea that the earthworks in the outskirts of Tikal, long assumed to hold a defensive purpose, are actually a series of filtration trenches used to harvest subsurface water (Silverstein et al., 2009).

Large regions around many Maya settlements were terraced for agriculture. Use of LiDAR is now allowing new insight into how pervasive terracing was in some regions, with nearly 90% of the landscape modified around Caracol (Chase et al., 2011). Lisa Lucero even proposes a theory where the ruling classes of the Maya obtained and maintained their power due to their control and management of water. When droughts destroyed their ability to control the water, the management systems collapsed (Lucero, 2002). With water stress clearly present in the

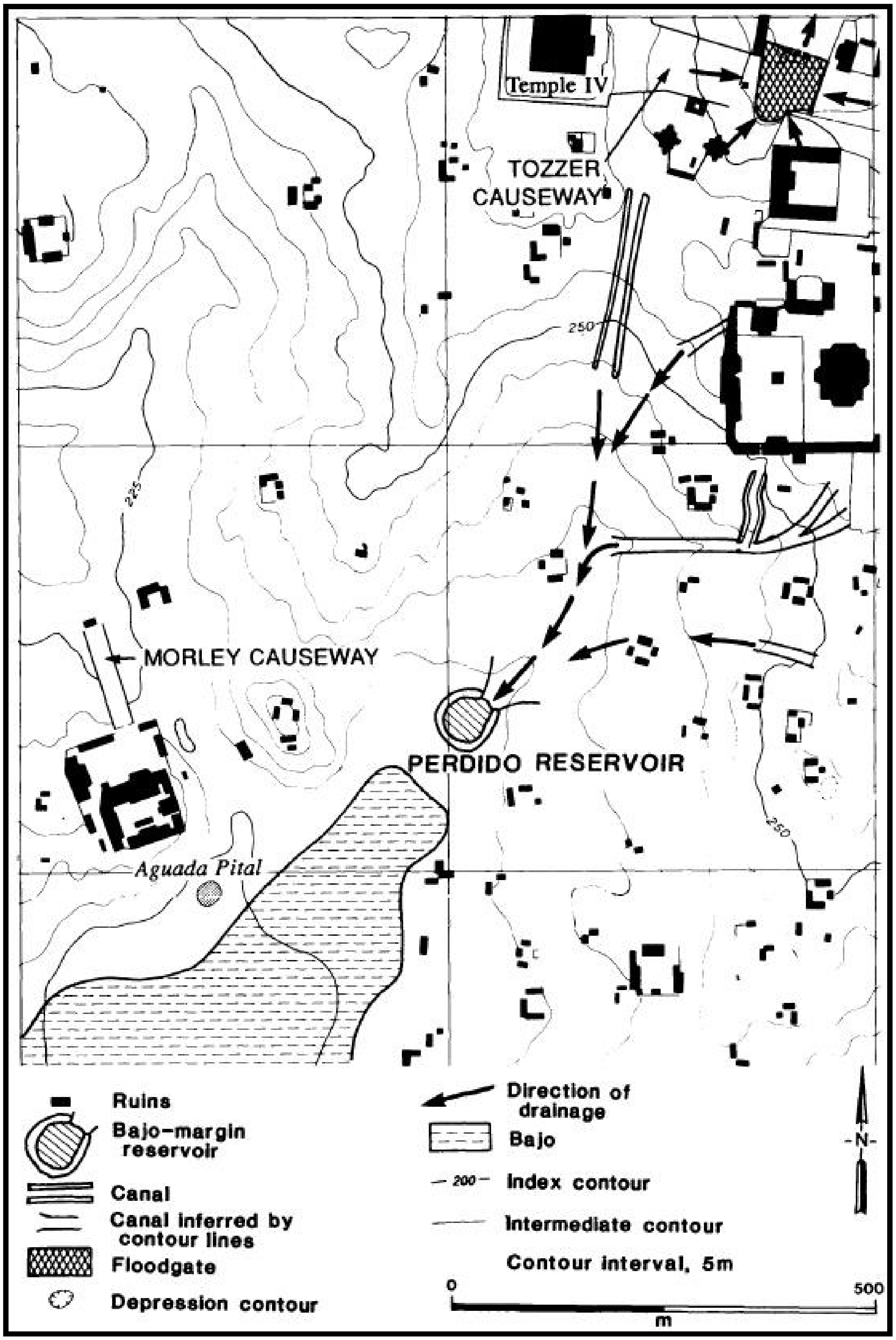

Figure 3.5. Map showing the flow of waters from part of Tikal to collection and holding regions (Scarborough and Gallopin, 1991)

minds of the ancient Maya, some research shifted to looking for physical evidence of droughts during the end of the Classic Maya period.

Sediment Studies

Most of the physical evidence for droughts during the Maya civilization comes from lacustrine deposits. The first of these studies came from Lake Chichancanab in the northern Yucatán Peninsula, which was selected for its unique lake properties: a closed hydrology, high microfossil abundance, and gypsum saturation. Theoretically, a decrease in rainfall and/or an increase in evaporation (indicating aridity) would result in gypsum supersaturation and subsequent precipitation onto the lakebed. A core was taken in 1993 resulting in a 9000-year sediment record. Most interesting was a 6 cm thick gypsum layer dating to 780-990 AD; this matched well with the accepted timing of the end of the Classic Period of the Maya (Hodell and Curtis, 1995). The authors point out that this finding has often been misinterpreted as a 200-year megadrought; in reality, the span was the probability distribution of the radiocarbon age and that cores of better resolution would be needed to better determine drought duration.

The lake was re-sampled in 2000 to retrieve two cores covering the past 2600 years. Prominent gypsum layers were found to be deposited twice between 770-870 AD and four times from 920-1100 AD. In between each of these timeframes was ~50 years of moister conditions. Hodell et al. (2005a) asserted that this study presented clear proof of “significant climate changes” during the Late Classic Period. After this study, sediment studies from other locations in the Maya region began to corroborate the idea that climate change had occurred around the decline of the Classic Maya civilization.

Several studies have been performed in the Mexican state of Quintana Roo near the Maya city of Cobá. Cores from Lake Punta Laguna were analyzed for oxygen and carbon isotopes from ostracods, gastropods, and inorganic calcium carbonate precipitate. Cores were also scanned along the red color bandwidth as a proxy for organic-rich sediments. Inorganic sources for oxygen isotopes presented large increases in $\delta^{18}O$ values at ~550 and 820 AD and a decrease at ~1000 AD. Organic sources (ostracods and gastropods) also exhibited a strong decrease in $\delta^{18}O$ values at ~1000 AD. Carbon isotope records from inorganic calcium carbonate reached maximum $\delta^{13}C$ values between ~550 and 690 AD. Combined, the core information was interpreted as showing a dry period at ~535-550 AD, coinciding with the proposed Maya Hiatus. This was followed by a return to wetter conditions until a series of dry events during the Late Classic Period, with the first beginning ~760-770 AD. The strongest dry period was estimated to have occurred in the mid-800s AD, and a final dry period beginning ~950-960 AD. Each of these dry events was interspaced with wetter decades, in agreement with other climate records that date back to the Late Classic Period (Curtis et al., 1996; Hodell et al., 2007).

Another project in Quintana Roo studied a lake situated near the center of a large Maya city. Lake Cobá was part of the large water complex of the city of Cobá. Cobá remained a strong and healthy power through the Terminal Classic Period before declining ~1100/1200 AD. An 8.8 m core was removed for study, covering over 7000 years of sedimentation. Pollen records around the time of the Maya collapse show an increase in trees at the expense of more weedy species, suggesting a decline in agriculture and disturbance. This trend later reverses suggesting a return of former practices, until after ~1240 AD when the forest pollen makes a dramatic comeback (Figure 3.6). Diatom records show a “fresh and deep-water period” during much of the Classic that the authors believe is not related to precipitation changes, but rather human alterations to the water system such as diking. While the sediments do not show evidence of drought in stable isotopes, the diking was possibly instigated by a need to provide a more stable water source during drier or variable times (Leyden et al., 1998).

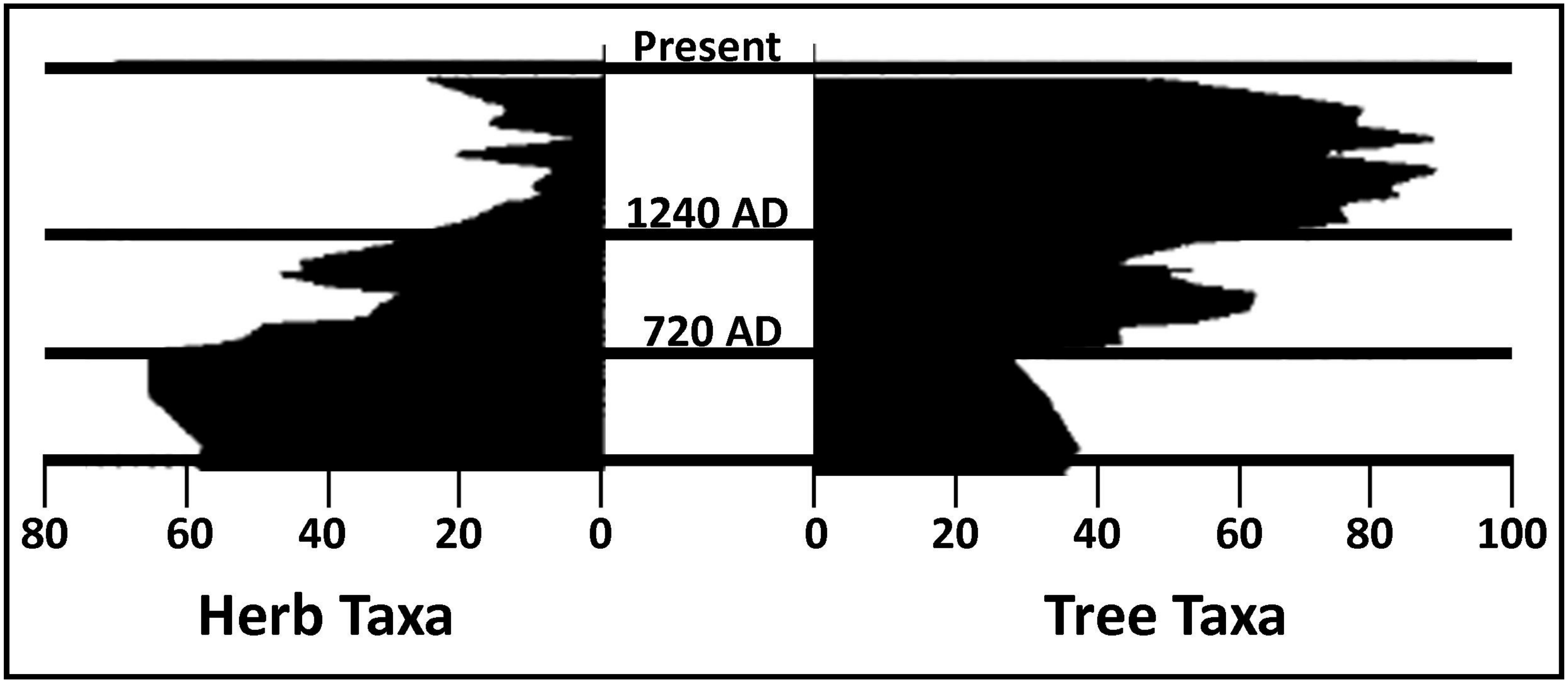

Figure 3.6. Pollen record from Lake Cobá illustrating the inverse relationships between tree and herb species. Tree increases are believed to be a response to land and city abandonment. Reproduced and simplified (Leyden et al., 1998)

Supporting Data from Surrounding Areas

Sites located around the periphery of Classic Maya activity have also been found to provide paleoenvironmental information. The Cariaco Basin in the Caribbean Sea off Venezuela has provided cores with bimonthly resolution spanning the Late Classic Period. High titanium concentrations in the sediment are linked to wetter periods, with low concentrations indicative of drier times. Multiyear droughts are suggested at 760, 810, 860, and 910 AD, on top of a general drying trend (Haug et al., 2003). Mangrove sediments from the Pacific coast of Guatemala present elemental and pollen records that also agree with an arid Late Classic Period. Interestingly, while Yucatán and Cariaco records suggest wetter conditions returning after ~950 AD, the mangrove sediments continue to show dry and variable precipitation for 300-500 more years. The mangrove record agrees with some Peten lake studies and is a reminder that changes in precipitation were unlikely to be consistent across the greater Maya region (Neff et al., 2006). Indeed, this variation in the scale, scope, and location of the droughts may explain why some Maya centers flourished during the Terminal Classic Period while others were deserted (Gill et al., 2007; Hodell et al., 2007).

A recent paper has published the first dendrochronologic record for Mesoamerica that dates back to the Late Classic. Dendrochronology is rare among paleorecords in that it can usually date events down to the exact year. Montezuma baldcypress trees from the Valley of Mexico provided evidence of four major droughts, including one during the Terminal Classic. This drought was dated to 897-922 AD, with lesser droughts at 810 and 860 AD as well. Later droughts coincided with the collapse of the Toltecs and famine recorded by the Aztecs (Stahle et al., 2011).

Papers not specifically searching for the Classic Maya droughts have also found evidence supporting the theory. A pollen study to determine vegetation changes in the Lacandon rain forest in Chiapas, Mexico found a decrease in lower montane rainforest taxa coinciding with an increase in pines from ~690-1220 AD. After this period pine pollen percentages decrease with a return of rainforest dominance. Pines are typically found in drier parts of the local landscape; while being excellent colonizers, pines cannot compete well with plants adapted to moister conditions. A decline in rainforest plants due to drought would provide an opportunity for pines to invade new locations. Once wetter conditions returned, the pines would be replaced by the rainforest taxa (Domínguez-Vázquez and Islebe, 2008).

Combined, the data gleaned from sediments in the region point to arid conditions prevailing at the time of the Late Classic and Terminal Classic decline of the Maya civilization. These arid conditions appear to take the form of several multiyear droughts separated by several decades of relatively moister conditions. While some special sediment cores can offer yearly laminae (Haug et al., 2003), most sediment studies are plagued by high levels of uncertainty in resolution. Changes in deposition rates and plateaus in the radiocarbon calibration curve limit the ability to focus on narrow time frames. In some cases, the resolution of a sample may be lower than the length of the dry events in question (Solleiro et al., 2007). Speleothem research can overcome much of the resolution issues frequent to sediments and is being used to refine and corroborate the pioneering work of the sediment studies.

Research from Belize

Limited paleoclimate research has been performed in the Vaca Plateau region of Belize, as the karst topography precludes the lakes and surface water needed for typical sediment studies. A recent study avoided the mainland entirely and retrieved sediment cores from a sinkhole located offshore Belize. This sinkhole, well-known to divers and tourists as the Blue Hole, appears to have begun flooding by rising sea levels sometime before 7-10 ka BP. The sediment appeared to have annual layers due to changes in ocean productivity over the year, and stable isotopes were sampled from various layers to create a chronology. Variations in $\delta^{18}O$ appear to correlate with other Holocene temperature curves with the highest values around 800 AD. A drop in $\delta^{13}C$ from 500-1000 AD might be explained as a result of Maya activities on the mainland, but carbon isotope variations in marine sediments can be very difficult to interpret (Gischler et al., 2008). Although providing insight into Holocene climate changes, the Blue Hole study falls victim to the same pitfalls as lacustrine studies on land.

One rather ingenious project examined sediments from within a cave near a Maya archaeological site. Though many caves in the area were utilized by the Maya for ritual, no evidence of Maya activity was found in this cave; thus, the sediments are assumed to be free from human disturbance. Carbon isotope analysis points to significant replacement of maize by native vegetation coinciding with the Preclassic Abandonment and Late Classic Period decline. The well-drained karst topography of the Vaca Plateau is believed to have magnified any drying trends throughout the Maya region. Little agricultural activity is indicated after ~800 AD, placing its abandonment early in the Late Classic decline and in agreement with theories stating that marginal areas such as the Vaca Plateau would be the first sites to be abandoned (Polk et al., 2007).

The Belizean stalagmite study by Webster et al. (2007) presented a previously unparalleled paleoclimate record for the Vaca Plateau. This study analyzed a stalagmite containing a 3300-year record from the Macal Chasm in the Vaca Plateau of Belize. The stalagmite was analyzed for reflectance, color, luminescence, $\delta^{13}C$ values, and $\delta^{18}O$ values. Luminescence records were collected at a data resolution of 0.5-3 years while each isotope sample covered 5-30 years at intervals of 10-70 years. Three major times of aridity were found between 100 BC and 1200 AD by correlating decreases in luminescence with maxima in $\delta^{13}C$ and

$\delta^{18}O$ values. The first two occurred at 141 AD and 517 AD, coinciding with the Preclassic Abandonment and Maya Hiatus, respectively. Both these relatively short times of drought were followed by a return to wetter conditions. The final arid period consisted of several droughts dating to 780, 910, 1074, and 1139 AD. These droughts are believed to be the most severe in the 3300-year record obtained from the stalagmite. Droughts dating to historical times are also observable in the speleothem record, helping verify the conclusions that predate written records. The arid peaks also correlate with highs in Bermuda Rise sea-surface temperatures and records from Lake Chichancanab, illustrating that the record is applicable to the larger Maya region (Webster et al., 2007).

CHAPTER 4
SPELEOTHEM RESEARCH

In recent years, speleothem research has become well-recognized for the many advantages for paleoclimate reconstruction it possesses over other physical sources. Speleothems contain records of meteoric water changes in a location typically protected from erosion for thousands of years. Stalagmites are by far the most common speleothem used for paleoclimate research. Stalagmites are typically formed when rain water absorbs CO_2 from the soil as it moves downward towards the limestone bedrock. This CO_2-rich water then dissolves carbonate from the limestone. If a cave exists in the bedrock, the water may drip from the cave ceiling onto the cave floor. Upon impact, the water will degas CO_2 and precipitate carbonate according to the equation:

$$Ca^{2+}{}_{(aq)} + 2HCO_3^-{}_{(aq)} \Longleftrightarrow CaCO_{3(s)} + H_2O + CO_2$$

Over time, this carbonate precipitate will grow upward, producing a stalagmite. Since the precipitated carbonate is partially derived from rainwater and soil CO_2, the carbonate contained in the stalagmite will preserve a record of the surface environment conditions. The orderly, horizontally-layered structure of stalagmites along their growth axes makes them more preferable for study than other speleothems such as stalactites (Lauritzen, 2005).

Perhaps the greatest advantage of speleothems is that they can be readily dated by uranium-series dating to a precision approaching ± 0.5% while avoiding the pitfalls of radiocarbon dating such as calibration and reservoir effects (McDermott, 2004). Such radiocarbon calibration typically offers date ranges during the Classic Period of approximately

200 years (McNeil et al., 2010), creating difficulties in correlating physical data with cultural events. Uranium-series dating works well for speleothems due to the inherent nature of their creation. ^{234}U is soluble in water and is picked up by the same water that is dissolving carbonate. When the calcite precipitates out of the water (creating the speleothem), some of the ^{234}U is deposited within the calcite lattice, where it will decay over time to ^{230}Th. ^{230}Th is not soluble in water and theoretically the only source of ^{230}Th will be from the decayed ^{234}U, enabling successful dating (Cheng et al., 2000). In reality, detrital sediment trapped in the speleothem can sometimes be a source of ^{230}Th contamination, and the ^{230}Th/^{234}U ratio must be corrected.

Visual information

Once sawn in half, optical observations of stalagmites can reveal a great deal of paleoclimate information. A simple visual analysis of light reflectance may reveal bands of dark detritus-rich layers surrounded by cleaner layers. Previous studies have proposed that the detritus-rich layers often represent arid periods when the drip water rate slowed or stopped, which prevented airborne dust from being washed off the stalagmite surface (Railsback et al., 1999; Webster et al., 2007). Natural color variation has been quantified by two different methods. The stalagmite can be scanned in grayscale, and then the variation in grayscale can be plotted over the history of the speleothem. Alternatively, a standardized color chart can be created, and the true color variations categorized and plotted (Webster et al., 2007).

A luminescence scan can be produced by exposing the cut stalagmite to ultraviolet light. Most of the luminescence stimulated by ultraviolet light is produced by fulvic and humic acids trapped in the stalagmite. Fulvic acids are released from plant roots while humic acids are byproducts of decomposition within soils. Both are related to overall soil productivity, and the increases in luminescence intensity are viewed as reflecting increases in productivity of the surrounding landscape (Baker et al., 1998; McGarry and Baker, 2000; Shopov et al., 1994). However, the luminescence intensity can be affected by several other factors besides concentration of fulvic and humic acids, including flow rate of the drip water, changes in speleothem growth rate, presence or absence of detrital grains, and aquifer depth (Baker et al., 1996).

Mineralogy and Petrography

The actual structure of stalagmites can provide much paleoenvironmental information. Typically, thin sections are created of the sample stalagmite and analyzed under a petrographic microscope. Calcium carbonate precipitates in speleothems as one of two minerals: calcite or aragonite. Identification of these minerals in commonly performed by thin section analysis, with x-ray diffraction available for confirmation. Determining the mineral composition of regions of a stalagmite is very important for two reasons. First, aragonite typically displays a $\delta^{13}C$ value ~3-5‰ greater and a $\delta^{18}O$ value ~1.75‰ greater than calcite (Frisia et al., 2002), and each mineral is associated with different trace elements (Railsback, 1999). If a stalagmite with alternating layers of aragonite and calcite is sampled for isotopes or trace elements, failure to correct for mineral changes will result in reading data variations due to mineral changes as environmental changes. Secondly, changes in mineral can be a direct signal of environmental changes (Frisia et al., 2002; Railsback et al., 1994). Aragonite deposition is associated with greater evaporation (Murray, 1954) and higher temperatures relative to calcite deposition (Burton and Walter, 1987; Morse et al., 1997).

Examination of the stalagmite under thin section can identify transitional changes between layers. In a 2011 paper, Railsback et al. described two types of layer boundaries along with their paleoenvironmental significance. Type E surfaces showed signs of layer erosion, particularly on the layer apex, and were associated with times of increased water flow. Type L surfaces had layers that were present on the layer apex of the stalagmite, but thinned before extending down the sides of the stalagmite. Type L surfaces were associated with aragonite and greater $\delta^{13}C$ values, and these surfaces were theorized to have formed during times of lesser water flow (Railsback et al., 2011).

$\delta^{18}O$ Studies

The $\delta^{18}O$ recorded in a stalagmite's calcium carbonate is assumed to reflect the $\delta^{18}O$ of the original meteoric water and any changes due to evaporation that occurs before carbonate precipitation (McDermott, 2004). The temperature of the cave environment plays a role in the equilibrium fractionation between water and calcite, but surface precipitation variations in $\delta^{18}O$ typically overwhelm the minor input from cave temperature. The 'amount effect' influence on oxygen isotopic ratios was previously mentioned, where increases in rainfall amount are associated with decreases in the rainfall's $\delta^{18}O$ (Rozanski, 1993). Conditions associated with changes in rainfall amounts may tend to exaggerate the corresponding stalagmite's $\delta^{18}O$ changes. Intense rainfalls tend to infiltrate soils quickly without much change in $\delta^{18}O$ due to the lack of evaporation, whereas lighter rains would tend to see increases in $\delta^{18}O$ due to the evaporative effect. While plants do not fractionate water, dense vegetation (a result of well-watered conditions) would decrease surface evaporation and more open vegetation would show increased surface evaporation (Lachniet, 2009). To summarize, lighter rains and arid conditions would result in sparser vegetation, leading to an increase in evaporation and $\delta^{18}O$ values. Theoretically, the new $\delta^{18}O$ would be greater than the original meteoric $\delta^{18}O$. More rains and wetter conditions would affect the $\delta^{18}O$ in a similar, but opposite, manner.

Kinetic fractionation occurs when the CO_2 concentration of the drip water is different from the cave's atmospheric CO_2 concentration. Kinetic fractionation can result in calcite or aragonite being precipitated out of equilibrium from the drip water, possibly erasing any paleotemperature information that would be preserved (Lachniet, 2009). Researchers can check for kinetic fractionation using 'Hendy criteria.' In a Hendy test, a single growth layer is sampled for evidence of correlation between $\delta^{13}C$ and $\delta^{18}O$ values. Determining the bounds of a single growth layer and drilling adequate samples from solely this layer is often a difficult task (McDermott, 2004). However, kinetic fractionation can aid in defining arid events as evaporation will fractionate the drip water to produce heavier $\delta^{13}C$ and $\delta^{18}O$ values. Assuming greater evaporation will occur in more arid periods, this fractionation will enforce the isotopic ratios that were already made heavier through lessened rainfall and vegetation changes (Brook, 1999).

$\delta^{13}C$ Studies

Much like with oxygen isotopes, calcite deposition on a stalagmite preserves the $^{13}C/^{12}C$ composition of the drip water. The $\delta^{13}C$ of the drip water is primarily influenced by the $\delta^{13}C$ of the soil CO_2. Greater amounts of vegetation will produce greater amounts of CO_2 that is enriched with ^{12}C. Drier conditions should lead to less vegetation and hence greater $\delta^{13}C$ values of the soil CO_2 (Baldini et al., 2005; Hesterberg and Siegenthaler, 1991). As stated previously, variations in $\delta^{13}C$ have often been attributed to changes in vegetation. C3 vegetation is reflected in speleothem carbonates with $\delta^{13}C$ values ranging from -14‰ to -6‰, compared to C4 $\delta^{13}C$ values of -6‰ to +2‰. Due to this vegetation basis, seasonal variations in $\delta^{13}C$ may exist; typical analysis samples, however, take in multiple years of deposition and seasonal variations should be limited (McDermott, 2004). Significant degassing will also enrich the remaining solution in ^{13}C, as ^{12}C is preferentially taken in the degassed CO_2 (Magaña et al., 1999). Because changes in plant species compositions would be limited and lagged on smaller timescales, degassing and vegetation amount are more likely to be the source of short-term variations.

Trace Elements and Inclusions

At present, the vast majority of speleothem studies focus on the stable isotopes of carbon and oxygen. A few studies have also looked into the ratios of several trace elements to attempt to determine any relation between trace element fluctuations and climatic fluctuations with limited conclusive results (Desmarchelier et al., 2006; Fairchild and Treble, 2009; Verheyden, 2004), although some evidence exists that Mg/Ca ratios increase during drier conditions (Huang et al., 2001) or warmer conditions (Roberts et al., 1998). The need for further examination into the links between trace elements and other information gleaned from speleothems has been noted in scientific literature (Perrette et al., 2000).

Finally, fluids and other objects trapped within a stalagmite's structure are a rarely tapped paleoenvironmental resource. Fluids within stalagmites have been tapped to extract noble gases and δD values. These data have been used to determine past temperatures and rainfall provenance (Fleitmann et al., 2003; Kipfer et al., 2002). Pollen can in some cases be recovered from stalagmites. Although not typically present in the same quantities normally found in palynological studies of lake sediments (around 1-5 pollen grains per gram of speleothem (McGarry and Caseldine, 2004)), the pollen found in stalagmites can nevertheless provide insight into previous environmental conditions of the sample site. Several studies have determined that the modern stalagmite pollen records match well with modern pollen assemblages and likely reflect local rather than regional pollen records (Brook et al., 1990; Brook and Nickmann, 1996; McGarry and Caseldine, 2004).

Drought Determination

After a speleothem is subjected to the analyses described above, the combined information can suggest the existence of previously occurring arid periods. To review, an arid period or event will exhibit many or all of the following signals within a relatively short timeframe:

- Visual color or grayscale indicative of high levels of detritus
- Low luminescence
- Switch from calcite to aragonite
- Type L surface boundaries (thinning or cessation of layer flank deposition)
- Higher $\delta^{18}O$ values
- Higher $\delta^{13}C$ values

CHAPTER 5
METHODS

Field Work

Field work was performed from May 9-17, 2010, in the Cayo District of Belize (Figure 5.1). The research group consisted of seven members: Dr. George A. Brook, Dr. Jim Webster, Dr. Philip Reeder, Dr. Jason Polk, Bill Reynolds, Pete Akers, and Ben Miller. All group members are either currently or previously involved in cave research and exploration. The main goal of the field research for Brook and Akers was to collect stalagmites for later analysis. A secondary goal was to examine multiple Maya archaeological sites in order to better understand the relationship between Maya settlement patterns and the local environments. Finally, the research group was observing the surrounding landscape for novel research opportunities that could be utilized as part of the current work.

Caves

Two days were dedicated to exploration and sampling of local caves. Three caves were investigated on property owned by Calico Jack's Village Resort: Box Tunich, Bega One, and Bega Two. Two vertical shaft cave entrances nearby were examined, but not entered nor explored. The three explored caves were all horizontal entrance caves with numerous Maya pottery shards indicating a long period of human impact (Figure 5.2). Box Tunich and Bega One have both been developed by Calico Jack's into tourist caves with the addition of metal stairways on steep locations in the caves, whereas Bega Two has been surveyed, but otherwise unaltered. Box Tunich is located on a hillside on the other side of the valley from Bega One and Bega Two. .

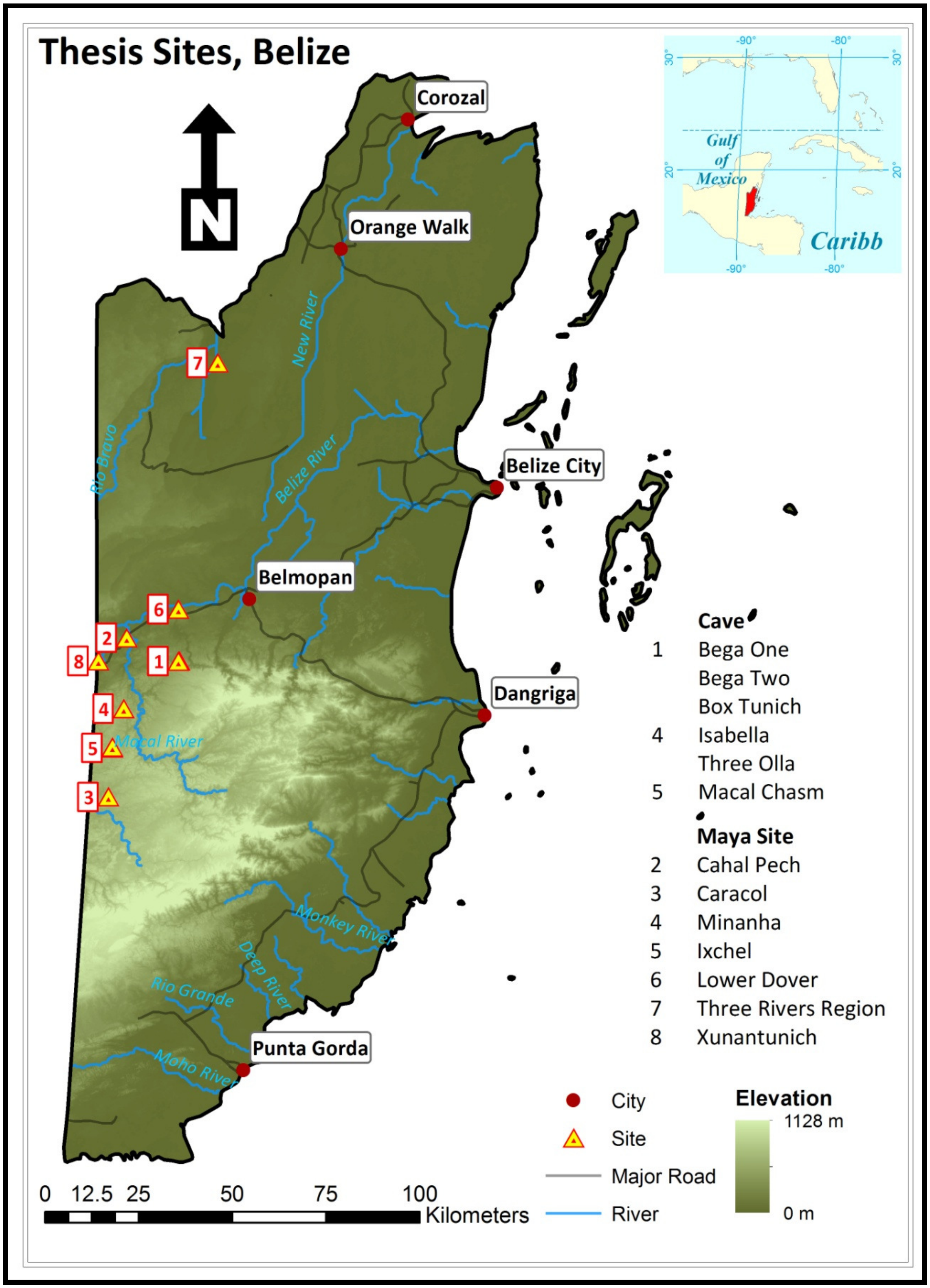

Figure 5.1. Map of Belize terrain, with caves and archaeological sites mentioned during field work labeled. The region of elevated terrain in south-central Belize is composed of the Vaca Plataeu (western portion) and the Maya Mountains (eastern portion).

Figure 5.2. Left: Entrance to Box Tunich Cave; Right: Pottery shards inside Box Tunich Cave

Bega Two is located on the same cliffside as Bega One, but at a higher elevation.

Two other caves were examined at a location on the Vaca Plateau near the Maya archaeological site of Minanha. Minanha is currently being excavated by a team from Trent University as part of the larger Vaca Plateau project. One cave is known as Isabella Cave; the cave was unique among those surveyed in being a very expansive room largely open to the external environment due to a cave collapse at an undetermined time in the past. The second cave explored was unnamed, but here referred to as Three Olla Cave. This cave was entered through a 10 m vertical shaft, and contained three rooms. Both caves contained Maya pots and pottery shards. Environmental data for select caves is given in Table 5.1.

Table 5.1. Temperature and humidity readings taken at select cave sites. Measured with a pen-type Thermohygrometer. Readings from within caves were taken from deep locations, often near stalagmite collection sites. The Three Olla readings were taken from directly outside the cave entrance.

Cave	**Temperature**	**Humidity**
Box Tunich	24.8°C	79%
Bega One	21.2°C	90%
Isabella	21.2°C	83%
Outside Three Olla	32.5-35.6°C	37-40%

Seven stalagmites were collected during field work. Stalagmites were collected using a chisel and rock hammer (Figure 5.3). A reciprocating saw was utilized in the removal of one stalagmite (BZBO3). The soda straw formations located above four stalagmites were also collected, plus an additional soda straw taken from a formation where water samples were collected. Information about collected stalagmites is presented in Table 5.2. Heights are approximate due to some stalagmites being retrieved in multiple pieces. BZBO2 was a small column, and current activity was unclear. Note that some information is missing for BZIS5; this stalagmite was found to have a large hollow section in the core of the stalagmite and judged

Figure 5.3. Jim Webster collecting stalagmite BZBO2 from Bega One cave with a rock hammer.

unsuitable for analysis. BZIS5 was thus not brought back to the University of Georgia for further research.

Table 5.2 Summary data for collected stalagmites. Stalagmites were labeled in the following manner: Two letter country label (BZ=Belize), two letter cave label, and number for order of acquisition.

Stalagmite Code	Cave	Activity	Approximate Height	Soda Straw Collected?
BZBT1	Box Tunich	Active	10.5 cm	No
BZBO2	Bega One	Unknown	78.0 cm	No
BZBO3	Bega One	Active	170.0 cm	Yes
BZBW4	Bega Two	Active	33.5 cm	Yes
BZIS5	Isabella	Active	Unknown	Yes
BZIS6	Isabella	Inactive	36.0 cm	No
BZTO7	Three Olla	Active	85.0 cm	Yes

Eight water samples were also collected for analysis. Four were taken of drip water coming off of formations around BZBO3 (Figure 5.4). Two were taken in Isabella cave: one solely of drip water coming off formations in the back of the cave, and one combining drip water with beads of condensation on the cave wall. One sample of drip water was taken in Bega Two around BZBW4. Finally, rainwater was collected during a brief, but heavy, rainstorm at Lower Dover Field Station on May 13, 2010.

Archaeological Sites

Maya archaeological sites were visited throughout the time of field work. These sites were visited in order to gain a feel for the water stresses and water mitigation methods relevant to the Classic Maya. In all, five Maya sites were visited: three were heavily excavated, restored, and open for public viewing, one was currently being excavated, but not restored, and one was unexcavated.

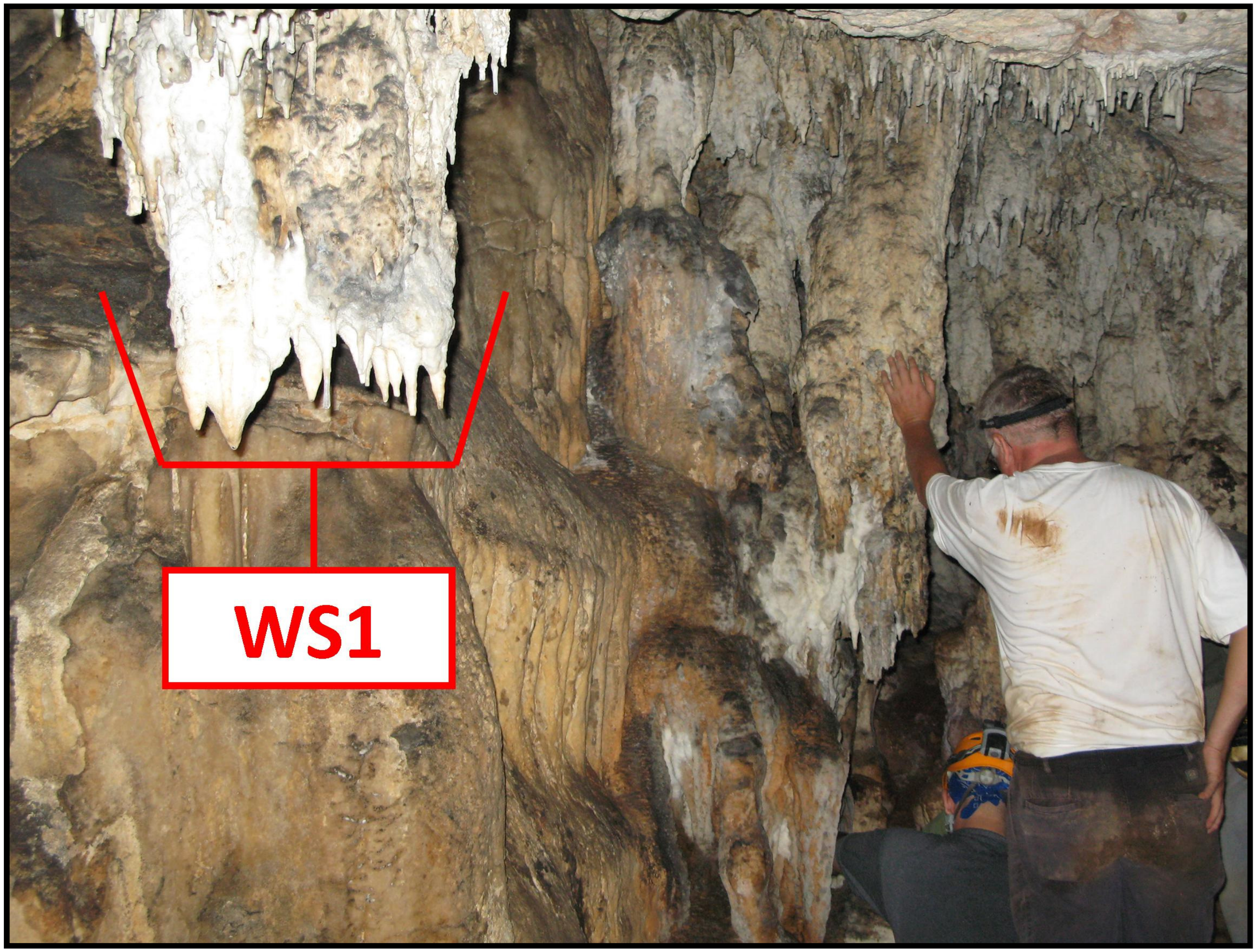

Figure 5.4. Cave formation where drip water sample WS1 was taken. Team members at right are collecting stalagmite BZBO3, indicating close proximity of WS1 to BZBO3.

The largest site visited was the city of Tikal in Guatemala. Tikal was a very important Maya city during the Classic Period. While large areas have been restored, many smaller structures remain unexamined due to the sheer number of structures. Several of the plazas appeared to support drainage towards what are believed to have been quarries doubling as aguadas (reservoirs), or perhaps quarries turned into aguadas. Possible aguadas at all sites were difficult to identify and analyze. Some aguadas have been surveyed in previous studies, but many have been obscured by a millennium of sedimentation.

Two smaller restored sites examined were Xunantunich and Cahal Pech. These sites are located in the Cayo District, Belize, near the Guatemala border. The sites are less than 20 km apart and are believed to have had similar-sized populations. Both of these sites are located on hilltops, which would aid in drainage. Several plazas and structures were located directly adjacent to very steep drop-offs. Presumed drainage channels were found leading away from plazas and across the face of El Castillo (Figure 5.5). With structured covered fully in stucco, runoff rates from rainstorms would have been quite rapid, and drainage channels would help prevent flooding and ponding.

The two unrestored sites visited were Minanha and Lower Dover. Minanha is located on the Vaca Plateau and is currently being excavated. The central portion of Minanha is dominated by a royal acropolis rising to one of the highest points in the local region (Figure 5.6). The surrounding landscape of the hills had been intensely terraced in ancient times. Excavations into the top of the acropolis have discovered a Classic temple and structures that were carefully filled and buried, suggesting that the previous royal court did not meet a particularly violent end (Iannone, 2005). The Lower Dover site is located outside of Unitedville, Belize (Figure 5.7). This site underwent excavation beginning in the summer of 2010, but simply had the understory cleared at the time of visitation. Although considered a small- to moderate-sized site, it.

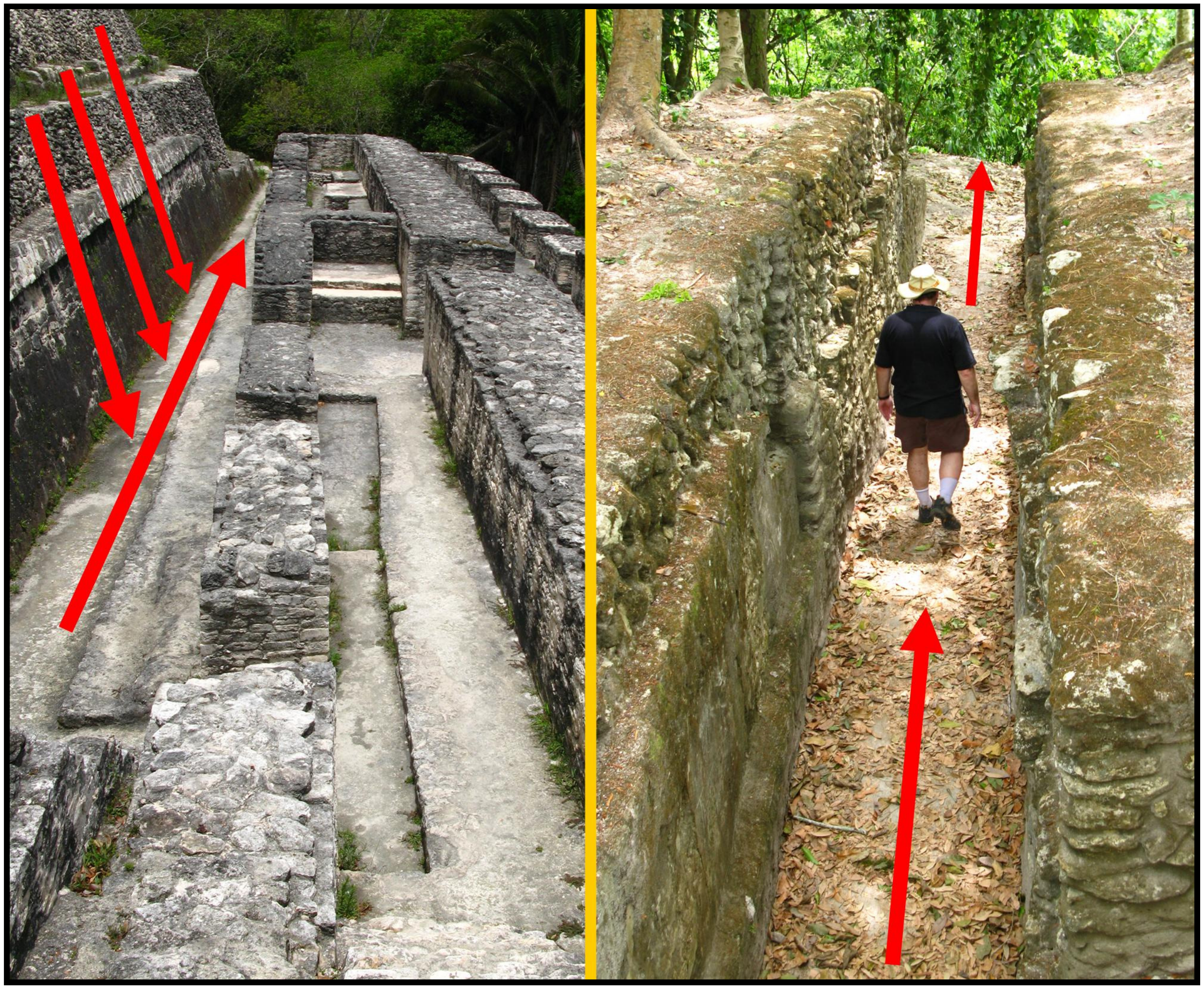

Figure 5.5. Maya drainage architecture, with red arrows indicating water flow. Left: The front of El Castillo at Xunantunich, with assumed drainage chute funneling water off pyramid face. Right: A drainage channel leading away from a plaza at Cahal Pech toward a hill drop off.

Figure 5.6. View across the Vaca Plateau from the apex of Minanha's main pyramid. A refreshing breeze and commanding view from such a height would have made for a prized location.

Figure 5.7. Jason Polk standing on an unexcavated structure located near Plaza B at the Lower Dover site.

nonetheless contains at least 5 plazas and multiple tall pyramid structures. Driving throughout the Cayo countryside, possible Maya ruins were commonplace, at some points occurring as little as every few kilometers. The highest concentration was found in the regions adjacent to the major river system of Belize (the Belize, Macal, and Mopan rivers)

Laboratory Work

Examination and analysis of the collected stalagmites was performed at the University of Georgia. Stalagmites were photographed prior to intrusive or destructive analysis (Figures 5.8 and 5.9). The stalagmites were also measured for physical dimensions, with each piece having a record for maximum vertical height, maximum and minimum base transverse diameter, and maximum and minimum top transverse diameter. A water-based rock saw was used to cut each stalagmite in half longitudinally. One half was saved for visual-based analysis while the other half was used for destructive sampling. The destructive sampling half was then sawn in half longitudinally again to create two pieces that were quarters of the original stalagmite. One quarter was used to drill for dating and isotope samples, while the other quarter was used to create thin sections.

BZBO2, a column, was collected in three pieces. The bottom two pieces were originally the stalagmite and the top piece was originally the stalactite prior to joining. After sawing the top piece of BZBO3, the stalagmite was found to have an eroded core upon which later deposition occurred. The top piece was retained for further study, but the remaining lower portions of the stalagmite were not considered suitable for further analysis. BZIS6 had an interior pitted with several odd pits and hollows. While the oddity of BZIS6 may prove useful for another study, the stalagmite was not pursued further for this project.

Dating

Each stalagmite had ten locations chosen for drilling in order to create a chronology (Figure 5.10). These locations were first chosen to set maximum and minimum ages, secondly to focus on zones of interesting crystal or color changes, and finally to fill out the remaining gaps in the drill sites. Each location had ~100 mg of sample collected by use of a dental drill (Figure 5.11). These samples were sent to the University of Minnesota for uranium-series dating. The uranium-series results returned as inconclusive dates due to a very low concentration of initial uranium present in the stalagmites. None of the samples contained greater than 50 ppb of ^{238}U, and most contained less than 10 ppb of ^{238}U. At these concentrations of uranium, calculated dates have large error terms and very small amounts of thorium contamination can skew results dramatically. A more thorough discussion of the uranium-series data can be found in the 'Results' section of this thesis.

Since uranium-series dating failed to precisely date the stalagmites as hoped, radiocarbon dating options were explored. Simple radiocarbon dating of the calcium carbonate matrix will not initially return correct ages. A certain percentage of the carbon contained within the stalagmite is composed of 'old carbon' from the limestone bedrock. This carbon has virtually nonexistent amounts of ^{14}C, and its inclusion within the radiocarbon sample will return ages older than the actual time of stalagmite growth. One method to deal with the old carbon problem is to determine a correction factor for the calcium carbonate samples. If the age of a sample can be determined by an alternative means, then the old carbon input can be calculated by comparing the accurate alternative age to the calcium carbonate radiocarbon age. The simplest method of finding an alternative age is to take a calcium carbonate sample from a location that should be recently deposited. Therefore, whatever age the calcium carbonate returns should be due to the input of old carbon; this technique requires the assumption,

Figure 5.8. Three collected stalagmites with 30 cm ruler for size comparison. BZBT1 has inset of the stalagmite from above, at same scale as side photo. BZBO2's furthest right piece was originally a stalactite prior to joining with the lower section to form a column. BZBO3 is arranged with its basal pieces above the upper portions. BZBT1 was collected from Box Tunich cave, while BZBO2 and BZBO3 were collected from Bega One Cave.

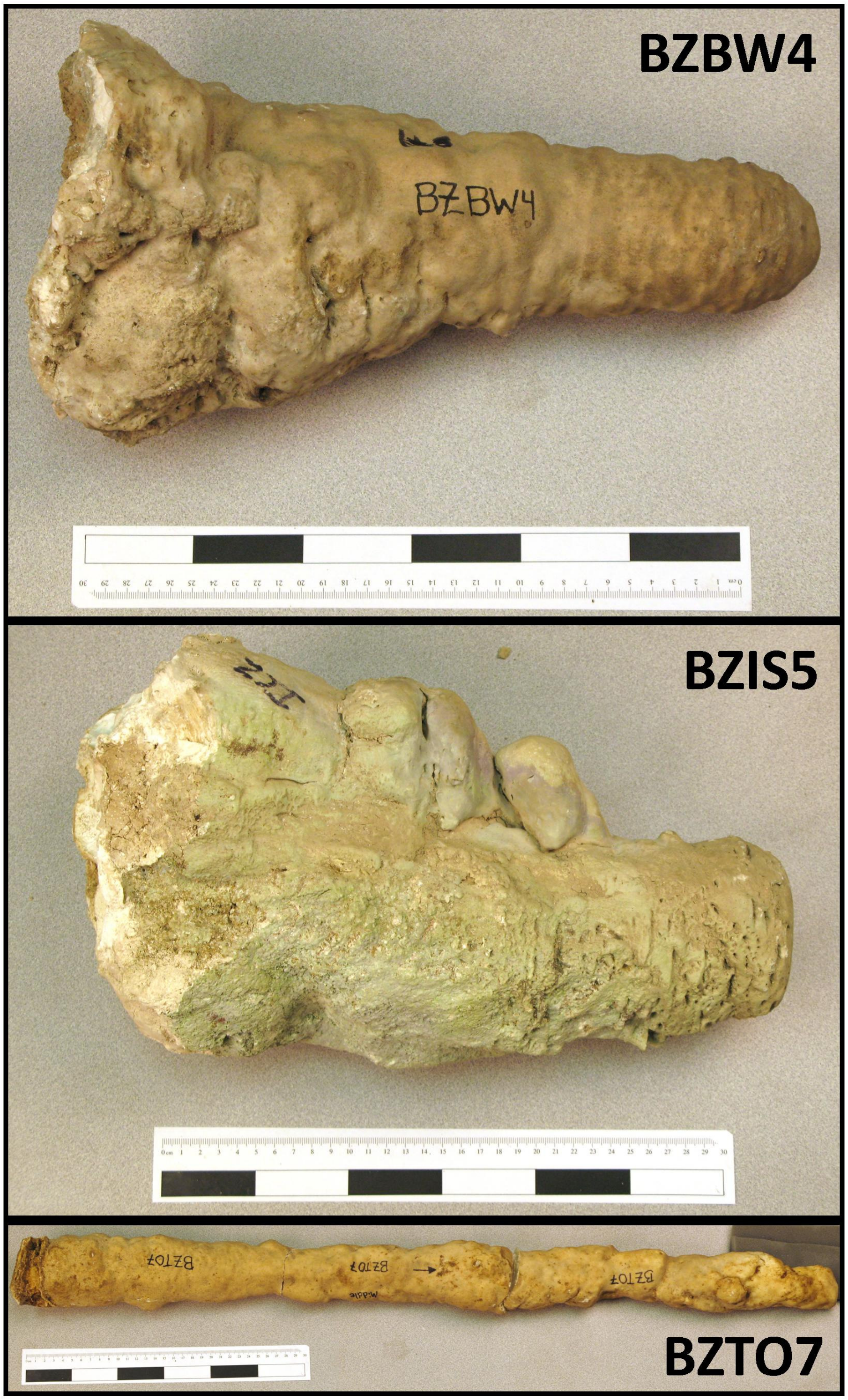

Figure 5.9. The other three stalagmites collected with 30 cm ruler for size comparison. BZBW4 was collected in Bega Two cave, BZIS5 was collected in Isabella cave, and BZTO7 was collected in Three Olla cave.

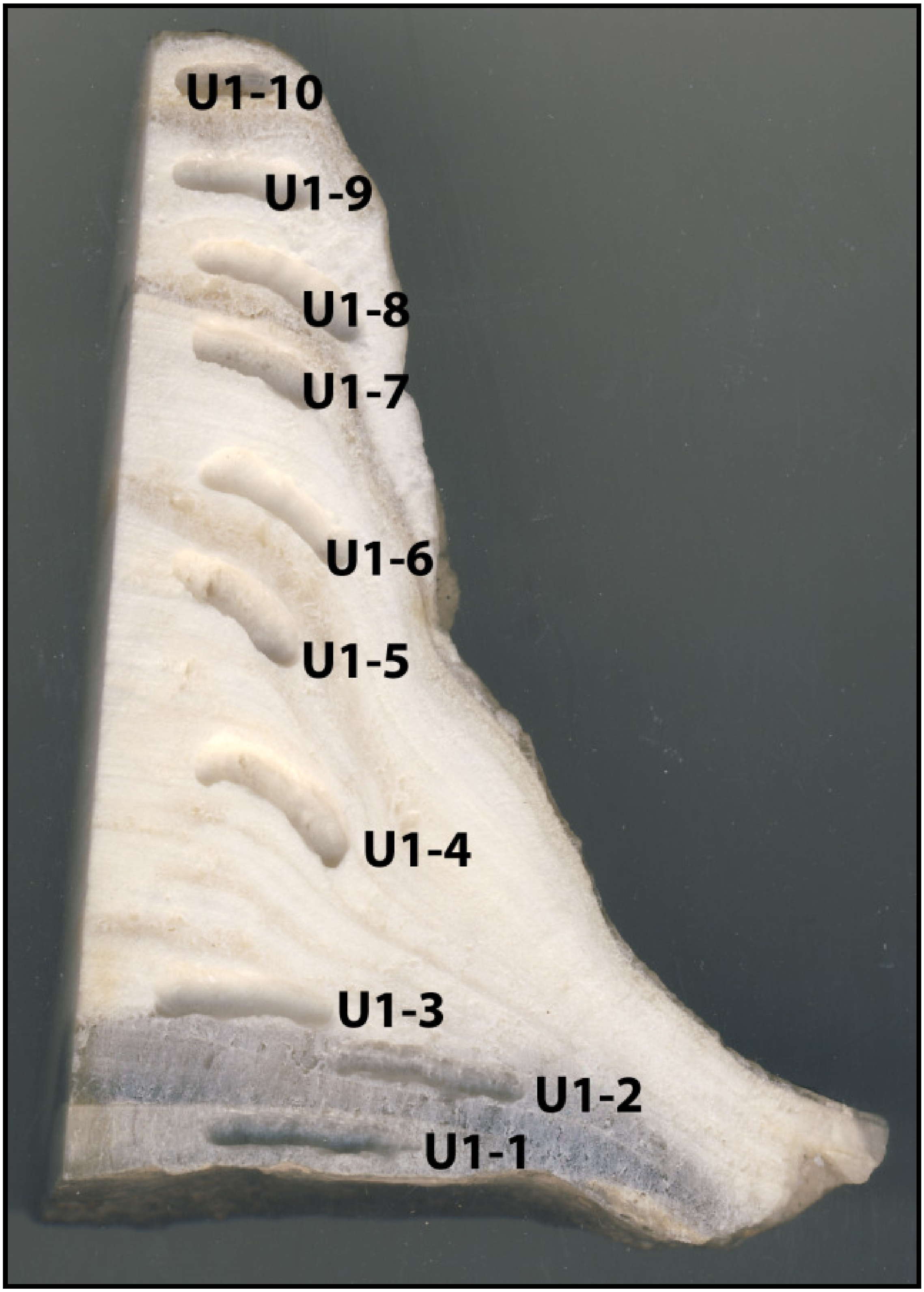

Figure 5.10. Locations of samples drilled for uranium-series dating on BZBT1.

Figure 5.11. Dental drill setup used to drill samples for uranium-series and radiocarbon dating.

however, that old carbon input has remained a constant rate over the growth life of the stalagmite.

Twelve calcium carbonate samples were drilled from BZBT1 for radiocarbon dating, with nine eventually sent for dating at the University of Georgia's Center for Applied Isotope Studies (CAIS). The sample sites were roughly located at the same interval as the prior uranium-series sample sites (Table 5.3). Sample RC1-10 was taken on the outer top layer of BZBT1, and should be a modern deposit. Approximately 20 mg of sample was drilled with a dental drill for analysis. A calcium carbonate sample was drilled from each of the five soda straws collected. Due to the relatively quick growth and transient nature of soda straws, the soda straw samples were to be used as a modern carbonate reference for their respective stalagmite or cave. At CAIS, the carbonate samples were reacted with 100% H_3PO_4 at 75°C for 1 hour to recover carbon dioxide. The resulting carbon dioxide was cryogenically purified from the other reaction products and catalytically converted to graphite using the method of described by Vogel et al. (Vogel et al., 1984). Graphite $^{14}C/^{13}C$ ratios were measured using the CAIS 0.5 MeV accelerator mass spectrometer. The sample ratios were compared to the ratio measured from the Oxalic Acid I (NBS SRM 4990). The sample $^{13}C/^{12}C$ ratios were measured separately using a stable isotope ratio mass spectrometer and expressed as $\delta^{13}C$ with respect to PDB, with an error of less than 0.1‰.

A second method of avoiding the old carbon issue is to date only organic carbon. In order to successfully obtain a radiocarbon date this way, the stalagmite must have trapped some organic material at some point during its growth. This organic material can then be extracted by dissolving the calcium carbonate matrix. Some stalagmites, such as BZBO3, appeared to have distinct sediment layers that might contain organic material. In contrast, other stalagmites, such as BZBT1, have no obvious layers that might contain organic material.

Table 5.3. Locations on BZBT1 where samples were taken for radiocarbon dating of calcium carbonate.

Sample Code	Depth (mm)
RC1-0	92 (Absolute base)
RC1-1	88
RC1-2	80
RC1-3	78
RC1-4	57
RC1-5	38
RC1-6	33
RC1-7	21
RC1-8	17
RC1-9	8
RC1-11	3
RC1-10	0 (Absolute top)

Organic extraction requires relatively large samples (1-5 g). These samples were collected as whole pieces of the stalagmite and not as drilled powder (Figure 5.12). The organic extraction samples were collected by using a rock saw to both obtain the desired region and remove any excess material. The spare pieces of stalagmite remaining after thin section preparation were the source for the organic extraction samples.

For BZBT1, four sites were originally chosen for organic extraction. Two sites were adjoining layers at the very base of the stalagmite, where sandy sediment was noted. A third site was from the 2DK zone, where no obvious sediment was observed. This site was selected partly to determine whether any recoverable amounts of organic material could be extracted from non-boundary regions. The fourth site was the 8DK zone and its boundaries with 7LT and 9LT. The 8DK layer showed some of the most interesting preliminary visual data and was a focus of much of the research. This layer did not appear to have any obvious sediment or organic material present to the naked eye, so this sample was also testing whether boundary layers could provide successful organics dates. Each of the organic extraction samples had a

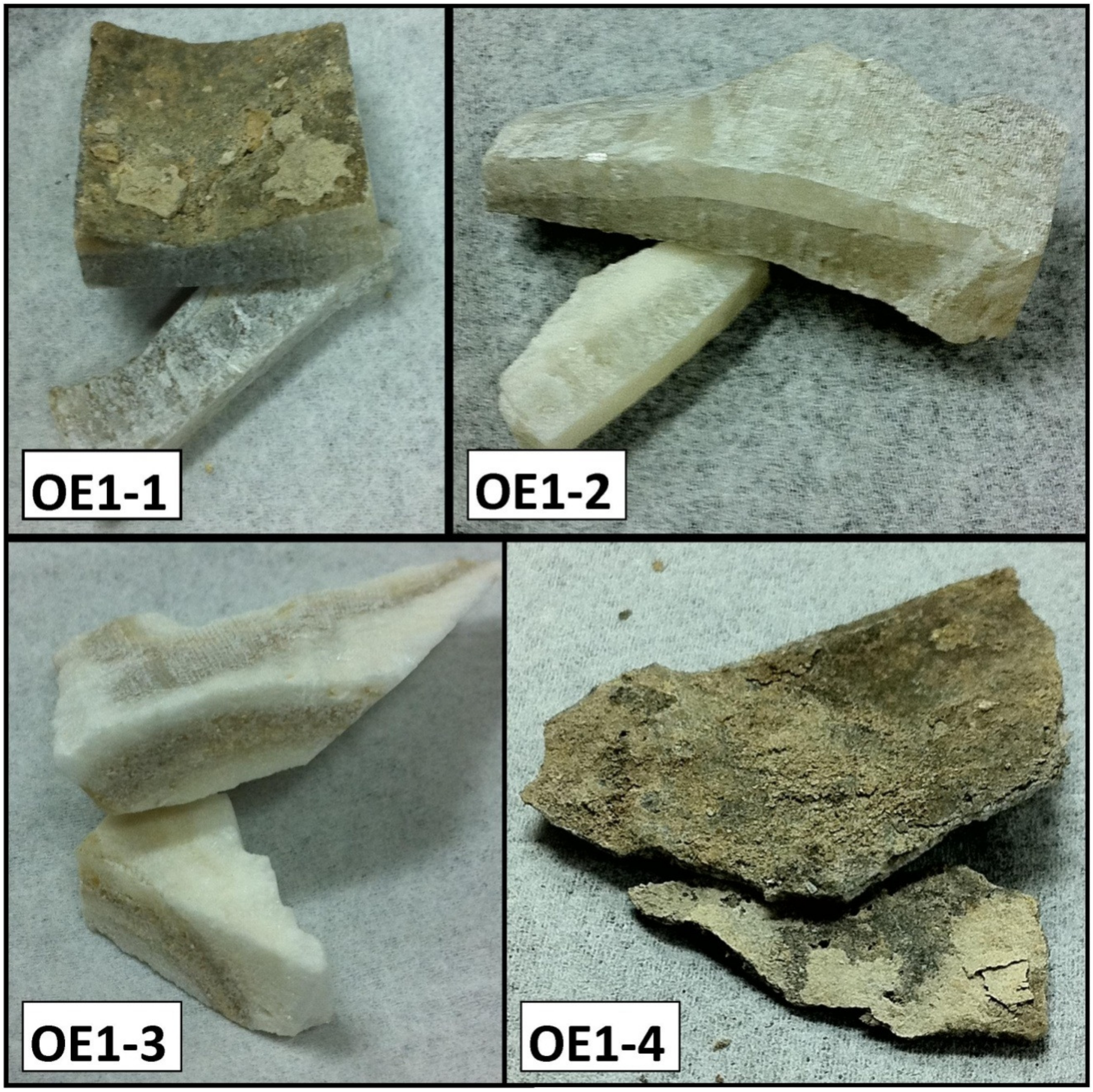

Figure 5.12. Samples taken from BZBT1 for organic extraction. Samples were sawn as whole pieces for processing, not drilled for a powder.

corresponding calcium carbonate radiocarbon sample; successful organic dates could then be used to help determine the old carbon input in the calcium carbonate samples.

After three of the organic samples were dated successfully (the two deepest and the 8DK samples), five additional sites on BZBT1 were chosen for sampling. One site was located in the uppermost light zone (11LT) where a slightly discolored chalky appearance was hopefully indicative of organic material. The other five samples were taken from locations between the base samples and the 8DK zone: one sample contained 4DK and its boundaries with 3LT and 4LT, a second sample contained 6DK and its boundaries with 5LT and 7LT, the third sample was taken from a layer within 5LT with visible detritus, and finally one sample was taken from the 11DK-12DK boundary. The 11DK-12DK boundary and visible detritus samples produced dates. The discolored chalky sample produced organic material, but not enough for dating, while the last two samples produced no organics. Unfortunately, no additional sample of the chalky zone existed and a date could not be produced from the upper region.

Once at CAIS, the stalagmite pieces were treated with HCl to remove carbonates at room temperature. The samples were then heated in acid conditions for 1 hour at 80°C. After that, the samples were washed with deionized water and dried at 60°C. For accelerator mass spectrometry analysis the cleaned organic sample was combusted at 900°C in evacuated / sealed ampoules in the presence of CuO. The carbon dioxide produced was then dated in the same method as the carbonate samples' carbon dioxide.

Visual

The remaining five stalagmites were imaged both in natural light and in ultraviolet light. For the natural light imaging, stalagmite halves were polished slightly and scanned in color at 1200 dpi on a Canon CanoScan 4400F. For the ultraviolet imaging, stalagmite halves were taken to a dark film-developing room and photographed with a Nikon D300 digital camera under handheld black lighting. An ultraviolet lens filter was placed on the camera to remove reflected ultraviolet light coming from the stalagmite. Using ArcMap and ERDAS Imagine software, seven transects were drawn down the central core of the stalagmites. All transects were parallel and roughly one pixel apart in the UV-stimulated luminescence images and four pixels apart in the scanned images (due to the higher resolution in the scanned images). Changes in color pixel value for red, green, and blue channels were recorded with ERDAS Imagine software over the length of the stalagmite. Data values from all seven transects were averaged together to produce a more representative record than a line of single pixels. The reflectance and UV-stimulated luminescence images were then converted to grayscale and contrast-enhanced in Photoshop. The grayscale images were then analyzed in the same manner as in the color images, aside from recording changes in grayscale pixel value rather than color channels.

Under natural light, BZBT1 shows a clear pattern of alternating dark and light zones. These zones were often used as reference points during drilling and later analysis. The zones were numbered starting at the top of the stalagmite, and assigned a suffix indicating whether the zone is dark (DK) or light (LT) (Table 5.4). Dark zones in BZBT1 were not dark due to detritus, but rather were dense translucent calcite which absorbs incoming light. The light zones in BZBT1 were composed of thinner, less dense calcite crystals which reflect incoming light to appear nearly white. Several very thin layers of denser calcite would typically exist within each light zone. These very thin layers were not individually labeled as separate zones; however, if an isotope drill sample crossed a thin dense layer, its existence was recorded.

Table 5.4. Named zones on stalagmite BZBT1. Range is measured along the central core of the stalagmite and indicates the distance of the bottom and top of the zone from the stalagmite base.

Zone Name	Range on BZBT1 (Depth, mm)
1DK	0.0-1.0
2LT	1.0-5.0
3DK	5.0-7.0
4LT	7.0-19.0
5DK	19.0-20.5
6LT	20.5-35.0
7DK	35.0-38.0
8LT	38.0-70.5
9DK	70.5-73.0
10LT	73.0-79.5
11DK	79.5-86.0
12DK	86.0-92.0

Isotope Sampling

Samples for stable isotope analysis (^{13}C and ^{18}O) were drilled with a Mechantek EO MicroMill (Figure 5.13). Each isotope sample contained 55-100 µg of calcium carbonate powder. Prior to drilling of the actual samples, a spare piece of the stalagmite would be experimentally drilled in order to determine what depth and length of the sampling path would produce the correct amount of powder. Samples were drilled at an interval of 500 µm with an HP-2 drill bit; at this interval, each sample path would slightly overlap and produce a continuous isotope record (Figure 5.14). Sampling paths were plotted though the associated MEO MicroMill System software. Once the paths were plotted, a surface profile of each path was measured for precise drilling. At the time of surface profiling, notes were taken about which layer a sample was located in, whether the sample fell on a boundary, and any other pertinent information. Each sample would then be drilled singly.

Figure 5.13. Micromill drilling apparatus (left) and attached computer (right) used for stable isotope and trace element sampling.

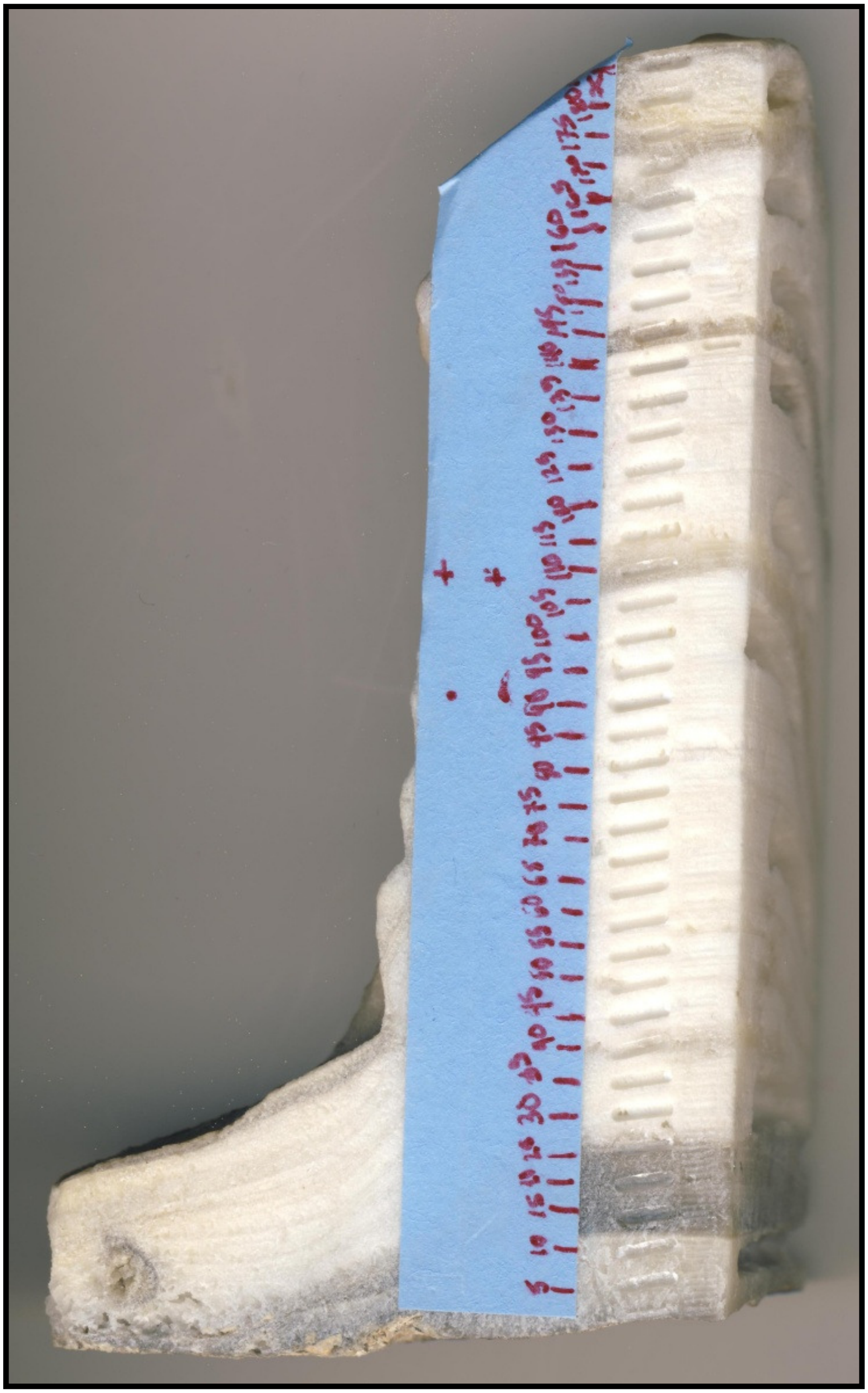

Figure 5.14. Stable isotope and trace element sample sites on BZBT1. The clearly visible troughs to the right of the blue tape are the trace element sample sites. Samples for stable isotope testing were taken in a continuous swath between the trace element sample sites and the edge. Numbers on the blue tape indicate the location of that particular isotope sample.

Drilled powder was collected onto wax weighing paper with a razor blade. The samples were weighed on a Mettler Toledo UMX2 balance and placed in a labeled vial. A modified vacuum cleaner was used to remove remaining powder from the stalagmite, drill bit, and work area. Compressed air was then blown on the stalagmite to remove any powder left by the vacuum cleaner. After cleaning the razor blade with Kimwipes, the next sample was drilled. Samples were personally driven (to avoid shaking the vials and spreading the powder over the vial surfaces during shipping) to the Alabama Stable Isotope Laboratory (Department of Geological Sciences, University of Alabama-Tuscaloosa) for analysis with a Gasbench II and a Delta Plus Isotope Ratio Mass Spectrometer using methods described by Lambert and Aharon (Lambert and Aharon, 2011).

For BZBT1, sampling paths for isotopes were typically ~2000 µm long and ~70-90 µm deep, with a drill speed of 70%. Depth was increased in regions of less dense calcium carbonate, to a maximum of 120 µm for five samples (BT1-84 to BT1-88). A total of 188 unique isotope samples were taken, representing the full growth of BZBT1. A Hendy test was not performed for several reasons. First, BZBT1 was collected from a rather shallow cave and almost certainly was not deposited under equilibrium conditions. As paleotemperature reconstruction was not an aim of this research, absolute isotope ratio values were not as important as the variation within the values. As previously mentioned, determining and sampling single growth layers is often difficult, especially with a stalagmite as small as BZBT1. Finally, the disequilibrium due to evaporation should enhance the variation present in the isotope ratio values.

Two isotope samples were taken from each of the five soda straws using the micromill as described previously. Sampling paths were ~3000 µm long and took two passes of 150 µm for a total of 300 µm deep, with a drill speed of 70%. The sampling paths were longer and deeper than those used in BZBT1 due to the low density of the soda straws' calcium carbonate and the curved drilling surface.

The water samples collected in Belize were also analyzed for stable isotopes, but were analyzed at the Center for Applied Isotope Studies at the University of Georgia, rather than at the University of Alabama.

Trace Element Sampling

Trace element samples were drilled from the stalagmites with the Mechantek EO MicroMill used for isotope sampling. Each trace element sample contained ~3 mg of drilled calcium carbonate powder measured on the Mettler Toledo UMX2 balance. As with the isotope drilling, length and depth of the sampling path were determined on a spare piece of the stalagmite. Samples were drilled at an interval of 2500 µm; this did not produce a continuous record, but a continuous trace element record was not considered necessary for this research (Figure 5.13). Aside from the interval difference, the method for trace element drilling was the same as the isotope drilling described above.

For BZBT1, sampling paths for trace elements were typically ~3500 µm long and had 5 passes of 150 µm for a total depth of 750 µm. Some denser layers only required 4 passes, while some more porous layers needed 6 passes. A total of 39 trace element samples were taken, representing the full growth of BZBT1. Trace element samples were also taken from the five soda straws. These samples were drilled with a dental drill, and their ~3 mg of drilled calcium carbonate powder was weighed out on a Mettler H10 balance. Eleven samples were taken: two from each soda straw, with three samples taken from SStr5.

After the powder was placed in a clean labeled vial, 3.0 mL of dilute HCl (5%·37%, 0.6N) was added to each sample. The sample solutions and some blanks of the dilute HCl were taken to the Chemical Analysis Lab at the University of Georgia for a 20 element ICP analysis. Water samples collected in Belize were also sent directly to the Chemical Analysis Laboratory for 20 element analysis without any chemical preparation. This analysis was performed on a Thermo Jarrell Ash Enviro 36 ICP Simultaneous Optical Emission Spectrograph. Once results were returned, the average element concentration from the dilute HCl was subtracted from the carbonate samples. Samples were also checked to determine whether their results were above the detection limits of the Thermo Jarrell Ash Enviro 36 ICP Simultaneous Optical Emission Spectrograph. Finally, the samples were standardized by assuming the calcium concentration was 40 wt%.

Thin Section Petrography

Thin section slides were created of each of the five stalagmites for microscopic analysis of their petrography. One quarter of each stalagmite was reserved for thin section production. This thin section quarter was sawn into pieces no greater than 60 mm long, 43 mm wide, and 10 mm thick (Figure 5.15). The top of each section was notched and the backside was labeled in the manner of “Stalagmite Code” – “# section from the top” (for example, BZBO2-8 is the eighth thin section from the top of BZBO2). The number of thin sections produced from a stalagmite depended on the overall size of the stalagmite (Table 5.5). The thin sections were sent to Quality Thin Sections, Tucson, AZ, for processing into 2” x 3” slides. Remnants of the thin section quarter not shipped to Quality Thin Sections were archived.

Finished slides were examined with a Leica DMLP microscope at magnifications of 2.5x, 4x, 10x, and 63x. Slides were examined for changes in crystal structure, visible detritus, evidence of layer erosion, and general layer dynamics. Images of select regions of the thin section slides were produced with Nikon Coolpix S3100 by taking the photograph though the

Figure 5.15. Two thin sections created from BZBT1 prior to slide preparation

right eyepiece. Photographs were then systematically taken of the entire BZBT1 thin section. These images were later joined into a large mosaic image using Adobe Photoshop (Figures 5.16 and 5.17). Images were color-matched, cropped, and rarely skewed, but otherwise unaltered. The resulting mosaic image was printed at large scale on a plotter, allowing for analysis of BZBT1's complete petrography at microscopic detail.

Table 5.5. The five stalagmites for which thin sections were created and the number of thin sections made from each.

Stalagmite	**Number of Thin Sections Created**
BZBT1	2
BZBO2	10
BZBO3	8
BZBW4	7
BZTO7	15

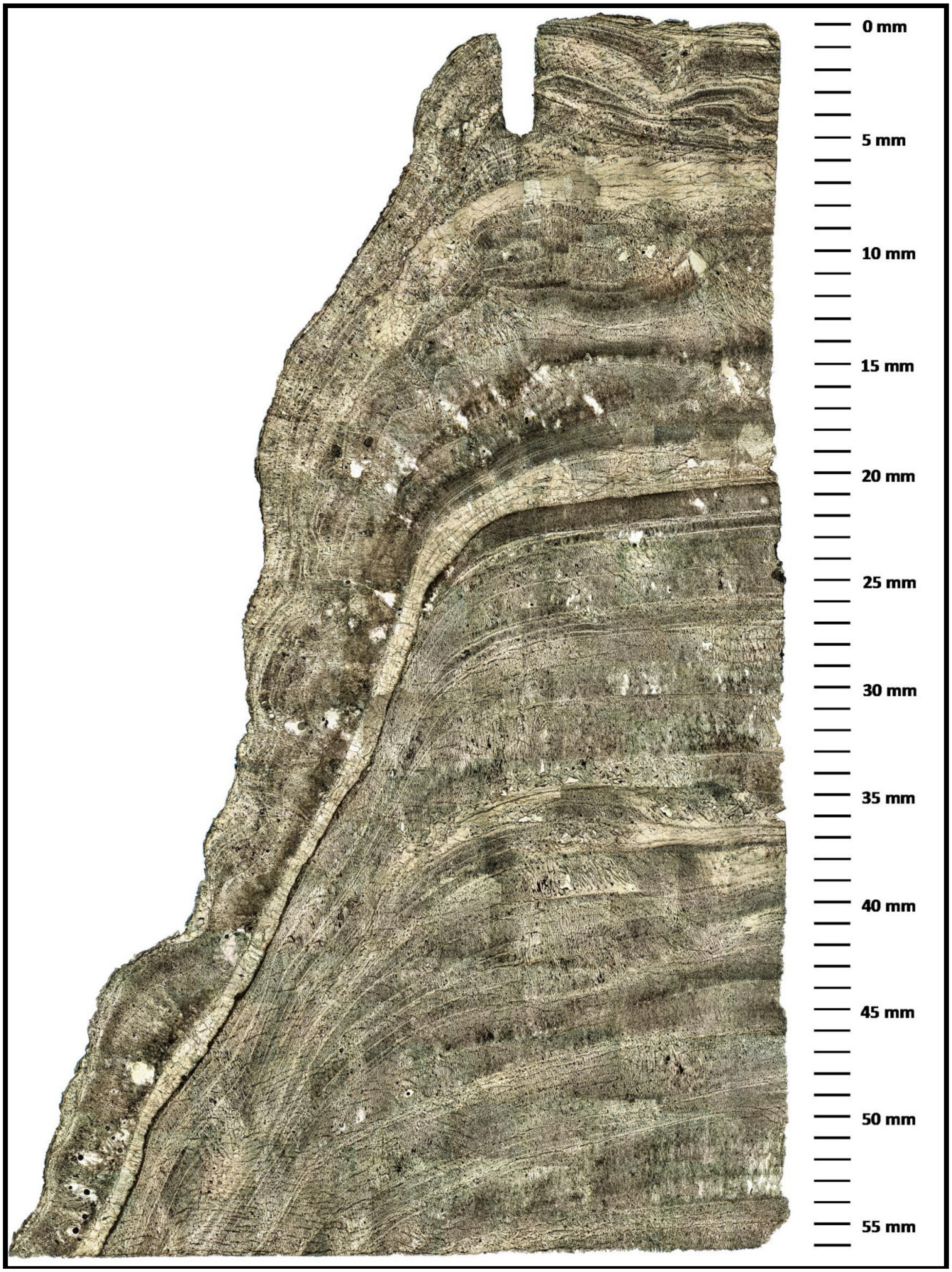

Figure 5.16. Mosaic image of the top thin section of BZBT1 with depth measurements at right.

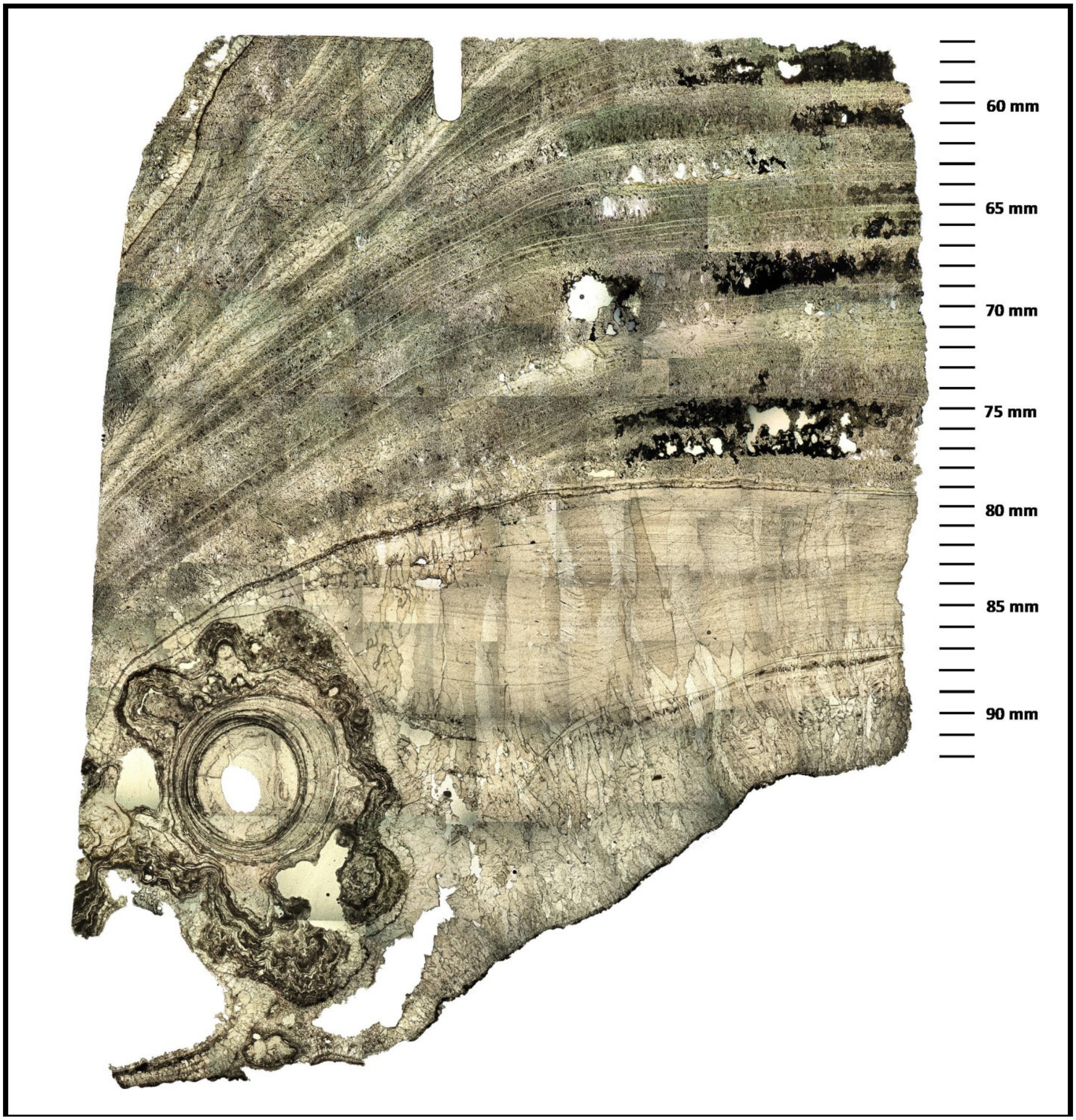

Figure 5.17. Mosaic image of the bottom thin section of BZBT1 with depth measurements at right.

CHAPTER 6
RESULTS

Stalagmite Selection

Initially, all five stalagmites were being processed and analyzed equally until a clearly superior stalagmite or stalagmites would become apparent. In the end, BZBT1 was chosen for the greatest level of analysis for several reasons. First, BZBT1 had the simplest inner structure with clear smooth layering as opposed to the indistinct or coralloid layering noted in the other stalagmites. The small size of BZBT1 allowed for a complete high-resolution record to be completed within a reasonable time. BZBT1 also produced one of the clearest chronologies initially, and this chronology was refined with later testing. Another stalagmite BZBO3 produced a radiocarbon age from organics that dated to 14037 cal yr BP. Although further analysis will be performed on BZBO3, it is beyond the scope of this thesis, and the following results and discussions will be primarily devoted to BZBT1.

Dating

Uranium-series Dating

Results from the uranium-series dating came back inconclusive. Initial uranium concentrations in all five stalagmites were extremely low (<50 ppb) (Table 6.1). At concentrations this low, thorium derived from uranium decay can be overshadowed by even slight amounts of detrital thorium or undetectable at young ages. As a result, ages calculated from these uranium and thorium concentrations have large error terms and often a nonlinear relationship with depth of the sampling location.

Nine samples were dated for BZBT1 (Table 6.2, Figure 6.1). Three of these samples were removed for being outliers: U1-1, U1-5B, and U1-9. The remaining six samples produced a somewhat linear relationship (Figure 6.1), and were used for comparison with the radiocarbon dates. These ages range from 1876±376 yr BP at 81 mm deep to 1065±203 yr BP at 17 mm deep.

High levels of ^{232}Th are commonly due to detritus being washed or blown onto the growing stalagmite, and samples showing these high ^{232}Th levels can be used to identify zones of increased detrital contamination. High levels (>235 ppt) of ^{232}Th are found at both the top and bottom of BZBT1, while the central region has lower values (<175 ppt).

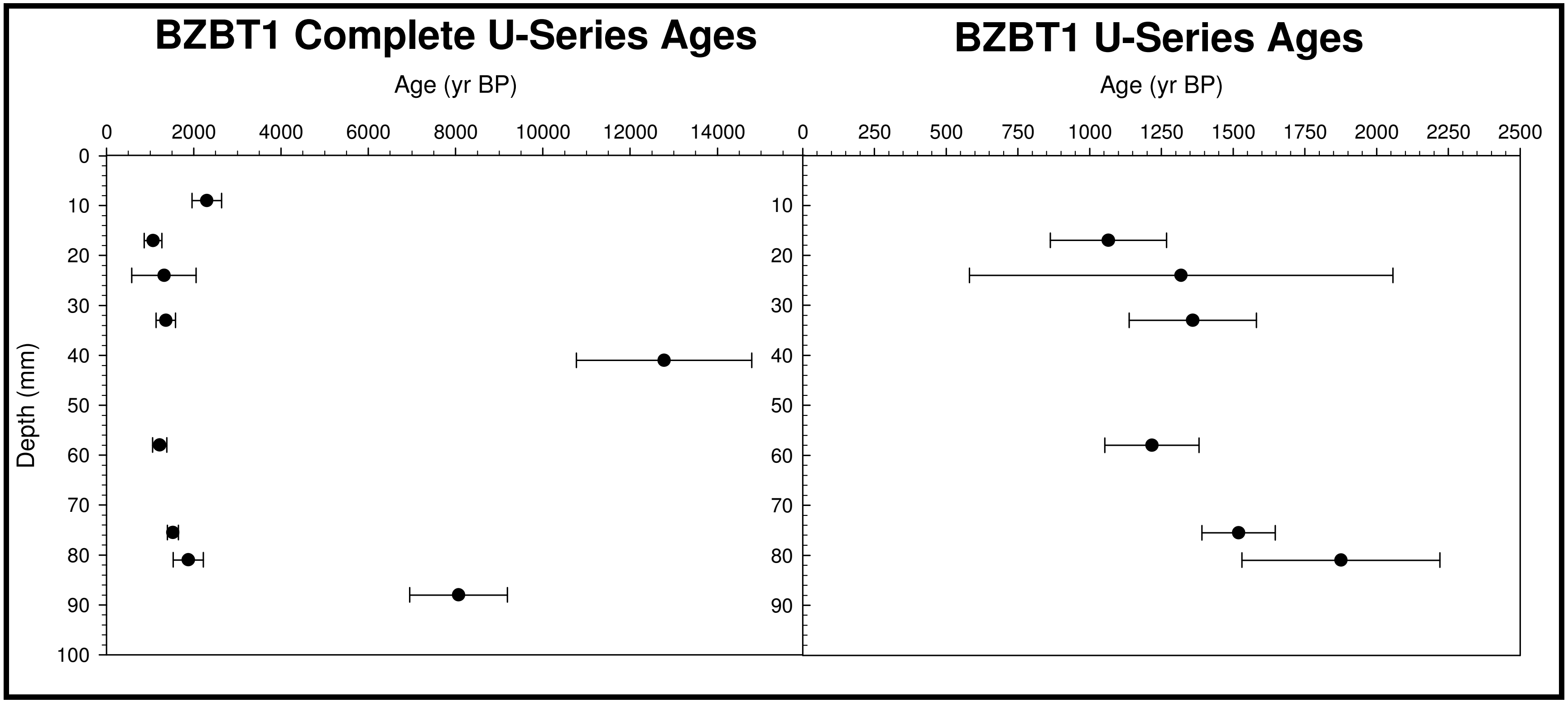

Figure 6.1. Left: All nine uranium-series age results from BZBT1, with error bars representing 95.4% confidence. Six ages are under 2000 years, while the remaining three ages range from 2298 to 12779 years. Right: The six ages under 2000 years old are plotted separately, showing a generally linear trend of ages increasing with depth. The trend reverses from 33 mm to 58 mm and combined with rather large error terms produces a chronology that is informative, but unreliable

Table 6.1. Data from during uranium-series dating for five Belizean stalagmites. Final ages are shown in the final column and in red. Samples labeled with a “B” were samples that were redrilled due to destruction of the original samples from lab error.

Sample	^{238}U (ppb)		^{232}Th (ppt)		$^{230}Th/^{232}Th$ (atomic x10^{-6})		$\delta^{234}U$ (measured)		$^{230}Th/^{238}U$ (activity)		^{230}Th Age (yr) (uncorrected)		$\delta^{234}U_{Initial}$ (corrected)		^{230}Th Age (yr BP) (corrected)	
U1-1	5.2	±0.0	672	±13	27	±1	1456.6	±12.6	0.2096	±0.0069	9642	±333	1490	±14	**8067**	**±1121**
U1-2	6.0	±0.0	235	±5	23	±1	1511.2	±19.0	0.0545	±0.0030	2387	±132	1520	±19	**1876**	**±345**
U1-3	44.1	±0.1	609	±12	49	±2	1610.7	±12.4	0.0412	±0.0016	1734	±67	1618	±12	**1519**	**±128**
U1-4	4.5	±0.0	66	±2	37	±3	1481.9	±8.2	0.0328	±0.0025	1451	±110	1487	±8	**1217**	**±164**
U1-5B	3.6	±0.0	175	±15	83	±13	1103.2	±17.8	0.2475	±0.0341	13508	±1963	1144	±20	**12779**	**±2009**
U1-6	3.8	±0.0	64	±2	33	±3	1236.5	±11.7	0.0334	±0.0032	1640	±159	1242	±12	**1359**	**±222**
U1-7	4.8	±0.0	385	±8	10	±1	1298.4	±11.6	0.0503	±0.0026	2408	±127	1303	±12	**1319**	**±738**
U1-8	46.7	±0.1	1090	±22	23	±1	1541.3	±14.5	0.0323	±0.0017	1393	±74	1546	±15	**1065**	**±203**
U1-9	49.1	±0.1	514	±10	91	±12	1575.9	±11.3	0.0580	±0.0076	2477	±326	1586	±11	**2298**	**±336**
U2-1B	9.4	±0.0	141	±3	2715	±57	3599.8	±11.6	2.4744	±0.0081	75290	±411	4451	±15	**75150**	**±415**
U2-2	2.1	±0.0	18	±1	305	±24	5658.8	±64.6	0.1557	±0.0083	2572	±141	5699	±65	**2476**	**±143**
U2-3	2.7	±0.0	23	±1	298	±16	5573.2	±32.8	0.1571	±0.0057	2630	±97	5614	±33	**2531**	**±101**
U2-4	3.2	±0.0	152	±3	49.4	±2.4	5812.1	±29.0	0.1446	±0.0064	2333	±105	5847	±29	**2068**	**±179**
U2-5B	3.3	±0.0	729	±15	15	±1	5234.2	±24.1	0.2076	±0.0088	3676	±158	5273	±27	**2576**	**±753**
U2-6	2.3	±0.0	177	±4	33	±2	5134.0	±37.7	0.1561	±0.0076	2801	±139	5169	±38	**2374**	**±294**
U2-7	2.5	±0.0	106	±2	82	±4	4908.8	±34.2	0.2092	±0.0083	3912	±159	4960	±35	**3646**	**±215**
U2-8	2.2	±0.0	287	±6	21	±1	5077.8	±35.7	0.1660	±0.0090	3009	±167	5112	±37	**2322**	**±473**
U2-9	2.1	±0.0	173	±4	31	±2	4835.2	±35.6	0.1587	±0.0091	2997	±175	4871	±36	**2521**	**±342**
U2-10	3.6	±0.0	28	±1	204	±9	4860.9	±21.9	0.0979	±0.0034	1833	±64	4886	±22	**1734**	**±70**

U3-2	6.0	±0.0	60	±1	4230	±103	1613.3	±12.7	2.5949	±0.0108	214777	±3446	2957	±37	**214642**	**±3447**
U3-4	8.6	±0.0	28	±1	16032	±488	2066.4	±7.6	3.1341	±0.0104	223541	±2317	3883	±29	**223462**	**±2319**
U3-5B	6.0	±0.0	40	±1	8608	±226	2439.1	±8.4	3.5044	±0.0120	217920	±2195	4511	±32	**217824**	**±2198**
U3-6	2.7	±0.0	476	±10	21	±1	6028.4	±28.7	0.2210	±0.0067	3469	±108	6075	±30	**2682**	**±526**
U3-7	3.3	±0.0	86	±2	113	±3	6091.5	±19.0	0.1805	±0.0039	2801	±61	6138	±19	**2634**	**±98**
U3-8	4.1	±0.0	35	±1	207	±7	6288.4	±16.7	0.1061	±0.0025	1595	±38	6316	±17	**1502**	**±45**
U3-9	2.0	±0.0	59	±1	90	±4	5937.4	±29.2	0.1627	±0.0071	2579	±114	5979	±29	**2394**	**±144**
U4-1	2.2	±0.0	412	±41	11	±1	1590.4	±31.3	0.1286	±0.0071	5526	±319	1606	±32	**3339**	**±1552**
U4-9B	1.3	±0.0	134	±4	20	±2	1556.4	±25.7	0.1217	±0.0089	5293	±398	1575	±26	**4094**	**±896**
U7-2	39.6	±0.1	1228	±25	17	±0	144.1	±2.5	0.0322	±0.0005	3107	±52	145	±2	**2256**	**±561**
U7-3	31.8	±0.1	329	±7	28	±2	145.8	±4.2	0.0179	±0.0010	1712	±100	146	±4	**1388**	**±211**
U7-4	35.9	±0.1	425	±9	24	±1	175.7	±5.4	0.0175	±0.0007	1634	±65	176	±5	**1280**	**±217**
U7-5B	34.7	±0.1	298	±6	29	±1	187.8	±3.1	0.0149	±0.0006	1376	±57	188	±3	**1105**	**±159**
U7-6	30.4	±0.1	236	±5	30	±2	190.9	±4.3	0.0140	±0.0008	1285	±73	191	±4	**1034**	**±153**
U7-7	28.0	±0.1	133	±3	40	±2	203.1	±4.4	0.0115	±0.0005	1049	±45	204	±4	**874**	**±92**
U7-8	43.3	±0.1	999	±20	14	±1	209.7	±4.4	0.0198	±0.0006	1801	±56	210	±4	**1185**	**±397**
U7-9B	13.8	±0.0	359	±7	14	±1	203.9	±5.1	0.0217	±0.0008	1983	±74	205	±5	**1292**	**±452**
U7-10	31.4	±0.1	419	±8	16	±1	182.8	±4.3	0.0130	±0.0004	1203	±39	183	±4	**813**	**±236**

Table 6.2. Uranium-series ages for BZBT1. Ages for samples U1-1, U1-5B, and U1-9 (italicized) were not used due to their excessively large ages relative to the other six samples.

Sample	Depth (mm)	^{230}Th Age (yr BP) corrected	
U1-1	*88*	*8067*	*±1121*
U1-2	81	1876	±345
U1-3	75.5	1519	±128
U1-4	58	1217	±164
U1-5B	*41*	*12779*	*±2009*
U1-6	33	1359	±222
U1-7	24	1319	±738
U1-8	17	1065	±203
U1-9	*9*	*2298*	*±336*

Radiocarbon Dating

Nine calcium carbonate samples from BZBT1 were dated by the AMS radiocarbon method (Table 6.3). These samples represented the full depth of BZBT1, with sample RC1-0 taken from the absolute base and RC1-10 taken from the absolute top surface. The other seven samples were either matched to locations where organics radiocarbon dating occurred or filled in gaps in the carbonate sampling intervals. Five samples chosen for organic extraction produced enough organic material for successful dating, while a sixth provided enough sample for a successful δ^{13}C value (Table 6.3).

The five organic ages produced a linear relationship aside from OE1-9 (Figure 6.2). Uncalibrated carbonate dates were older than the corresponding organics dates in all cases. This is expected from old carbon input from the limestone bedrock. The three deepest carbonate dates appear to occur on a different, younger trend line than the shallower samples. All three deepest samples were taken from the basal layers comprised of a calcite quite different than the rest of BZBT1. The difference in age between carbonates and organics was quite varied, ranging from 310 years in RC1-0 & OE1-1 to 840 years in RC1-4 & OE1-6. The

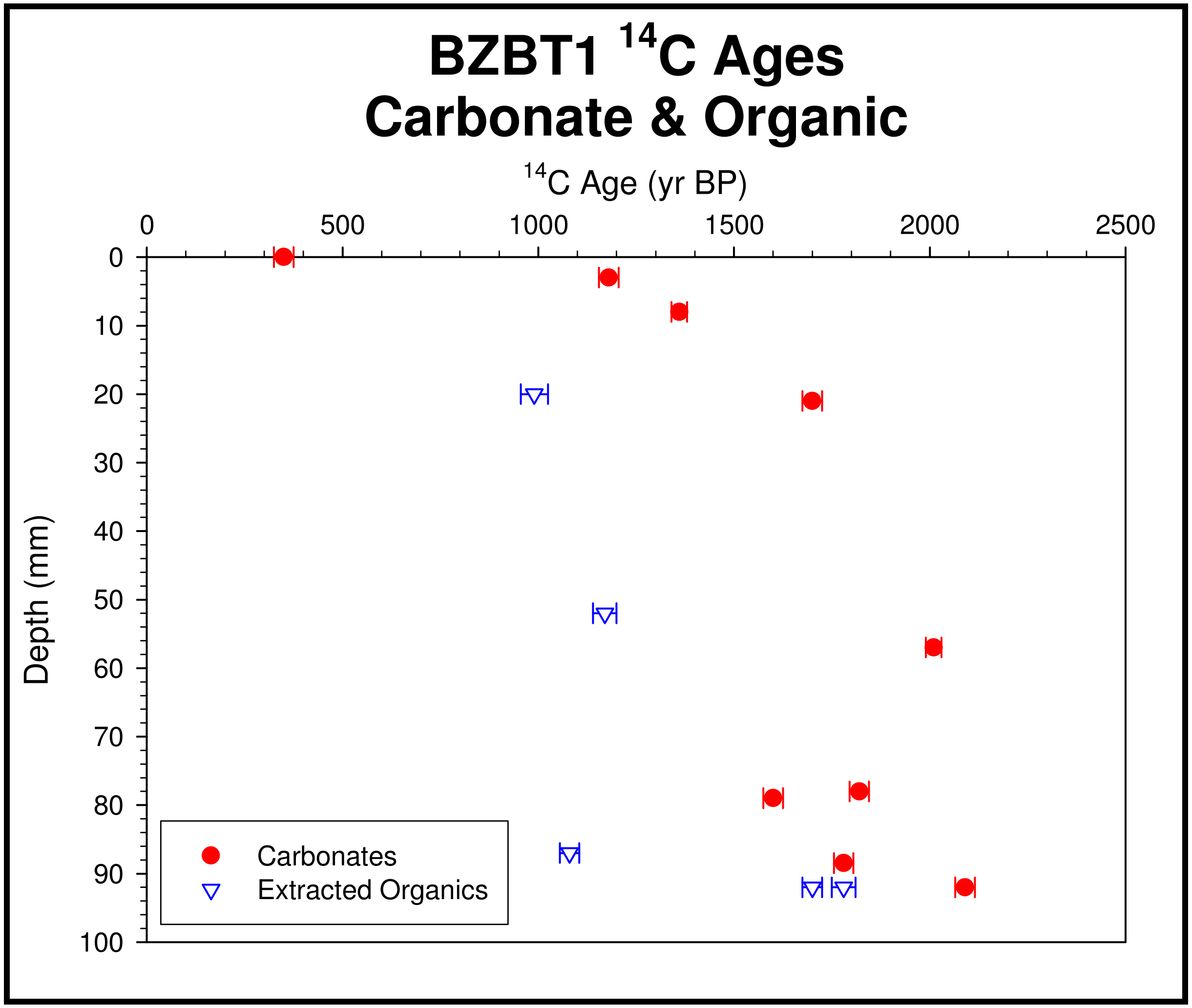

Figure 6.2. Each sample successfully dated by radiocarbon dating is plotted above, with error bars representing one standard deviation. Organic extraction produced five ages, while nine carbonate ages were produced.

unpaired carbonate samples had different relationships to the general organic age trend depending on their position: the deepest three samples were 300-400 years older than the trend, while shallower samples were 500-850 years older. Because of the variations in differences, a consistent correction factor for old carbon could not be determined.

Table 6.3. Radiocarbon dating data as received from the Center for Applied Isotope Studies, University of Georgia.

Sample ID	Depth (mm)	Material	$\delta^{13}C$ (‰V-PDB)	^{14}C age years Yr BP	±	pMC	±
RC1-10	0	carbonate	-2.6	350	25	95.71	0.28
RC1-11	3	carbonate	-8.0	1180	25	86.37	0.25
RC1-9	8	carbonate	-7.1	1360	20	84.40	0.22
RC1-7	21	carbonate	-7.8	1700	25	80.90	0.25
RC1-4	57	carbonate	-10.6	2010	20	77.86	0.22
RC1-3	78	carbonate	-10.1	1820	25	79.62	0.23
RC1-2	80	carbonate	-7.0	1600	25	81.09	0.25
RC1-1	88.5	carbonate	-8.8	1780	25	80.10	0.27
RC1-0	92	carbonate	-5.6	2090	25	77.12	0.25
OE1-3	20	organics	-23.0	990	35	88.41	0.37
OE1-6	52	organics	-21.5	1170	30	86.40	0.31
OE1-2	83	organics	-21.9	n/a		n/a	
OE1-9	87	organics	-24.9	1080	25	87.41	0.26
OE1-1	92	organics	-24.2	1780	30	80.15	0.29
OE1-4	92	organics	-24.9	1700	25	80.93	0.25

The radiocarbon ages appear to indicate relatively stable growth from the stalagmite's genesis until sometime after RC1-11. The young carbonate age of RC1-10 seems to indicate a modern deposit, but if BZBT1 grew continuously until present, its growth rate must have slowed radically during deposition of the top ~3 mm. If the growth rate did not slow, BZBT1 would have become inactive several centuries ago, and RC1-10 may be from carbonate deposited from nearby splashing water or recent reactivation.

The ages for extracted organic material were calibrated using Oxcal and CALIB14C with IntCal09, with ranges presented representing 95.4% certainty (Table 6.4). Carbonate samples were not calibrated, as the varying amounts of old carbon present would skew any calibration attempts.

Table 6.4. Calibrated radiocarbon dates of organic material extracted from sections of BZBT1. Dates calibrated by Oxcal and CALIB14C using IntCal09. All age ranges have a 95.4% confidence.

Sample	Depth (mm)	^{14}C Age Median (yr BP) calibrated	^{14}C Age Range (yr BP) calibrated
OE1-3	20	907	795-963
OE1-6	52	1094	984-1174
OE1-9	87	984	933-1055
OE1-4	92	1603	1540-1693
OE1-1	92	1703	1614-1814

Visual

The reflectance images of BZBT1 (Figure 6.3) had pixel values reported at an interval of 0.0206 mm, for a total of 4476 pixel values spanning the entire growth axis of the stalagmite. The color analysis revealed that all three color channels (blue, green, and red) followed the same pattern of variation, with correlations between the three colors ranging from 0.971-0.995. The grayscale pattern also correlated well with the three color channels (0.960-0.979), and the grayscale data were used in later analysis as representative of the scanned reflectance image. The grayscale reflectance transect clearly illustrates the 12 zones of alternating dark and light carbonate, along with several minor variations in color (Figure 6.4). Grayscale values for reflectance are listed in Appendix 1.

Pixel values in the UV-stimulated luminescence images of BZBT1 (Figure 6.3) are at an interval of 0.0624 mm, for a total of 1475 pixel values spanning the entire growth axis of the stalagmite. In contrast to the reflectance image, the color channels for the luminescence image did not follow identical patterns. The red and blue channels were often mirrored (correlation = -0.149), with a peak in the blue associated with a trough in the red. The green channel was typically somewhere between the blue and red channels, but tended to resemble the blue channel (correlation = 0.749) more than the red channel (correlation = 0.380). The luminescence produced by ultraviolet stimulation in a stalagmite is yellowish-green, so the green channel here is taken as the best representative of changes in luminescence. Fortunately, the grayscale image produced a pattern (Figure 6.5) that matched very well with the green channel (correlation = 0.959), and the grayscale data values were used in later analysis as representative of the UV-stimulated luminescence image.

UV-stimulated luminescence variations are highly irregular. Marked minimum values are centered at 0 mm and 19 mm, while the region from 70-92 mm fluctuates around a much lower average than the rest of the stalagmite. Low reflectance zones 1DK, 5DK, 11DK, and 12DK are also dark in the luminescence image, but 3DK, 7DK, and 9DK are not significantly different from typical variations along the stalagmite axis. Marked minima elsewhere in the luminescence plot (15, 43, 50, 58, 61, and 74 mm) are matched by peaks in the reflectance plot. Grayscale values for UV-stimulated luminescence are listed in Appendix 2.

Trace Elements

The concentrations of eight elements (Ba, Cd, Co, Cr, Mn, Mo, Ni, Sr) were never above analytical detection limits and so are not reported here. The average elemental concentrations from the four blank samples of HCl were subtracted from the remaining 12 elements' concentrations. Assuming calcium to be 40% by weight of the original calcium carbonate sample, all samples were standardized and converted from parts per million to weight percent. Four elements (B, Si, Na, Zn) had elemental concentrations fully explained by the average blank sample concentrations and so were not considered further. Previous experience with this particular ICP machine's results cast doubt upon the validity of any potassium results. This,

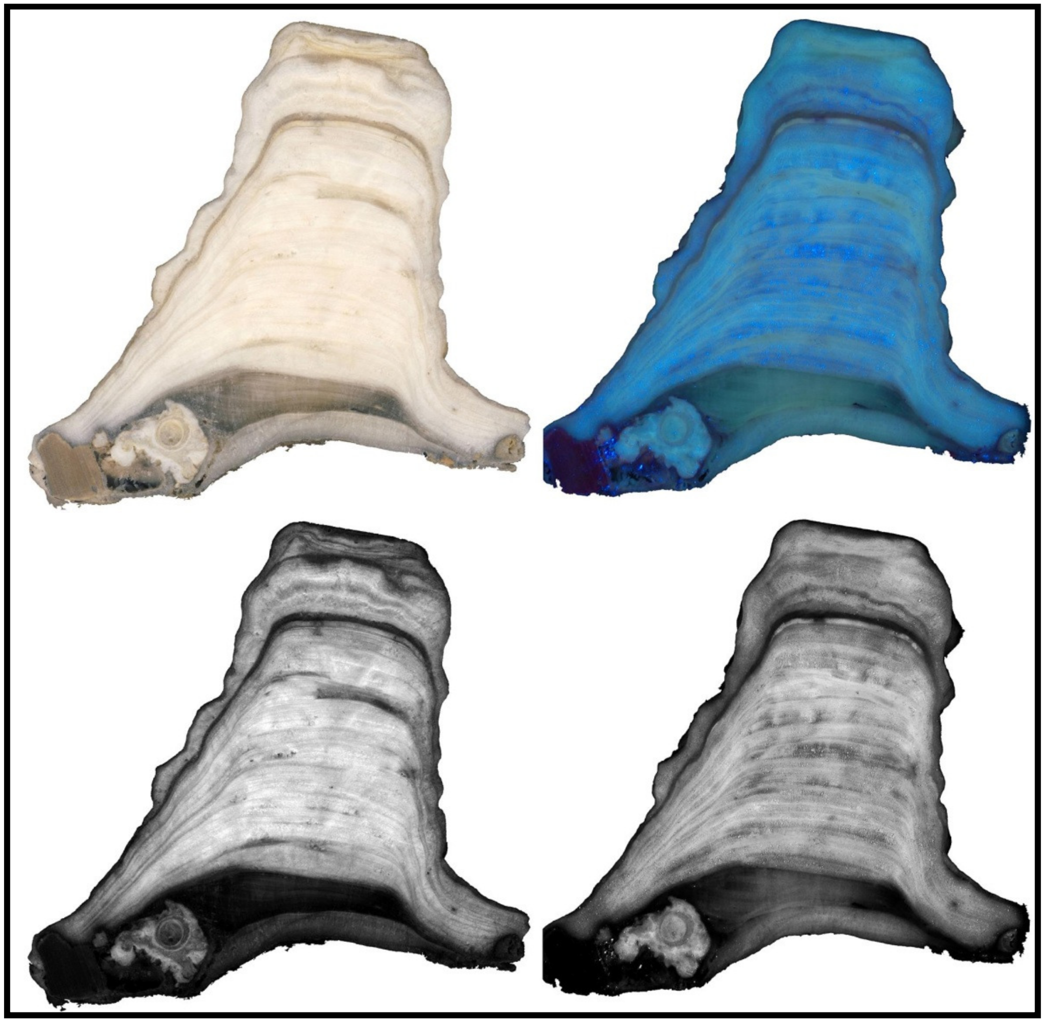

Figure 6.3. Top: True color images of BZBT1 reflectance (left) and ultraviolet-stimulated luminescence (right). Bottom: Grayscale images of BZBT1 reflectance (left) and ultraviolet-stimulated luminescence. Grayscale images have been contrast- and brightness-enhanced.

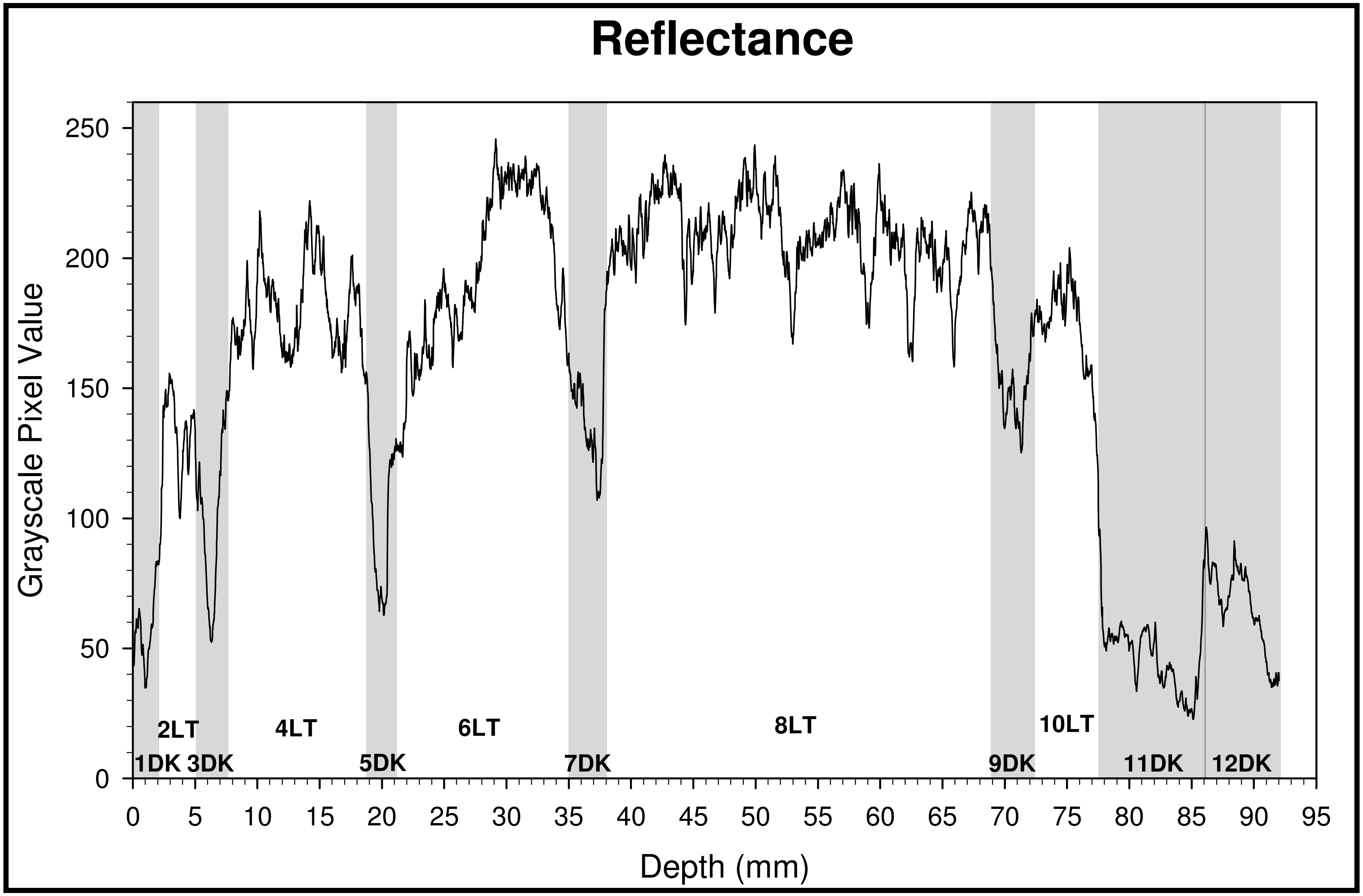

Figure 6.4. Variations in the grayscale pixel value of BZBT1's reflected light. Shaded zones are darker regions of BZBT1 and are composed of translucent dense calcite. The 12 naked eye-observed zones of BZBT1 are labeled along the bottom.

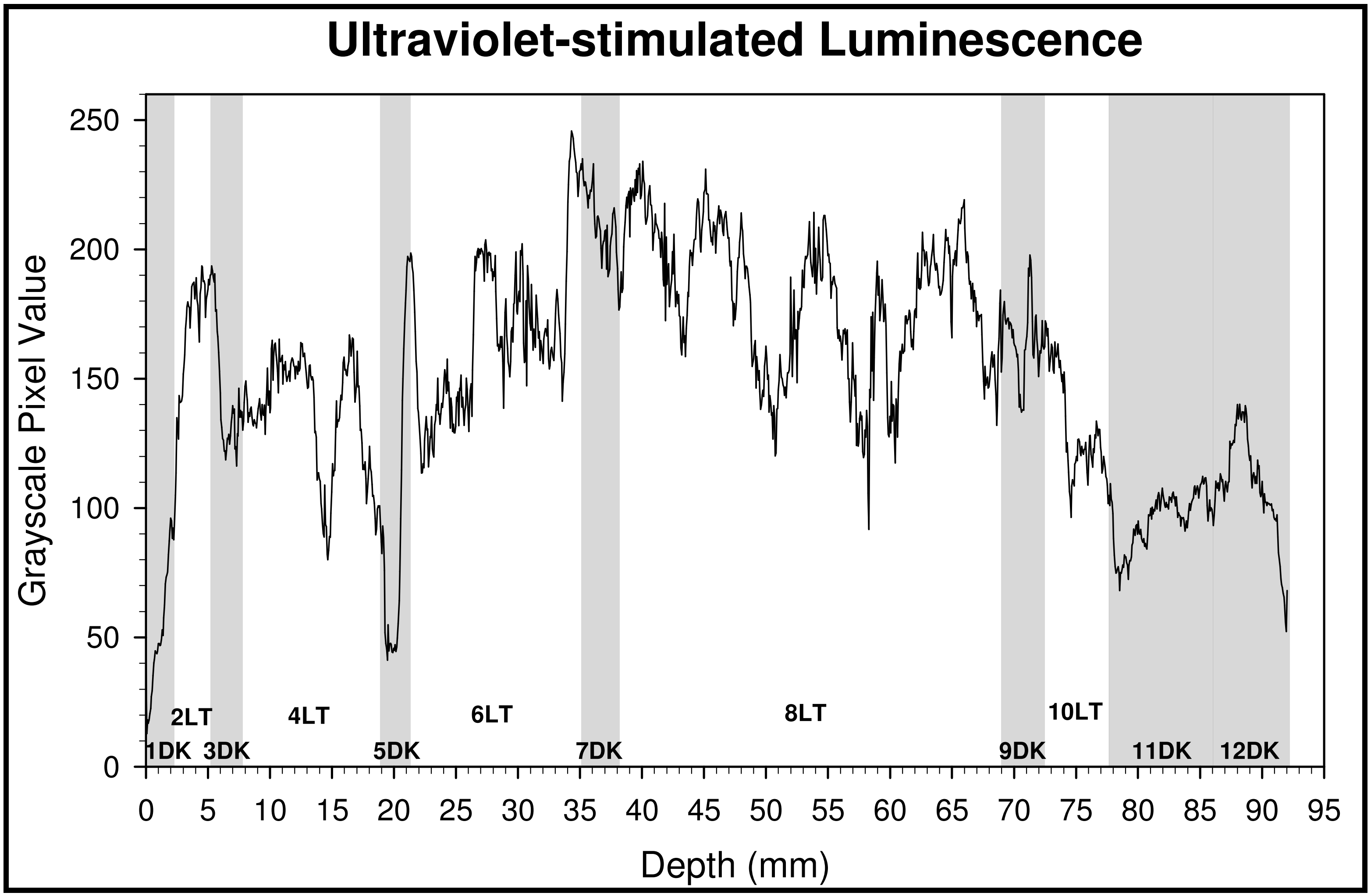

Figure 6.5. Variations in the grayscale pixel value of BZBT1 luminescence observed under ultraviolet light. Shaded zones are darker reflected light regions of BZBT1 and are translucent dense calcite. The 12 naked eye-observed zones of BZBT1 are labeled along the bottom.

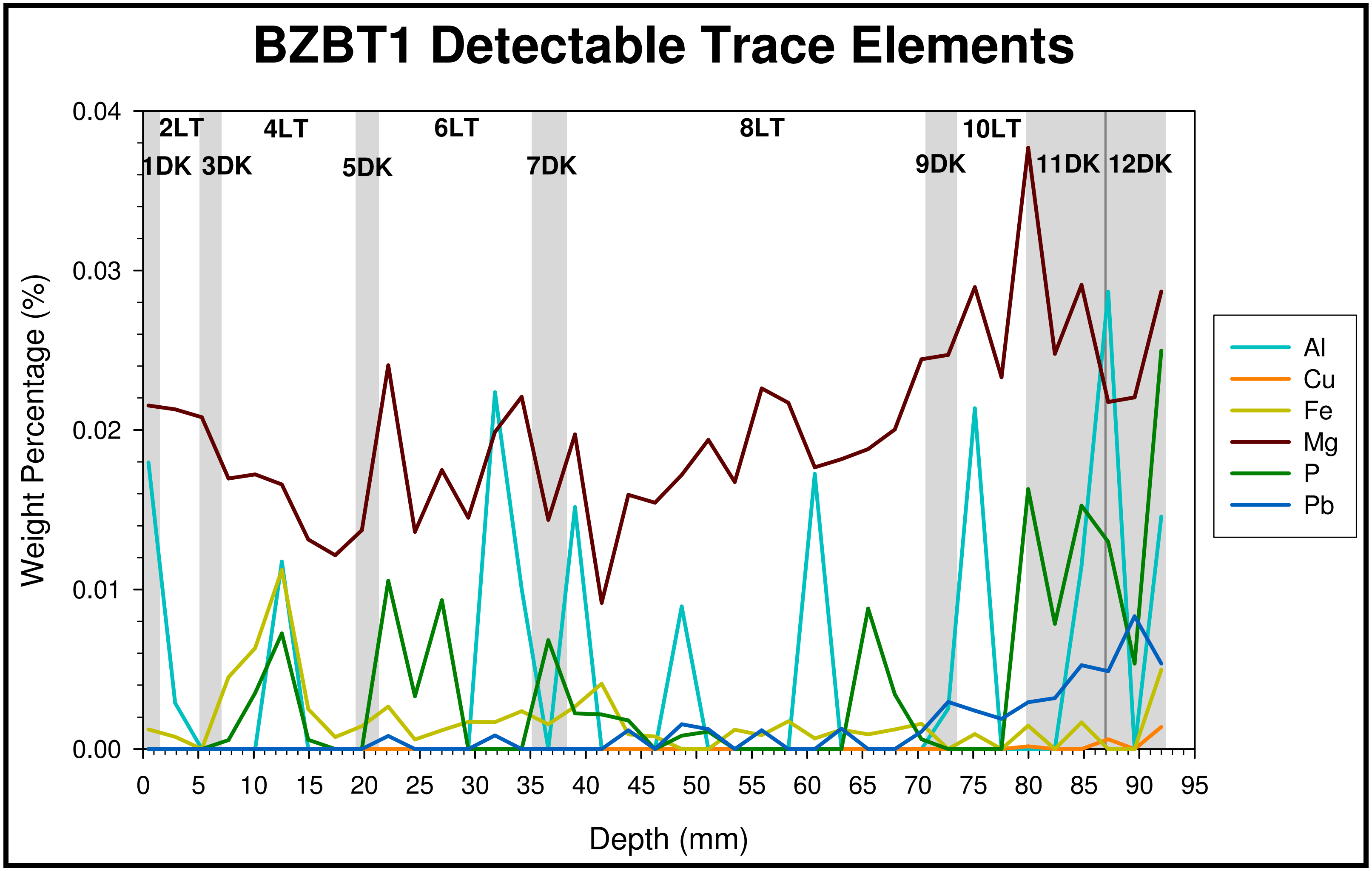

Figure 6.6. Results of trace element sampling in BZBT1. Trace elements are more common towards the base of the stalagmite and also from approximately 20-40 mm in depth. The 12 naked eye-observed zones of BZBT1 are labeled along the top.

along with the low concentrations of potassium reported, resulted in the potassium results being discarded. Excluding calcium, the remaining six elements were Al, Cu, Fe, Mg, P, and Pb. Only magnesium remained above detectable limits for all 39 sample sites (Figure 6.6). Magnesium is typically found as a trace element only in calcite and not in aragonite, providing evidence that BZBT1 is made solely of calcite. Copper was detectable in only three samples. Iron maintained a very low, yet detectable, concentration for most of the samples, while aluminum, phosphorus, and lead had relatively large spikes in concentration as well as samples where values of these elements were below detection limits. A full list of trace element concentrations is contained in Appendix 3.

The five drip water samples from cave formations all contained calcium, magnesium, sodium, and silicon above detectable limits. Boron, molybdenum, strontium, and zinc were detected in at least one of the samples. The sample containing rainwater had small amounts of calcium, magnesium, and sodium (Table 6.5).

Table 6.5. Trace elements detected in water samples taken in the field. Shaded cells indicate that the water sample did not contain detectable amounts of that element. All samples were drip water aside from WS8, which was rainwater.

		Elemental Concentration (ppm)							
ID	Location	B	Ca	Mg	Mo	Na	Si	Sr	Zn
WS1	Bega One		55.56	2.662	0.0638	6.538	4.085	0.0505	
WS2	Bega One	0 .2113	59.87	3.400		18.75	9.817	0.0626	0.1017
WS3	Bega One		45.37	1.566		3.702	2.392		
WS4	Bega One		45.14	1.367		3.118	2.009		
WS5	Isabella		66.22	2.268		7.144	3.642		0.0806
WS8	Lower Dover		4.842	0.1201			0.7488		

Trace elements in the soda straw samples were averaged to present a single elemental concentration for each of the five soda straws. Detectable elements were similar to those found in BZBT1 (Al, Cu, Fe, Mg, P, Pb), with the addition of chromium, molybdenum, and zinc (Table 6.6).

Table 6.6. Trace elements detected in soda straws taken above collected stalagmites (except SStr2, which was taken from near the site of WS1). Concentrations are expressed at weight percent (assuming calcium to be 40%) and multiplied by 1000 for easier interpretation. Shaded cells indicate that the soda straw did not contain detectable amounts of that element.

				Elemental Concentration (wt % * 1000)						
ID	**Cave**	**Al**	**Cr**	**Cu**	**Fe**	**Mg**	**Mo**	**P**	**Pb**	**Zn**
SStr1	Bega One	1.340	7.488	50.97	27.90	47.54	3.028	39.94	19.64	4.032
SStr2	Bega One	14.15	2.845	40.71	6.245	41.42		37.13	13.66	2.809
Sstr3	Bega Two			53.40		48.76		60.83	18.27	3.252
Sstr4	Isabella	5.904	5.354	27.91		36.42		27.52	14.24	1.470
Sstr5	Three Olla	5.882	7.033	34.23		38.48		35.41	16.41	1.800

Stable Isotopes

Stable isotope values in the 188 samples from BZBT1 are reported with respect to V-PDB (Figure 6.7). Values for $\delta^{13}C$ ranged from -12.3 to -2.0‰, with a mean of -9.3‰. Values for $\delta^{18}O$ ranged from -6.6 to -1.9‰, with a mean of -3.7‰. The first 80 samples had a 1-sigma error for $\delta^{13}C$ and $\delta^{18}O$ of ±0.11 and 0.09, respectively, the next 80 had errors for $\delta^{13}C$ and $\delta^{18}O$ of ±0.05 and 0.10, respectively, and the final 28 samples had errors for $\delta^{13}C$ and $\delta^{18}O$ of ±0.05 and 0.14, respectively. Variation in one of the isotope ratios was often mirrored in the other, with a correlation between $\delta^{13}C$ and $\delta^{18}O$ of 0.72 (Figure 6.8).

$\delta^{13}C$ and $\delta^{18}O$ attain maximum values at 79-86 mm, which corresponds exactly to samples taken from the 11DK zone. At the start of this zone, $\delta^{13}C$ jumps by 6.7‰ and $\delta^{18}O$ by 1.5‰ and then falls at the end of the zone by the same amount. After the end of 11DK until

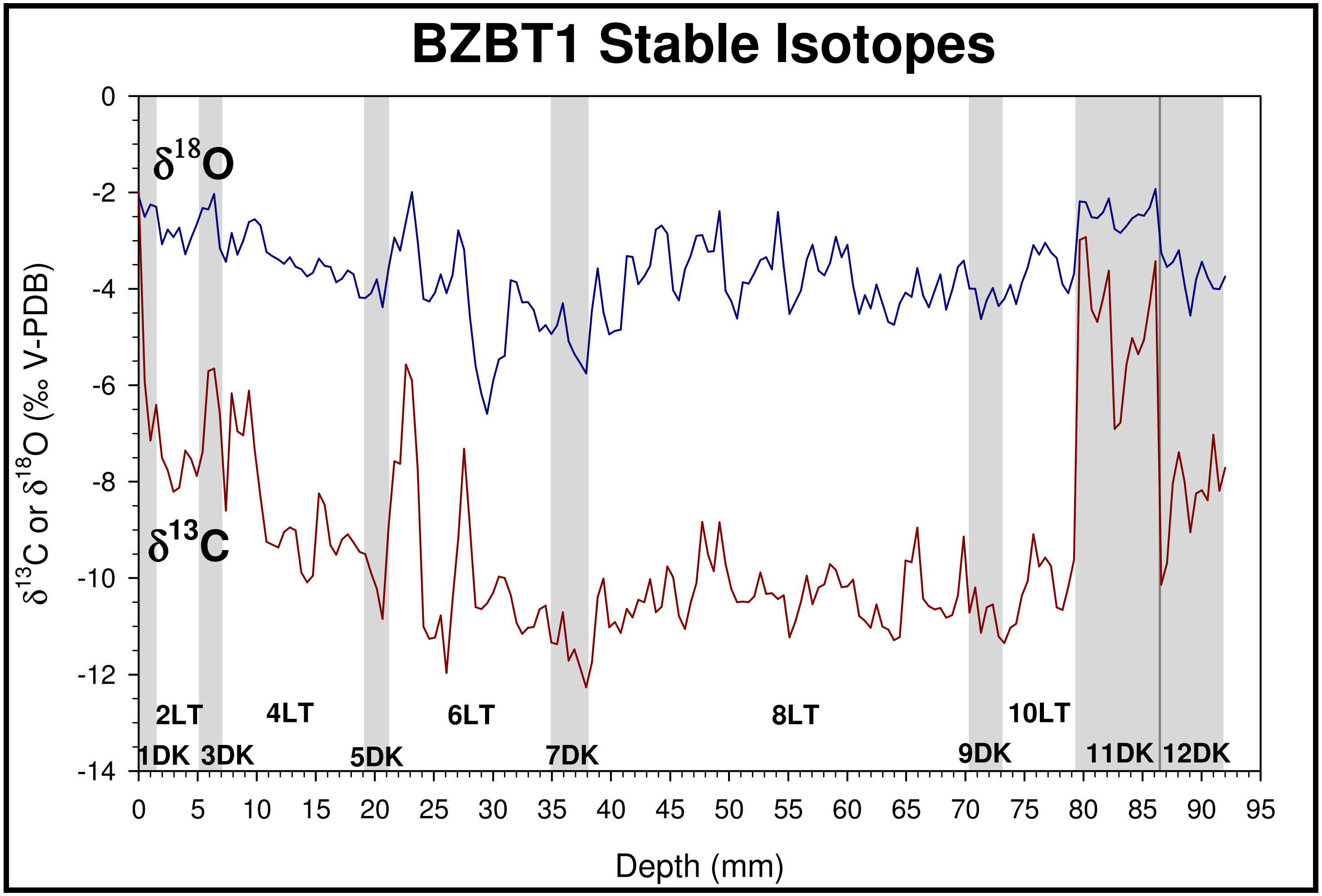

Figure 6.7. Isotopic ratios plotted over the sample range of BZBT1. Carbon isotopes are plotted along the bottom, and oxygen isotopes are plotted along the top. Of particular note is the double spike from 20-28 mm. The large increase from 79-86 mm perfectly corresponds to the zone 11DK. The 12 naked eye-observed zones of BZBT1 are labeled along the bottom.

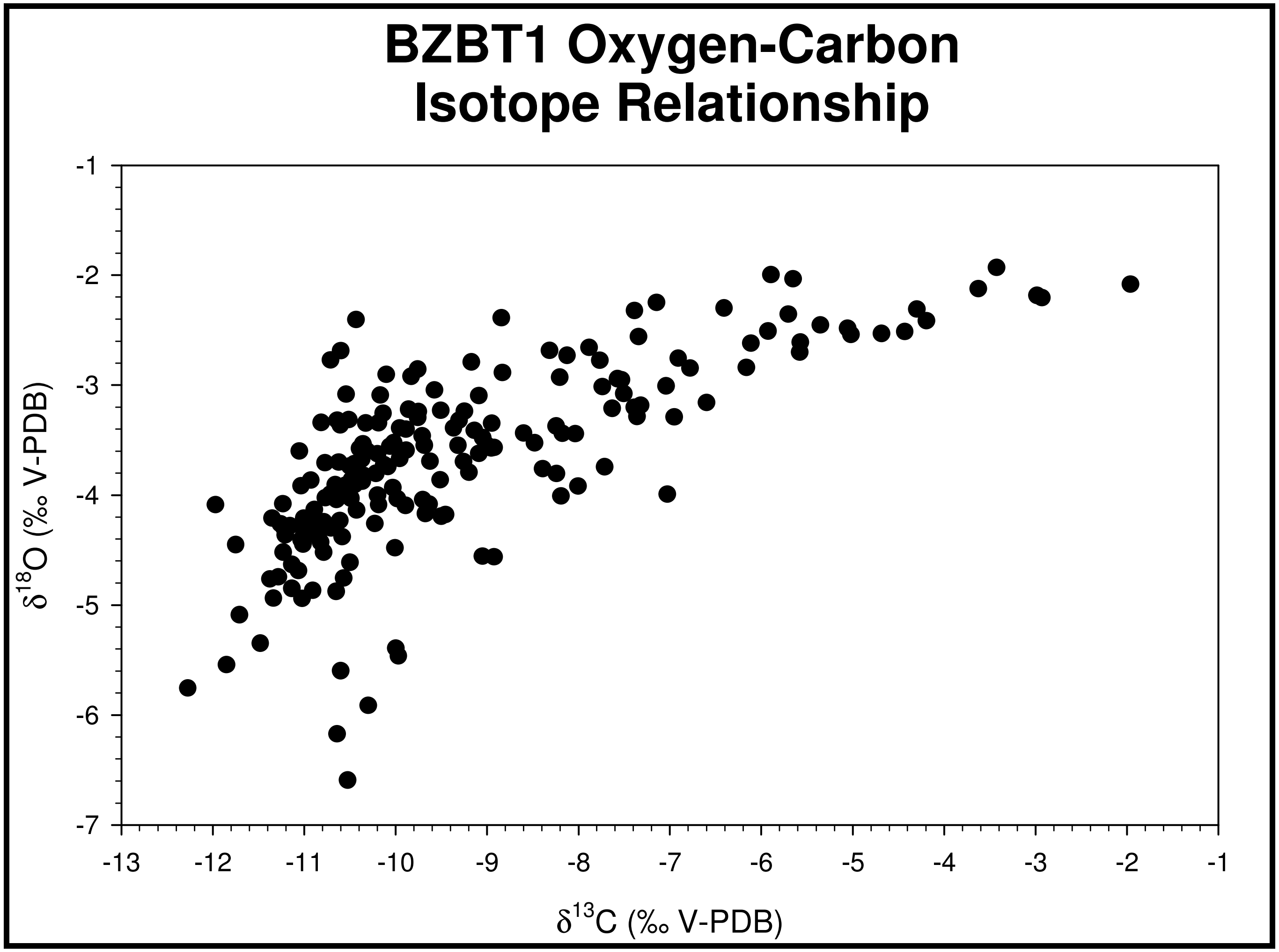

Figure 6.8. Each individual isotope sample from BZBT1 is plotted according to its stable isotopic ratio values. Larger values in one isotopic ratio are associated with larger values in the other isotopic ratio, and vice versa.

28.5 mm, $\delta^{13}C$ values fluctuate around an average of -10.5‰ and never reach a value greater than -8.8‰. During this same interval, the $\delta^{18}O$ values follow the same general pattern of peaks and troughs observed in the $\delta^{13}C$ values, with an average of -4.0‰ and a maximum of -2.4‰. Both $\delta^{13}C$ and $\delta^{18}O$ have low values at 38 mm, where $\delta^{13}C$ reaches its lowest value in the record of -12.4‰ and $\delta^{18}O$ reaches a local minimum value of -5.8‰. One point of difference between the two isotope plots occurs at 29.5 mm. Here, $\delta^{18}O$ attains its lowest value of -6.6‰, while $\delta^{13}C$ values are low but not significantly low.

Both isotopic ratios have a sharp spike at 27.5 mm, with $\delta^{13}C$ and $\delta^{18}O$ rising by 3.2‰ and 3.4‰, respectively, from the low values at 29.5 mm. Isotopic ratios peak again at 23 mm with values greater than any point since the 11DK zone ($\delta^{13}C$ = -5.6‰, $\delta^{18}O$ = -2.0‰) before dropping to another minimum at 20.7 mm. Aside from the high values throughout zone 11DK, this double spike is the most striking aspect of the isotopic plots, particularly in the $\delta^{13}C$ values.

After the double spike, the isotopic values increase steadily but with sharp peaks from 5-10 mm. These peaks are quite large in the $\delta^{13}C$ values (a sudden increase of 3.1‰), but not unusual in the $\delta^{18}O$ values. At the very top of the stalagmite the $\delta^{13}C$ value jumps to -2.0‰, the highest value in the record, and while the $\delta^{18}O$ value does not increase as sharply, it reaches -2.1‰, close to its maximum value.

Drip water samples produced $\delta^{18}O$ values ranging from -3.6 to +0.8‰ V-SMOW, and the average drip water $\delta^{18}O$ for the Bega One cave was -2.5‰ V-SMOW. The sample of rainwater that fell at Lower Dover had a $\delta^{18}O$ value of -1.0‰ V-SMOW (Table 6.7).

Two samples were taken from each soda straw for isotope analysis (Table 6.8). These samples were from separate locations on the soda straw (typically one towards the top and one towards the bottom). Though the soda straws were small enough that the distance between samples was not large (typically under 1 cm), the isotopic values often varied greatly in magnitude. The two samples from Sstr3 varied by 6.8‰ and 1.0‰ for $\delta^{13}C$ and $\delta^{18}O$, respectively. Samples from Sstr4 and Sstr5 did not vary nearly as much. Overall, soda straws from Bega One cave had lower $\delta^{13}C$ and $\delta^{18}O$ values than the straws from Bega Two, Isabella, and Three Olla caves.

Table 6.7. Oxygen stable isotopic ratios for six water samples. Note that these samples are reported relative to V-SMOW, rather than V-PDB as with the carbonate samples; however, the V-SMOW values have also been converted to V-PDB for carbonate comparison.

ID	**Location**	**Source**	**$\delta^{18}O$ (‰ V-SMOW)**	**$\delta^{18}O$ (‰ V-PDB)**
WS1	Bega One	Drip water	-2.3±0.6	-32.2±0.6
WS2	Bega One	Drip water	-1.2±0.1	-31.1±0.1
WS3	Bega One	Drip water	-2.7±0.2	-32.6±0.2
WS4	Bega One	Drip water	-3.6±0.2	-33.5±0.2
WS5	Isabella	Drip water	+0.8±0.2	-29.2±0.2
WS8	Lower Dover	Rain	-1.0±0.2	-31.0±0.2

Table 6.8. Oxygen stable isotopic ratios for soda straws taken above collected stalagmites (except SStr2, which was taken from near the site of WS1). Each soda straw had two samples taken for isotopic analysis.

			Sample 1		**Sample 2**	
ID	**Cave**	**Stalagmite**	**$\delta^{13}C$ (‰ V-PDB)**	**$\delta^{18}O$ (‰ V- PDB)**	**$\delta^{13}C$ (‰ V- PDB)**	**$\delta^{18}O$ (‰ V- PDB)**
SStr1	Bega One	BZBO3	-14.3	-4.7	-10.4	-3.6
SStr2	Bega One	N/A	-14.2	-4.5	-13.5	-3.9
Sstr3	Bega Two	BZBW4	-13.5	-2.2	-6.7	-1.2
Sstr4	Isabella	BZIS5	-8.4	-2.0	-8.7	-2.0
Sstr5	Three Olla	BZTO7	-9.8	-4.1	-8.3	-4.0

Petrography

The petrography of BZBT1 ranged through multiple calcite crystal fabrics. The twelve zones defined by visual inspection varied in appearance because of variations in crystal fabric. Dark zones are typically dense sparry calcite (Figure 6.9), while lighter zones are comprised of multiple layers of smaller calcite crystals which are often growing at varied angles to give a braided appearance (Figure 6.10). This braided pattern was also reported in the Webster et al. Belize stalagmite (Webster et al., 2007), but does not seem to be a common speleothem fabric.

The region of BZBT1 from 0-19 mm is very irregular compared to rest of the stalagmite. Zones 1DK and 2LT are comprised of undulating layers irregularly alternating between blocky calcite and smaller calcite crystals. However, there is no clear difference between 1DK and 2LT when viewed through the microscope. These layers do not appear to be truncated or thin in a recognizable pattern. Zone 3DK is a prominent thick layer of dense blocky calcite. Zone 4LT returns to the undulating pattern observed in 1DK and 2LT, but lacks layers of dense calcite. Some sections of 4LT (predominately towards the outer flanks) contain more needle-like crystals than anywhere else in the stalagmite (Figure 6.11). Some of these needle-like crystals form fan-like clusters, but do not show the sweeping extinction in cross-polarized light common to aragonite. The bottommost layers of 4LT are much more regular and similar to other lighter zones of BZBT1. These regular layers contain very fine braided crystals and several thin interruptions of denser calcite. They also thin out and disappear toward the flanks of BZBT1 and could be classified as L-type layers following Railsback et al. (2011).

Zone 5DK is the most striking and noticeable layer in all of BZBT1. It is comprised of sparry dense calcite and is 1.5 mm thick at the growth axis. 5DK maintains much of its thickness down the flanks of BZBT1 and is identifiable as a dark layer even in the flat deposits surrounding the base. The boundary between 5DK and 6LT contains a layer of detritus, thickest on the flanks, but still present at the central axis. The crystals in 5DK above the detrital layer are not optically in line with the crystals in 6LT below this layer, whereas all other zonal boundaries maintain some form of optical continuity (Figure 6.12). Directly below this detritus in zone 6LT

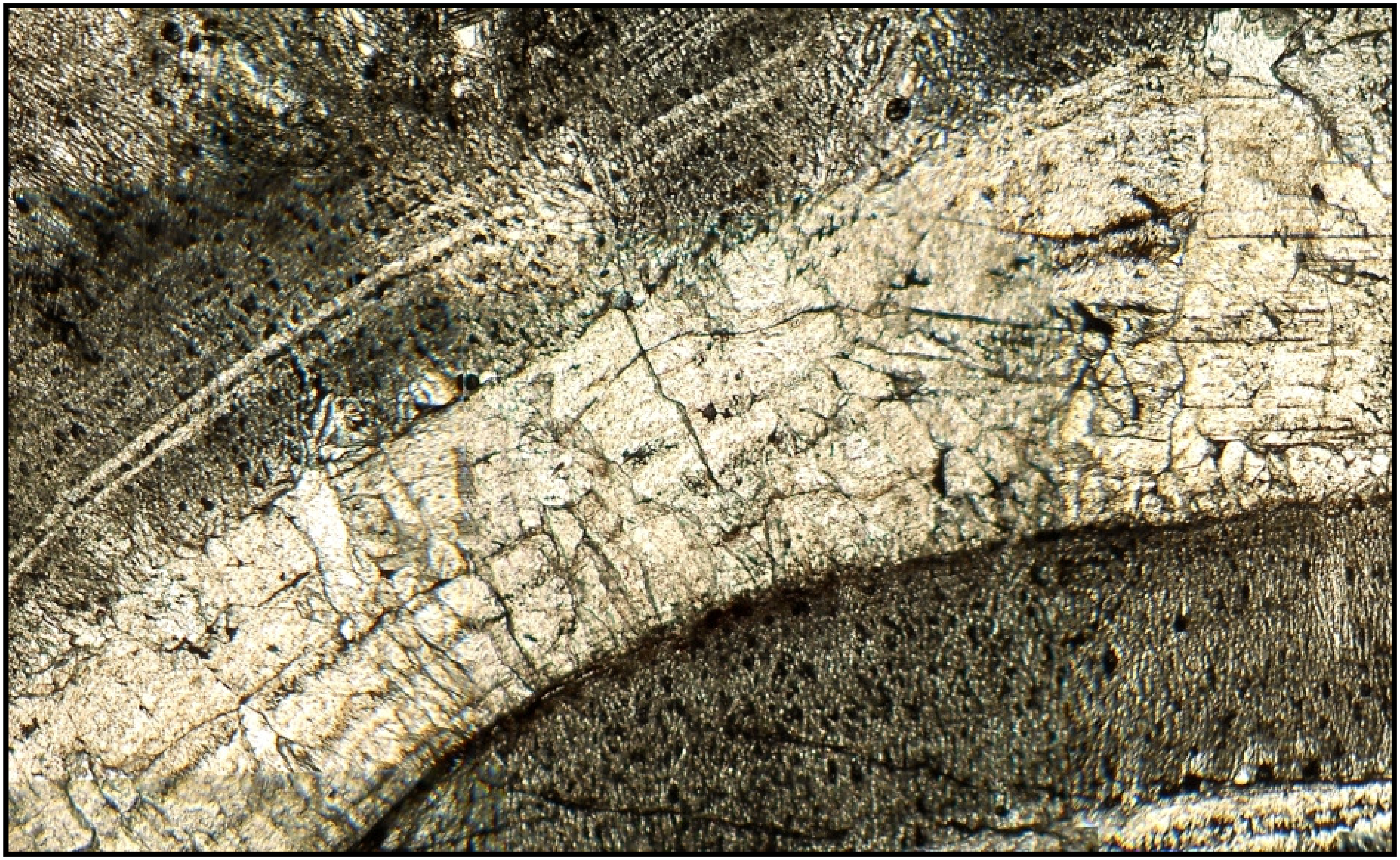

Figure 6.9. A layer of dense sparry calcite can be seen here between two non-dense calcite regions.

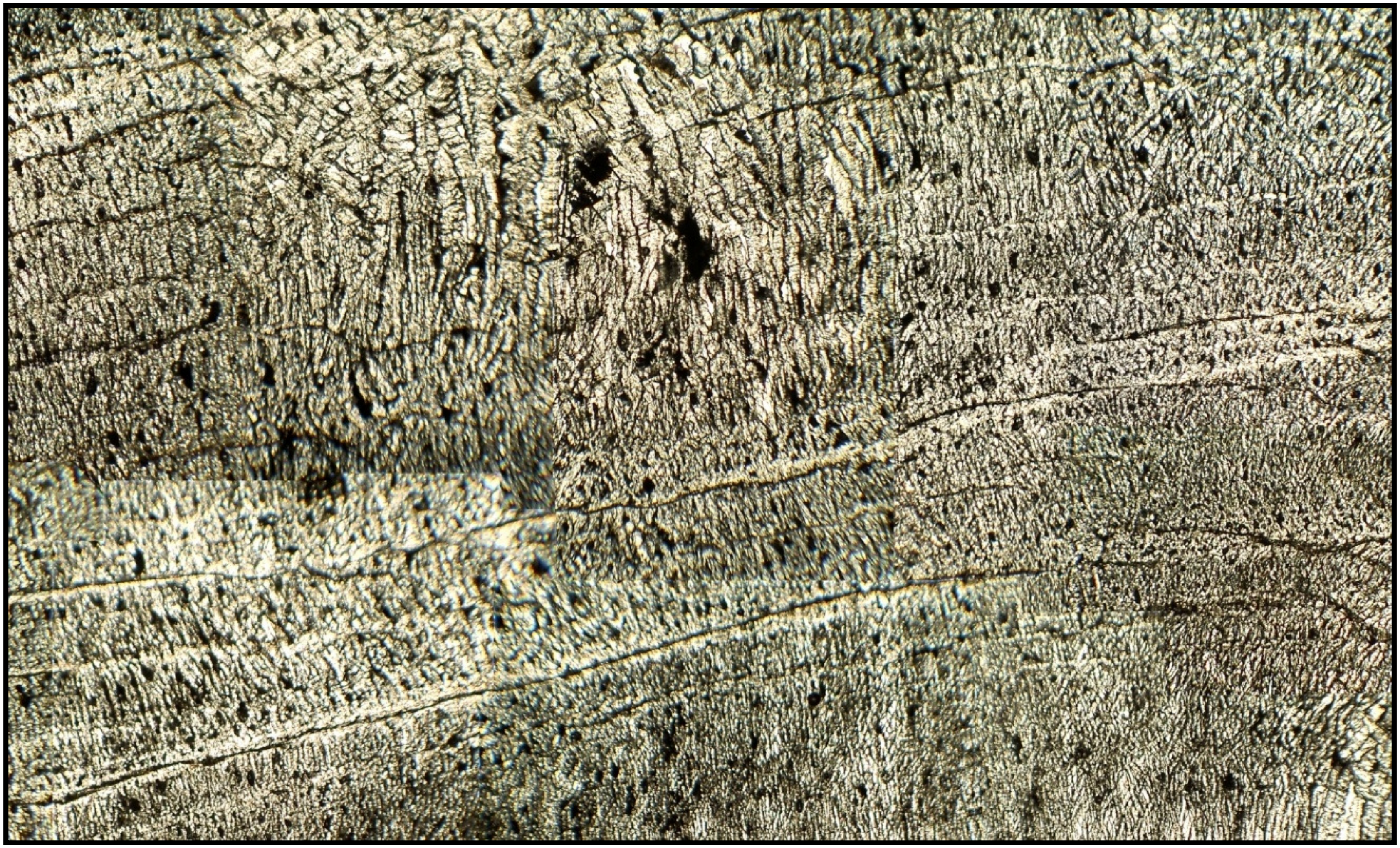

Figure 6.10. A region typifying the braided fabric layers. interspaced with thin layers of denser calcite.

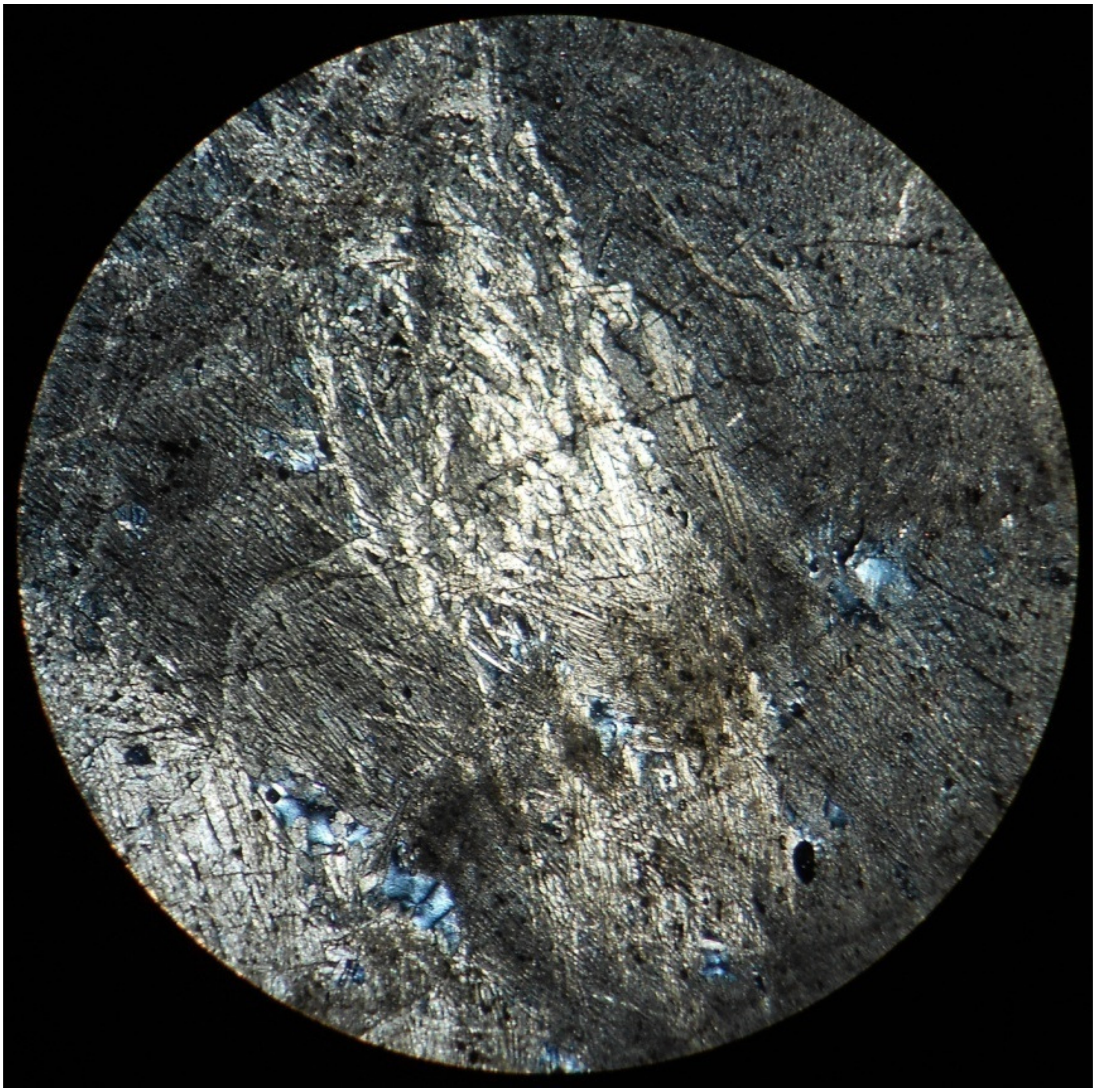

Figure 6.11. Some of the elongated needle crystals present in 4LT viewed under cross-polarized light. Although the needle-shape and fan-shaped clusters (producing the wavy layer boundary) suggest aragonite, extinction patterns and present of magnesium are more indicative of calcite.

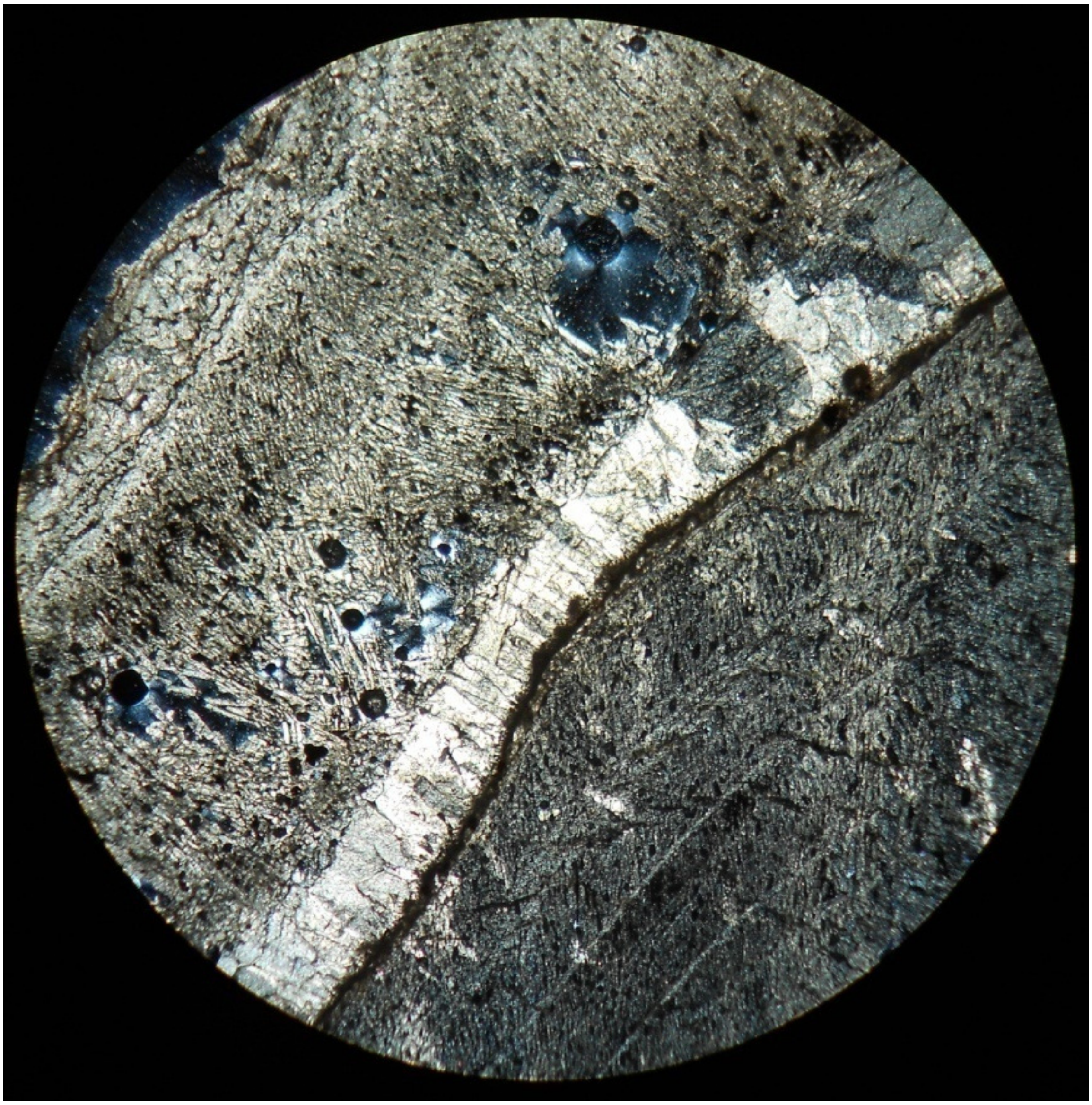

Figure 6.12. The bright white layer is 5DK, with 4LT to the left and 6LT to the right. Note the dark detrital layer between 5DK and 6LT. Contrast the lack of optical continuity between 5DK and 6LT with the continuity present between 4LT and 5DK. Viewed under cross-polarized light.

is a ~1 mm thick layer comprised of very fine braided crystals. This layer, though relatively thick at its apex, thins rapidly to nothing toward the flanks.

The remainder of 6LT is comprised of multiple layers of braided calcite, each separated by very thin layers of denser calcite. The width and thickness of each of these layers is highly variable. At ~23 mm several L-type layers are clustered together over approximately 1 mm. Directly below that are two thick (~1.0mm) braided calcite layers that maintain their thickness down the flanks, followed by another set of L-type layers at ~27 mm. This deeper set of L-type layers are not densely packed as the upper set in 6LT, nor do they taper away as quickly. Once again, a set of wider layers lies beneath the L-type layers, extending 2 mm (Figure 6.13). A third set of L-type layers exists at ~31 mm, although these are even less dense and tapered than the previous L-type layers. The remaining section of 6LT is composed of a final set of wider layers. Zone 7DK is a thick layer of denser calcite, but not nearly as well-defined as 5DK. Toward the flanks the crystal fabric changes from a solid sparry block into a dense braided calcite and finally into the regular braided calcite. This transition is not orderly and reverses in some sections, producing a patchwork of dense calcite and braided calcite.

Below 7DK is 8LT, the largest zone extending from 38-70.5 mm. The growth for nearly the entire zone is quite stable and uneventful. Layers thicken and thin, but never dramatically or to the degree observed in 6LT. The most notable thinning occurs from 56-60.5 mm in depth, but the thinning is subtle and gradual. The remaining portion of 8LT is comprised of regular and non-L-type braided calcite layers, separated by the denser calcite interruptions. Some of the braided layers are quite porous at the growth axis (51-55, 57-59, 67-68.5mm), but these layers do not appear otherwise abnormal in thickness or thinning.

Zone 9DK is similar to 7DK in its pattern of dense calcite near the growth axis transitioning to braided calcite towards the flanks, but 9DK is much more regular in its

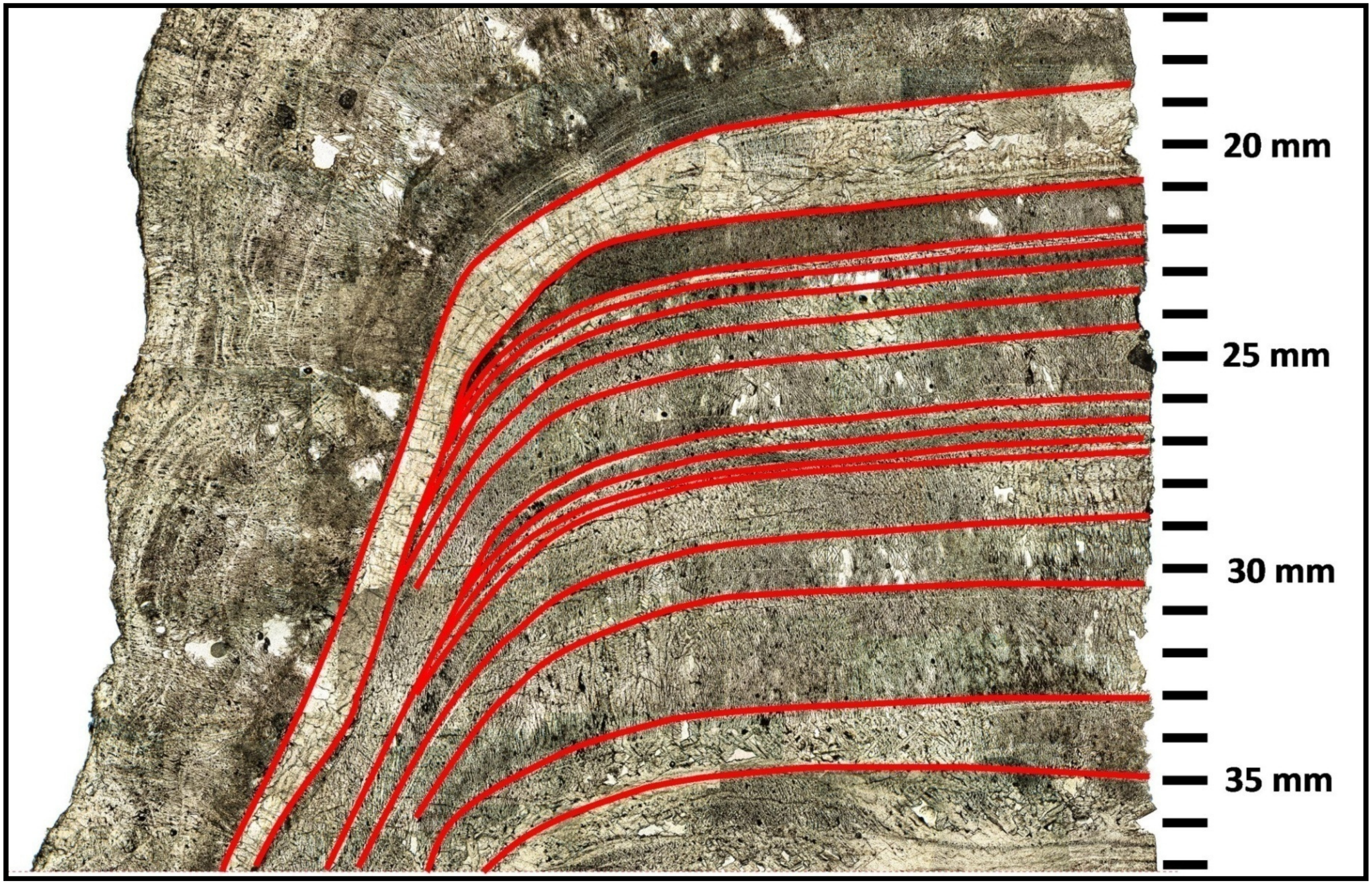

Figure 6.13. A portion of the BZBT1 thin section with layer boundaries highlighted in red. The wide dense calcite layer at 20 mm is 5DK. Significant thinning (vertical distance) and narrowing (horizontal distance) of layers occurs at ~23 mm and ~27 mm.

transition. Zone 10LT appears very similar to 8LT in its range of crystal fabrics. The layers from 75-78 mm near the growth axis are extremely porous and rapidly thin toward the flanks after ~19.5 mm. The boundary between 10LT and 11DK is defined by a clear double line. The exact nature of this double line is unclear, but most likely is an optical artifact created at the boundary between two crystal growth faces. Small amounts of clay-sized detritus may also be present in the double line, but the layers on either side maintain optical continuity (Figure 6.14). This boundary shows signs of dissolution and layer erosion indicative of a Type E boundary (Railsback et al., 2011). The erosion does not appear to be severe.

Towards the flanks, 11DK seems to “bleed over” the clear boundary zone and the lowermost layers of 10LT are a sparry calcite rather than the typical braided calcite located near the central axis. A possible explanation for this “bleeding” is that the greater flow and deposition located near the central axis allowed the crystal fabric to be created closer to its environmental equilibrium (in this case, the braided calcite). The lessened flow on the outer flanks produced crystals more prone to simply building on top of the already present crystal lattice of 11DK. It may also be a result of the erosional boundary.

Although both 11DK and 12DK are both composed of sparry dense calcite, they are readily distinguished petrographically (Figure 6.15). Zone 11DK contains massive columnar calcite crystals, up to 2 mm wide and some extending the entire length of 11DK. Very fine layering can be seen within the crystals, but the layers are not defined enough to determine changes in thickness. The boundary with 12DK is marked by a transition from the organized massive columnar calcite of 11DK to a more chaotic calcite composed of smaller spars ranging from nearly equant to columnar.

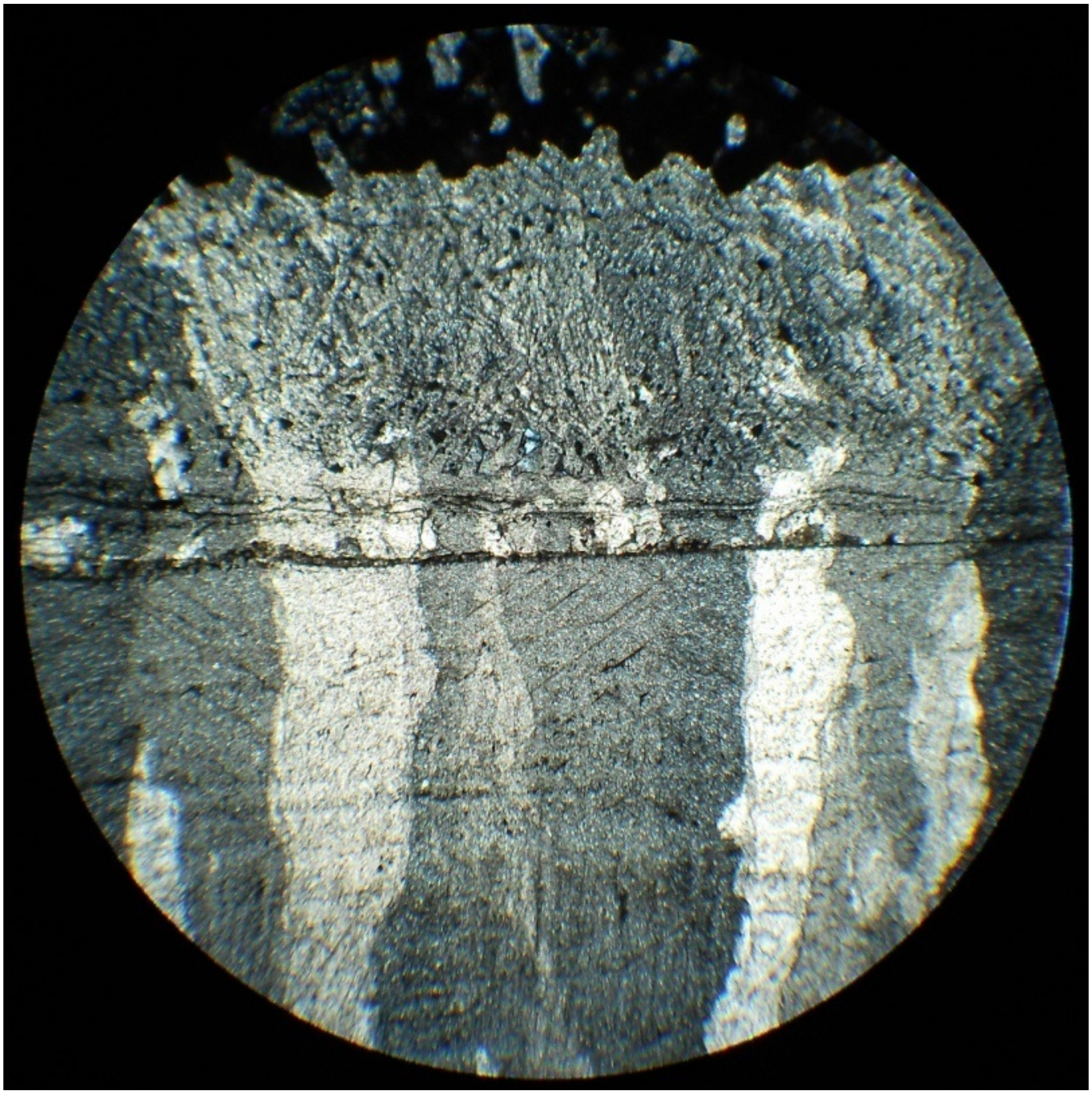

Figure 6.14. The double line boundary between 10LT (top of image) and 11DK (bottom of image). Despite the dramatically different crystal fabrics, optical and thus crystallographic continuity is maintained. Viewed under cross-polarized light.

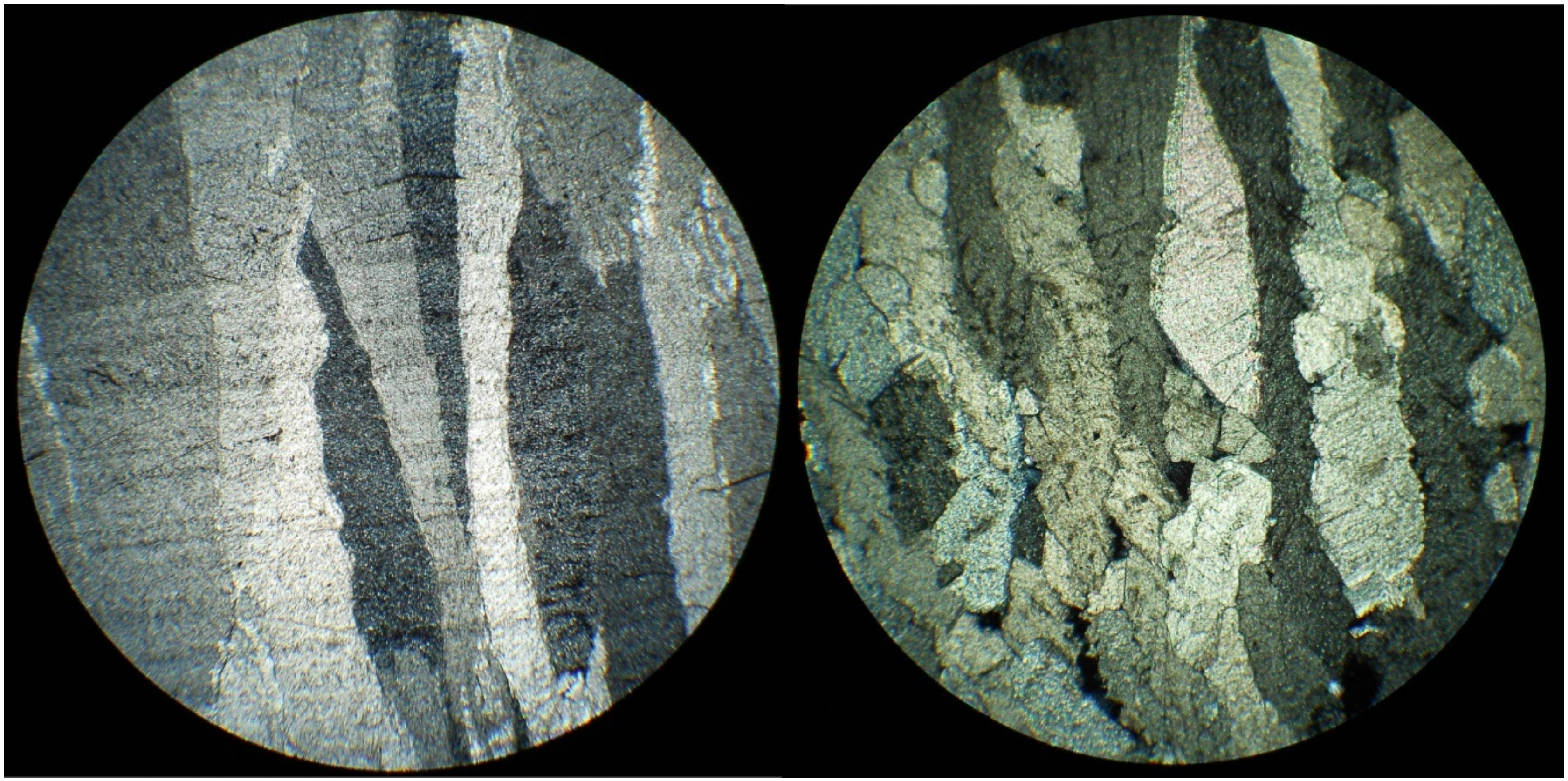

Figure 6.15. Massive columnar calcite of 11DK (left) and the more chaotic calcite of 12DK (right). Viewed under cross-polarized light.

CHAPTER 7
DISCUSSION

Chronology

The calibrated organic radiocarbon ages and uncalibrated carbonate ages can be compared to determine the most robust chronology for BZBT1 (Figure 7.1). There is no clear petrographic evidence for periods of erosion other than one location: an eroded boundary at 79.5 mm. The two youngest organic ages come from a region of relatively stable growth with no apparent interruptions. An eroded boundary separates these two dated samples from the three oldest dates. Oddly, the organic sample from 87 mm is 110 years younger than the sample from 52 mm. There were not enough recoverable organics present in the topmost layers of BZBT1 to produce a radiocarbon date, despite multiple attempts. Carbonate ages in these layers suggest continued stable growth until at least the shallowest 3 mm. The very young carbonate age from the topmost layer does not fit well with the rest of the carbonate ages; this sample comes from a dense calcite layer covering the uppermost 1 mm. This dense calcite layer is associated with extreme values in both the $\delta^{13}C$ and luminescence records. Because of these aberrations the chronology for BZBT1 has been created for all portions except the uppermost 1 mm, and data from this uppermost 1 mm has been disregarded.

The chronology trend line was constructed in a series of steps, combining data from both the organics and carbonate samples. The erosional discontinuity at 79.5 mm provided a distinct boundary separating the upper portion of BZBT1 from the basal portion. These portions differentiated in petrography (the upper portion being primarily braided calcite, in contrast to the dense sparry basal portion) and average stable isotope values (the basal portion having much greater values). As mentioned previously, the carbonate ages in the basal portion appear to adhere to a different, younger trend than the upper carbonate ages. Therefore, the trend line for BZBT1's chronology would be independently calculated in two sections: an upper trend and a basal trend.

The upper trend was first calculated by plotting a linear trend between the two organic ages. The carbonate ages differ in age from the organic trend by 370-880 years, but the general carbonate trend is similar to the organic trend. Organic material in a moist tropical environment typically has a short residence time , but the residence time can be up to 100-200 years (Shang and Tiessen, 1997). Thus, the organic trend line created for the upper portion is likely too old. To account for the organic residence time, the organic trend line must be shifted younger; the exact amount of year to shift the upper organic trend line would be determined after determining the age-depth relationship of the basal portion of the stalagmite first.

The age-depth relationship in the basal section was calculated as the linear trend fitted to the three organic ages is this section of the stalagmite. This simple trend predicts a date of -19.5 cal yr BP at the 79.5 mm boundary, which is clearly incorrect. A possible explanation is that the deepest two organics samples were taken from a location directly below the absolute base of BZBT1. Because these samples were not actually contained within the basal carbonate deposits of BZBT1 and could predate the initiation of BZBT1 growth by a longer period than initially assumed. If this is true, then the lowest two ages may be older than their depth of 92 mm would seemingly indicate. The three carbonate ages from the basal portion are aligned in a linear manner. Over the short distance and homogeneous petrography of the basal portion, input of old carbon should not vary a great deal; therefore, the trend of the carbonate ages would be reflective of the actual growth rate. The age-depth relationship for the basal portion was thus given the same slope as the carbonate age trend.

A final combined trend line was created by joining the upper trend with the basal trend at the 79.5 boundary. Although it appears that a portion of the record has been lost to erosion at the boundary, the exact duration of the lost record cannot be determined. Based on petrographic analysis, the amount lost appears to be quite small and within the general error assumptions of the trend line. The combined trend was then located in such a manner to satisfy the actual organic sample ages as much as possible. This resulted in a chronology beginning at 1192 cal yr BP and reaching 955 cal yr BP at the 79.5 mm boundary. The rate of growth then increased for the upper portion of BZBT1, ending at 496 cal yr BP at 1 mm in depth. The BZBT1 record would then contain the last few centuries of the Classic Period and a large portion of the Postclassic Period.

Placing the chronology trend in this location required assuming that OE1-9 had an age that did not require adjustment due to residence time, but that the other organic sample ages did require a residence time adjustment less than 200 years. Out of necessity, the age trend line in Figure 7.1 must be regarded as an approximation of the true age-depth relationship, although it is likely to be a close approximation. The exact age at each depth may not be known, but a small range of possible ages can be created. The given organic sample age establishes an oldest age boundary for the depth it originates from, and the youngest possible age should not more than 200 years younger than this. For the placement of the trend as described above and shown in Figure 7.1, the trend adjustment was ~190 years younger than the age range of the two upper organic samples. The two organic samples from the very base of BZBT1 were adjusted by -385 years; this is greater than the 200 year limit, but it is likely that the sediment source of the organic material was not deposited immediately prior to the initiation of BZBT1’s growth. Finally, OE1-9 is actually 40 years younger than the trend age, but this was considered acceptable. Later comparison with other paleoclimate records would aid in narrowing down which exact trend adjustment was best. Because the chronology for BZBT1 is comprised of two distinct growth rates, the age interval for proxy samples is different between the upper and basal portion (Table 7.1).

All the uranium-series age ranges are either equal in age or older than the organic ages and trend (Figure 7.2). If the organic ages are the most accurate, then this arrangement of uranium-series ages is expected; any uranium-series samples contaminated by external thorium would show ages older than the organic age trend line.

Table 7.1. Range of intervals between proxy samples taken from BZBT1. Intervals are greater in the basal portion than the upper portion because the growth rate was slower.

	Interval between Samples (Years)	
Proxy	**Upper Portion**	**Basal Portion**
Natural light reflectance	0.11	0.35
Luminescence	0.36	1.06
Stable isotopes	2.88	8.39
Trace elements	12.66	36.50

The successful extraction and dating of organics from within a speleothem represents a powerful tool for accurate dating of speleothems. A chronology derived solely from dating included organic material typically has a larger probability range (due to calibration) and more limited age range than a uranium-series chronology. In addition, determining the organic residence time can be difficult and adds more uncertainty. However, some regions and samples (such as this study's Belize site) may naturally have low uranium concentrations or high detrital levels that make uranium-series dating difficult or impossible. In these cases, dating of organic material in stalagmite carbonate may be the only accurate dating method available. Even in speleothems successfully dated by the uranium-series method, organic dating can be utilized as a check to ensure that the chronology derived from the uranium-series approach is accurate.

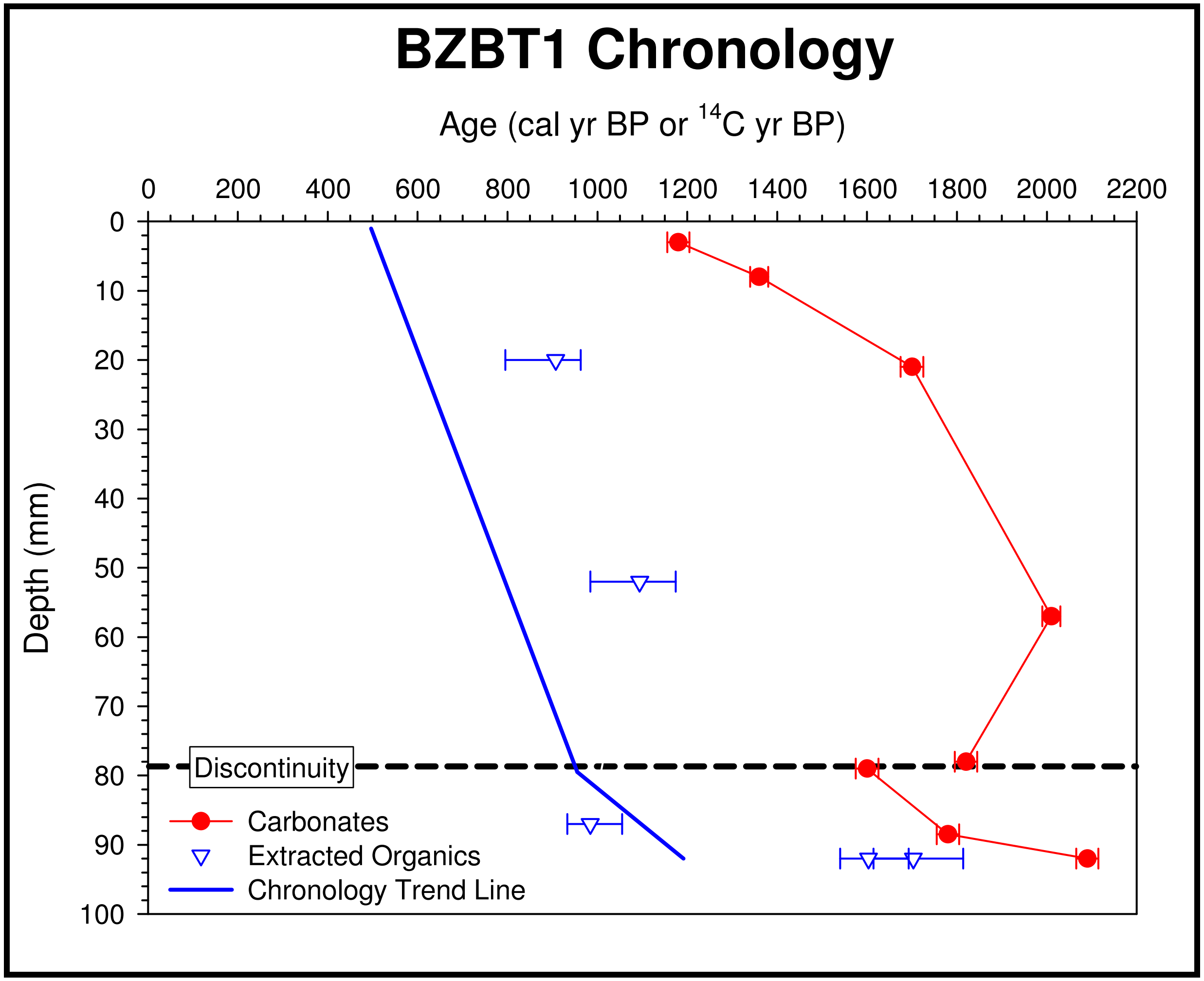

Figure 7.1. Trend line used for the BZBT1 chronology with radiocarbon ages from both carbonate (red circles, closed) and extracted organics (blue triangles, open), along with error ranges. Carbonate dates are uncalibrated and measured in ^{14}C years, whereas organic ages have been calibrated and are plotted in calendar years.

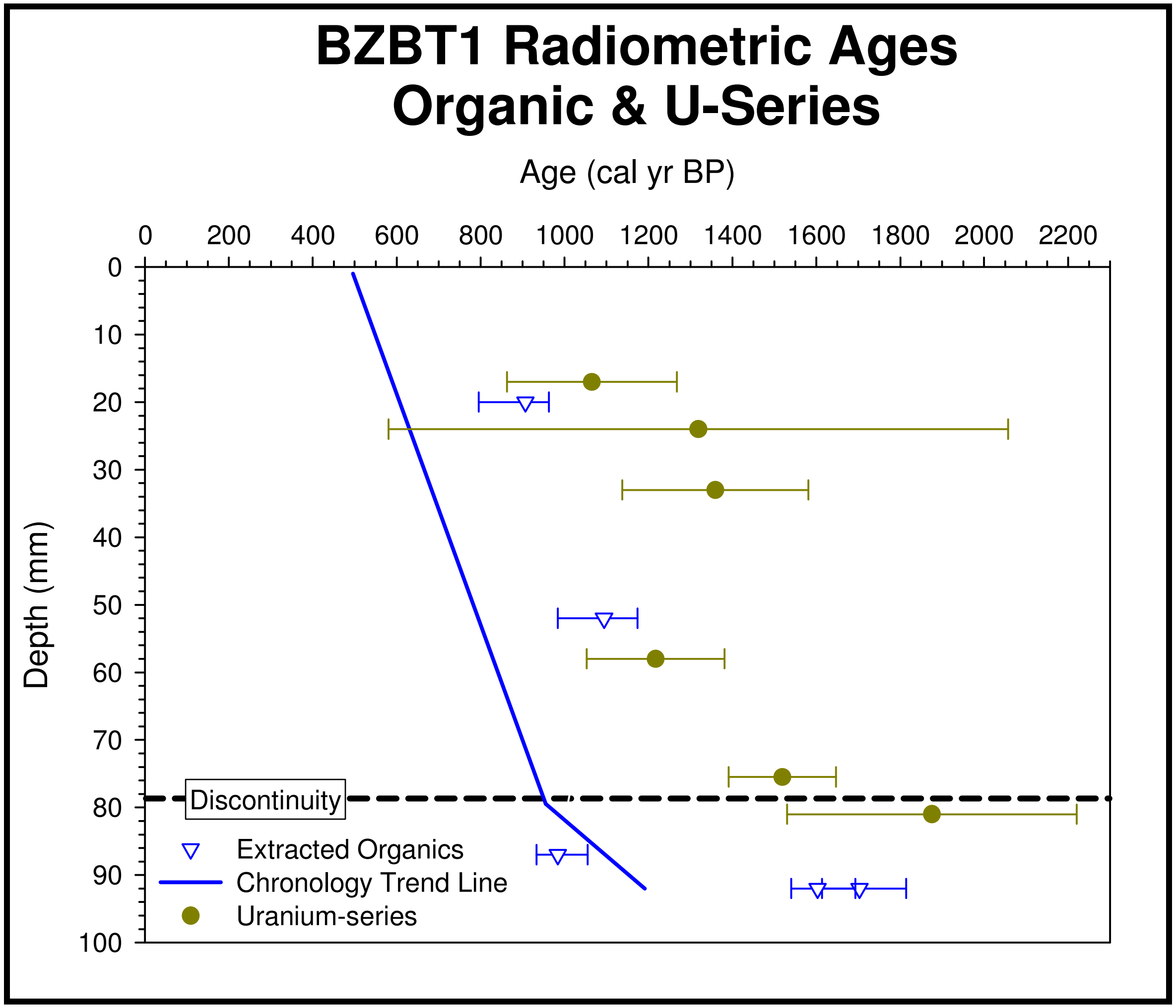

Figure 7.2. Trend line used for the BZBT1 chronology with radiometric ages from both uranium-series (olive circles, closed) and extracted organics (blue triangles, open), along with error ranges. Uranium-series ages are always older or equal to comparable organics ages.

The BZBT1 Paleoenvironmental Record

The BZBT1 paleoenvironmental record consists of three major units (Figure 7.3). The basal unit (Unit 1) extends from 79.5-92 mm in depth and contains zones 11DK and 12DK. This unit is composed of dense calcite layers that are thicker than other dense calcite layers elsewhere in BZBT1. Unit 2, the central portion of BZBT1, extends from 19-80 mm in depth and includes zones 5DK to 10LT. Unit 2 is characterized by a limited but still varied assortment of crystal fabrics and general agreement among the various paleoenvironmental proxies. Unit 3 comprises the upper portion of BZBT1. Unit 3 extends from 0-19 mm in depth and includes zones 1DK to 4LT.

Generally, the climate signal derived from the stable isotope record was also observed in petrographic analysis (Figure 7.4). Upon examination of trace element data, magnesium showed an overall pattern similar to the $\delta^{18}O$ record. None of the other trace element patterns agreed consistently with any of the other proxies, although some major peaks and troughs in the isotopes corresponded with similar peaks and troughs in phosphorus and aluminum. Light and dark zones in the reflectance data were not consistently associated with a wet/dry dichotomy from the other proxies. Some of the dark zones (3DK, 5DK, 11DK, 12DK) were quite obvious under thin section analysis, while others (1DK, 7DK, 9DK) were less clearly defined and difficult to distinguish from surrounding zones.

In addition, the luminescence record did not always support the isotope data. BZBT1 has many widely varying crystal fabrics in a short distance, although the changes in crystal fabric do not skew the luminescence value consistently. Many of the small dense calcite zones (7DK, 9DK) and the thin layers of dense calcite within the lighter zones show high luminescence values, but the most striking thin dense calcite zone (5DK) has some of the lowest luminescence values. The low luminescence values in 5DK would suggest arid conditions, but the zone

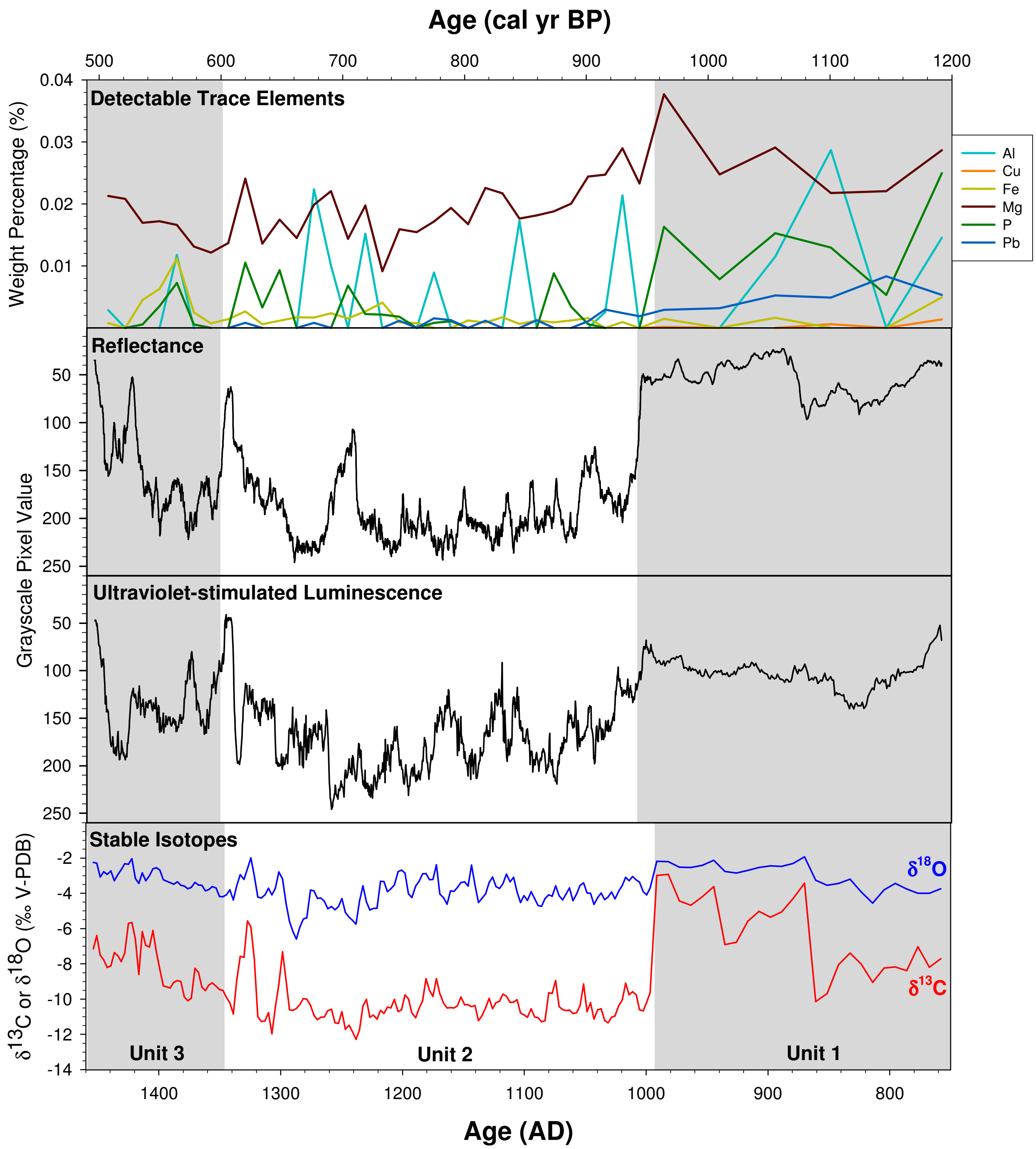

Figure 7.3. Five paleoenvironmental proxy records derived from BZBT1. The ultraviolet-stimulated luminescence and both stable isotope records, combined with the petrographic record, provided the best data for paleoclimate reconstruction. The three units as described in the paleoenvironmental record are identified. Exact width and location of the three units is slightly different between the drilled records (trace elements, stable isotopes) and the visual records (reflectance and luminescence) because the records were taken from different faces of the cut BZBT1

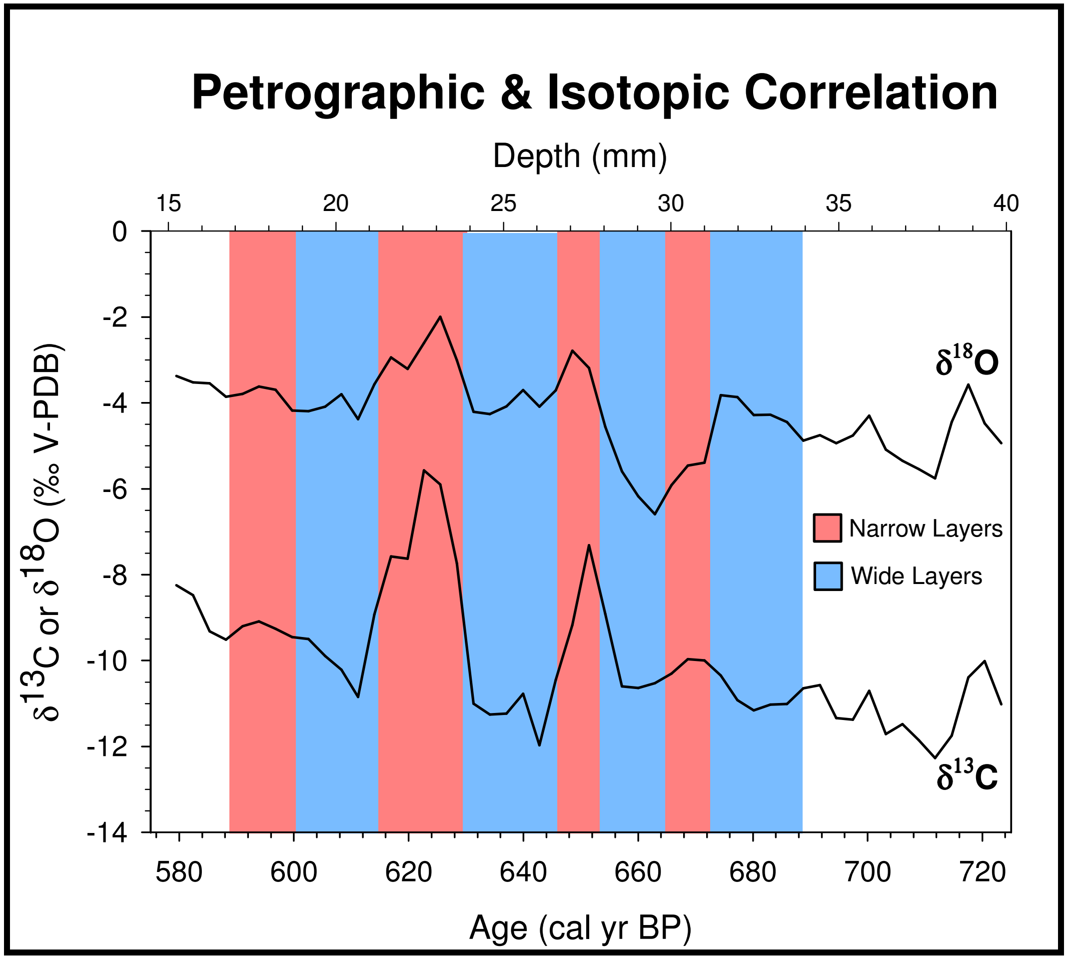

Figure 7.4. The stable isotope record for a select region of BZBT1 overlain with petrographic information. Pink zones are composed of thin layers with reduced or nonexistent growth towards the flanks (L-type layering). Blue zones are composed of much thicker layers that maintain much of their width towards and down the flanks. Narrow layers are associated with greater $\delta^{13}C$ and $\delta^{18}O$ values, and wide layers are associated with lower $\delta^{13}C$ and $\delta^{18}O$ values.

maintains its distinction and much of its width down the entire flanks of BZBT1 (indicative of wet conditions). Similarly, while many sections of braided calcite with L-type layering have low luminescence values, an obvious L-type layer at 21.5 mm deep has a very high luminescence. Outside of these two regions, the luminescence data agree very well with both the stable isotope and petrographic data.

The basal unit ranges from 955-1192 cal yr BP (758-995 AD) and contains several features that are not found elsewhere in BZBT1. Please note that years listed in this section are derived from the trend line and are not indicative of accuracy down to the actual year. Reflectance and luminescence maintain low values with limited variability, while magnesium, phosphorus, and lead are found at higher levels than in the rest of BZBT1. Both $\delta^{13}C$ and $\delta^{18}O$ values in the basal region are high and suggest drier conditions. The 11DK zone in particular contains the highest average $\delta^{13}C$ and $\delta^{18}O$ values of the entire stalagmite, with both an abrupt increase and decrease to these high values. The stable isotopes suggest that a major arid interval occurred during the length of the 11DK zone (955-1078 cal yr BP [872-995 AD]), with extremely rapid transitions to and from the arid interval. Initially, petrographic analysis appears to offer conflicting paleoclimatic signals in the basal region. The dense, blocky calcite in both the 11DK and 12DK zones is assumed to be indicative of wetter conditions, with the 11DK zone having the largest calcite spars. However, upon closer inspection, both these dense zones have very fine layering and are not particularly wide. The exact precipitation-crystal relationship needed to produce the braided fabric is not known, and dense calcite may be produced in this environment during extremely dry conditions.

The boundary between 11DK and 10LT shows signs of erosion, most likely due to large volumes of water. Layer erosion helps to explain why the transition from the arid 11DK was so abrupt: the record showing a more subtle climate shift is not present due to erosion. Major erosion does not appear to have occurred, so the shift from very arid to very wet still occurred in a relatively short timeframe.

The middle unit of BZBT1 (19-79.5 mm range) provides the most stable paleoclimate record from BZBT1 and dates to 601-955 cal yr BP (995-1349 AD). The change in crystal fabric from dense and blocky to braided made layering more visible. In addition, any thinning of these layers away from the growth axis is much more noticeable in the braided fabric. Two organic dates are taken from this unit and provide a reliable chronology. Much of the lower portion of Unit 2 (29-80 cal yr BP {583-991 AD}) is characterized by subtle changes in both petrography and stable isotopes. Thinning and narrowing of layers generally coincided with higher stable isotope values, suggesting more arid conditions from 929-946 cal yr BP (1004-1021 AD), 818-844 cal yr BP (1106-1132 AD), and 666-675 cal yr BP (1275-1284 AD). The $\delta^{18}O$ record suggests an otherwise relatively stable climate from 841-964 cal yr BP (956-1109 AD), followed by more variable and overall drier conditions from 736-841 cal yr BP (1109-1214 AD). Low luminescence values at 780, 820, and 840 cal yr BP (1110, 1130, and 1170 AD) support the isotope data of drier conditions around these times.

The climate remains variable from 660-736 cal yr BP (1214-1290 AD), but, given lower isotope values and higher luminescence, was wetter than the preceding times. In fact, there are two intervals of much wetter conditions centered on 663 cal yr BP (1287 AD) and 710 cal yr BP (1240 AD). The $\delta^{13}C$ record is variable in Unit 2 but also shows a trend towards wetter conditions from 660-736 cal yr BP (1214-1290 AD) with very wet conditions at 710 cal yr BP (1240 AD).

The region from 19-29 mm contains one of the strongest paleoclimate signals of BZBT1. Major peaks in $\delta^{13}C$ and $\delta^{18}O$ values at 23 and 27.5 mm coincide with L-type layering in the petrographic record and much lower luminescence. The stable isotope and petrographic evidence combined suggests two severe droughts centered at 625 cal yr BP (1325 AD) and 651 cal yr BP (1299 AD), both with rapid onset and rapid decline. This second drought appears to have lasted 2-3 times longer than the first drought. The detrital layer at 21 mm suggests that there was little or no calcite deposition prior to deposition of zone 5DK carbonates, most likely due to a reduced input of water to the cave. The dense calcite of 5DK coincides with a second return to somewhat wetter conditions at 610 cal yr BP (1340 AD).

The proxies in Unit 3 suggest an overall increase in aridity until deposition stopped. This is indicated by long-term increases in both $\delta^{13}C$ and $\delta^{18}O$ to values higher than those recorded during earlier droughts. A series of L-type layers directly above 5DK coincides with slight increases in $\delta^{13}C$ and $\delta^{18}O$ suggesting moderately dry conditions from 588-601 cal yr BP (1349-1362 AD) and there is also evidence of a dry interval around 578 cal yr BP (1372 AD).

Higher isotope values from 5.2-10.3 mm coupled with lower luminescence and higher reflectance suggest a dry interval from 521-551 cal yr BP (1399-1429 AD) with a brief respite at 534 cal yr BP (1416 AD). The dry conditions abated somewhat after 520 cal yr BP (1430 AD), although the climate continued to be drier than during most of the period from ~675-950 cal yr BP (~1000-1275 AD). Finally, from 502 cal yr BP (1448 AD) until the chronology ends at 496 cal yr BP (1454 AD), the various proxy climate records indicate a rapid change to conditions nearly as dry as during 11DK. The uppermost values for $\delta^{13}C$ (not included in the chronology since they occur in the 1 mm excluded zone) rapidly increase to their greatest values present in the record. The extremely high $\delta^{13}C$ values may indicate very dry conditions on the ground above the cave with low levels of CO_2 in the soil resulting in more carbon in soil waters coming from the bedrock as opposed to the soil air.

The paleoenvironmental record from BZBT1 suggests several periods of wetter- and drier-than-average climate since 750 AD (Figure 7.5). The isotopic, reflectance, and

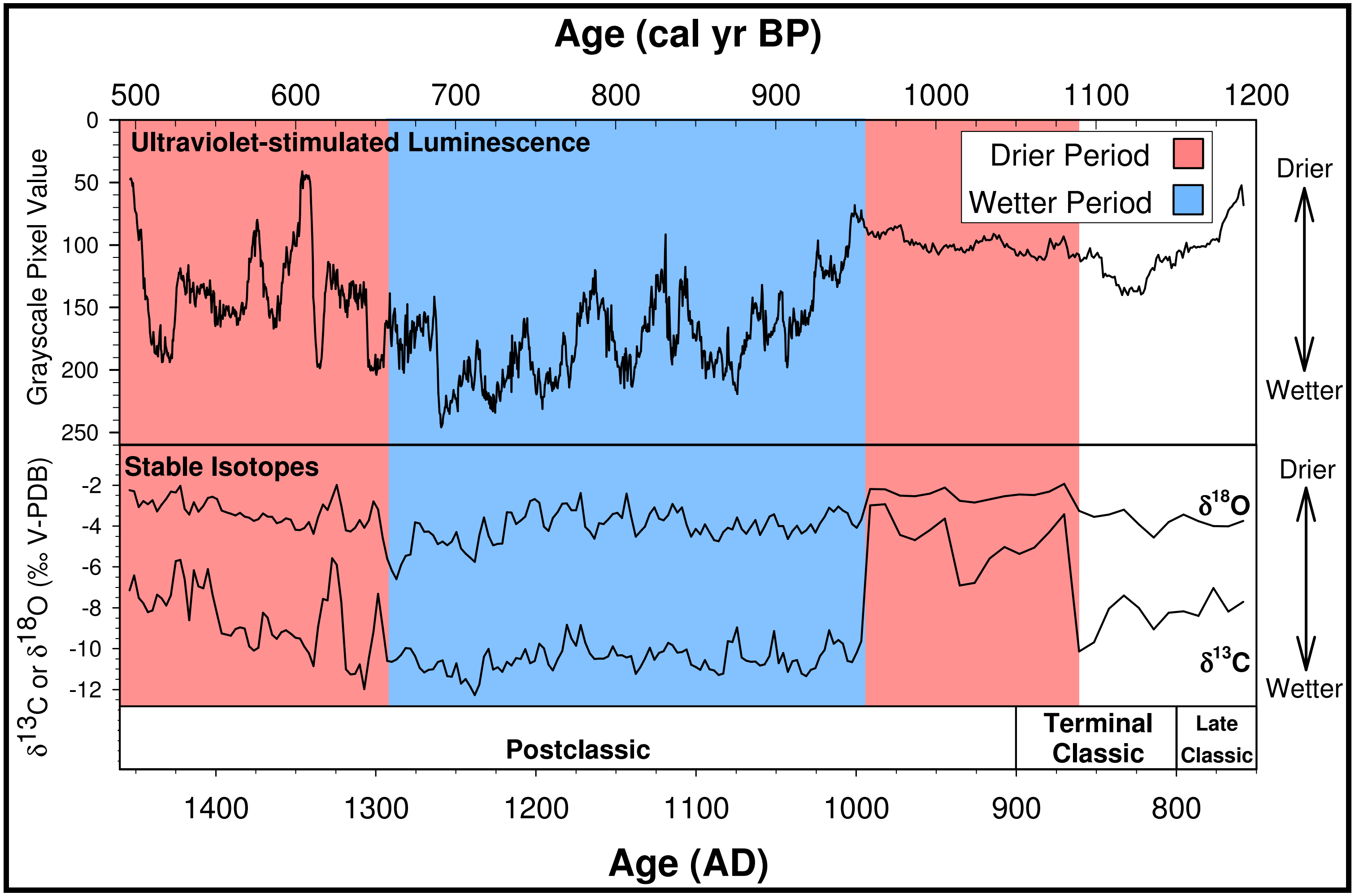

Figure 7.5. Broadly-defined wetter and drier periods primarily defined from luminescence and stable isotopic data and supported by petrographic analysis. Although the general trend in each period is either wetter or drier than the overall average, great variability and climatic swings from wet to dry still occur within each period. Mesoamerican chronological periods are listed along the bottom.

luminescence data from the basal zones of BZBT1 (11DK and 12DK) suggests this was a period of drier conditions from 955-1191 cal yr BP (758-995 AD). The 11DK zone (955-1078 cal yr BP [872-995 AD]) was extremely dry in particular, showing up as a raised plateau in the stable isotope record. The climate was wetter from 665-955 cal yr BP (995-1285 AD), but several smaller fluctuations within that wetter climate occurred (typically at intervals of 40-50 years). Finally, there was a marked, lasting trend towards a lengthy period of quite dry conditions that finished with an end to deposition on the stalagmite not long after 496 cal yr BP (1454 AD).

Comparison with Maya Cultural History

Much of the Late Classic period was a time of expanding population and cultural development among the Maya. The record from BZBT1 suggests that nearly the Late Classic and early Terminal Classic were neither wetter nor drier than average. During this period, major centers like Tikal, Caracol, and Calakmul either expanded or maintained their power, while several intermediate and frontier settlements rapidly developed (Chase et al., 2011; Houston and Inomata, 2009). Many of these frontier cities were located on less-than-ideal agricultural locations, such as the arid Vaca Plateau. Consistent rainfall would enable successful crop cultivation in areas too dry for productive farming in drier regimes. Stable rainfall would ensure dependable harvests, which in turn would help to fortify the power of any elite ruling class through a stable food supply. Stable governance would theoretically also allow for greater trade, an increased ability and motivation to defuse political crises through diplomatic means, and lessened reasons for small-scale conflict.

Partway through the Terminal Classic, the region entered a drier phase, coinciding with the abandonment of cities and cultural decline. Many cities were likely stable enough that drought stress on agriculture was not enough for wholesale destruction of the Maya Classic civilization, particularly in a region where drought occurs even during wetter periods. However, political, trade, and economic systems that were based on resource availability during wetter times were likely not well-adapted to operating in the new arid normal. The cumulative effect of decades of resource scarcity and political mismanagement likely proved overwhelming for many cities and leaders. Wars and skirmishes over resources would likely occur as rulers attempted to take advantage of weaker cities and stave off their own turmoil. Refugees would add additional pressures upon the increasingly few stable cities as people abandoned the marginal frontier settlements.

The climate remained dry for the first 100 years of the Postclassic Period. Several sites experienced a renaissance (Tikal) or florescence (Chichén Itzá, Seibal) after the initial Late Classic Maya decline of the Late and Terminal Classic. It would seem strange that if climate played a major role in the initial collapse that some sites would recover during equally dry conditions. Equally intriguing is that although the climate ameliorates to wetter conditions after 1000 AD, the Maya lowlands continue to remain depopulated (although several sites in the Yucatán continue to flourish). It appears likely that although droughts played a role in the initial Terminal Classic decline, other factors (likely political or social) prevented the return of the Classic Maya.

Comparison with Other Paleoenvironmental Records

The record from BZBT1 was compared with other paleoclimate records from around the world (Table 7.2) to explore similarities and teleconnections and displayed graphically in Figures 7.6 and 7.7 (NOAA Paleoclimatology Program (http://www.ncdc.noaa.gov/paleo/paleo.html)).

Table 7.2. Brief description of paleoclimate records compared with the BZBT1 record.

Site Name	**Site Location**	**Source Material**	**Proxy**	**Citation**
Cariaco Basin (Lea)	Caribbean Sea, Venezuela	Planktonic foraminifera	Sea surface temperatures	(Lea et al., 2003)
Cariaco Basin (Haug)	Caribbean Sea, Venezuela	Ocean sediment	Titanium concentration	(Haug et al., 2001)
Chilibrillo Cave	Panama	Stalagmite	$\delta^{18}O$, $\delta^{13}C$	(Lachniet et al., 2004b)
Huangye Cave	Gansu Province, China	Stalagmite	$\delta^{18}O$	(Tan et al., 2011)
Lake Chichancanab	Yucatán, Mexico	Lake sediment	Density	(Hodell et al., 2005)
Lake Punta Laguna	Yucatán, Mexico	Ostracod, gastropod	$\delta^{18}O$, $\delta^{13}C$	(Curtis et al., 1996)
Macal Chasm	Vaca Plateau, Belize	Stalagmite	Luminescence	(Webster et al., 2007)
Quelccaya Ice Cap	Peru	Ice core	Particle count	(Thompson and Mosley-Thompson, 1989)
Shihua Cave	Beijing, China	Stalagmite	Temperature anomaly	(Tan et al., 2003)
Spannagel Cave	Central Alps, Austria	Stalagmite	$\delta^{18}O$	(Mangini et al., 2005)
Tzabnah Cave	Yucatán, Mexico	Stalagmite	$\delta^{18}O$	(Medina-Elizalde et al., 2010)
Wanxiang Cave	Gansu Province, China	Stalagmite	$\delta^{18}O$	(Zhang et al., 2008)

The Chilibrillo Cave record (Lachniet et al., 2004b) suggests an arid period coinciding with the first arid period of BZBT1 during the late Terminal Classic and early Postclassic. Aside from a wet phase around 970 AD, the climate remains dry in the Chilibrillo record throughout the remainder of the Postclassic. Unfortunately, the Chilibrillo record ends prior to the onset of BZBT1's final arid period. Chilibrillo Cave is located on the Isthmus of Panama and may have a climate influenced by the Pacific Ocean to a greater degree than the general Maya homeland. The $\delta^{13}C$ record over the life of the Chilibrillo Cave record is unusual in that the oldest values are nearly equal to the $\delta^{18}O$ values but increase steadily over time until they are almost 4‰ higher

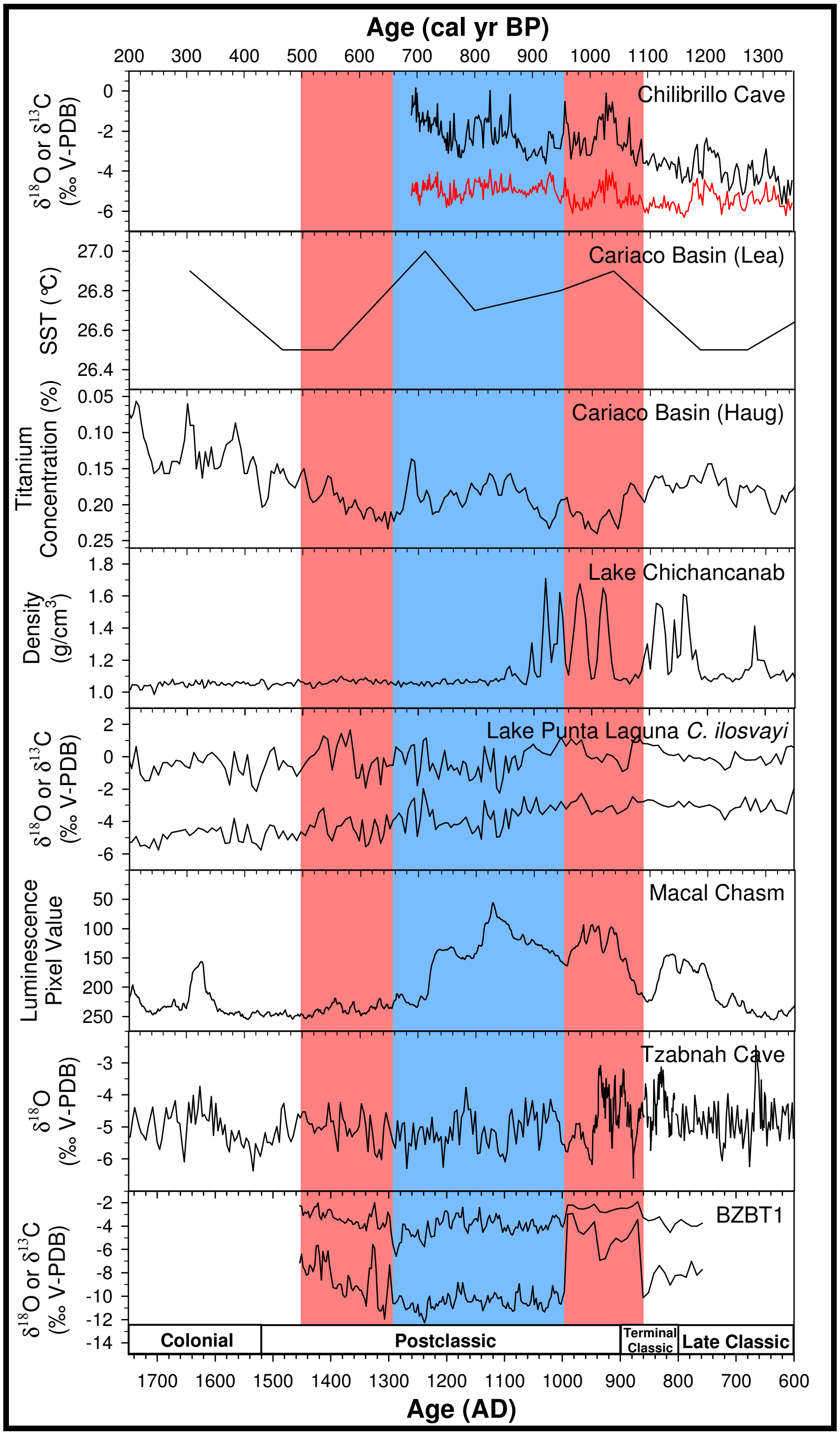

Figure 7.6. Paleoenvironmental records from Mesoamerica and nearby regions. Red zones correspond to drier periods in the BZBT1 record, while the blue zones correspond to wetter periods in the BZBT1 record. All records have been plotted so that peaks represent greater aridity.

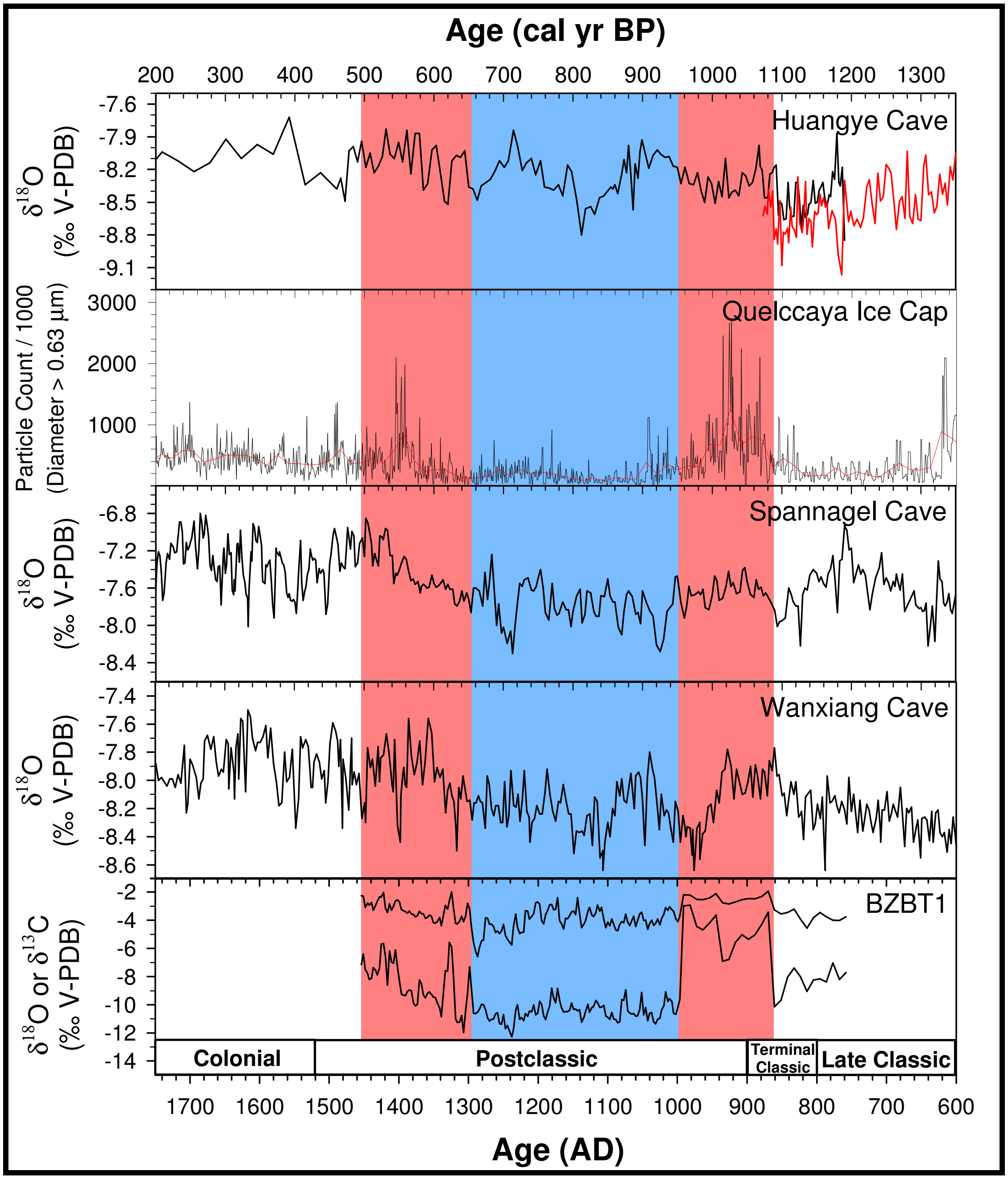

Figure 7.7. Paleoenvironmental records from other regions in the world (Spannagel Cave is in Austria, Quelccaya Ice Cap is in Peru, Wanxiang and Huangye Caves are in China) in comparison with the BZBT1 record. Red zones correspond to drier periods in the BZBT1 record, while the blue zones correspond to wetter periods in the BZBT1 record. All records have been plotted so that peaks represent greater aridity. Huangye Cave's record is derived from two stalagmites (one in black, other in red) and a running average of particle count (red line) has been overlain on the Quelccaya Ice Cap data.

than corresponding $\delta^{18}O$ values. As a result, Chilibrillo Cave may not be a strong record for comparison.

The two records from the Cariaco Basin correlate somewhat with the BZBT1 record. Although the sea surface temperature (SST) record of Lea et al. (2003) has low resolution, the wetter period of the Late Classic is associated with low SST, while the Terminal Classic and beginning of the Postclassic are associated with higher SST. The SST declines from 940-1150 AD, correlating with the beginning of BZBT1's wetter period. A local maximum in SST that occurs around 1250 AD has no comparable extreme in the BZBT1 record, and the final dry period of BZBT1 coincides with a rapid decline in SST. In the Haug et al. (2001) Cariaco Basin record, low titanium concentrations are indicative of drier times. This record indicates a drier interval in the Late and Terminal Classic that ends 80 years earlier first arid period in the BZBT1 record. Although much of the Postclassic appears drier in this record than in the BZBT1 record, the overall pattern of a steady increase in aridity toward 1500-1200 AD, followed by a steady decline toward 1300 AD can be found in both the Haug et al. (2001) Cariaco Basin record and BZBT1's $\delta^{18}O$ record. A steady increase in aridity from 1300 AD onward can also be found in both records.

Data from Lake Chichancanab, Lake Punta Laguna (*Cytheridella ilosvayi*-derived record), and Macal Chasm (Curtis et al., 1996; Hodell et al., 2005; Webster et al., 2007) all show a similar pattern of wet Late Classic, droughts occurring over much of the Terminal Classic, a return to wetter conditions, and finally an extended drought beginning in the Postclassic. The precise date of each climate transition varies between records, and all are slightly different than the BZBT1 record. These three data sets record a transition to the Terminal Classic dry interval within 25 years of 780 AD, prior to the intitiation of the BZBT1 record. The wet interval's central date varies the most: from 890 AD at Lake Chichancanab to 920 AD at Lake Punta Laguna to either 850 AD or 990 AD at Macal Chasm (the 850 AD date seems to match best, but there is a less pronounced wet interval is present at 990 AD, as well). The duration of the wet interval is fairly consistent across all records at 60-80 years. This wet period may exist in the BZBT1 record as either the lower stable isotope values prior to the first arid period or possibly the slight decrease in stable isotope values in the middle of the first arid period. The onset of the Postclassic droughts varies from 920-1000 AD, but all are relatively close to the first arid period of BZBT1.

The Tzabnah Cave record from Yucatán, Mexico (Medina-Elizalde et al., 2010) matches the BZBT1 record of a dry Postclassic Period beginning. The onset of a wetter period in the Postclassic is 60 years earlier than in the BZBT1 record. After a wet period that ends around 1000 AD, the Tzabnah Cave record fluctuates, but no clear wet or dry trends can be found.

Records from around the world offer insight into whether the climatic change from 800-1100 AD was limited to Mesoamerica or was worldwide (Figure 7.7). East Asian climate has been found to be linked to changes originating in the North Atlantic (Li et al., 2008); since the climate of Belize is heavily influence by the Atlantic, significant changes in Mesoamerican climate may also appear in Chinese records. Huangye Cave (Tan et al., 2011) in Gansu Province, China, suggests a dry late Terminal Classic beginning at nearly the same time at the start of the first BZBT1 arid period. The rest of the Postclassic shows much greater $\delta^{18}O$ variability than the BZBT1 record. The Wanxiang Cave record (Zhang et al., 2008), also from Gansu Province, China, matches with very well with BZBT1's record. An arid period for Wanxiang cave begins and ends ~50 earlier than the first BZBT1 record, but appears to be of a similar duration. A wetter middle Postclassic transitions to a drier period around 1350 AD in a pattern analogous to BZBT1's record.

The Spannagel Cave record (Mangini et al., 2005) from the Central Alps of Austria does not show an extremely dry period at the beginning of the Postclassic, but the record beginning 1250 AD is very similar to the BZBT1 record. Both records show a wet anomaly at 1250 AD followed by a sharp spike to a short-lived very dry period. Both records then show increasing aridity from 1300-1450 AD. Finally, the Quelccaya Ice Cap record may show the greatest correlation to the BZBT1 record. An extended period of high particle counts in found within the first dry period of BZBT1 before dropping to low levels (indicating less dry conditions) for much of the Postclassic. Another period of high particle counts occurs within the last BZBT1 dry period, although the largest peak occurs 100 years after the clear double spike present in the BZBT1 stable isotope records.

The comparison with all the other paleoclimate record offers mixed, but generally supportive insight into both the validity of the BZBT1 chronology and the wider regional and worldwide climate from 700-1500 AD. The best agreement amongst the records is during the first BZBT1 dry period from 870-1000 AD; all the records show evidence of drier conditions within 100 years of this interval. Some records (Haug's Cariaco record, Tzabnah Cave, Wanxiang Cave) show this dry period beginning and ending earlier than BZBT1's record, while others (Lake Chichancanab, Macal Chasm, Lake Punta Laguna) show evidence of this dry period lasting later than the BZBT1 record suggests. The gradual increasing aridity found in BZBT1's final dry period has analogs in a few records, although the peak aridity often occurs around 100 years later in the other records than the BZBT1 record. The intervening time (identified as a wetter period in the BZBT1 record) is usually uneventful in the other paleorecords and does not provide a strong argument for or against correlation with the BZBT1 record.

Overall, the chronology chosen for BZBT1 is believed to be supported by comparison with other regional and worldwide paleorecords. Although the BZBT1 record does not always perfectly agree with the other records, it should be understood that the other paleorecords often do not agree well with each other either. The BZBT1 paleoclimate record often occupies a middle ground between the other conflicting paleoclimate records, suggesting that chronology chosen for BZBT1 is accurate and close to reality.

CHAPTER 8
CONCLUSIONS

A 92 mm stalagmite from the Cayo District of Belize (BZBT1) has provided a paleoclimate record spanning 695 years. Although uranium-series dating proved difficult because of low uranium concentrations, it was possible to develop a reliable chronology by dating both organic material trapped in the stalagmite and calcium carbonate using the AMS radiocarbon method. After the chronology was adjusted to account for organic residence time, the period of growth was dated to 495-1190 cal yr BP (760-1455 AD). Six climatic proxies were measured and analyzed to produce a paleoclimatic record: reflectance, ultraviolet-stimulated luminescence, $\delta^{18}O$, $\delta^{13}C$, trace element concentrations, and petrographic characteristics. These proxies reveal major changes in precipitation amount during the deposition of the stalagmite BZBT1.

Three periods of wetter or drier climate have been identified: the dry periods from 955-1080 cal yr BP (870-995 AD) and 495-665 cal yr BP (1285-1455 AD) and an intervening wet period from 665-955 cal yr BP (995-1285 AD). Within each of these climate periods, there were smaller-scale variations indicating several individual droughts alternating with wetter periods. Stalagmite BZBT1 was being deposited during end of the Classic Period and continuing through much of the Postclassic Period of the Maya civilization, including the decline and abandonment of the Classic Maya cities and culture towards the end of the Classic Period.

The Late Classic through Postclassic was a time of shifting climate in Mesoamerica. The pattern of dry-wet-dry periods noted in BZBT1 appears in many records not only from Mesoamerica, but also around the world. The exact onset and duration of each of these periods varies from record to record, but this is not unexpected with spatially-diverse records. Although the climate across Mesoamerica had a general dry-wet-dry trend, local conditions no doubt would have varied greatly within the overall trend. Local variations in climate can help to explain why some Maya cities were able to prosper while other cities were abandoned during the Late Classic. The Late Classic florescence of Maya culture occurred during a time of wetter conditions, but a shift to drier conditions during the Terminal Classic and early Postclassic would have greatly strained a population accustomed to more rainfall.

Due to the porous limestone bedrock, many Maya sites were entirely dependent upon rainwater for daily water use and agriculture; a shortage in water supply could provoke instability within many cities and regions. The Terminal Classic decline noted in Maya archaeology coincides with an overall drier climate and several individual droughts. Climate is likely not to have been the sole factor of the Maya collapse, but it surely played a major antagonizing or perhaps even instigating role in the initial decline of the Classic Maya civilization.

REFERENCES

Acuna-Soto, R., Stahle, D.W., Therrell, M.D., Chavez, S.G., and Cleaveland, M.K., 2005, Drought, epidemic disease, and the fall of classic period cultures in Mesoamerica (AD 750-950). Hemorrhagic fevers as a cause of massive population loss: Medical Hypotheses, v. 65, p. 405-409.

Aimers, J.J., 2007, What Maya collapse? Terminal classic variation in the Maya lowlands: Journal of Archaeological Research, v. 15, p. 329-377.

Arz, H.W., Lamy, F., and Patzold, J., 2006, A pronounced dry event recorded around 4.2 ka in brine sediments from the northern Red Sea: Quaternary Research, v. 66, p. 432-441.

Baker, A., Barnes, W.L., and Smart, P.L., 1996, Speleothem luminescence intensity and spectral characteristics: Signal calibration and a record of palaeovegetation change: Chemical Geology, v. 130, p. 65-76.

Baker, A., Genty, D., and Smart, P.L., 1998, High-resolution records of soil humification and paleoclimate change from variations in speleothem luminescence excitation and emission wavelengths: Geology, v. 26, p. 903-906.

Baldini, J.U.L., McDermott, F., Baker, A., Baldini, L.M., Mattey, D.P., and Railsback, L.B., 2005, Biomass effects on stalagmite growth and isotope ratios: A 20th century analogue from Wiltshire, England: Earth and Planetary Science Letters, v. 240, p. 486-494.

Bar-Matthews, M., Ayalon, A., Kaufman, A., and Wasserburg, G.J., 1999, The Eastern Mediterranean paleoclimate as a reflection of regional events: Soreq cave, Israel: Earth and Planetary Science Letters, v. 166, p. 85-95.

Beach, T., Luzzadder-Beach, S., Dunning, N., and Cook, D., 2008, Human and natural impacts on fluvial and karst depressions of the Maya Lowlands: Geomorphology, v. 101, p. 308-331.

Bender, M.M., 1971, Variations in the 13C/12C ratios of plants in relation to the pathway of photosynthetic carbon dioxide fixation: Phytochemistry, v. 10, p. 1239-1244.

Brenner, M., Hodell, D.A., Curtis, J.H., Rosenmeier, M.F., Anselmetti, F.S., and Ariztegui, D., 2003, Paleolimnological Approaches for Inferring Past Climate Change in the Maya Region: Recent Advances and Methodological Limitations, *in* Gómez-Pompa, A., Allen, M.F., Fedick, S.L., and Jiménez-Osornio, J.J., eds., The Lowland Maya Area: Three Millennia at the Human-Wildland Interface: Binghampton, NY, The Haworth Press, Inc., p. 45-75.

Brook, G.A., 1999, Arid zone paleoenvironmental records from cave speleothems, *in* Singhvi, A.K., Derbyshire, E., ed., Paleoenvironmental Reconstruction in Arid Lands: New Delhi, Oxford & IBH Publishing Co. Pvt. Ltd., p. 217-262.

Brook, G.A., Burney, D.A., and Cowart, J.B., 1990, Desert paleoenvironmental data from cave speleothems with examples from the Chihuahuan, Somali-Chalbi, and Kalahari deserts: Palaeogeography Palaeoclimatology Palaeoecology, v. 76, p. 311-329.

Brook, G.A., and Nickmann, R.J., 1996, Evidence of late Quaternary environments in northwestern Georgia from sediments preserved in Red Spider Cave: Physical Geography, v. 17, p. 465-484.

Burton, E.A., and Walter, L.M., 1987, Relative precipitation rates of aragonite and Mg calcite from seawater - temperature or carbonate ion control: Geology, v. 15, p. 111-114.

Carrion, J.S., 2002, Patterns and processes of Late Quaternary environmental change in a montane region of southwestern Europe: Quaternary Science Reviews, v. 21, p. 2047-2066.

Chase, A.F., Chase, D.Z., Weishampel, J.F., Drake, J.B., Shrestha, R.L., Slatton, K.C., Awe, J.J., and Carter, W.E., 2011, Airborne LiDAR, archaeology, and the ancient Maya landscape at Caracol, Belize: Journal of Archaeological Science, v. 38, p. 387-398.

Cheng, H., Edwards, R.L., Hoff, J., Gallup, C.D., Richards, D.A., and Asmerom, Y., 2000, The half-lives of uranium-234 and thorium-230: Chemical Geology, v. 169, p. 17-33.

Cullen, H.M., deMenocal, P.B., Hemming, S., Hemming, G., Brown, F.H., Guilderson, T., and Sirocko, F., 2000, Climate change and the collapse of the Akkadian empire: Evidence from the deep sea: Geology, v. 28, p. 379-382.

Curtis, J.H., Hodell, D.A., and Brenner, M., 1996, Climate variability on the Yucatan Peninsula (Mexico) during the past 3500 years, and implications for Maya Cultural Evolution: Quaternary Research, v. 46, p. 37-47.

Demarest, A.A., Rice, P.M., and Rice, D.S., 2004, The Terminal Classic in the Maya Lowlands:Collapse, Transition, and Transformation: Boulder, University Press of Colorado.

deMenocal, P.B., 2001, Cultural responses to climate change during the Late Holocene: Science, v. 292, p. 667-673.

Desmarchelier, J.M., Hellstrom, J.C., and McCulloch, M.T., 2006, Rapid trace element analysis of speleothems by ELA-ICP-MS: Chemical Geology, v. 231, p. 102-117.

Diamond, J., 2005, Collapse: How Societies Choose to Fail or Succeed: New York, Viking.

Domínguez-Vázquez, G., and Islebe, G.A., 2008, Protracted drought during the late Holocene in the Lacandon rain forest, Mexico: Vegetation History and Archaeobotany, v. 17, p. 327-333.

Drysdale, R., Zanchetta, G., Hellstrom, J., Maas, R., Fallick, A., Pickett, M., Cartwright, I., and Piccini, L., 2006, Late Holocene drought responsible for the collapse of Old World civilizations is recorded in an Italian cave flowstone: Geology, v. 34, p. 101-104.

Emery, K.F., 2007, Assessing the impact of ancient Maya animal use: Journal for Nature Conservation, v. 15, p. 184-195.

—, 2008, A Zooarchaeological Test for Dietary Resource Depression at the End of the Classic Period in the Petexbatun, Guatemala: Human Ecology, v. 36, p. 617-634.

Emery, K.F., and Thornton, E.K., 2008, A regional perspective on biotic change during the Classic Maya occupation using zooarchaeological isotopic chemistry: Quaternary International, v. 191, p. 131-143.

Fairchild, I.J., and Treble, P.C., 2009, Trace elements in speleothems as recorders of environmental change: Quaternary Science Reviews, v. 28, p. 449-468.

Faust, A., and Ashkenazy, Y., 2007, Excess in precipitation as a cause for settlement decline along the Israeli coastal plain during the third millennium BC: Quaternary Research, v. 68, p. 37-44.

Fedick, S.L., 2010, The Maya Forest: Destroyed or cultivated by the ancient Maya?: Proceedings of the National Academy of Sciences, v. 107, p. 953-954.

Fleitmann, D., Burns, S.J., Neff, U., Mangini, A., and Matter, A., 2003, Changing moisture sources over the last 330,000 years in Northern Oman from fluid-inclusion evidence in speleothems: Quaternary Research, v. 60, p. 223-232.

Frisia, S., Borsato, A., Fairchild, I.J., McDermott, F., and Selmo, E.M., 2002, Aragonite-calcite relationships in speleothems (Grotte de Clamouse, France): Environment, fabrics, and carbonate geochemistry: Journal of Sedimentary Research, v. 72, p. 687-699.

Furley, P.A., and Newey, W.W., 1979, Variations in plant-communities with topography over tropical limestone soils: Journal of Biogeography, v. 6, p. 1-15.

Gill, R.B., Mayewski, P.A., Nyberg, J., Haug, G.H., and Peterson, L.C., 2007, Drought and the Maya collapse: Ancient Mesoamerica, v. 18, p. 283-302.

Gischler, E., Shinn, E.A., Oschmann, W., Fiebig, J., and Buster, N.A., 2008, A 1500-Year Holocene Caribbean Climate Archive from the Blue Hole, Lighthouse Reef, Belize: Journal of Coastal Research, v. 24, p. 1495-1505.

Haug, G.H., Gunther, D., Peterson, L.C., Sigman, D.M., Hughen, K.A., and Aeschlimann, B., 2003, Climate and the collapse of Maya civilization: Science, v. 299, p. 1731-1735.

Haug, G.H., Hughen, K.A., Sigman, D.M., Peterson, L.C., and Röhl, U., 2001, Southward Migration of the Intertropical Convergence Zone Through the Holocene: Science, v. 293, p. 1304-1308.

Hesterberg, R., and Siegenthaler, U., 1991, Production and stable isotopic composition of CO2 in a soil near Bern, Switzerland: Tellus B, v. 43, p. 197-205.

Hodell, D.A., Brenner, M., and Curtis, J.H., 2005, Terminal Classic drought in the northern Maya lowlands inferred from multiple sediment cores in Lake Chichancanab (Mexico): Quaternary Science Reviews, v. 24, p. 1413-1427.

—, 2007, Climate and cultural history of the northeastern Yucatan Peninsula, Quintana Roo, Mexico: Climatic Change, v. 83, p. 215-240.

Hodell, D.A., and Curtis, J.H., 1995, Possible role of climate in the collapse of classic Maya civilization.: Nature, v. 375, p. 391.

Houston, S.D., and Inomata, T., 2009, The Classic Maya: New York, NY, Cambridge University Press.

Huang, H.M., Fairchild, I.J., Borsato, A., Frisia, S., Cassidy, N.J., McDermott, F., and Hawkesworth, C.J., 2001, Seasonal variations in Sr, Mg and P in modern speleothems (Grotta di Ernesto, Italy): Chemical Geology, v. 175, p. 429-448.

Huffman, G., Bolvin, D., Nelkin, E., Wolff, D., Adler, R., Gu, G., Hong, Y., Bowman, K., and Stocker, E., 2007, The TRMM Multisatellite Precipitation Analysis (TMPA): Quasi-Global, Multiyear, Combined-Sensor Precipitation Estimates at Fine Scales: Journal of Hydrometeorology, v. 8, p. 38-55.

IAEA/WMO, 2006, Global Network of Isotopes in Precipitation. The GNIP Database: http://www.iaea.org/water.

Iannone, G., 2005, The rise and fall of an ancient Maya petty royal court: Latin American Antiquity, v. 16, p. 26-44.

Inomata, T., Ponciano, E., Chinchilla, O., Roman, O., Breuil-Martinez, V., and Santos, O., 2004, An unfinished temple at the Classic Maya Centre of Aguateca, Guatemala: Antiquity, v. 78, p. 798-811.

Kaniewski, D., Paulissen, E., Van Campo, E., Al-Maqdissi, M., Bretschneider, J., and Van Lerberghe, K., 2008, Middle East coastal ecosystem response to middle-to-late Holocene abrupt climate changes: Proceedings of the National Academy of Sciences of the United States of America, v. 105, p. 13941-13946.

Kipfer, R., Aeschbach-Hertig, W., Peeters, F., and Stute, M., 2002, Noble Gases in Lakes and Ground Waters: Reviews in Mineralogy and Geochemistry, v. 47, p. 615-700.

Kummerow, C., Barnes, W., Kozu, T., Shiue, J., and Simpson, J., 1998, The Tropical Rainfall Measuring Mission (TRMM) Sensor Package: Journal of Atmospheric and Oceanic Technology, v. 15, p. 809-817.

Lachniet, M.S., 2009, Climatic and environmental controls on speleothem oxygen-isotope values: Quaternary Science Reviews, v. 28, p. 412-432.

Lachniet, M.S., Asmerom, Y., Burns, S.J., Patterson, W.P., Polyak, V.J., and Seltzer, G.O., 2004a, Tropical response to the 8200 yr BP cold event? Speleothem isotopes indicate a weakened early Holocene monsoon in Costa Rica: Geology, v. 32, p. 957-960.

Lachniet, M.S., Burns, S.J., Piperno, D.R., Asmerom, Y., Polyak, V.J., Moy, C.M., and Christenson, K., 2004b, A 1500-year El Nino/Southern Oscillation and rainfall history for the Isthmus of Panama from speleothem calcite: Journal of Geophysical Research-Atmospheres, v. 109.

Lambert, W.J., and Aharon, P., 2011, Controls on dissolved inorganic carbon and [delta]13C in cave waters from DeSoto Caverns: Implications for speleothem [delta]13C assessments: Geochimica et Cosmochimica Acta, v. 75, p. 753-768.

Lauritzen, S.-E., 2005, Reconstructing Holocene Climate Records from Speleothems, *in* Mackay, A., Battarbee, R., Birks, J., and Oldfield, F., eds., Global Change in the Holocene: London, Arnold, p. 242-263.

Lea, D.W., Pak, D.K., Peterson, L.C., and Hughen, K.A., 2003, Synchroneity of Tropical and High-Latitude Atlantic Temperatures over the Last Glacial Termination: Science, v. 301, p. 1361-1364.

LeCount, L.J., and Yaeger, J., 2010, Classic Maya Provincial Politics: Xunantunich and its Hinterlands: Tucson, University of Arizona Press.

Leyden, B.W., Brenner, M., and Dahlin, B.H., 1998, Cultural and climatic history of Coba, a lowland Maya city in Quintana Roo, Mexico: Quaternary Research, v. 49, p. 111-122.

Li, J., Yu, R., and Zhou, T., 2008, Teleconnection between NAO and Climate Downstream of the Tibetan Plateau: Journal of Climate, v. 21, p. 4680-4690.

Lucero, L.J., 2002, The collapse of the Classic Maya: A case for the role of water control: American Anthropologist, v. 104, p. 814-826.

Magaña, V., Amador, J.A., and Medina, S., 1999, The midsummer drought over Mexico and Central America: Journal of Climate, v. 12, p. 1577.

Magny, M., Vanniere, B., Zanchetta, G., Fouache, E., Touchais, G., Petrika, L., Coussot, C., Walter-Simonnet, A.V., and Arnaud, F., 2009, Possible complexity of the climatic event around 4300-3800 cal. BP in the central and western Mediterranean: Holocene, v. 19, p. 823-833.

Mangini, A., Spötl, C., and Verdes, P., 2005, Reconstruction of temperature in the Central Alps during the past 2000 yr from a $\delta^{18}O$ stalagmite record: Earth and Planetary Science Letters, v. 235, p. 741-751.

Marcus, J., 2003, Recent advances in Maya archaeology: Journal of Archaeological Research, v. 11, p. 71-148.

Marr, J.S., and Kiracofe, J.B., 2000, Was the huey cocoliztli a haemorrhagic fever?: Medical History, v. 44, p. 341-362.

McDermott, F., 2004, Palaeo-climate reconstruction from stable isotope variations in speleothems: a review: Quaternary Science Reviews, v. 23, p. 901-918.

McGarry, S.F., and Baker, A., 2000, Organic acid fluorescence: applications to speleothem palaeoenvironmental reconstruction: Quaternary Science Reviews, v. 19, p. 1087-1101.

McGarry, S.F., and Caseldine, C., 2004, Speleothem palynology: an undervalued tool in Quaternary studies: Quaternary Science Reviews, v. 23, p. 2389-2404.

McNeil, C.L., Burney, D.A., and Burney, L.P., 2010, Evidence disputing deforestation as the cause for the collapse of the ancient Maya polity of Copan, Honduras: Proceedings of the National Academy of Sciences, v. 107, p. 1017-1022.

Medina-Elizalde, M., Burns, S.J., Lea, D.W., Asmerom, Y., von Gunten, L., Polyak, V., Vuille, M., and Karmalkar, A., 2010, High resolution stalagmite climate record from the Yucatán

Peninsula spanning the Maya terminal classic period: Earth and Planetary Science Letters, v. 298, p. 255-262.
Moberg, A., Sonechkin, D.M., Holmgren, K., Datsenko, N.M., KarlÃ©n, W.r., and Lauritzen, S.-E., 2005, Highly variable Northern Hemisphere temperatures reconstructed from low- and high-resolution proxy data: Nature, v. 433, p. 613-617.
Morse, J.W., Wang, Q.W., and Tsio, M.Y., 1997, Influences of temperature and Mg:Ca ratio on CaCO3 precipitates from seawater: Geology, v. 25, p. 85-87.
Murray, J.W., 1954, The deposition of calcite and aragonite in caves: Journal of Geology, v. 62.
Neff, H., Pearsall, D.M., Jones, J.G., de Pieters, B.A., and Freidel, D.E., 2006, Climate change and population history in the Pacific Lowlands of Southern Mesoamerica: Quaternary Research, v. 65, p. 390-400.
Pablo Bernal, J., Lachniet, M., McCulloch, M., Mortimer, G., Morales, P., and Cienfuegos, E., 2011, A speleothem record of Holocene climate variability from southwestern Mexico: Quaternary Research, v. 75, p. 104-113.
Penn, M.G., Sutton, D.A., and Monro, A., 2004, Vegetation of the Greater Maya Mountains, Belize: Systematics and Biodiversity, v. 2, p. 21-44.
Perrette, Y., Delannoy, J.-J., Bolvin, H., Cordonnier, M., Destombes, J.-L., Zhilinskaya, E.A., and Aboukais, A., 2000, Comparative study of a stalagmite sample by stratigraphy, laser induced fluorescence spectroscopy, EPR spectrometry and reflectance imaging: Chemical Geology, v. 162, p. 221-243.
Polk, J.S., van Beynen, P.E., and Reeder, P.P., 2007, Late Holocene environmental reconstruction using cave sediments from Belize: Quaternary Research, v. 68, p. 53-63.
Proskouriakoff, T., 1993, Maya History: Austin, TX, University of Texas Press.
Railsback, L., 1999, Patterns in the compositions, properties, and geochemistry of carbonate minerals: Carbonates and Evaporites, v. 14, p. 1-20.
Railsback, L.B., Brook, G.A., Chen, J., Kalin, R., and Fleisher, C.J., 1994, Environmental controls on the petrology of a late Holocene speleothem from Botswana with annual layers of aragonite and calcite: Journal of Sedimentary Research Section a-Sedimentary Petrology and Processes, v. 64, p. 147-155.
Railsback, L.B., Brook, G.A., and Webster, J.W., 1999, Petrology and paleoenvironmental significance of detrital sand and silt in a stalagmite from Drotsky's Cave, Botswana: Physical Geography, v. 20, p. 331-347.
Railsback, L.B., Liang, F., Vidal Romaní, J.R., Grandal-d'Anglade, A., Vaqueiro Rodríguez, M., Santos Fidalgo, L., Fernández Mosquera, D., Cheng, H., and Edwards, R.L., 2011, Petrographic and isotopic evidence for Holocene long-term climate change and shorter-term environmental shifts from a stalagmite from the Serra do Courel of northwestern Spain, and implications for climatic history across Europe and the Mediterranean: Palaeogeography, Palaeoclimatology, Palaeoecology, v. 305, p. 172-184.
Reeder, P., Brinkmann, R., and Alt, E., 1996, Karstification on the Northern Vaca Plateau, Belize: Journal of Cave and Karst Studies, v. 58, p. 121-130.
Roberts, M.S., Smart, P.L., and Baker, A., 1998, Annual trace element variations in a Holocene speleothem: Earth and Planetary Science Letters, v. 154, p. 237-246.
Ross, N.J., 2011, Modern tree species composition reflects ancient Maya "forest gardens" in northwest Belize: Ecological Applications, v. 21, p. 75-84.
Rozanski, K., Araguas-Araguas, L, Gonfiantini, R, 1993, Isotopic patterns of modern global precipitation, *in* Swart PK, L.K., McKenzie J, Savin S, ed., Climate change in continental isotopic records: Washington, District of Columbia, American Geophyscial Union, p. 1-36.

Scarborough, V.L., and Gallopin, G.G., 1991, A water storage adaptation in the Maya lowlands: Science, v. 251, p. 658-662.
Shang, C., and Tiessen, H., 1997, Organic Matter Lability in A Tropical Oxisol: Evidence From Shifting Cultivation, Chemical Oxidation, Particle Size, Density, and Magnetic Fractionations: Soil Science, v. 162, p. 795-807.
Shopov, Y.Y., Ford, D.C., and Schwarcz, H.P., 1994, Luminescent microbanding in speleothems: High-resolution chronology and paleoclimate: Geology, v. 22, p. 407-410.
Silverstein, J.E., Webster, D., Martinez, H., and Soto, A., 2009, Rethinking the great earthwork of Tikal: a hydraulic hypothesis for the classic Maya polity: Ancient Mesoamerica, v. 20, p. 45-58.
Solleiro, E., Sedov, S., Macias, J.L., and Pi, T., 2007, Late holocene paleopedological records contained in tephra from El Chichon volcano, Chiapas, Mexico: Catena, v. 71, p. 444-455.
Stahle, D.W., Diaz, J.V., Burnette, D.J., Paredes, J.C., Heim, R.R., Fye, F.K., Soto, R.A., Therrell, M.D., Cleaveland, M.K., and Stahle, D.K., 2011, Major Mesoamerican droughts of the past millennium: Geophysical Research Letters, v. 38.
Stanley, J.D., Krom, M.D., Cliff, R.A., and Woodward, J.C., 2003, Short contribution: Nile flow failure at the end of the old kingdom, Egypt: Strontium isotopic and petrologic evidence: Geoarchaeology-an International Journal, v. 18, p. 395-402.
Tan, L., Cai, Y., An, Z., Edwards, R.L., Cheng, H., Shen, C.-C., and Zhang, H., 2011, Centennial-to decadal-scale monsoon precipitation variability in the semi-humid region, northern China during the last 1860 years: Records from stalagmites in Huangye Cave: Holocene, v. 21, p. 287-296.
Tan, M., Liu, T.S., Hou, J.Z., Qin, X.G., Zhang, H.C., and Li, T.Y., 2003, Cyclic rapid warming on centennial-scale revealed by a 2650-year stalagmite record of warm season temperature: Geophysical Research Letters, v. 30.
Thompson, L., and Mosley-Thompson, E., 1989, One-half millenia of tropical climate variability as record in the stratigraphy of the Quelccaya Ice Cap, Per: American Geophysical Union, v. Geophysical Monograph 55.
Verheyden, S., 2004, Trace elements in speleothems: a short review of the state of the art: International Journal of Speleology, v. 33, p. 95-101.
Vogel, J.C., 1980, Fractionation of the Carbon Isotopes During Photosynthesis: Berlin, Springer-Verlag.
Vogel, J.S., Southon, J.R., Nelson, D.E., and Brown, T.A., 1984, Performance of catalytically condensed carbon for use in accelerator mass spectrometry: Nuclear Instruments and Methods in Physics Research Section B: Beam Interactions with Materials and Atoms, v. 5, p. 289-293.
Webb, E.A., Schwarcz, H.P., and Healy, P.F., 2004, Detection of ancient maize in lowland Maya soils using stable carbon isotopes: evidence from Caracol, Belize: Journal of Archaeological Science, v. 31, p. 1039-1052.
Webster, D., 2000, The not so peaceful civilization: A review of Maya war: Journal of World Prehistory, v. 14, p. 65-119.
—, 2007, The uses and abuses of the ancient Maya, The Emergence of the Modern World Conference Otzenhausen, Germany : Organizers Jared Diamond and James Robinson
Webster, J.W., Brook, G.A., Railsback, L.B., Cheng, H., Edwards, R.L., Alexander, C., and Reeder, P.P., 2007, Stalagmite evidence from Belize indicating significant droughts at the time of Preclassic Abandonment, the Maya Hiatus, and the Classic Maya collapse: Palaeogeography Palaeoclimatology Palaeoecology, v. 250, p. 1-17.

Zhang, P., Cheng, H., Edwards, R.L., Chen, F., Wang, Y., Yang, X., Liu, J., Tan, M., Wang, X., Liu, J., An, C., Dai, Z., Zhou, J., Zhang, D., Jia, J., Jin, L., and Johnson, K.R., 2008, A Test of Climate, Sun, and Culture Relationships from an 1810-Year Chinese Cave Record: Science, v. 322, p. 940-942.

Zielhofer, C., and Faust, D., 2008, Mid- and late Holocene fluvial chronology of Tunisia: Quaternary Science Reviews, v. 27, p. 580-588.

APPENDIX 1

REFLECTANCE DATA

Distance (mm)	Age (cal yr BP)	Grayscale Pixel Value
0.000	N/A	45.14
0.021	N/A	45.57
0.041	N/A	46.57
0.062	N/A	44.86
0.082	N/A	43.43
0.103	N/A	45.14
0.123	N/A	46.57
0.144	N/A	48.00
0.164	N/A	52.71
0.185	N/A	56.43
0.206	N/A	56.57
0.226	N/A	57.00
0.247	N/A	56.00
0.267	N/A	58.00
0.288	N/A	61.29
0.308	N/A	61.14
0.329	N/A	58.43
0.350	N/A	58.14
0.370	N/A	58.14
0.391	N/A	58.57
0.411	N/A	57.86
0.432	N/A	60.00
0.452	N/A	62.14
0.473	N/A	62.00
0.493	N/A	64.43
0.514	N/A	65.29
0.535	N/A	64.00
0.555	N/A	64.00
0.576	N/A	62.29
0.596	N/A	61.71
0.617	N/A	60.86
0.637	N/A	59.43
0.658	N/A	57.86
0.679	N/A	54.00

0.699	N/A	50.14
0.720	N/A	47.43
0.740	N/A	48.00
0.761	N/A	49.00
0.781	N/A	50.00
0.802	N/A	51.43
0.822	N/A	51.43
0.843	N/A	50.00
0.864	N/A	47.14
0.884	N/A	46.00
0.905	N/A	43.43
0.925	N/A	42.29
0.946	N/A	40.29
0.966	N/A	36.86
0.987	N/A	34.86
1.007	496.31	34.86
1.028	496.43	35.00
1.049	496.55	34.86
1.069	496.67	35.00
1.090	496.79	35.43
1.110	496.91	38.14
1.131	497.03	38.43
1.151	497.15	38.86
1.172	497.27	40.57
1.193	497.39	44.29
1.213	497.51	47.00
1.234	497.63	48.71
1.254	497.75	49.57
1.275	497.87	49.71
1.295	497.99	50.00
1.316	498.11	50.29
1.336	498.23	50.00
1.357	498.35	50.86
1.378	498.47	52.29
1.398	498.59	52.71
1.419	498.71	53.71
1.439	498.83	55.29
1.460	498.95	56.14
1.480	499.07	58.43
1.501	499.19	59.29
1.521	499.31	58.71

1.542	499.43	58.00
1.563	499.55	58.00
1.583	499.67	58.57
1.604	499.79	59.14
1.624	499.91	60.86
1.645	500.03	63.57
1.665	500.15	66.43
1.686	500.27	68.43
1.707	500.39	70.29
1.727	500.51	72.14
1.748	500.63	72.86
1.768	500.75	73.71
1.789	500.88	76.14
1.809	501.00	78.43
1.830	501.12	79.71
1.850	501.24	81.71
1.871	501.36	83.29
1.892	501.48	81.57
1.912	501.60	82.14
1.933	501.72	83.43
1.953	501.84	83.00
1.974	501.96	83.14
1.994	502.08	82.29
2.015	502.20	83.00
2.036	502.32	83.57
2.056	502.44	83.14
2.077	502.56	82.14
2.097	502.68	83.00
2.118	502.80	83.43
2.138	502.92	84.86
2.159	503.04	88.29
2.179	503.16	89.86
2.200	503.28	90.14
2.221	503.40	90.00
2.241	503.52	93.71
2.262	503.64	97.43
2.282	503.76	105.00
2.303	503.88	111.43
2.323	504.00	111.43
2.344	504.12	112.43
2.364	504.24	112.43

2.385	504.36	116.00
2.406	504.48	127.43
2.426	504.60	141.14
2.447	504.72	143.29
2.467	504.84	143.00
2.488	504.96	138.86
2.508	505.08	141.71
2.529	505.20	143.57
2.550	505.32	141.57
2.570	505.44	142.29
2.591	505.56	145.57
2.611	505.68	148.00
2.632	505.80	149.29
2.652	505.92	149.43
2.673	506.04	145.43
2.693	506.16	144.00
2.714	506.28	142.86
2.735	506.40	142.86
2.755	506.52	143.71
2.776	506.64	143.57
2.796	506.76	143.14
2.817	506.88	143.57
2.837	507.00	147.71
2.858	507.12	147.57
2.879	507.24	148.71
2.899	507.36	150.14
2.920	507.48	152.71
2.940	507.60	155.71
2.961	507.72	154.86
2.981	507.84	152.71
3.002	507.96	154.86
3.022	508.08	151.86
3.043	508.20	152.57
3.064	508.32	152.86
3.084	508.44	152.57
3.105	508.56	153.43
3.125	508.68	153.00
3.146	508.81	152.86
3.166	508.93	152.14
3.187	509.05	150.57
3.207	509.17	149.71

3.228	509.29	149.43
3.249	509.41	148.86
3.269	509.53	147.29
3.290	509.65	148.71
3.310	509.77	147.14
3.331	509.89	145.43
3.351	510.01	142.00
3.372	510.13	139.43
3.393	510.25	136.43
3.413	510.37	132.86
3.434	510.49	132.86
3.454	510.61	133.14
3.475	510.73	135.00
3.495	510.85	134.29
3.516	510.97	134.86
3.536	511.09	133.71
3.557	511.21	130.43
3.578	511.33	128.86
3.598	511.45	126.29
3.619	511.57	120.86
3.639	511.69	116.43
3.660	511.81	112.14
3.680	511.93	109.29
3.701	512.05	108.57
3.721	512.17	104.00
3.742	512.29	102.71
3.763	512.41	100.43
3.783	512.53	100.00
3.804	512.65	100.86
3.824	512.77	101.57
3.845	512.89	103.43
3.865	513.01	106.71
3.886	513.13	107.57
3.907	513.25	111.57
3.927	513.37	114.71
3.948	513.49	117.00
3.968	513.61	118.43
3.989	513.73	118.86
4.009	513.85	122.57
4.030	513.97	126.00
4.050	514.09	125.71

4.071	514.21	126.29
4.092	514.33	129.00
4.112	514.45	129.86
4.133	514.57	130.57
4.153	514.69	134.14
4.174	514.81	133.86
4.194	514.93	134.29
4.215	515.05	137.00
4.236	515.17	136.86
4.256	515.29	136.86
4.277	515.41	137.43
4.297	515.53	136.43
4.318	515.65	134.71
4.338	515.77	135.29
4.359	515.89	134.57
4.379	516.01	129.57
4.400	516.13	123.57
4.421	516.25	118.86
4.441	516.37	117.86
4.462	516.49	116.86
4.482	516.62	117.86
4.503	516.74	119.14
4.523	516.86	122.00
4.544	516.98	126.57
4.564	517.10	127.86
4.585	517.22	131.43
4.606	517.34	132.14
4.626	517.46	133.14
4.647	517.58	134.71
4.667	517.70	136.57
4.688	517.82	139.57
4.708	517.94	137.71
4.729	518.06	139.00
4.750	518.18	139.57
4.770	518.30	139.00
4.791	518.42	139.43
4.811	518.54	138.43
4.832	518.66	139.00
4.852	518.78	140.29
4.873	518.90	138.71
4.893	519.02	139.29

4.914	519.14	141.71
4.935	519.26	140.43
4.955	519.38	137.43
4.976	519.50	135.29
4.996	519.62	133.86
5.017	519.74	130.29
5.037	519.86	123.86
5.058	519.98	121.00
5.079	520.10	115.43
5.099	520.22	110.71
5.120	520.34	108.43
5.140	520.46	107.43
5.161	520.58	107.43
5.181	520.70	106.43
5.202	520.82	105.14
5.222	520.94	103.00
5.243	521.06	106.57
5.264	521.18	110.43
5.284	521.30	114.00
5.305	521.42	118.57
5.325	521.54	121.00
5.346	521.66	121.57
5.366	521.78	120.86
5.387	521.90	116.29
5.407	522.02	112.00
5.428	522.14	108.86
5.449	522.26	106.86
5.469	522.38	105.57
5.490	522.50	106.71
5.510	522.62	106.29
5.531	522.74	106.43
5.551	522.86	108.00
5.572	522.98	106.57
5.593	523.10	106.00
5.613	523.22	104.00
5.634	523.34	100.43
5.654	523.46	99.71
5.675	523.58	99.86
5.695	523.70	98.86
5.716	523.82	96.86
5.736	523.94	92.71

5.757	524.06	89.43
5.778	524.18	86.71
5.798	524.30	86.29
5.819	524.42	85.43
5.839	524.55	83.57
5.860	524.67	81.57
5.880	524.79	80.86
5.901	524.91	78.86
5.922	525.03	76.29
5.942	525.15	74.14
5.963	525.27	71.29
5.983	525.39	68.86
6.004	525.51	66.57
6.024	525.63	65.14
6.045	525.75	65.71
6.065	525.87	64.86
6.086	525.99	65.00
6.107	526.11	62.00
6.127	526.23	60.71
6.148	526.35	59.29
6.168	526.47	58.14
6.189	526.59	58.43
6.209	526.71	57.29
6.230	526.83	54.29
6.250	526.95	53.29
6.271	527.07	52.86
6.292	527.19	53.14
6.312	527.31	53.00
6.333	527.43	52.43
6.353	527.55	53.43
6.374	527.67	53.14
6.394	527.79	55.00
6.415	527.91	57.14
6.436	528.03	57.43
6.456	528.15	59.14
6.477	528.27	60.14
6.497	528.39	61.14
6.518	528.51	61.29
6.538	528.63	63.00
6.559	528.75	63.57
6.579	528.87	67.29

6.600	528.99	69.86
6.621	529.11	71.86
6.641	529.23	76.14
6.662	529.35	80.14
6.682	529.47	82.00
6.703	529.59	84.29
6.723	529.71	86.29
6.744	529.83	90.57
6.764	529.95	92.86
6.785	530.07	98.14
6.806	530.19	103.43
6.826	530.31	104.29
6.847	530.43	105.57
6.867	530.55	106.43
6.888	530.67	107.57
6.908	530.79	108.29
6.929	530.91	108.00
6.950	531.03	112.57
6.970	531.15	116.14
6.991	531.27	118.14
7.011	531.39	118.00
7.032	531.51	117.71
7.052	531.63	116.57
7.073	531.75	118.29
7.093	531.87	123.86
7.114	531.99	128.00
7.135	532.11	132.14
7.155	532.23	132.86
7.176	532.35	134.29
7.196	532.48	133.29
7.217	532.60	133.14
7.237	532.72	137.86
7.258	532.84	141.57
7.279	532.96	138.14
7.299	533.08	137.29
7.320	533.20	137.43
7.340	533.32	137.43
7.361	533.44	135.43
7.381	533.56	136.71
7.402	533.68	134.71
7.422	533.80	134.29

7.443	533.92	137.29
7.464	534.04	141.14
7.484	534.16	146.00
7.505	534.28	146.29
7.525	534.40	148.86
7.546	534.52	149.00
7.566	534.64	148.00
7.587	534.76	148.86
7.607	534.88	146.43
7.628	535.00	145.29
7.649	535.12	145.29
7.669	535.24	145.43
7.690	535.36	147.14
7.710	535.48	146.71
7.731	535.60	148.43
7.751	535.72	149.00
7.772	535.84	149.14
7.793	535.96	152.71
7.813	536.08	158.86
7.834	536.20	160.29
7.854	536.32	161.14
7.875	536.44	167.29
7.895	536.56	167.29
7.916	536.68	168.00
7.936	536.80	169.57
7.957	536.92	172.57
7.978	537.04	175.86
7.998	537.16	176.43
8.019	537.28	175.00
8.039	537.40	175.86
8.060	537.52	177.00
8.080	537.64	175.29
8.101	537.76	175.00
8.122	537.88	174.43
8.142	538.00	174.14
8.163	538.12	172.86
8.183	538.24	170.00
8.204	538.36	167.43
8.224	538.48	166.71
8.245	538.60	167.14
8.265	538.72	167.14

8.286	538.84	166.71
8.307	538.96	167.71
8.327	539.08	168.14
8.348	539.20	170.57
8.368	539.32	173.29
8.389	539.44	173.14
8.409	539.56	168.57
8.430	539.68	162.71
8.450	539.80	161.14
8.471	539.92	161.86
8.492	540.04	163.43
8.512	540.16	166.57
8.533	540.28	170.00
8.553	540.41	169.00
8.574	540.53	166.57
8.594	540.65	163.86
8.615	540.77	163.29
8.636	540.89	162.71
8.656	541.01	163.57
8.677	541.13	164.71
8.697	541.25	165.43
8.718	541.37	169.00
8.738	541.49	172.43
8.759	541.61	170.71
8.779	541.73	169.00
8.800	541.85	168.57
8.821	541.97	172.29
8.841	542.09	172.43
8.862	542.21	171.00
8.882	542.33	170.14
8.903	542.45	176.14
8.923	542.57	173.00
8.944	542.69	174.00
8.964	542.81	176.29
8.985	542.93	175.14
9.006	543.05	174.00
9.026	543.17	175.29
9.047	543.29	177.43
9.067	543.41	182.29
9.088	543.53	185.86
9.108	543.65	189.00

9.129	543.77	189.14
9.150	543.89	196.00
9.170	544.01	199.00
9.191	544.13	196.86
9.211	544.25	191.57
9.232	544.37	190.71
9.252	544.49	189.57
9.273	544.61	185.43
9.293	544.73	183.57
9.314	544.85	181.57
9.335	544.97	184.00
9.355	545.09	183.86
9.376	545.21	181.71
9.396	545.33	177.29
9.417	545.45	175.71
9.437	545.57	175.57
9.458	545.69	176.29
9.479	545.81	172.00
9.499	545.93	171.00
9.520	546.05	171.86
9.540	546.17	169.71
9.561	546.29	168.43
9.581	546.41	167.86
9.602	546.53	164.29
9.622	546.65	159.57
9.643	546.77	157.71
9.664	546.89	157.29
9.684	547.01	160.71
9.705	547.13	162.71
9.725	547.25	167.14
9.746	547.37	168.86
9.766	547.49	170.14
9.787	547.61	169.00
9.807	547.73	169.29
9.828	547.85	171.43
9.849	547.97	171.57
9.869	548.09	173.86
9.890	548.21	176.43
9.910	548.34	177.29
9.931	548.46	182.71
9.951	548.58	189.00

9.972	548.70	190.00
9.993	548.82	190.71
10.013	548.94	195.86
10.034	549.06	203.43
10.054	549.18	202.43
10.075	549.30	202.14
10.095	549.42	202.71
10.116	549.54	200.71
10.136	549.66	201.14
10.157	549.78	205.00
10.178	549.90	208.86
10.198	550.02	218.14
10.219	550.14	216.57
10.239	550.26	214.57
10.260	550.38	215.43
10.280	550.50	212.71
10.301	550.62	209.29
10.322	550.74	206.43
10.342	550.86	202.57
10.363	550.98	200.00
10.383	551.10	200.71
10.404	551.22	201.86
10.424	551.34	201.00
10.445	551.46	197.86
10.465	551.58	198.57
10.486	551.70	196.86
10.507	551.82	195.14
10.527	551.94	191.14
10.548	552.06	191.43
10.568	552.18	192.00
10.589	552.30	192.14
10.609	552.42	189.86
10.630	552.54	190.00
10.650	552.66	189.29
10.671	552.78	190.29
10.692	552.90	187.86
10.712	553.02	185.00
10.733	553.14	187.86
10.753	553.26	187.14
10.774	553.38	186.43
10.794	553.50	185.29

10.815	553.62	185.86
10.836	553.74	190.57
10.856	553.86	191.57
10.877	553.98	192.57
10.897	554.10	192.86
10.918	554.22	191.86
10.938	554.34	190.14
10.959	554.46	186.14
10.979	554.58	186.14
11.000	554.70	184.29
11.021	554.82	181.71
11.041	554.94	179.71
11.062	555.06	179.14
11.082	555.18	180.86
11.103	555.30	183.57
11.123	555.42	186.57
11.144	555.54	189.29
11.164	555.66	189.14
11.185	555.78	189.29
11.206	555.90	191.29
11.226	556.02	191.86
11.247	556.15	190.29
11.267	556.27	191.00
11.288	556.39	190.86
11.308	556.51	189.00
11.329	556.63	188.43
11.350	556.75	184.29
11.370	556.87	184.14
11.391	556.99	183.71
11.411	557.11	184.43
11.432	557.23	186.86
11.452	557.35	185.43
11.473	557.47	184.57
11.493	557.59	181.29
11.514	557.71	181.43
11.535	557.83	182.57
11.555	557.95	178.71
11.576	558.07	176.86
11.596	558.19	177.29
11.617	558.31	175.57
11.637	558.43	179.71

11.658	558.55	181.57
11.679	558.67	183.29
11.699	558.79	184.43
11.720	558.91	181.57
11.740	559.03	177.86
11.761	559.15	178.00
11.781	559.27	176.43
11.802	559.39	171.43
11.822	559.51	170.86
11.843	559.63	170.71
11.864	559.75	169.43
11.884	559.87	166.86
11.905	559.99	165.86
11.925	560.11	167.43
11.946	560.23	164.71
11.966	560.35	165.14
11.987	560.47	163.86
12.007	560.59	161.86
12.028	560.71	163.57
12.049	560.83	162.14
12.069	560.95	165.29
12.090	561.07	165.29
12.110	561.19	167.43
12.131	561.31	168.14
12.151	561.43	170.43
12.172	561.55	165.43
12.193	561.67	162.57
12.213	561.79	161.57
12.234	561.91	159.86
12.254	562.03	162.43
12.275	562.15	163.29
12.295	562.27	163.57
12.316	562.39	164.14
12.336	562.51	160.71
12.357	562.63	160.43
12.378	562.75	160.29
12.398	562.87	161.00
12.419	562.99	163.57
12.439	563.11	162.00
12.460	563.23	160.57
12.480	563.35	161.29

12.501	563.47	161.00
12.522	563.59	163.57
12.542	563.71	164.43
12.563	563.83	166.86
12.583	563.95	167.00
12.604	564.08	165.14
12.624	564.20	161.86
12.645	564.32	159.43
12.665	564.44	158.14
12.686	564.56	158.29
12.707	564.68	158.43
12.727	564.80	159.71
12.748	564.92	161.71
12.768	565.04	162.71
12.789	565.16	160.71
12.809	565.28	159.57
12.830	565.40	160.71
12.850	565.52	163.14
12.871	565.64	164.29
12.892	565.76	164.86
12.912	565.88	162.43
12.933	566.00	164.57
12.953	566.12	165.57
12.974	566.24	165.86
12.994	566.36	168.57
13.015	566.48	172.29
13.036	566.60	173.14
13.056	566.72	172.57
13.077	566.84	171.14
13.097	566.96	169.57
13.118	567.08	170.29
13.138	567.20	176.57
13.159	567.32	181.71
13.179	567.44	181.71
13.200	567.56	174.29
13.221	567.68	168.29
13.241	567.80	164.29
13.262	567.92	164.57
13.282	568.04	167.29
13.303	568.16	166.71
13.323	568.28	169.43

13.344	568.40	172.14
13.364	568.52	172.57
13.385	568.64	173.00
13.406	568.76	173.86
13.426	568.88	173.14
13.447	569.00	176.14
13.467	569.12	180.71
13.488	569.24	182.00
13.508	569.36	184.57
13.529	569.48	187.86
13.550	569.60	186.86
13.570	569.72	187.29
13.591	569.84	186.29
13.611	569.96	185.43
13.632	570.08	183.00
13.652	570.20	187.86
13.673	570.32	193.14
13.693	570.44	193.57
13.714	570.56	193.86
13.735	570.68	196.43
13.755	570.80	203.29
13.776	570.92	206.00
13.796	571.04	209.43
13.817	571.16	210.71
13.837	571.28	209.43
13.858	571.40	206.14
13.879	571.52	208.57
13.899	571.64	212.86
13.920	571.76	213.86
13.940	571.88	208.71
13.961	572.01	203.86
13.981	572.13	203.71
14.002	572.25	203.29
14.022	572.37	203.29
14.043	572.49	205.43
14.064	572.61	209.29
14.084	572.73	210.43
14.105	572.85	212.86
14.125	572.97	215.57
14.146	573.09	216.43
14.166	573.21	219.43

14.187	573.33	221.00
14.207	573.45	222.00
14.228	573.57	219.43
14.249	573.69	219.86
14.269	573.81	218.43
14.290	573.93	215.86
14.310	574.05	216.00
14.331	574.17	213.14
14.351	574.29	210.14
14.372	574.41	207.86
14.393	574.53	204.14
14.413	574.65	201.57
14.434	574.77	198.86
14.454	574.89	195.14
14.475	575.01	194.00
14.495	575.13	194.00
14.516	575.25	197.14
14.536	575.37	196.71
14.557	575.49	194.86
14.578	575.61	193.86
14.598	575.73	196.86
14.619	575.85	199.29
14.639	575.97	198.71
14.660	576.09	200.57
14.680	576.21	202.43
14.701	576.33	204.71
14.722	576.45	207.00
14.742	576.57	209.29
14.763	576.69	212.00
14.783	576.81	212.57
14.804	576.93	212.29
14.824	577.05	212.29
14.845	577.17	210.14
14.865	577.29	209.57
14.886	577.41	212.00
14.907	577.53	212.29
14.927	577.65	209.71
14.948	577.77	210.29
14.968	577.89	206.29
14.989	578.01	206.86
15.009	578.13	205.14

15.030	578.25	201.86
15.050	578.37	198.43
15.071	578.49	195.57
15.092	578.61	195.57
15.112	578.73	195.00
15.133	578.85	193.57
15.153	578.97	194.43
15.174	579.09	194.29
15.194	579.21	197.86
15.215	579.33	195.57
15.236	579.45	197.71
15.256	579.57	201.00
15.277	579.69	206.00
15.297	579.81	208.43
15.318	579.94	207.14
15.338	580.06	203.71
15.359	580.18	199.86
15.379	580.30	195.00
15.400	580.42	192.00
15.421	580.54	192.57
15.441	580.66	189.86
15.462	580.78	188.00
15.482	580.90	186.00
15.503	581.02	187.29
15.523	581.14	185.57
15.544	581.26	184.29
15.565	581.38	184.00
15.585	581.50	181.14
15.606	581.62	184.14
15.626	581.74	181.29
15.647	581.86	179.00
15.667	581.98	179.57
15.688	582.10	179.14
15.708	582.22	177.29
15.729	582.34	177.14
15.750	582.46	175.57
15.770	582.58	176.43
15.791	582.70	176.86
15.811	582.82	175.71
15.832	582.94	173.29
15.852	583.06	172.14

15.873	583.18	173.71
15.893	583.30	174.57
15.914	583.42	171.71
15.935	583.54	171.00
15.955	583.66	169.43
15.976	583.78	169.86
15.996	583.90	165.57
16.017	584.02	161.57
16.037	584.14	162.00
16.058	584.26	161.86
16.079	584.38	162.29
16.099	584.50	162.57
16.120	584.62	162.57
16.140	584.74	164.57
16.161	584.86	165.00
16.181	584.98	163.86
16.202	585.10	164.14
16.222	585.22	167.86
16.243	585.34	166.86
16.264	585.46	166.14
16.284	585.58	165.86
16.305	585.70	169.57
16.325	585.82	169.43
16.346	585.94	171.43
16.366	586.06	174.29
16.387	586.18	176.86
16.407	586.30	175.00
16.428	586.42	174.14
16.449	586.54	172.00
16.469	586.66	170.71
16.490	586.78	164.71
16.510	586.90	162.57
16.531	587.02	163.43
16.551	587.14	166.57
16.572	587.26	169.71
16.593	587.38	167.43
16.613	587.50	168.00
16.634	587.62	164.57
16.654	587.74	164.14
16.675	587.87	163.57
16.695	587.99	161.86

16.716	588.11	160.29
16.736	588.23	159.43
16.757	588.35	156.29
16.778	588.47	156.00
16.798	588.59	157.29
16.819	588.71	157.71
16.839	588.83	158.86
16.860	588.95	163.14
16.880	589.07	167.00
16.901	589.19	162.57
16.922	589.31	162.43
16.942	589.43	161.43
16.963	589.55	162.71
16.983	589.67	172.86
17.004	589.79	176.00
17.024	589.91	167.57
17.045	590.03	168.14
17.065	590.15	162.43
17.086	590.27	158.14
17.107	590.39	160.29
17.127	590.51	165.43
17.148	590.63	170.14
17.168	590.75	167.86
17.189	590.87	171.00
17.209	590.99	172.29
17.230	591.11	174.29
17.250	591.23	175.29
17.271	591.35	178.29
17.292	591.47	177.43
17.312	591.59	180.57
17.333	591.71	182.71
17.353	591.83	185.71
17.374	591.95	187.86
17.394	592.07	186.29
17.415	592.19	186.57
17.436	592.31	186.57
17.456	592.43	189.57
17.477	592.55	191.14
17.497	592.67	194.14
17.518	592.79	198.57
17.538	592.91	200.43

17.559	593.03	199.43
17.579	593.15	199.00
17.600	593.27	200.00
17.621	593.39	201.14
17.641	593.51	195.86
17.662	593.63	194.29
17.682	593.75	190.86
17.703	593.87	189.29
17.723	593.99	190.43
17.744	594.11	189.71
17.765	594.23	188.14
17.785	594.35	188.00
17.806	594.47	184.43
17.826	594.59	183.86
17.847	594.71	184.43
17.867	594.83	182.29
17.888	594.95	181.71
17.908	595.07	186.29
17.929	595.19	188.00
17.950	595.31	188.43
17.970	595.43	189.00
17.991	595.55	187.57
18.011	595.68	189.43
18.032	595.80	189.14
18.052	595.92	189.00
18.073	596.04	186.57
18.093	596.16	187.86
18.114	596.28	186.86
18.135	596.40	190.14
18.155	596.52	188.86
18.176	596.64	189.43
18.196	596.76	186.00
18.217	596.88	182.00
18.237	597.00	178.14
18.258	597.12	176.57
18.279	597.24	172.86
18.299	597.36	170.00
18.320	597.48	171.71
18.340	597.60	170.00
18.361	597.72	171.71
18.381	597.84	172.86

18.402	597.96	168.14
18.422	598.08	163.43
18.443	598.20	158.29
18.464	598.32	158.71
18.484	598.44	157.29
18.505	598.56	157.14
18.525	598.68	156.29
18.546	598.80	154.71
18.566	598.92	154.71
18.587	599.04	154.86
18.607	599.16	155.43
18.628	599.28	154.29
18.649	599.40	153.86
18.669	599.52	151.71
18.690	599.64	152.00
18.710	599.76	154.71
18.731	599.88	156.29
18.751	600.00	155.57
18.772	600.12	155.57
18.793	600.24	154.00
18.813	600.36	153.14
18.834	600.48	150.57
18.854	600.60	148.86
18.875	600.72	147.86
18.895	600.84	143.71
18.916	600.96	138.29
18.936	601.08	135.00
18.957	601.20	132.57
18.978	601.32	128.71
18.998	601.44	127.00
19.019	601.56	126.86
19.039	601.68	124.57
19.060	601.80	119.71
19.080	601.92	116.57
19.101	602.04	114.14
19.122	602.16	109.71
19.142	602.28	106.71
19.163	602.40	106.14
19.183	602.52	105.71
19.204	602.64	105.29
19.224	602.76	102.14

19.245	602.88	101.43
19.265	603.00	100.57
19.286	603.12	98.71
19.307	603.24	95.29
19.327	603.36	91.43
19.348	603.48	89.00
19.368	603.61	86.86
19.389	603.73	85.86
19.409	603.85	82.71
19.430	603.97	80.57
19.450	604.09	79.71
19.471	604.21	79.43
19.492	604.33	80.71
19.512	604.45	80.14
19.533	604.57	77.57
19.553	604.69	76.86
19.574	604.81	76.71
19.594	604.93	74.71
19.615	605.05	72.43
19.636	605.17	72.43
19.656	605.29	72.14
19.677	605.41	72.29
19.697	605.53	71.14
19.718	605.65	69.86
19.738	605.77	68.43
19.759	605.89	67.00
19.779	606.01	65.57
19.800	606.13	64.29
19.821	606.25	66.57
19.841	606.37	69.14
19.862	606.49	69.71
19.882	606.61	70.86
19.903	606.73	72.43
19.923	606.85	73.71
19.944	606.97	72.71
19.965	607.09	70.71
19.985	607.21	69.57
20.006	607.33	68.86
20.026	607.45	68.14
20.047	607.57	67.29
20.067	607.69	67.43

20.088	607.81	67.14
20.108	607.93	66.43
20.129	608.05	64.43
20.150	608.17	62.86
20.170	608.29	62.71
20.191	608.41	63.43
20.211	608.53	65.71
20.232	608.65	66.71
20.252	608.77	66.57
20.273	608.89	67.43
20.293	609.01	67.00
20.314	609.13	67.43
20.335	609.25	68.14
20.355	609.37	69.57
20.376	609.49	69.86
20.396	609.61	70.57
20.417	609.73	74.57
20.437	609.85	81.29
20.458	609.97	94.14
20.479	610.09	103.14
20.499	610.21	108.86
20.520	610.33	112.86
20.540	610.45	116.00
20.561	610.57	117.00
20.581	610.69	118.00
20.602	610.81	119.86
20.622	610.93	121.00
20.643	611.05	122.43
20.664	611.17	121.71
20.684	611.29	122.57
20.705	611.41	121.71
20.725	611.54	121.00
20.746	611.66	119.71
20.766	611.78	121.43
20.787	611.90	124.57
20.807	612.02	124.29
20.828	612.14	124.29
20.849	612.26	121.43
20.869	612.38	120.57
20.890	612.50	121.86
20.910	612.62	124.86

20.931	612.74	125.00
20.951	612.86	123.29
20.972	612.98	124.86
20.993	613.10	122.71
21.013	613.22	125.71
21.034	613.34	127.57
21.054	613.46	127.29
21.075	613.58	127.57
21.095	613.70	125.71
21.116	613.82	125.86
21.136	613.94	130.57
21.157	614.06	128.71
21.178	614.18	128.86
21.198	614.30	127.57
21.219	614.42	126.57
21.239	614.54	126.29
21.260	614.66	127.29
21.280	614.78	128.00
21.301	614.90	127.57
21.322	615.02	126.00
21.342	615.14	126.57
21.363	615.26	127.43
21.383	615.38	126.86
21.404	615.50	125.43
21.424	615.62	126.43
21.445	615.74	128.29
21.465	615.86	129.14
21.486	615.98	129.29
21.507	616.10	128.57
21.527	616.22	126.29
21.548	616.34	125.14
21.568	616.46	128.14
21.589	616.58	127.86
21.609	616.70	125.43
21.630	616.82	126.71
21.650	616.94	124.14
21.671	617.06	123.57
21.692	617.18	124.86
21.712	617.30	129.14
21.733	617.42	133.43
21.753	617.54	136.43

21.774	617.66	134.71
21.794	617.78	134.29
21.815	617.90	135.00
21.836	618.02	136.29
21.856	618.14	137.00
21.877	618.26	136.86
21.897	618.38	137.00
21.918	618.50	138.86
21.938	618.62	142.14
21.959	618.74	147.14
21.979	618.86	153.00
22.000	618.98	161.71
22.021	619.10	162.71
22.041	619.22	165.86
22.062	619.34	167.86
22.082	619.47	167.00
22.103	619.59	166.43
22.123	619.71	165.86
22.144	619.83	167.43
22.165	619.95	169.43
22.185	620.07	171.00
22.206	620.19	171.86
22.226	620.31	171.86
22.247	620.43	170.14
22.267	620.55	168.14
22.288	620.67	168.57
22.308	620.79	167.43
22.329	620.91	163.29
22.350	621.03	159.71
22.370	621.15	156.43
22.391	621.27	154.29
22.411	621.39	149.57
22.432	621.51	148.57
22.452	621.63	147.86
22.473	621.75	147.14
22.493	621.87	147.00
22.514	621.99	147.71
22.535	622.11	147.57
22.555	622.23	148.57
22.576	622.35	150.29
22.596	622.47	154.14

22.617	622.59	159.00
22.637	622.71	163.43
22.658	622.83	162.86
22.679	622.95	161.14
22.699	623.07	155.86
22.720	623.19	153.57
22.740	623.31	156.57
22.761	623.43	160.57
22.781	623.55	161.71
22.802	623.67	163.14
22.822	623.79	162.43
22.843	623.91	161.00
22.864	624.03	159.57
22.884	624.15	158.14
22.905	624.27	157.00
22.925	624.39	154.86
22.946	624.51	156.57
22.966	624.63	154.71
22.987	624.75	153.29
23.007	624.87	153.14
23.028	624.99	156.29
23.049	625.11	157.14
23.069	625.23	156.00
23.090	625.35	154.71
23.110	625.47	156.43
23.131	625.59	155.86
23.151	625.71	158.86
23.172	625.83	157.14
23.193	625.95	156.86
23.213	626.07	159.71
23.234	626.19	162.57
23.254	626.31	165.14
23.275	626.43	165.86
23.295	626.55	164.57
23.316	626.67	163.29
23.336	626.79	165.43
23.357	626.91	165.43
23.378	627.03	167.71
23.398	627.15	170.00
23.419	627.27	176.57
23.439	627.40	183.86

23.460	627.52	182.57
23.480	627.64	181.29
23.501	627.76	177.43
23.522	627.88	172.57
23.542	628.00	168.29
23.563	628.12	169.00
23.583	628.24	164.57
23.604	628.36	162.43
23.624	628.48	162.00
23.645	628.60	162.00
23.665	628.72	161.57
23.686	628.84	162.14
23.707	628.96	161.86
23.727	629.08	162.86
23.748	629.20	166.14
23.768	629.32	166.57
23.789	629.44	163.86
23.809	629.56	162.86
23.830	629.68	160.57
23.850	629.80	158.29
23.871	629.92	157.57
23.892	630.04	159.29
23.912	630.16	157.43
23.933	630.28	157.29
23.953	630.40	161.43
23.974	630.52	162.00
23.994	630.64	161.57
24.015	630.76	165.57
24.036	630.88	165.57
24.056	631.00	161.43
24.077	631.12	158.71
24.097	631.24	160.86
24.118	631.36	166.00
24.138	631.48	172.86
24.159	631.60	176.71
24.179	631.72	174.86
24.200	631.84	175.57
24.221	631.96	176.71
24.241	632.08	178.71
24.262	632.20	177.43
24.282	632.32	178.86

24.303	632.44	179.71
24.323	632.56	179.29
24.344	632.68	177.14
24.365	632.80	180.57
24.385	632.92	181.71
24.406	633.04	182.00
24.426	633.16	185.29
24.447	633.28	185.14
24.467	633.40	181.00
24.488	633.52	184.14
24.508	633.64	186.71
24.529	633.76	186.57
24.550	633.88	184.29
24.570	634.00	184.14
24.591	634.12	179.71
24.611	634.24	182.14
24.632	634.36	184.14
24.652	634.48	187.86
24.673	634.60	187.71
24.693	634.72	185.29
24.714	634.84	184.14
24.735	634.96	184.71
24.755	635.08	182.86
24.776	635.21	180.71
24.796	635.33	183.43
24.817	635.45	187.14
24.837	635.57	188.00
24.858	635.69	190.14
24.879	635.81	190.71
24.899	635.93	191.71
24.920	636.05	194.00
24.940	636.17	196.00
24.961	636.29	195.00
24.981	636.41	192.29
25.002	636.53	190.71
25.022	636.65	188.71
25.043	636.77	188.43
25.064	636.89	187.00
25.084	637.01	190.14
25.105	637.13	189.00
25.125	637.25	188.29

25.146	637.37	185.00
25.166	637.49	184.57
25.187	637.61	185.57
25.208	637.73	183.00
25.228	637.85	181.29
25.249	637.97	183.14
25.269	638.09	182.43
25.290	638.21	184.43
25.310	638.33	186.14
25.331	638.45	183.71
25.351	638.57	181.57
25.372	638.69	181.86
25.393	638.81	180.71
25.413	638.93	179.57
25.434	639.05	178.43
25.454	639.17	176.86
25.475	639.29	177.29
25.495	639.41	176.43
25.516	639.53	175.00
25.536	639.65	173.29
25.557	639.77	174.29
25.578	639.89	175.14
25.598	640.01	170.86
25.619	640.13	169.29
25.639	640.25	164.00
25.660	640.37	160.86
25.680	640.49	159.00
25.701	640.61	158.00
25.722	640.73	161.71
25.742	640.85	164.00
25.763	640.97	166.57
25.783	641.09	170.14
25.804	641.21	174.00
25.824	641.33	179.14
25.845	641.45	182.14
25.865	641.57	182.00
25.886	641.69	181.71
25.907	641.81	181.00
25.927	641.93	178.57
25.948	642.05	180.29
25.968	642.17	180.00

25.989	642.29	180.57
26.009	642.41	177.29
26.030	642.53	177.43
26.050	642.65	173.71
26.071	642.77	173.86
26.092	642.89	170.86
26.112	643.01	169.29
26.133	643.14	168.86
26.153	643.26	168.14
26.174	643.38	169.00
26.194	643.50	170.43
26.215	643.62	170.00
26.236	643.74	168.43
26.256	643.86	168.57
26.277	643.98	169.71
26.297	644.10	170.86
26.318	644.22	169.00
26.338	644.34	171.43
26.359	644.46	170.14
26.379	644.58	169.71
26.400	644.70	171.57
26.421	644.82	168.86
26.441	644.94	170.57
26.462	645.06	173.43
26.482	645.18	175.43
26.503	645.30	179.14
26.523	645.42	179.29
26.544	645.54	181.14
26.565	645.66	184.86
26.585	645.78	185.57
26.606	645.90	182.29
26.626	646.02	181.71
26.647	646.14	185.29
26.667	646.26	189.14
26.688	646.38	190.86
26.708	646.50	191.43
26.729	646.62	188.43
26.750	646.74	191.43
26.770	646.86	189.29
26.791	646.98	187.00
26.811	647.10	187.71

26.832	647.22	187.57
26.852	647.34	187.00
26.873	647.46	186.71
26.893	647.58	188.57
26.914	647.70	189.43
26.935	647.82	187.57
26.955	647.94	186.71
26.976	648.06	184.57
26.996	648.18	184.86
27.017	648.30	186.00
27.037	648.42	185.71
27.058	648.54	183.71
27.079	648.66	184.57
27.099	648.78	187.14
27.120	648.90	187.71
27.140	649.02	188.43
27.161	649.14	188.71
27.181	649.26	186.43
27.202	649.38	184.43
27.222	649.50	180.71
27.243	649.62	183.86
27.264	649.74	182.86
27.284	649.86	182.29
27.305	649.98	182.00
27.325	650.10	181.43
27.346	650.22	182.29
27.366	650.34	182.86
27.387	650.46	179.86
27.408	650.58	179.86
27.428	650.70	180.29
27.449	650.82	180.57
27.469	650.94	179.14
27.490	651.07	181.57
27.510	651.19	185.14
27.531	651.31	186.29
27.551	651.43	188.57
27.572	651.55	195.00
27.593	651.67	198.14
27.613	651.79	197.57
27.634	651.91	196.00
27.654	652.03	194.57

27.675	652.15	190.43
27.695	652.27	193.00
27.716	652.39	195.00
27.736	652.51	195.71
27.757	652.63	193.29
27.778	652.75	191.57
27.798	652.87	194.14
27.819	652.99	198.57
27.839	653.11	196.86
27.860	653.23	195.14
27.880	653.35	194.86
27.901	653.47	195.43
27.922	653.59	195.71
27.942	653.71	196.57
27.963	653.83	200.71
27.983	653.95	199.00
28.004	654.07	198.86
28.024	654.19	204.00
28.045	654.31	210.29
28.065	654.43	213.57
28.086	654.55	213.43
28.107	654.67	214.29
28.127	654.79	214.57
28.148	654.91	211.29
28.168	655.03	209.29
28.189	655.15	206.86
28.209	655.27	206.86
28.230	655.39	209.57
28.250	655.51	210.29
28.271	655.63	207.57
28.292	655.75	206.86
28.312	655.87	207.43
28.333	655.99	210.57
28.353	656.11	214.71
28.374	656.23	216.14
28.394	656.35	216.71
28.415	656.47	219.57
28.436	656.59	222.86
28.456	656.71	223.29
28.477	656.83	223.29
28.497	656.95	222.71

28.518	657.07	219.14
28.538	657.19	215.43
28.559	657.31	215.29
28.579	657.43	214.57
28.600	657.55	217.29
28.621	657.67	219.14
28.641	657.79	220.43
28.662	657.91	220.57
28.682	658.03	222.86
28.703	658.15	218.43
28.723	658.27	221.57
28.744	658.39	220.29
28.765	658.51	221.29
28.785	658.63	219.43
28.806	658.75	221.43
28.826	658.87	222.43
28.847	659.00	220.00
28.867	659.12	223.57
28.888	659.24	229.00
28.908	659.36	229.14
28.929	659.48	230.71
28.950	659.60	233.14
28.970	659.72	234.71
28.991	659.84	234.43
29.011	659.96	234.86
29.032	660.08	237.00
29.052	660.20	240.57
29.073	660.32	240.86
29.093	660.44	240.57
29.114	660.56	243.71
29.135	660.68	245.86
29.155	660.80	243.57
29.176	660.92	241.00
29.196	661.04	242.29
29.217	661.16	235.14
29.237	661.28	235.86
29.258	661.40	234.43
29.279	661.52	233.71
29.299	661.64	232.00
29.320	661.76	234.71
29.340	661.88	232.29

29.361	662.00	230.29
29.381	662.12	231.00
29.402	662.24	232.00
29.422	662.36	230.29
29.443	662.48	227.00
29.464	662.60	226.57
29.484	662.72	223.14
29.505	662.84	219.71
29.525	662.96	219.00
29.546	663.08	222.71
29.566	663.20	231.00
29.587	663.32	234.00
29.608	663.44	235.14
29.628	663.56	232.00
29.649	663.68	230.71
29.669	663.80	225.71
29.690	663.92	222.86
29.710	664.04	222.86
29.731	664.16	226.86
29.751	664.28	224.29
29.772	664.40	225.57
29.793	664.52	227.71
29.813	664.64	228.14
29.834	664.76	231.14
29.854	664.88	231.14
29.875	665.00	233.29
29.895	665.12	231.29
29.916	665.24	229.29
29.936	665.36	229.86
29.957	665.48	230.00
29.978	665.60	231.57
29.998	665.72	228.43
30.019	665.84	231.57
30.039	665.96	232.43
30.060	666.08	231.86
30.080	666.20	230.86
30.101	666.32	235.29
30.122	666.44	233.43
30.142	666.56	233.86
30.163	666.68	236.71
30.183	666.80	232.57

30.204	666.93	226.14
30.224	667.05	230.29
30.245	667.17	232.43
30.265	667.29	233.71
30.286	667.41	232.14
30.307	667.53	233.00
30.327	667.65	234.86
30.348	667.77	233.71
30.368	667.89	230.43
30.389	668.01	230.00
30.409	668.13	227.57
30.430	668.25	226.14
30.450	668.37	229.71
30.471	668.49	232.29
30.492	668.61	232.14
30.512	668.73	233.71
30.533	668.85	235.71
30.553	668.97	236.14
30.574	669.09	236.00
30.594	669.21	234.43
30.615	669.33	231.86
30.636	669.45	229.43
30.656	669.57	229.71
30.677	669.69	229.71
30.697	669.81	229.43
30.718	669.93	227.29
30.738	670.05	226.29
30.759	670.17	225.29
30.779	670.29	225.71
30.800	670.41	228.14
30.821	670.53	228.57
30.841	670.65	223.57
30.862	670.77	224.00
30.882	670.89	224.29
30.903	671.01	230.00
30.923	671.13	232.14
30.944	671.25	233.00
30.965	671.37	235.29
30.985	671.49	235.57
31.006	671.61	233.86
31.026	671.73	230.00

31.047	671.85	226.57
31.067	671.97	228.57
31.088	672.09	229.57
31.108	672.21	230.00
31.129	672.33	231.14
31.150	672.45	231.57
31.170	672.57	231.29
31.191	672.69	232.71
31.211	672.81	231.00
31.232	672.93	230.71
31.252	673.05	234.00
31.273	673.17	233.86
31.293	673.29	233.29
31.314	673.41	232.86
31.335	673.53	230.71
31.355	673.65	231.71
31.376	673.77	230.00
31.396	673.89	232.57
31.417	674.01	234.57
31.437	674.13	234.43
31.458	674.25	233.00
31.479	674.37	232.57
31.499	674.49	238.14
31.520	674.61	239.14
31.540	674.74	237.86
31.561	674.86	237.43
31.581	674.98	233.14
31.602	675.10	232.71
31.622	675.22	229.71
31.643	675.34	225.43
31.664	675.46	223.86
31.684	675.58	224.71
31.705	675.70	228.43
31.725	675.82	224.57
31.746	675.94	225.29
31.766	676.06	226.86
31.787	676.18	228.57
31.808	676.30	227.57
31.828	676.42	229.14
31.849	676.54	230.29
31.869	676.66	230.00

31.890	676.78	228.57
31.910	676.90	227.43
31.931	677.02	225.86
31.951	677.14	224.29
31.972	677.26	224.86
31.993	677.38	225.43
32.013	677.50	229.00
32.034	677.62	233.43
32.054	677.74	229.71
32.075	677.86	227.71
32.095	677.98	226.86
32.116	678.10	228.14
32.136	678.22	228.14
32.157	678.34	231.00
32.178	678.46	232.29
32.198	678.58	233.29
32.219	678.70	234.29
32.239	678.82	231.86
32.260	678.94	233.00
32.280	679.06	234.14
32.301	679.18	231.57
32.322	679.30	232.00
32.342	679.42	232.00
32.363	679.54	231.29
32.383	679.66	231.57
32.404	679.78	233.00
32.424	679.90	236.29
32.445	680.02	234.14
32.465	680.14	234.00
32.486	680.26	235.57
32.507	680.38	234.29
32.527	680.50	233.86
32.548	680.62	234.14
32.568	680.74	235.29
32.589	680.86	234.57
32.609	680.98	232.43
32.630	681.10	233.14
32.651	681.22	231.29
32.671	681.34	227.71
32.692	681.46	226.43
32.712	681.58	225.29

32.733	681.70	223.57
32.753	681.82	221.43
32.774	681.94	221.57
32.794	682.06	221.29
32.815	682.18	219.43
32.836	682.30	219.14
32.856	682.42	218.57
32.877	682.54	222.14
32.897	682.67	224.14
32.918	682.79	223.43
32.938	682.91	221.71
32.959	683.03	219.57
32.979	683.15	220.71
33.000	683.27	219.00
33.021	683.39	216.86
33.041	683.51	217.71
33.062	683.63	219.29
33.082	683.75	218.14
33.103	683.87	220.71
33.123	683.99	221.00
33.144	684.11	223.43
33.165	684.23	223.86
33.185	684.35	224.29
33.206	684.47	226.57
33.226	684.59	227.29
33.247	684.71	225.00
33.267	684.83	222.14
33.288	684.95	222.00
33.308	685.07	218.71
33.329	685.19	217.29
33.350	685.31	215.71
33.370	685.43	215.29
33.391	685.55	215.43
33.411	685.67	219.43
33.432	685.79	217.86
33.452	685.91	216.43
33.473	686.03	217.43
33.493	686.15	214.29
33.514	686.27	211.71
33.535	686.39	209.86
33.555	686.51	208.14

33.576	686.63	207.71
33.596	686.75	211.57
33.617	686.87	213.00
33.637	686.99	212.43
33.658	687.11	211.14
33.679	687.23	210.43
33.699	687.35	212.00
33.720	687.47	210.29
33.740	687.59	207.43
33.761	687.71	205.86
33.781	687.83	205.14
33.802	687.95	205.86
33.822	688.07	204.14
33.843	688.19	202.29
33.864	688.31	200.86
33.884	688.43	196.43
33.905	688.55	192.71
33.925	688.67	188.57
33.946	688.79	187.71
33.966	688.91	186.86
33.987	689.03	184.43
34.008	689.15	184.00
34.028	689.27	182.29
34.049	689.39	182.43
34.069	689.51	180.71
34.090	689.63	180.00
34.110	689.75	181.57
34.131	689.87	181.43
34.151	689.99	180.29
34.172	690.11	177.71
34.193	690.23	176.43
34.213	690.35	174.00
34.234	690.47	174.14
34.254	690.60	173.71
34.275	690.72	172.57
34.295	690.84	174.00
34.316	690.96	176.57
34.336	691.08	177.57
34.357	691.20	177.29
34.378	691.32	177.86
34.398	691.44	181.43

34.419	691.56	181.86
34.439	691.68	183.14
34.460	691.80	186.71
34.480	691.92	189.00
34.501	692.04	193.29
34.522	692.16	195.86
34.542	692.28	196.14
34.563	692.40	193.86
34.583	692.52	193.14
34.604	692.64	191.86
34.624	692.76	188.14
34.645	692.88	184.00
34.665	693.00	182.43
34.686	693.12	180.43
34.707	693.24	176.43
34.727	693.36	173.86
34.748	693.48	173.57
34.768	693.60	171.29
34.789	693.72	169.43
34.809	693.84	167.43
34.830	693.96	164.14
34.851	694.08	161.43
34.871	694.20	159.43
34.892	694.32	158.71
34.912	694.44	159.86
34.933	694.56	159.29
34.953	694.68	162.14
34.974	694.80	162.00
34.994	694.92	163.43
35.015	695.04	161.00
35.036	695.16	158.00
35.056	695.28	156.29
35.077	695.40	157.14
35.097	695.52	156.29
35.118	695.64	155.43
35.138	695.76	155.43
35.159	695.88	152.71
35.179	696.00	151.14
35.200	696.12	148.86
35.221	696.24	149.00
35.241	696.36	148.86

35.262	696.48	149.43
35.282	696.60	148.71
35.303	696.72	146.43
35.323	696.84	146.29
35.344	696.96	145.86
35.365	697.08	146.00
35.385	697.20	147.71
35.406	697.32	148.14
35.426	697.44	151.57
35.447	697.56	151.86
35.467	697.68	151.43
35.488	697.80	147.29
35.508	697.92	144.57
35.529	698.04	144.00
35.550	698.16	144.71
35.570	698.28	143.86
35.591	698.40	143.29
35.611	698.53	144.00
35.632	698.65	142.43
35.652	698.77	144.57
35.673	698.89	146.86
35.693	699.01	150.43
35.714	699.13	153.29
35.735	699.25	155.00
35.755	699.37	156.29
35.776	699.49	153.57
35.796	699.61	150.14
35.817	699.73	150.43
35.837	699.85	153.29
35.858	699.97	155.29
35.879	700.09	155.43
35.899	700.21	155.29
35.920	700.33	155.71
35.940	700.45	153.86
35.961	700.57	152.71
35.981	700.69	148.86
36.002	700.81	145.14
36.022	700.93	143.29
36.043	701.05	145.43
36.064	701.17	147.29
36.084	701.29	147.57

36.105	701.41	149.29
36.125	701.53	151.71
36.146	701.65	147.71
36.166	701.77	147.14
36.187	701.89	143.14
36.208	702.01	140.00
36.228	702.13	138.71
36.249	702.25	137.43
36.269	702.37	134.57
36.290	702.49	134.00
36.310	702.61	135.00
36.331	702.73	133.86
36.351	702.85	133.14
36.372	702.97	131.57
36.393	703.09	129.86
36.413	703.21	129.43
36.434	703.33	128.43
36.454	703.45	127.57
36.475	703.57	129.00
36.495	703.69	130.57
36.516	703.81	128.00
36.536	703.93	126.86
36.557	704.05	127.43
36.578	704.17	128.86
36.598	704.29	126.14
36.619	704.41	127.14
36.639	704.53	128.29
36.660	704.65	130.29
36.680	704.77	129.29
36.701	704.89	127.43
36.722	705.01	129.71
36.742	705.13	134.00
36.763	705.25	132.57
36.783	705.37	132.00
36.804	705.49	130.43
36.824	705.61	129.86
36.845	705.73	130.00
36.865	705.85	130.00
36.886	705.97	126.57
36.907	706.09	123.71
36.927	706.21	122.86

36.948	706.34	121.57
36.968	706.46	123.14
36.989	706.58	127.29
37.009	706.70	128.57
37.030	706.82	131.57
37.051	706.94	133.57
37.071	707.06	134.57
37.092	707.18	132.00
37.112	707.30	128.00
37.133	707.42	127.29
37.153	707.54	125.57
37.174	707.66	122.00
37.194	707.78	119.71
37.215	707.90	114.00
37.236	708.02	110.86
37.256	708.14	109.14
37.277	708.26	107.00
37.297	708.38	108.71
37.318	708.50	109.43
37.338	708.62	108.43
37.359	708.74	109.57
37.379	708.86	110.29
37.400	708.98	109.29
37.421	709.10	108.29
37.441	709.22	107.86
37.462	709.34	108.57
37.482	709.46	108.71
37.503	709.58	109.29
37.523	709.70	109.71
37.544	709.82	111.43
37.565	709.94	115.00
37.585	710.06	118.43
37.606	710.18	120.57
37.626	710.30	122.71
37.647	710.42	121.71
37.667	710.54	121.00
37.688	710.66	122.43
37.708	710.78	124.71
37.729	710.90	129.14
37.750	711.02	133.14
37.770	711.14	142.71

37.791	711.26	152.00
37.811	711.38	160.71
37.832	711.50	168.57
37.852	711.62	175.29
37.873	711.74	180.43
37.893	711.86	180.00
37.914	711.98	180.43
37.935	712.10	182.00
37.955	712.22	181.57
37.976	712.34	183.71
37.996	712.46	187.29
38.017	712.58	187.71
38.037	712.70	188.14
38.058	712.82	192.00
38.079	712.94	194.86
38.099	713.06	190.86
38.120	713.18	189.86
38.140	713.30	190.57
38.161	713.42	190.86
38.181	713.54	192.14
38.202	713.66	194.00
38.222	713.78	196.43
38.243	713.90	196.86
38.264	714.02	196.86
38.284	714.14	197.29
38.305	714.27	199.29
38.325	714.39	201.14
38.346	714.51	200.14
38.366	714.63	201.86
38.387	714.75	202.29
38.408	714.87	202.86
38.428	714.99	204.29
38.449	715.11	203.57
38.469	715.23	207.29
38.490	715.35	206.00
38.510	715.47	204.43
38.531	715.59	202.86
38.551	715.71	202.57
38.572	715.83	201.14
38.593	715.95	199.29
38.613	716.07	196.29

38.634	716.19	194.00
38.654	716.31	193.57
38.675	716.43	194.57
38.695	716.55	198.29
38.716	716.67	199.86
38.736	716.79	202.86
38.757	716.91	206.57
38.778	717.03	211.29
38.798	717.15	209.71
38.819	717.27	203.00
38.839	717.39	204.86
38.860	717.51	205.00
38.880	717.63	206.14
38.901	717.75	205.29
38.922	717.87	202.86
38.942	717.99	203.29
38.963	718.11	202.43
38.983	718.23	203.14
39.004	718.35	205.43
39.024	718.47	206.43
39.045	718.59	208.57
39.065	718.71	211.29
39.086	718.83	210.86
39.107	718.95	212.43
39.127	719.07	211.14
39.148	719.19	209.86
39.168	719.31	210.71
39.189	719.43	211.43
39.209	719.55	208.86
39.230	719.67	205.57
39.251	719.79	205.43
39.271	719.91	205.00
39.292	720.03	205.29
39.312	720.15	203.71
39.333	720.27	200.86
39.353	720.39	203.00
39.374	720.51	206.71
39.394	720.63	205.14
39.415	720.75	205.86
39.436	720.87	203.86
39.456	720.99	202.43

39.477	721.11	201.57
39.497	721.23	201.57
39.518	721.35	202.71
39.538	721.47	204.71
39.559	721.59	203.86
39.579	721.71	203.71
39.600	721.83	202.14
39.621	721.95	202.14
39.641	722.07	201.14
39.662	722.20	199.14
39.682	722.32	198.29
39.703	722.44	197.29
39.723	722.56	198.86
39.744	722.68	202.43
39.765	722.80	205.43
39.785	722.92	210.43
39.806	723.04	216.57
39.826	723.16	216.29
39.847	723.28	214.29
39.867	723.40	210.86
39.888	723.52	207.57
39.908	723.64	203.71
39.929	723.76	199.29
39.950	723.88	198.86
39.970	724.00	196.86
39.991	724.12	196.14
40.011	724.24	196.57
40.032	724.36	195.43
40.052	724.48	197.86
40.073	724.60	202.29
40.093	724.72	206.86
40.114	724.84	209.57
40.135	724.96	211.43
40.155	725.08	208.29
40.176	725.20	208.71
40.196	725.32	205.43
40.217	725.44	205.43
40.237	725.56	204.29
40.258	725.68	201.29
40.279	725.80	199.14
40.299	725.92	198.00

40.320	726.04	196.43
40.340	726.16	196.00
40.361	726.28	193.29
40.381	726.40	190.43
40.402	726.52	194.00
40.422	726.64	197.71
40.443	726.76	201.14
40.464	726.88	204.86
40.484	727.00	210.86
40.505	727.12	211.29
40.525	727.24	210.43
40.546	727.36	209.29
40.566	727.48	210.29
40.587	727.60	209.57
40.608	727.72	216.00
40.628	727.84	216.86
40.649	727.96	220.00
40.669	728.08	223.29
40.690	728.20	219.29
40.710	728.32	219.14
40.731	728.44	220.57
40.751	728.56	222.71
40.772	728.68	224.43
40.793	728.80	219.00
40.813	728.92	215.86
40.834	729.04	216.71
40.854	729.16	217.00
40.875	729.28	215.86
40.895	729.40	212.71
40.916	729.52	210.29
40.936	729.64	206.29
40.957	729.76	200.86
40.978	729.88	201.00
40.998	730.00	200.00
41.019	730.13	201.71
41.039	730.25	203.43
41.060	730.37	203.57
41.080	730.49	206.71
41.101	730.61	209.86
41.122	730.73	215.57
41.142	730.85	218.14

41.163	730.97	220.29
41.183	731.09	221.71
41.204	731.21	222.00
41.224	731.33	218.43
41.245	731.45	213.00
41.265	731.57	207.43
41.286	731.69	206.43
41.307	731.81	207.14
41.327	731.93	209.86
41.348	732.05	208.71
41.368	732.17	211.71
41.389	732.29	215.57
41.409	732.41	214.71
41.430	732.53	215.57
41.451	732.65	219.14
41.471	732.77	221.14
41.492	732.89	220.29
41.512	733.01	223.71
41.533	733.13	225.57
41.553	733.25	223.57
41.574	733.37	224.29
41.594	733.49	224.00
41.615	733.61	226.29
41.636	733.73	226.57
41.656	733.85	229.00
41.677	733.97	231.14
41.697	734.09	232.43
41.718	734.21	229.43
41.738	734.33	232.00
41.759	734.45	230.86
41.779	734.57	229.43
41.800	734.69	228.86
41.821	734.81	227.00
41.841	734.93	225.14
41.862	735.05	222.57
41.882	735.17	221.00
41.903	735.29	222.43
41.923	735.41	224.43
41.944	735.53	225.71
41.965	735.65	228.00
41.985	735.77	228.29

42.006	735.89	227.14
42.026	736.01	226.86
42.047	736.13	223.43
42.067	736.25	222.57
42.088	736.37	224.00
42.108	736.49	227.14
42.129	736.61	227.14
42.150	736.73	230.00
42.170	736.85	226.43
42.191	736.97	222.43
42.211	737.09	221.00
42.232	737.21	223.14
42.252	737.33	226.29
42.273	737.45	226.71
42.294	737.57	225.43
42.314	737.69	225.43
42.335	737.81	223.86
42.355	737.93	224.86
42.376	738.06	225.43
42.396	738.18	225.00
42.417	738.30	223.29
42.437	738.42	224.14
42.458	738.54	225.00
42.479	738.66	227.71
42.499	738.78	226.43
42.520	738.90	224.43
42.540	739.02	230.14
42.561	739.14	234.57
42.581	739.26	236.00
42.602	739.38	236.86
42.622	739.50	235.00
42.643	739.62	232.71
42.664	739.74	235.14
42.684	739.86	237.00
42.705	739.98	238.71
42.725	740.10	239.71
42.746	740.22	237.00
42.766	740.34	235.86
42.787	740.46	234.71
42.808	740.58	234.29
42.828	740.70	236.14

42.849	740.82	236.29
42.869	740.94	233.29
42.890	741.06	231.00
42.910	741.18	232.43
42.931	741.30	231.86
42.951	741.42	230.71
42.972	741.54	229.71
42.993	741.66	227.71
43.013	741.78	224.57
43.034	741.90	225.14
43.054	742.02	224.00
43.075	742.14	223.43
43.095	742.26	224.43
43.116	742.38	223.71
43.136	742.50	227.43
43.157	742.62	231.57
43.178	742.74	231.71
43.198	742.86	232.71
43.219	742.98	231.43
43.239	743.10	228.43
43.260	743.22	226.00
43.280	743.34	224.43
43.301	743.46	225.00
43.322	743.58	228.86
43.342	743.70	230.86
43.363	743.82	233.29
43.383	743.94	235.71
43.404	744.06	232.29
43.424	744.18	232.00
43.445	744.30	233.43
43.465	744.42	232.14
43.486	744.54	229.86
43.507	744.66	228.14
43.527	744.78	230.00
43.548	744.90	231.00
43.568	745.02	232.43
43.589	745.14	230.57
43.609	745.26	230.43
43.630	745.38	227.43
43.651	745.50	226.86
43.671	745.62	226.00

43.692	745.74	226.43
43.712	745.87	224.71
43.733	745.99	224.71
43.753	746.11	224.43
43.774	746.23	224.43
43.794	746.35	223.43
43.815	746.47	223.14
43.836	746.59	226.29
43.856	746.71	227.00
43.877	746.83	224.71
43.897	746.95	224.00
43.918	747.07	223.43
43.938	747.19	222.00
43.959	747.31	226.29
43.979	747.43	228.57
44.000	747.55	226.43
44.021	747.67	221.29
44.041	747.79	218.43
44.062	747.91	214.43
44.082	748.03	210.00
44.103	748.15	199.57
44.123	748.27	196.71
44.144	748.39	195.86
44.165	748.51	196.71
44.185	748.63	197.57
44.206	748.75	199.29
44.226	748.87	198.57
44.247	748.99	194.71
44.267	749.11	190.43
44.288	749.23	185.86
44.308	749.35	181.14
44.329	749.47	175.71
44.350	749.59	175.14
44.370	749.71	174.57
44.391	749.83	174.43
44.411	749.95	179.00
44.432	750.07	183.86
44.452	750.19	188.14
44.473	750.31	196.43
44.494	750.43	207.43
44.514	750.55	209.14

44.535	750.67	208.14
44.555	750.79	210.57
44.576	750.91	212.14
44.596	751.03	212.71
44.617	751.15	213.71
44.637	751.27	215.00
44.658	751.39	214.29
44.679	751.51	214.29
44.699	751.63	211.71
44.720	751.75	208.29
44.740	751.87	204.00
44.761	751.99	203.86
44.781	752.11	201.71
44.802	752.23	200.00
44.822	752.35	196.71
44.843	752.47	192.14
44.864	752.59	190.00
44.884	752.71	190.00
44.905	752.83	190.57
44.925	752.95	192.86
44.946	753.07	193.14
44.966	753.19	195.29
44.987	753.31	194.71
45.008	753.43	197.29
45.028	753.55	201.00
45.049	753.67	204.71
45.069	753.80	207.43
45.090	753.92	209.29
45.110	754.04	210.29
45.131	754.16	210.71
45.151	754.28	212.71
45.172	754.40	215.57
45.193	754.52	215.43
45.213	754.64	213.00
45.234	754.76	211.43
45.254	754.88	208.86
45.275	755.00	210.00
45.295	755.12	209.86
45.316	755.24	209.71
45.336	755.36	210.00
45.357	755.48	208.71

45.378	755.60	208.29
45.398	755.72	205.00
45.419	755.84	201.43
45.439	755.96	203.43
45.460	756.08	204.29
45.480	756.20	206.43
45.501	756.32	209.00
45.522	756.44	211.57
45.542	756.56	216.71
45.563	756.68	218.86
45.583	756.80	219.71
45.604	756.92	217.71
45.624	757.04	212.43
45.645	757.16	210.86
45.665	757.28	205.00
45.686	757.40	203.00
45.707	757.52	205.00
45.727	757.64	205.29
45.748	757.76	208.43
45.768	757.88	210.00
45.789	758.00	207.86
45.809	758.12	207.14
45.830	758.24	206.71
45.851	758.36	209.14
45.871	758.48	210.86
45.892	758.60	208.14
45.912	758.72	211.29
45.933	758.84	210.14
45.953	758.96	207.43
45.974	759.08	208.57
45.994	759.20	211.29
46.015	759.32	212.43
46.036	759.44	210.00
46.056	759.56	211.86
46.077	759.68	211.00
46.097	759.80	210.14
46.118	759.92	211.14
46.138	760.04	213.57
46.159	760.16	217.57
46.179	760.28	217.29
46.200	760.40	217.71

46.221	760.52	218.29
46.241	760.64	221.14
46.262	760.76	218.57
46.282	760.88	216.43
46.303	761.00	216.86
46.323	761.12	213.71
46.344	761.24	213.86
46.365	761.36	211.00
46.385	761.48	209.57
46.406	761.60	208.00
46.426	761.73	205.29
46.447	761.85	202.43
46.467	761.97	199.86
46.488	762.09	201.29
46.508	762.21	200.86
46.529	762.33	200.43
46.550	762.45	198.43
46.570	762.57	198.00
46.591	762.69	198.29
46.611	762.81	195.14
46.632	762.93	194.86
46.652	763.05	192.00
46.673	763.17	186.71
46.694	763.29	183.14
46.714	763.41	181.29
46.735	763.53	179.00
46.755	763.65	180.71
46.776	763.77	184.71
46.796	763.89	188.29
46.817	764.01	191.86
46.837	764.13	193.14
46.858	764.25	197.57
46.879	764.37	200.57
46.899	764.49	202.00
46.920	764.61	203.14
46.940	764.73	202.29
46.961	764.85	205.57
46.981	764.97	207.86
47.002	765.09	209.71
47.022	765.21	213.29
47.043	765.33	216.29

47.064	765.45	216.00
47.084	765.57	215.86
47.105	765.69	213.29
47.125	765.81	209.71
47.146	765.93	208.71
47.166	766.05	207.29
47.187	766.17	206.71
47.208	766.29	205.29
47.228	766.41	207.71
47.249	766.53	206.43
47.269	766.65	208.29
47.290	766.77	211.43
47.310	766.89	214.57
47.331	767.01	216.57
47.351	767.13	218.00
47.372	767.25	217.57
47.393	767.37	215.43
47.413	767.49	213.86
47.434	767.61	213.14
47.454	767.73	214.14
47.475	767.85	215.86
47.495	767.97	213.14
47.516	768.09	210.86
47.536	768.21	212.57
47.557	768.33	211.00
47.578	768.45	210.00
47.598	768.57	209.43
47.619	768.69	210.43
47.639	768.81	208.29
47.660	768.93	208.00
47.680	769.05	207.43
47.701	769.17	204.71
47.722	769.29	202.57
47.742	769.41	201.43
47.763	769.53	199.00
47.783	769.66	199.29
47.804	769.78	197.14
47.824	769.90	195.00
47.845	770.02	195.57
47.865	770.14	193.57
47.886	770.26	193.14

47.907	770.38	192.14
47.927	770.50	194.29
47.948	770.62	196.86
47.968	770.74	199.57
47.989	770.86	205.29
48.009	770.98	209.00
48.030	771.10	210.71
48.051	771.22	211.86
48.071	771.34	212.86
48.092	771.46	212.00
48.112	771.58	207.71
48.133	771.70	205.71
48.153	771.82	204.00
48.174	771.94	204.29
48.194	772.06	208.14
48.215	772.18	207.14
48.236	772.30	208.86
48.256	772.42	208.00
48.277	772.54	208.71
48.297	772.66	209.71
48.318	772.78	215.57
48.338	772.90	218.71
48.359	773.02	221.14
48.379	773.14	223.71
48.400	773.26	223.00
48.421	773.38	220.86
48.441	773.50	221.00
48.462	773.62	219.14
48.482	773.74	221.43
48.503	773.86	223.29
48.523	773.98	223.43
48.544	774.10	221.86
48.565	774.22	224.00
48.585	774.34	225.29
48.606	774.46	226.00
48.626	774.58	227.57
48.647	774.70	229.29
48.667	774.82	230.00
48.688	774.94	228.29
48.708	775.06	226.14
48.729	775.18	223.29

48.750	775.30	218.86
48.770	775.42	218.14
48.791	775.54	218.43
48.811	775.66	222.00
48.832	775.78	226.71
48.852	775.90	229.00
48.873	776.02	229.00
48.894	776.14	226.86
48.914	776.26	226.14
48.935	776.38	222.57
48.955	776.50	223.43
48.976	776.62	229.43
48.996	776.74	234.29
49.017	776.86	234.29
49.037	776.98	234.71
49.058	777.10	237.71
49.079	777.22	237.43
49.099	777.34	238.29
49.120	777.46	238.00
49.140	777.59	238.14
49.161	777.71	238.57
49.181	777.83	236.14
49.202	777.95	236.00
49.222	778.07	234.86
49.243	778.19	230.29
49.264	778.31	227.71
49.284	778.43	225.43
49.305	778.55	222.57
49.325	778.67	219.86
49.346	778.79	222.14
49.366	778.91	226.57
49.387	779.03	233.43
49.408	779.15	231.00
49.428	779.27	228.86
49.449	779.39	225.86
49.469	779.51	227.00
49.490	779.63	226.86
49.510	779.75	230.00
49.531	779.87	229.86
49.551	779.99	226.57
49.572	780.11	222.86

49.593	780.23	224.57
49.613	780.35	226.71
49.634	780.47	224.29
49.654	780.59	221.43
49.675	780.71	223.86
49.695	780.83	223.14
49.716	780.95	223.57
49.736	781.07	224.71
49.757	781.19	224.29
49.778	781.31	225.57
49.798	781.43	227.29
49.819	781.55	226.86
49.839	781.67	232.14
49.860	781.79	240.00
49.880	781.91	240.57
49.901	782.03	242.57
49.922	782.15	242.43
49.942	782.27	243.43
49.963	782.39	240.43
49.983	782.51	238.43
50.004	782.63	234.00
50.024	782.75	234.29
50.045	782.87	230.86
50.065	782.99	226.71
50.086	783.11	225.86
50.107	783.23	224.43
50.127	783.35	224.43
50.148	783.47	224.14
50.168	783.59	224.71
50.189	783.71	223.71
50.209	783.83	221.71
50.230	783.95	220.57
50.251	784.07	218.57
50.271	784.19	218.14
50.292	784.31	217.57
50.312	784.43	219.71
50.333	784.55	217.43
50.353	784.67	217.29
50.374	784.79	216.71
50.394	784.91	215.86
50.415	785.03	214.43

50.436	785.15	210.29
50.456	785.27	208.14
50.477	785.40	207.29
50.497	785.52	210.86
50.518	785.64	213.29
50.538	785.76	213.29
50.559	785.88	214.00
50.579	786.00	216.57
50.600	786.12	221.43
50.621	786.24	224.14
50.641	786.36	230.00
50.662	786.48	231.86
50.682	786.60	232.29
50.703	786.72	230.71
50.723	786.84	232.43
50.744	786.96	233.14
50.765	787.08	231.00
50.785	787.20	230.71
50.806	787.32	225.71
50.826	787.44	223.29
50.847	787.56	220.57
50.867	787.68	221.29
50.888	787.80	220.71
50.908	787.92	216.86
50.929	788.04	218.14
50.950	788.16	219.71
50.970	788.28	217.43
50.991	788.40	217.14
51.011	788.52	216.71
51.032	788.64	217.29
51.052	788.76	220.29
51.073	788.88	218.71
51.094	789.00	217.71
51.114	789.12	217.43
51.135	789.24	215.86
51.155	789.36	211.71
51.176	789.48	214.00
51.196	789.60	216.57
51.217	789.72	220.14
51.237	789.84	218.00
51.258	789.96	219.14

51.279	790.08	218.43
51.299	790.20	221.14
51.320	790.32	220.43
51.340	790.44	222.57
51.361	790.56	220.57
51.381	790.68	220.71
51.402	790.80	226.00
51.422	790.92	228.86
51.443	791.04	231.71
51.464	791.16	235.71
51.484	791.28	235.29
51.505	791.40	234.71
51.525	791.52	236.29
51.546	791.64	236.43
51.566	791.76	239.29
51.587	791.88	235.57
51.608	792.00	232.29
51.628	792.12	231.29
51.649	792.24	227.86
51.669	792.36	227.57
51.690	792.48	228.57
51.710	792.60	231.14
51.731	792.72	229.29
51.751	792.84	231.71
51.772	792.96	229.86
51.793	793.08	229.00
51.813	793.20	224.57
51.834	793.33	220.14
51.854	793.45	216.71
51.875	793.57	216.29
51.895	793.69	216.57
51.916	793.81	218.71
51.937	793.93	218.29
51.957	794.05	217.57
51.978	794.17	219.43
51.998	794.29	216.14
52.019	794.41	217.14
52.039	794.53	212.29
52.060	794.65	212.00
52.080	794.77	209.57
52.101	794.89	206.71

52.122	795.01	203.71
52.142	795.13	201.14
52.163	795.25	200.86
52.183	795.37	199.71
52.204	795.49	199.86
52.224	795.61	197.57
52.245	795.73	202.57
52.265	795.85	202.29
52.286	795.97	197.43
52.307	796.09	197.14
52.327	796.21	196.71
52.348	796.33	194.14
52.368	796.45	192.86
52.389	796.57	193.00
52.409	796.69	192.71
52.430	796.81	194.00
52.451	796.93	197.00
52.471	797.05	201.86
52.492	797.17	202.43
52.512	797.29	202.29
52.533	797.41	200.71
52.553	797.53	198.43
52.574	797.65	194.86
52.594	797.77	191.71
52.615	797.89	192.14
52.636	798.01	193.43
52.656	798.13	198.14
52.677	798.25	198.29
52.697	798.37	195.29
52.718	798.49	191.71
52.738	798.61	189.14
52.759	798.73	187.43
52.779	798.85	184.43
52.800	798.97	180.57
52.821	799.09	178.00
52.841	799.21	173.43
52.862	799.33	171.29
52.882	799.45	169.71
52.903	799.57	171.14
52.923	799.69	170.71
52.944	799.81	170.43

52.965	799.93	169.86
52.985	800.05	167.00
53.006	800.17	169.00
53.026	800.29	170.14
53.047	800.41	171.14
53.067	800.53	174.00
53.088	800.65	176.43
53.108	800.77	178.86
53.129	800.89	180.00
53.150	801.01	180.43
53.170	801.13	184.14
53.191	801.26	187.00
53.211	801.38	186.57
53.232	801.50	188.71
53.252	801.62	188.86
53.273	801.74	191.86
53.294	801.86	195.00
53.314	801.98	203.86
53.335	802.10	204.29
53.355	802.22	204.14
53.376	802.34	204.14
53.396	802.46	206.29
53.417	802.58	200.57
53.437	802.70	195.86
53.458	802.82	196.00
53.479	802.94	197.43
53.499	803.06	201.57
53.520	803.18	205.57
53.540	803.30	207.14
53.561	803.42	208.29
53.581	803.54	207.57
53.602	803.66	205.86
53.622	803.78	202.86
53.643	803.90	201.43
53.664	804.02	201.86
53.684	804.14	199.57
53.705	804.26	199.86
53.725	804.38	199.14
53.746	804.50	200.43
53.766	804.62	200.86
53.787	804.74	201.71

53.808	804.86	203.00
53.828	804.98	204.29
53.849	805.10	204.14
53.869	805.22	202.14
53.890	805.34	199.14
53.910	805.46	199.14
53.931	805.58	198.86
53.951	805.70	200.57
53.972	805.82	202.86
53.993	805.94	203.57
54.013	806.06	206.00
54.034	806.18	207.71
54.054	806.30	207.71
54.075	806.42	210.57
54.095	806.54	208.57
54.116	806.66	208.14
54.137	806.78	205.71
54.157	806.90	200.14
54.178	807.02	204.57
54.198	807.14	207.00
54.219	807.26	209.00
54.239	807.38	208.57
54.260	807.50	209.57
54.280	807.62	210.71
54.301	807.74	208.43
54.322	807.86	206.00
54.342	807.98	206.43
54.363	808.10	207.71
54.383	808.22	203.14
54.404	808.34	203.86
54.424	808.46	204.00
54.445	808.58	203.43
54.465	808.70	203.86
54.486	808.82	202.00
54.507	808.94	201.71
54.527	809.06	200.86
54.548	809.19	201.14
54.568	809.31	204.29
54.589	809.43	204.43
54.609	809.55	206.14
54.630	809.67	209.43

54.651	809.79	212.86
54.671	809.91	213.57
54.692	810.03	212.29
54.712	810.15	212.14
54.733	810.27	209.00
54.753	810.39	208.14
54.774	810.51	205.00
54.794	810.63	207.14
54.815	810.75	209.43
54.836	810.87	204.14
54.856	810.99	205.71
54.877	811.11	205.00
54.897	811.23	204.71
54.918	811.35	205.43
54.938	811.47	206.14
54.959	811.59	206.14
54.979	811.71	205.57
55.000	811.83	207.71
55.021	811.95	205.00
55.041	812.07	205.00
55.062	812.19	205.43
55.082	812.31	205.86
55.103	812.43	205.57
55.123	812.55	207.00
55.144	812.67	208.86
55.165	812.79	207.29
55.185	812.91	205.86
55.206	813.03	204.00
55.226	813.15	204.00
55.247	813.27	204.43
55.267	813.39	205.29
55.288	813.51	206.71
55.308	813.63	209.00
55.329	813.75	210.00
55.350	813.87	209.29
55.370	813.99	206.00
55.391	814.11	204.29
55.411	814.23	204.29
55.432	814.35	208.14
55.452	814.47	209.86
55.473	814.59	210.71

55.494	814.71	212.14
55.514	814.83	212.00
55.535	814.95	214.00
55.555	815.07	214.29
55.576	815.19	214.86
55.596	815.31	211.57
55.617	815.43	212.14
55.637	815.55	206.71
55.658	815.67	207.57
55.679	815.79	207.57
55.699	815.91	208.57
55.720	816.03	210.29
55.740	816.15	215.43
55.761	816.27	214.43
55.781	816.39	211.43
55.802	816.51	212.71
55.822	816.63	213.71
55.843	816.75	212.57
55.864	816.87	210.29
55.884	816.99	208.14
55.905	817.12	208.71
55.925	817.24	209.57
55.946	817.36	211.00
55.966	817.48	213.86
55.987	817.60	219.29
56.008	817.72	220.29
56.028	817.84	220.00
56.049	817.96	221.29
56.069	818.08	220.57
56.090	818.20	216.86
56.110	818.32	217.57
56.131	818.44	219.29
56.151	818.56	219.29
56.172	818.68	217.57
56.193	818.80	215.57
56.213	818.92	213.14
56.234	819.04	213.57
56.254	819.16	212.71
56.275	819.28	208.71
56.295	819.40	206.71
56.316	819.52	208.71

56.337	819.64	210.71
56.357	819.76	210.14
56.378	819.88	209.00
56.398	820.00	208.14
56.419	820.12	210.86
56.439	820.24	211.43
56.460	820.36	212.86
56.480	820.48	215.29
56.501	820.60	214.00
56.522	820.72	218.14
56.542	820.84	218.57
56.563	820.96	220.29
56.583	821.08	221.43
56.604	821.20	222.29
56.624	821.32	221.57
56.645	821.44	223.43
56.665	821.56	221.43
56.686	821.68	221.43
56.707	821.80	219.71
56.727	821.92	219.43
56.748	822.04	220.43
56.768	822.16	221.43
56.789	822.28	225.00
56.809	822.40	226.43
56.830	822.52	227.57
56.851	822.64	229.71
56.871	822.76	233.00
56.892	822.88	227.71
56.912	823.00	230.00
56.933	823.12	229.57
56.953	823.24	231.57
56.974	823.36	233.00
56.994	823.48	233.29
57.015	823.60	233.86
57.036	823.72	232.00
57.056	823.84	233.57
57.077	823.96	233.29
57.097	824.08	231.29
57.118	824.20	228.57
57.138	824.32	228.29
57.159	824.44	225.29

57.179	824.56	221.71
57.200	824.68	221.14
57.221	824.80	221.43
57.241	824.93	225.14
57.262	825.05	224.57
57.282	825.17	224.71
57.303	825.29	225.43
57.323	825.41	224.14
57.344	825.53	221.14
57.365	825.65	220.00
57.385	825.77	217.29
57.406	825.89	214.29
57.426	826.01	210.14
57.447	826.13	208.00
57.467	826.25	209.14
57.488	826.37	215.14
57.508	826.49	220.29
57.529	826.61	217.57
57.550	826.73	214.43
57.570	826.85	217.57
57.591	826.97	219.29
57.611	827.09	223.71
57.632	827.21	224.86
57.652	827.33	226.00
57.673	827.45	227.71
57.694	827.57	227.71
57.714	827.69	222.14
57.735	827.81	216.43
57.755	827.93	212.29
57.776	828.05	209.14
57.796	828.17	215.29
57.817	828.29	223.00
57.837	828.41	222.86
57.858	828.53	225.43
57.879	828.65	228.43
57.899	828.77	228.71
57.920	828.89	224.71
57.940	829.01	221.29
57.961	829.13	216.71
57.981	829.25	215.14
58.002	829.37	213.71

58.022	829.49	211.29
58.043	829.61	215.57
58.064	829.73	218.00
58.084	829.85	218.71
58.105	829.97	217.29
58.125	830.09	215.86
58.146	830.21	209.86
58.166	830.33	207.71
58.187	830.45	206.00
58.208	830.57	211.43
58.228	830.69	216.29
58.249	830.81	219.00
58.269	830.93	217.57
58.290	831.05	217.71
58.310	831.17	214.43
58.331	831.29	213.43
58.351	831.41	213.43
58.372	831.53	212.00
58.393	831.65	208.00
58.413	831.77	205.14
58.434	831.89	200.71
58.454	832.01	197.14
58.475	832.13	194.71
58.495	832.25	195.14
58.516	832.37	194.00
58.537	832.49	194.14
58.557	832.61	194.29
58.578	832.73	194.29
58.598	832.86	194.29
58.619	832.98	193.86
58.639	833.10	196.71
58.660	833.22	198.00
58.680	833.34	196.57
58.701	833.46	196.71
58.722	833.58	195.00
58.742	833.70	195.00
58.763	833.82	194.29
58.783	833.94	193.00
58.804	834.06	188.43
58.824	834.18	185.43
58.845	834.30	182.71

58.865	834.42	178.14
58.886	834.54	174.57
58.907	834.66	176.57
58.927	834.78	178.71
58.948	834.90	178.14
58.968	835.02	178.57
58.989	835.14	182.86
59.009	835.26	180.86
59.030	835.38	178.43
59.051	835.50	175.29
59.071	835.62	174.86
59.092	835.74	174.71
59.112	835.86	173.14
59.133	835.98	175.29
59.153	836.10	177.86
59.174	836.22	182.00
59.194	836.34	184.00
59.215	836.46	185.57
59.236	836.58	187.86
59.256	836.70	190.43
59.277	836.82	189.71
59.297	836.94	189.86
59.318	837.06	190.29
59.338	837.18	191.86
59.359	837.30	193.43
59.379	837.42	194.57
59.400	837.54	191.86
59.421	837.66	192.43
59.441	837.78	194.00
59.462	837.90	198.71
59.482	838.02	207.14
59.503	838.14	207.86
59.523	838.26	205.14
59.544	838.38	206.29
59.565	838.50	205.14
59.585	838.62	201.14
59.606	838.74	201.00
59.626	838.86	203.43
59.647	838.98	209.71
59.667	839.10	213.43
59.688	839.22	217.00

59.708	839.34	217.14
59.729	839.46	219.57
59.750	839.58	221.57
59.770	839.70	224.43
59.791	839.82	227.57
59.811	839.94	229.71
59.832	840.06	231.00
59.852	840.18	232.00
59.873	840.30	232.29
59.894	840.42	232.14
59.914	840.54	236.29
59.935	840.66	235.43
59.955	840.79	233.29
59.976	840.91	228.14
59.996	841.03	225.29
60.017	841.15	224.43
60.037	841.27	220.43
60.058	841.39	221.14
60.079	841.51	218.29
60.099	841.63	218.71
60.120	841.75	221.86
60.140	841.87	221.14
60.161	841.99	221.00
60.181	842.11	220.86
60.202	842.23	216.71
60.222	842.35	212.71
60.243	842.47	209.86
60.264	842.59	209.71
60.284	842.71	211.43
60.305	842.83	214.14
60.325	842.95	218.00
60.346	843.07	221.14
60.366	843.19	224.14
60.387	843.31	219.29
60.408	843.43	215.71
60.428	843.55	212.29
60.449	843.67	212.29
60.469	843.79	212.43
60.490	843.91	213.00
60.510	844.03	214.00
60.531	844.15	213.29

60.551	844.27	210.71
60.572	844.39	208.71
60.593	844.51	209.43
60.613	844.63	211.00
60.634	844.75	211.71
60.654	844.87	213.71
60.675	844.99	215.57
60.695	845.11	215.43
60.716	845.23	218.71
60.737	845.35	216.00
60.757	845.47	211.86
60.778	845.59	207.43
60.798	845.71	202.00
60.819	845.83	199.14
60.839	845.95	198.57
60.860	846.07	197.29
60.880	846.19	198.86
60.901	846.31	206.43
60.922	846.43	209.86
60.942	846.55	209.71
60.963	846.67	207.86
60.983	846.79	207.57
61.004	846.91	204.29
61.024	847.03	204.43
61.045	847.15	203.71
61.065	847.27	206.86
61.086	847.39	209.14
61.107	847.51	209.86
61.127	847.63	209.71
61.148	847.75	209.86
61.168	847.87	206.86
61.189	847.99	204.43
61.209	848.11	203.57
61.230	848.23	206.71
61.251	848.35	209.14
61.271	848.47	213.00
61.292	848.59	213.14
61.312	848.72	210.43
61.333	848.84	209.57
61.353	848.96	207.14
61.374	849.08	206.43

61.394	849.20	208.14
61.415	849.32	207.14
61.436	849.44	207.00
61.456	849.56	203.14
61.477	849.68	202.71
61.497	849.80	200.71
61.518	849.92	199.00
61.538	850.04	199.43
61.559	850.16	200.14
61.580	850.28	202.57
61.600	850.40	200.14
61.621	850.52	200.43
61.641	850.64	200.86
61.662	850.76	204.86
61.682	850.88	207.71
61.703	851.00	204.57
61.723	851.12	204.29
61.744	851.24	204.57
61.765	851.36	206.14
61.785	851.48	207.00
61.806	851.60	209.14
61.826	851.72	209.86
61.847	851.84	213.00
61.867	851.96	211.43
61.888	852.08	211.29
61.908	852.20	207.00
61.929	852.32	204.86
61.950	852.44	201.43
61.970	852.56	196.57
61.991	852.68	193.86
62.011	852.80	193.71
62.032	852.92	191.86
62.052	853.04	193.57
62.073	853.16	190.00
62.094	853.28	188.14
62.114	853.40	188.43
62.135	853.52	187.43
62.155	853.64	185.43
62.176	853.76	181.43
62.196	853.88	173.00
62.217	854.00	167.43

62.237	854.12	163.71
62.258	854.24	163.29
62.279	854.36	164.43
62.299	854.48	163.57
62.320	854.60	163.57
62.340	854.72	162.00
62.361	854.84	163.29
62.381	854.96	164.86
62.402	855.08	166.57
62.422	855.20	167.29
62.443	855.32	167.43
62.464	855.44	167.29
62.484	855.56	167.43
62.505	855.68	165.14
62.525	855.80	164.57
62.546	855.92	162.43
62.566	856.04	160.86
62.587	856.16	160.29
62.608	856.28	161.14
62.628	856.40	163.86
62.649	856.52	169.86
62.669	856.65	172.43
62.690	856.77	175.00
62.710	856.89	179.86
62.731	857.01	182.86
62.751	857.13	185.00
62.772	857.25	183.71
62.793	857.37	185.86
62.813	857.49	189.71
62.834	857.61	198.71
62.854	857.73	202.71
62.875	857.85	203.14
62.895	857.97	205.43
62.916	858.09	207.57
62.937	858.21	209.71
62.957	858.33	208.57
62.978	858.45	208.86
62.998	858.57	211.43
63.019	858.69	208.43
63.039	858.81	205.71
63.060	858.93	205.86

63.080	859.05	206.29
63.101	859.17	203.29
63.122	859.29	202.29
63.142	859.41	201.14
63.163	859.53	198.57
63.183	859.65	200.29
63.204	859.77	201.57
63.224	859.89	201.14
63.245	860.01	201.57
63.265	860.13	207.43
63.286	860.25	210.57
63.307	860.37	215.57
63.327	860.49	213.43
63.348	860.61	212.86
63.368	860.73	211.86
63.389	860.85	211.00
63.409	860.97	214.43
63.430	861.09	211.57
63.451	861.21	210.00
63.471	861.33	208.43
63.492	861.45	208.71
63.512	861.57	208.71
63.533	861.69	208.00
63.553	861.81	211.71
63.574	861.93	211.71
63.594	862.05	209.00
63.615	862.17	207.29
63.636	862.29	205.86
63.656	862.41	206.14
63.677	862.53	206.43
63.697	862.65	205.29
63.718	862.77	202.14
63.738	862.89	203.00
63.759	863.01	203.57
63.780	863.13	201.86
63.800	863.25	202.29
63.821	863.37	203.29
63.841	863.49	205.00
63.862	863.61	202.57
63.882	863.73	201.71
63.903	863.85	200.00

63.923	863.97	202.00
63.944	864.09	207.29
63.965	864.21	209.14
63.985	864.33	207.43
64.006	864.46	208.43
64.026	864.58	205.86
64.047	864.70	204.14
64.067	864.82	209.57
64.088	864.94	210.43
64.108	865.06	209.86
64.129	865.18	211.14
64.150	865.30	214.14
64.170	865.42	214.00
64.191	865.54	210.14
64.211	865.66	202.71
64.232	865.78	200.86
64.252	865.90	198.57
64.273	866.02	194.71
64.294	866.14	191.57
64.314	866.26	195.57
64.335	866.38	199.57
64.355	866.50	203.14
64.376	866.62	206.29
64.396	866.74	207.14
64.417	866.86	203.57
64.437	866.98	200.43
64.458	867.10	198.71
64.479	867.22	197.29
64.499	867.34	194.71
64.520	867.46	193.00
64.540	867.58	189.00
64.561	867.70	186.86
64.581	867.82	188.71
64.602	867.94	192.71
64.622	868.06	193.43
64.643	868.18	195.43
64.664	868.30	194.14
64.684	868.42	193.00
64.705	868.54	195.86
64.725	868.66	194.71
64.746	868.78	193.14

64.766	868.90	193.71
64.787	869.02	195.43
64.808	869.14	196.57
64.828	869.26	195.86
64.849	869.38	192.00
64.869	869.50	189.43
64.890	869.62	189.14
64.910	869.74	187.14
64.931	869.86	188.86
64.951	869.98	190.14
64.972	870.10	191.57
64.993	870.22	194.14
65.013	870.34	195.86
65.034	870.46	198.14
65.054	870.58	197.71
65.075	870.70	199.43
65.095	870.82	199.14
65.116	870.94	198.43
65.137	871.06	198.57
65.157	871.18	200.29
65.178	871.30	202.57
65.198	871.42	205.00
65.219	871.54	205.14
65.239	871.66	207.57
65.260	871.78	208.00
65.280	871.90	210.57
65.301	872.02	207.43
65.322	872.14	202.29
65.342	872.26	200.86
65.363	872.39	200.14
65.383	872.51	199.29
65.404	872.63	201.29
65.424	872.75	204.00
65.445	872.87	202.29
65.465	872.99	201.57
65.486	873.11	203.86
65.507	873.23	201.14
65.527	873.35	200.00
65.548	873.47	197.43
65.568	873.59	195.29
65.589	873.71	189.43

65.609	873.83	186.71
65.630	873.95	185.14
65.651	874.07	181.86
65.671	874.19	182.71
65.692	874.31	181.14
65.712	874.43	180.86
65.733	874.55	180.00
65.753	874.67	179.14
65.774	874.79	175.86
65.794	874.91	172.00
65.815	875.03	167.14
65.836	875.15	163.86
65.856	875.27	161.43
65.877	875.39	161.14
65.897	875.51	159.43
65.918	875.63	158.29
65.938	875.75	159.00
65.959	875.87	161.57
65.980	875.99	164.57
66.000	876.11	169.29
66.021	876.23	174.57
66.041	876.35	176.43
66.062	876.47	177.14
66.082	876.59	178.14
66.103	876.71	179.86
66.123	876.83	180.00
66.144	876.95	181.00
66.165	877.07	184.57
66.185	877.19	186.00
66.206	877.31	185.86
66.226	877.43	185.86
66.247	877.55	187.86
66.267	877.67	187.00
66.288	877.79	186.14
66.308	877.91	187.71
66.329	878.03	189.43
66.350	878.15	189.86
66.370	878.27	191.43
66.391	878.39	189.57
66.411	878.51	192.43
66.432	878.63	192.86

66.452	878.75	190.86
66.473	878.87	192.14
66.494	878.99	192.43
66.514	879.11	194.86
66.535	879.23	199.14
66.555	879.35	200.57
66.576	879.47	201.29
66.596	879.59	203.43
66.617	879.71	205.57
66.637	879.83	206.57
66.658	879.95	204.86
66.679	880.07	205.43
66.699	880.19	205.43
66.720	880.32	204.86
66.740	880.44	204.71
66.761	880.56	205.14
66.781	880.68	205.00
66.802	880.80	202.57
66.822	880.92	201.43
66.843	881.04	203.29
66.864	881.16	203.57
66.884	881.28	204.14
66.905	881.40	203.86
66.925	881.52	207.43
66.946	881.64	211.43
66.966	881.76	210.14
66.987	881.88	211.00
67.008	882.00	211.86
67.028	882.12	213.29
67.049	882.24	216.29
67.069	882.36	218.86
67.090	882.48	218.43
67.110	882.60	218.00
67.131	882.72	217.29
67.151	882.84	219.29
67.172	882.96	221.00
67.193	883.08	221.86
67.213	883.20	219.86
67.234	883.32	219.86
67.254	883.44	219.14
67.275	883.56	220.57

67.295	883.68	224.57
67.316	883.80	225.29
67.337	883.92	223.71
67.357	884.04	220.43
67.378	884.16	218.14
67.398	884.28	216.86
67.419	884.40	217.71
67.439	884.52	214.00
67.460	884.64	214.43
67.480	884.76	214.14
67.501	884.88	216.43
67.522	885.00	218.00
67.542	885.12	217.00
67.563	885.24	218.29
67.583	885.36	216.43
67.604	885.48	217.57
67.624	885.60	215.71
67.645	885.72	214.29
67.665	885.84	214.14
67.686	885.96	213.29
67.707	886.08	212.00
67.727	886.20	210.43
67.748	886.32	208.14
67.768	886.44	210.57
67.789	886.56	207.29
67.809	886.68	203.43
67.830	886.80	200.86
67.851	886.92	197.29
67.871	887.04	194.86
67.892	887.16	193.86
67.912	887.28	196.43
67.933	887.40	200.14
67.953	887.52	205.14
67.974	887.64	210.57
67.994	887.76	211.14
68.015	887.88	210.00
68.036	888.00	209.71
68.056	888.12	210.00
68.077	888.25	212.57
68.097	888.37	211.14
68.118	888.49	214.14

68.138	888.61	213.71
68.159	888.73	211.86
68.180	888.85	210.00
68.200	888.97	210.71
68.221	889.09	213.00
68.241	889.21	210.14
68.262	889.33	213.71
68.282	889.45	219.00
68.303	889.57	217.43
68.323	889.69	217.00
68.344	889.81	217.57
68.365	889.93	217.14
68.385	890.05	219.71
68.406	890.17	220.57
68.426	890.29	218.43
68.447	890.41	215.57
68.467	890.53	217.14
68.488	890.65	218.86
68.508	890.77	220.29
68.529	890.89	220.14
68.550	891.01	216.71
68.570	891.13	213.71
68.591	891.25	212.00
68.611	891.37	209.71
68.632	891.49	215.00
68.652	891.61	216.71
68.673	891.73	217.00
68.694	891.85	212.86
68.714	891.97	213.43
68.735	892.09	210.71
68.755	892.21	211.29
68.776	892.33	213.00
68.796	892.45	209.43
68.817	892.57	204.29
68.837	892.69	200.43
68.858	892.81	196.00
68.879	892.93	195.57
68.899	893.05	195.14
68.920	893.17	196.43
68.940	893.29	194.43
68.961	893.41	193.00

68.981	893.53	191.71
69.002	893.65	191.43
69.022	893.77	189.00
69.043	893.89	189.43
69.064	894.01	184.14
69.084	894.13	182.29
69.105	894.25	183.14
69.125	894.37	182.00
69.146	894.49	178.00
69.166	894.61	175.71
69.187	894.73	174.57
69.208	894.85	173.29
69.228	894.97	171.00
69.249	895.09	168.57
69.269	895.21	168.71
69.290	895.33	167.00
69.310	895.45	165.43
69.331	895.57	163.57
69.351	895.69	163.14
69.372	895.81	166.57
69.393	895.93	166.71
69.413	896.05	165.00
69.434	896.18	161.00
69.454	896.30	158.86
69.475	896.42	157.00
69.495	896.54	154.43
69.516	896.66	152.43
69.537	896.78	150.00
69.557	896.90	151.00
69.578	897.02	153.86
69.598	897.14	155.57
69.619	897.26	153.29
69.639	897.38	151.57
69.660	897.50	152.14
69.680	897.62	152.14
69.701	897.74	152.43
69.722	897.86	151.71
69.742	897.98	154.14
69.763	898.10	156.71
69.783	898.22	156.00
69.804	898.34	153.71

69.824	898.46	149.71
69.845	898.58	144.71
69.865	898.70	140.71
69.886	898.82	140.43
69.907	898.94	138.14
69.927	899.06	136.00
69.948	899.18	135.57
69.968	899.30	134.71
69.989	899.42	134.57
70.009	899.54	134.86
70.030	899.66	135.71
70.051	899.78	136.43
70.071	899.90	137.86
70.092	900.02	139.86
70.112	900.14	140.86
70.133	900.26	139.86
70.153	900.38	140.14
70.174	900.50	141.57
70.194	900.62	142.86
70.215	900.74	145.71
70.236	900.86	146.29
70.256	900.98	148.57
70.277	901.10	148.86
70.297	901.22	150.14
70.318	901.34	149.71
70.338	901.46	149.57
70.359	901.58	148.86
70.380	901.70	148.86
70.400	901.82	150.57
70.421	901.94	147.00
70.441	902.06	146.43
70.462	902.18	145.57
70.482	902.30	147.00
70.503	902.42	147.14
70.523	902.54	150.86
70.544	902.66	153.43
70.565	902.78	151.71
70.585	902.90	152.71
70.606	903.02	155.14
70.626	903.14	157.29
70.647	903.26	154.86

70.667	903.38	152.43
70.688	903.50	154.00
70.708	903.62	151.86
70.729	903.74	150.43
70.750	903.86	147.43
70.770	903.99	143.14
70.791	904.11	142.43
70.811	904.23	139.29
70.832	904.35	137.29
70.852	904.47	135.29
70.873	904.59	135.71
70.894	904.71	134.43
70.914	904.83	134.71
70.935	904.95	136.29
70.955	905.07	140.00
70.976	905.19	142.29
70.996	905.31	140.57
71.017	905.43	140.14
71.037	905.55	138.71
71.058	905.67	137.00
71.079	905.79	136.43
71.099	905.91	136.14
71.120	906.03	135.14
71.140	906.15	134.43
71.161	906.27	135.43
71.181	906.39	137.00
71.202	906.51	135.86
71.223	906.63	132.86
71.243	906.75	131.29
71.264	906.87	128.14
71.284	906.99	126.57
71.305	907.11	125.29
71.325	907.23	125.29
71.346	907.35	127.57
71.366	907.47	126.29
71.387	907.59	127.29
71.408	907.71	128.57
71.428	907.83	128.86
71.449	907.95	134.86
71.469	908.07	137.71
71.490	908.19	139.71

71.510	908.31	143.71
71.531	908.43	146.71
71.551	908.55	148.71
71.572	908.67	150.86
71.593	908.79	150.71
71.613	908.91	147.86
71.634	909.03	146.14
71.654	909.15	145.71
71.675	909.27	147.00
71.695	909.39	150.86
71.716	909.51	151.00
71.737	909.63	151.86
71.757	909.75	152.71
71.778	909.87	153.43
71.798	909.99	154.71
71.819	910.11	154.43
71.839	910.23	152.43
71.860	910.35	151.86
71.880	910.47	157.00
71.901	910.59	155.71
71.922	910.71	158.43
71.942	910.83	160.71
71.963	910.95	163.29
71.983	911.07	162.43
72.004	911.19	161.43
72.024	911.31	160.43
72.045	911.43	162.43
72.065	911.55	166.00
72.086	911.67	169.57
72.107	911.79	175.14
72.127	911.92	177.14
72.148	912.04	178.86
72.168	912.16	177.29
72.189	912.28	176.00
72.209	912.40	172.86
72.230	912.52	171.86
72.251	912.64	170.00
72.271	912.76	171.71
72.292	912.88	170.29
72.312	913.00	170.43
72.333	913.12	170.14

72.353	913.24	173.43
72.374	913.36	175.86
72.394	913.48	178.86
72.415	913.60	178.86
72.436	913.72	177.57
72.456	913.84	179.86
72.477	913.96	178.57
72.497	914.08	178.43
72.518	914.20	179.57
72.538	914.32	179.00
72.559	914.44	182.00
72.580	914.56	184.14
72.600	914.68	180.71
72.621	914.80	180.14
72.641	914.92	178.14
72.662	915.04	175.43
72.682	915.16	177.14
72.703	915.28	175.86
72.723	915.40	175.29
72.744	915.52	175.57
72.765	915.64	179.00
72.785	915.76	181.57
72.806	915.88	181.43
72.826	916.00	179.57
72.847	916.12	176.57
72.867	916.24	179.14
72.888	916.36	178.86
72.908	916.48	179.43
72.929	916.60	177.57
72.950	916.72	177.14
72.970	916.84	174.86
72.991	916.96	172.43
73.011	917.08	171.29
73.032	917.20	170.71
73.052	917.32	172.86
73.073	917.44	171.71
73.094	917.56	172.43
73.114	917.68	173.43
73.135	917.80	174.14
73.155	917.92	174.71
73.176	918.04	174.57

73.196	918.16	172.57
73.217	918.28	170.14
73.237	918.40	167.86
73.258	918.52	168.86
73.279	918.64	169.14
73.299	918.76	170.00
73.320	918.88	169.43
73.340	919.00	171.57
73.361	919.12	174.57
73.381	919.24	174.43
73.402	919.36	174.43
73.423	919.48	175.14
73.443	919.60	175.00
73.464	919.72	175.14
73.484	919.85	175.43
73.505	919.97	173.57
73.525	920.09	173.71
73.546	920.21	173.00
73.566	920.33	174.57
73.587	920.45	177.00
73.608	920.57	176.86
73.628	920.69	175.86
73.649	920.81	176.57
73.669	920.93	177.43
73.690	921.05	176.14
73.710	921.17	175.71
73.731	921.29	177.43
73.751	921.41	178.71
73.772	921.53	182.86
73.793	921.65	184.29
73.813	921.77	184.43
73.834	921.89	186.86
73.854	922.01	187.71
73.875	922.13	188.14
73.895	922.25	191.43
73.916	922.37	195.00
73.937	922.49	192.57
73.957	922.61	189.57
73.978	922.73	187.86
73.998	922.85	185.57
74.019	922.97	183.43

74.039	923.09	184.14
74.060	923.21	187.57
74.080	923.33	186.57
74.101	923.45	186.14
74.122	923.57	185.86
74.142	923.69	187.14
74.163	923.81	182.00
74.183	923.93	182.00
74.204	924.05	185.86
74.224	924.17	188.00
74.245	924.29	188.43
74.265	924.41	190.86
74.286	924.53	192.14
74.307	924.65	193.57
74.327	924.77	192.29
74.348	924.89	190.00
74.368	925.01	189.57
74.389	925.13	188.29
74.409	925.25	192.29
74.430	925.37	192.71
74.451	925.49	196.86
74.471	925.61	198.14
74.492	925.73	194.43
74.512	925.85	188.86
74.533	925.97	184.43
74.553	926.09	182.14
74.574	926.21	182.43
74.594	926.33	182.14
74.615	926.45	178.57
74.636	926.57	179.43
74.656	926.69	176.43
74.677	926.81	178.57
74.697	926.93	183.71
74.718	927.05	185.00
74.738	927.17	186.29
74.759	927.29	185.71
74.780	927.41	184.86
74.800	927.53	181.57
74.821	927.65	177.00
74.841	927.78	174.00
74.862	927.90	175.71

74.882	928.02	177.00
74.903	928.14	179.14
74.923	928.26	181.57
74.944	928.38	184.00
74.965	928.50	187.86
74.985	928.62	193.86
75.006	928.74	197.57
75.026	928.86	194.43
75.047	928.98	191.57
75.067	929.10	192.29
75.088	929.22	192.29
75.108	929.34	190.29
75.129	929.46	191.86
75.150	929.58	194.14
75.170	929.70	199.86
75.191	929.82	204.00
75.211	929.94	203.00
75.232	930.06	202.14
75.252	930.18	200.14
75.273	930.30	199.29
75.294	930.42	195.29
75.314	930.54	191.29
75.335	930.66	190.29
75.355	930.78	189.86
75.376	930.90	188.57
75.396	931.02	187.43
75.417	931.14	189.14
75.437	931.26	190.71
75.458	931.38	192.00
75.479	931.50	187.43
75.499	931.62	183.43
75.520	931.74	181.43
75.540	931.86	180.57
75.561	931.98	183.71
75.581	932.10	184.86
75.602	932.22	190.71
75.623	932.34	191.00
75.643	932.46	191.14
75.664	932.58	190.71
75.684	932.70	186.57
75.705	932.82	185.86

75.725	932.94	185.14
75.746	933.06	182.86
75.766	933.18	179.00
75.787	933.30	175.86
75.808	933.42	177.86
75.828	933.54	182.43
75.849	933.66	182.00
75.869	933.78	184.00
75.890	933.90	185.00
75.910	934.02	185.00
75.931	934.14	183.29
75.951	934.26	179.71
75.972	934.38	176.86
75.993	934.50	176.00
76.013	934.62	174.43
76.034	934.74	175.14
76.054	934.86	173.86
76.075	934.98	171.29
76.095	935.10	171.29
76.116	935.22	169.71
76.137	935.34	167.71
76.157	935.46	166.57
76.178	935.59	165.86
76.198	935.71	166.71
76.219	935.83	164.29
76.239	935.95	160.29
76.260	936.07	158.86
76.280	936.19	156.57
76.301	936.31	156.43
76.322	936.43	155.00
76.342	936.55	155.29
76.363	936.67	153.57
76.383	936.79	154.57
76.404	936.91	153.57
76.424	937.03	153.71
76.445	937.15	154.14
76.465	937.27	153.57
76.486	937.39	155.00
76.507	937.51	156.86
76.527	937.63	160.71
76.548	937.75	162.57

76.568	937.87	161.00
76.589	937.99	156.43
76.609	938.11	155.00
76.630	938.23	157.43
76.651	938.35	157.71
76.671	938.47	154.86
76.692	938.59	154.43
76.712	938.71	154.71
76.733	938.83	155.00
76.753	938.95	156.57
76.774	939.07	155.29
76.794	939.19	156.14
76.815	939.31	155.57
76.836	939.43	156.00
76.856	939.55	156.57
76.877	939.67	156.43
76.897	939.79	157.43
76.918	939.91	158.71
76.938	940.03	158.86
76.959	940.15	157.86
76.980	940.27	158.86
77.000	940.39	155.14
77.021	940.51	151.43
77.041	940.63	149.00
77.062	940.75	148.43
77.082	940.87	146.14
77.103	940.99	146.71
77.123	941.11	143.29
77.144	941.23	139.29
77.165	941.35	138.57
77.185	941.47	138.43
77.206	941.59	137.71
77.226	941.71	138.86
77.247	941.83	140.29
77.267	941.95	138.00
77.288	942.07	137.14
77.308	942.19	136.14
77.329	942.31	133.14
77.350	942.43	130.00
77.370	942.55	126.00
77.391	942.67	124.14

77.411	942.79	124.29
77.432	942.91	122.14
77.452	943.03	120.71
77.473	943.15	118.43
77.494	943.27	113.29
77.514	943.39	105.14
77.535	943.52	97.57
77.555	943.64	93.86
77.576	943.76	93.29
77.596	943.88	95.29
77.617	944.00	95.86
77.637	944.12	94.57
77.658	944.24	90.57
77.679	944.36	87.71
77.699	944.48	85.71
77.720	944.60	81.43
77.740	944.72	73.43
77.761	944.84	65.86
77.781	944.96	62.43
77.802	945.08	62.00
77.823	945.20	65.86
77.843	945.32	60.43
77.864	945.44	57.43
77.884	945.56	57.00
77.905	945.68	56.14
77.925	945.80	55.00
77.946	945.92	53.29
77.966	946.04	51.86
77.987	946.16	51.29
78.008	946.28	50.57
78.028	946.40	51.29
78.049	946.52	51.71
78.069	946.64	52.14
78.090	946.76	51.71
78.110	946.88	50.14
78.131	947.00	49.00
78.151	947.12	50.29
78.172	947.24	50.86
78.193	947.36	51.71
78.213	947.48	51.57
78.234	947.60	52.29

78.254	947.72	53.43
78.275	947.84	54.43
78.295	947.96	54.86
78.316	948.08	56.29
78.337	948.20	57.29
78.357	948.32	57.86
78.378	948.44	57.43
78.398	948.56	56.29
78.419	948.68	55.57
78.439	948.80	54.29
78.460	948.92	53.57
78.480	949.04	52.71
78.501	949.16	53.57
78.522	949.28	54.14
78.542	949.40	55.29
78.563	949.52	55.29
78.583	949.64	55.71
78.604	949.76	55.71
78.624	949.88	55.71
78.645	950.00	54.57
78.666	950.12	54.29
78.686	950.24	54.29
78.707	950.36	53.00
78.727	950.48	52.14
78.748	950.60	51.71
78.768	950.72	52.57
78.789	950.84	53.43
78.809	950.96	54.00
78.830	951.08	54.71
78.851	951.20	54.57
78.871	951.32	53.86
78.892	951.45	53.00
78.912	951.57	54.00
78.933	951.69	54.43
78.953	951.81	54.29
78.974	951.93	54.57
78.994	952.05	54.29
79.015	952.17	53.29
79.036	952.29	53.43
79.056	952.41	53.00
79.077	952.53	52.29

79.097	952.65	52.29
79.118	952.77	53.00
79.138	952.89	53.43
79.159	953.01	54.43
79.180	953.13	55.43
79.200	953.25	56.71
79.221	953.37	57.71
79.241	953.49	58.43
79.262	953.61	58.57
79.282	953.73	59.57
79.303	953.85	59.86
79.323	953.97	59.71
79.344	954.09	60.43
79.365	954.21	60.14
79.385	954.33	59.29
79.406	954.45	58.29
79.426	954.57	58.43
79.447	954.69	58.71
79.467	954.81	58.00
79.488	954.93	58.14
79.508	955.16	58.14
79.529	955.55	57.43
79.550	955.94	57.29
79.570	956.33	56.86
79.591	956.72	56.71
79.611	957.11	55.00
79.632	957.50	54.29
79.652	957.89	54.86
79.673	958.28	55.43
79.694	958.67	55.00
79.714	959.06	55.29
79.735	959.45	55.29
79.755	959.84	55.14
79.776	960.23	54.71
79.796	960.61	54.71
79.817	961.00	55.14
79.837	961.39	55.00
79.858	961.78	55.29
79.879	962.17	55.14
79.899	962.56	53.86
79.920	962.95	53.29

79.940	963.34	52.14
79.961	963.73	51.57
79.981	964.12	49.00
80.002	964.51	50.14
80.023	964.90	50.29
80.043	965.29	51.71
80.064	965.68	51.43
80.084	966.07	52.29
80.105	966.46	51.86
80.125	966.85	52.29
80.146	967.24	52.00
80.166	967.63	52.00
80.187	968.02	52.43
80.208	968.41	52.57
80.228	968.80	53.00
80.249	969.19	52.71
80.269	969.58	51.29
80.290	969.96	50.71
80.310	970.35	49.00
80.331	970.74	47.71
80.351	971.13	46.29
80.372	971.52	44.57
80.393	971.91	43.57
80.413	972.30	42.29
80.434	972.69	40.00
80.454	973.08	37.86
80.475	973.47	36.43
80.495	973.86	36.00
80.516	974.25	36.43
80.537	974.64	35.00
80.557	975.03	35.00
80.578	975.42	33.43
80.598	975.81	33.86
80.619	976.20	35.86
80.639	976.59	37.43
80.660	976.98	39.43
80.680	977.37	40.00
80.701	977.76	41.57
80.722	978.15	42.86
80.742	978.54	44.57
80.763	978.92	46.57

80.783	979.31	47.14
80.804	979.70	48.57
80.824	980.09	50.43
80.845	980.48	52.00
80.866	980.87	52.29
80.886	981.26	53.71
80.907	981.65	54.00
80.927	982.04	54.86
80.948	982.43	55.00
80.968	982.82	54.57
80.989	983.21	55.14
81.009	983.60	55.43
81.030	983.99	56.43
81.051	984.38	56.57
81.071	984.77	56.71
81.092	985.16	56.57
81.112	985.55	56.57
81.133	985.94	57.29
81.153	986.33	57.29
81.174	986.72	57.86
81.194	987.11	58.14
81.215	987.50	57.29
81.236	987.88	57.00
81.256	988.27	57.29
81.277	988.66	57.57
81.297	989.05	57.43
81.318	989.44	56.43
81.338	989.83	57.71
81.359	990.22	57.29
81.380	990.61	58.29
81.400	991.00	58.29
81.421	991.39	59.00
81.441	991.78	58.57
81.462	992.17	58.29
81.482	992.56	59.00
81.503	992.95	58.71
81.523	993.34	58.14
81.544	993.73	57.86
81.565	994.12	56.86
81.585	994.51	56.00
81.606	994.90	54.86

81.626	995.29	53.71
81.647	995.68	51.43
81.667	996.07	50.00
81.688	996.46	49.43
81.708	996.85	49.43
81.729	997.23	48.29
81.750	997.62	48.29
81.770	998.01	47.43
81.791	998.40	47.71
81.811	998.79	47.43
81.832	999.18	47.14
81.852	999.57	47.86
81.873	999.96	47.29
81.894	1000.35	48.43
81.914	1000.74	50.00
81.935	1001.13	50.57
81.955	1001.52	51.86
81.976	1001.91	52.14
81.996	1002.30	53.29
82.017	1002.69	54.86
82.037	1003.08	57.00
82.058	1003.47	59.00
82.079	1003.86	60.00
82.099	1004.25	59.14
82.120	1004.64	57.43
82.140	1005.03	55.00
82.161	1005.42	52.29
82.181	1005.81	50.43
82.202	1006.19	47.71
82.223	1006.58	44.43
82.243	1006.97	43.43
82.264	1007.36	42.14
82.284	1007.75	41.00
82.305	1008.14	39.71
82.325	1008.53	39.00
82.346	1008.92	39.86
82.366	1009.31	39.29
82.387	1009.70	38.43
82.408	1010.09	38.57
82.428	1010.48	37.71
82.449	1010.87	36.71

82.469	1011.26	36.57
82.490	1011.65	37.29
82.510	1012.04	38.71
82.531	1012.43	39.29
82.551	1012.82	40.29
82.572	1013.21	41.14
82.593	1013.60	41.29
82.613	1013.99	40.71
82.634	1014.38	39.14
82.654	1014.77	37.86
82.675	1015.16	36.71
82.695	1015.54	35.57
82.716	1015.93	35.43
82.737	1016.32	34.86
82.757	1016.71	34.86
82.778	1017.10	35.57
82.798	1017.49	35.57
82.819	1017.88	35.29
82.839	1018.27	36.14
82.860	1018.66	37.43
82.880	1019.05	38.00
82.901	1019.44	39.29
82.922	1019.83	38.71
82.942	1020.22	39.43
82.963	1020.61	40.43
82.983	1021.00	41.29
83.004	1021.39	42.29
83.024	1021.78	43.43
83.045	1022.17	43.00
83.066	1022.56	42.57
83.086	1022.95	42.71
83.107	1023.34	43.00
83.127	1023.73	41.71
83.148	1024.12	42.14
83.168	1024.50	42.71
83.189	1024.89	43.29
83.209	1025.28	44.29
83.230	1025.67	44.57
83.251	1026.06	43.86
83.271	1026.45	42.86
83.292	1026.84	42.71

83.312	1027.23	42.00
83.333	1027.62	42.86
83.353	1028.01	43.57
83.374	1028.40	42.43
83.394	1028.79	42.29
83.415	1029.18	41.14
83.436	1029.57	41.86
83.456	1029.96	41.71
83.477	1030.35	41.71
83.497	1030.74	42.00
83.518	1031.13	41.71
83.538	1031.52	40.86
83.559	1031.91	39.86
83.580	1032.30	39.86
83.600	1032.69	39.14
83.621	1033.08	38.71
83.641	1033.46	37.57
83.662	1033.85	36.57
83.682	1034.24	35.71
83.703	1034.63	35.00
83.723	1035.02	34.00
83.744	1035.41	32.29
83.765	1035.80	30.86
83.785	1036.19	30.14
83.806	1036.58	30.71
83.826	1036.97	30.43
83.847	1037.36	28.57
83.867	1037.75	28.71
83.888	1038.14	27.71
83.908	1038.53	27.43
83.929	1038.92	28.43
83.950	1039.31	29.14
83.970	1039.70	29.57
83.991	1040.09	29.57
84.011	1040.48	29.71
84.032	1040.87	29.71
84.052	1041.26	30.00
84.073	1041.65	31.14
84.094	1042.04	32.43
84.114	1042.43	32.57
84.135	1042.81	32.86

84.155	1043.20	33.00
84.176	1043.59	32.71
84.196	1043.98	33.43
84.217	1044.37	33.57
84.237	1044.76	33.14
84.258	1045.15	31.71
84.279	1045.54	30.43
84.299	1045.93	28.86
84.320	1046.32	28.29
84.340	1046.71	28.14
84.361	1047.10	27.29
84.381	1047.49	26.71
84.402	1047.88	26.86
84.423	1048.27	26.00
84.443	1048.66	26.00
84.464	1049.05	26.86
84.484	1049.44	26.43
84.505	1049.83	28.00
84.525	1050.22	29.86
84.546	1050.61	30.86
84.566	1051.00	28.43
84.587	1051.39	28.14
84.608	1051.77	28.14
84.628	1052.16	27.43
84.649	1052.55	26.00
84.669	1052.94	25.29
84.690	1053.33	24.14
84.710	1053.72	24.00
84.731	1054.11	24.29
84.751	1054.50	25.71
84.772	1054.89	25.86
84.793	1055.28	26.43
84.813	1055.67	26.14
84.834	1056.06	25.86
84.854	1056.45	25.57
84.875	1056.84	25.29
84.895	1057.23	26.14
84.916	1057.62	26.57
84.937	1058.01	25.71
84.957	1058.40	26.71
84.978	1058.79	26.71

84.998	1059.18	26.71
85.019	1059.57	26.00
85.039	1059.96	25.71
85.060	1060.35	24.71
85.080	1060.74	23.14
85.101	1061.12	22.71
85.122	1061.51	22.86
85.142	1061.90	22.86
85.163	1062.29	23.00
85.183	1062.68	24.14
85.204	1063.07	25.71
85.224	1063.46	26.57
85.245	1063.85	28.86
85.266	1064.24	29.71
85.286	1064.63	32.00
85.307	1065.02	34.29
85.327	1065.41	37.71
85.348	1065.80	39.14
85.368	1066.19	38.71
85.389	1066.58	36.00
85.409	1066.97	33.71
85.430	1067.36	31.43
85.451	1067.75	30.57
85.471	1068.14	31.57
85.492	1068.53	33.71
85.512	1068.92	34.86
85.533	1069.31	37.71
85.553	1069.70	39.14
85.574	1070.08	41.29
85.594	1070.47	43.29
85.615	1070.86	45.29
85.636	1071.25	45.43
85.656	1071.64	46.43
85.677	1072.03	46.86
85.697	1072.42	47.43
85.718	1072.81	48.14
85.738	1073.20	50.86
85.759	1073.59	53.86
85.780	1073.98	54.57
85.800	1074.37	56.14
85.821	1074.76	58.57

85.841	1075.15	61.57
85.862	1075.54	66.71
85.882	1075.93	72.14
85.903	1076.32	76.57
85.923	1076.71	80.43
85.944	1077.10	83.00
85.965	1077.49	83.86
85.985	1077.88	82.71
86.006	1078.27	80.86
86.026	1078.66	81.86
86.047	1079.04	83.29
86.067	1079.43	85.71
86.088	1079.82	89.43
86.108	1080.21	91.29
86.129	1080.60	93.29
86.150	1080.99	95.86
86.170	1081.38	96.57
86.191	1081.77	95.57
86.211	1082.16	95.57
86.232	1082.55	94.00
86.252	1082.94	92.57
86.273	1083.33	90.57
86.294	1083.72	88.00
86.314	1084.11	85.29
86.335	1084.50	83.00
86.355	1084.89	81.71
86.376	1085.28	80.71
86.396	1085.67	80.00
86.417	1086.06	78.14
86.437	1086.45	76.86
86.458	1086.84	75.57
86.479	1087.23	75.00
86.499	1087.62	75.43
86.520	1088.01	74.71
86.540	1088.39	75.00
86.561	1088.78	76.57
86.581	1089.17	78.14
86.602	1089.56	80.43
86.623	1089.95	80.86
86.643	1090.34	81.43
86.664	1090.73	82.57

86.684	1091.12	83.00
86.705	1091.51	83.14
86.725	1091.90	82.29
86.746	1092.29	82.29
86.766	1092.68	82.29
86.787	1093.07	82.57
86.808	1093.46	81.86
86.828	1093.85	82.71
86.849	1094.24	82.00
86.869	1094.63	81.86
86.890	1095.02	81.43
86.910	1095.41	81.57
86.931	1095.80	82.43
86.951	1096.19	81.71
86.972	1096.58	80.86
86.993	1096.97	80.29
87.013	1097.35	78.57
87.034	1097.74	76.43
87.054	1098.13	76.00
87.075	1098.52	75.71
87.095	1098.91	74.00
87.116	1099.30	71.71
87.137	1099.69	70.29
87.157	1100.08	70.14
87.178	1100.47	70.00
87.198	1100.86	68.14
87.219	1101.25	66.71
87.239	1101.64	66.86
87.260	1102.03	66.86
87.280	1102.42	66.86
87.301	1102.81	68.29
87.322	1103.20	68.57
87.342	1103.59	68.43
87.363	1103.98	68.86
87.383	1104.37	68.71
87.404	1104.76	67.86
87.424	1105.15	65.71
87.445	1105.54	63.14
87.466	1105.93	62.86
87.486	1106.32	61.14
87.507	1106.70	60.00

87.527	1107.09	58.43
87.548	1107.48	58.57
87.568	1107.87	59.71
87.589	1108.26	61.29
87.609	1108.65	63.00
87.630	1109.04	63.57
87.651	1109.43	64.14
87.671	1109.82	64.29
87.692	1110.21	64.71
87.712	1110.60	64.57
87.733	1110.99	64.57
87.753	1111.38	65.29
87.774	1111.77	65.43
87.794	1112.16	65.57
87.815	1112.55	65.57
87.836	1112.94	65.71
87.856	1113.33	65.00
87.877	1113.72	65.86
87.897	1114.11	66.43
87.918	1114.50	69.00
87.938	1114.89	70.00
87.959	1115.28	70.14
87.980	1115.66	69.57
88.000	1116.05	69.71
88.021	1116.44	69.86
88.041	1116.83	70.14
88.062	1117.22	70.71
88.082	1117.61	71.86
88.103	1118.00	73.57
88.123	1118.39	74.86
88.144	1118.78	76.00
88.165	1119.17	76.14
88.185	1119.56	76.86
88.206	1119.95	76.43
88.226	1120.34	77.57
88.247	1120.73	78.14
88.267	1121.12	78.00
88.288	1121.51	77.71
88.309	1121.90	76.57
88.329	1122.29	76.29
88.350	1122.68	77.00

88.370	1123.07	78.86
88.391	1123.46	83.86
88.411	1123.85	87.86
88.432	1124.24	91.29
88.452	1124.62	89.71
88.473	1125.01	87.43
88.494	1125.40	84.71
88.514	1125.79	84.00
88.535	1126.18	84.29
88.555	1126.57	83.57
88.576	1126.96	82.43
88.596	1127.35	81.57
88.617	1127.74	82.14
88.637	1128.13	81.57
88.658	1128.52	80.86
88.679	1128.91	80.14
88.699	1129.30	81.43
88.720	1129.69	80.71
88.740	1130.08	79.71
88.761	1130.47	79.29
88.781	1130.86	79.43
88.802	1131.25	79.14
88.823	1131.64	78.43
88.843	1132.03	78.57
88.864	1132.42	79.43
88.884	1132.81	79.71
88.905	1133.20	81.00
88.925	1133.59	82.14
88.946	1133.97	82.57
88.966	1134.36	81.57
88.987	1134.75	80.43
89.008	1135.14	77.86
89.028	1135.53	77.71
89.049	1135.92	76.57
89.069	1136.31	76.57
89.090	1136.70	76.14
89.110	1137.09	76.86
89.131	1137.48	76.29
89.151	1137.87	76.43
89.172	1138.26	76.43
89.193	1138.65	76.00

89.213	1139.04	76.00
89.234	1139.43	76.57
89.254	1139.82	78.86
89.275	1140.21	80.29
89.295	1140.60	80.71
89.316	1140.99	81.29
89.337	1141.38	79.43
89.357	1141.77	78.00
89.378	1142.16	77.43
89.398	1142.55	77.71
89.419	1142.93	78.00
89.439	1143.32	77.29
89.460	1143.71	77.29
89.480	1144.10	76.57
89.501	1144.49	75.71
89.522	1144.88	75.86
89.542	1145.27	74.14
89.563	1145.66	73.00
89.583	1146.05	72.00
89.604	1146.44	72.29
89.624	1146.83	71.29
89.645	1147.22	71.71
89.666	1147.61	70.86
89.686	1148.00	70.43
89.707	1148.39	69.29
89.727	1148.78	67.14
89.748	1149.17	66.86
89.768	1149.56	66.43
89.789	1149.95	64.57
89.809	1150.34	63.57
89.830	1150.73	63.86
89.851	1151.12	63.00
89.871	1151.51	62.00
89.892	1151.89	61.71
89.912	1152.28	62.14
89.933	1152.67	62.00
89.953	1153.06	61.86
89.974	1153.45	60.86
89.994	1153.84	61.00
90.015	1154.23	59.57
90.036	1154.62	59.00

90.056	1155.01	59.29
90.077	1155.40	60.00
90.097	1155.79	60.86
90.118	1156.18	61.71
90.138	1156.57	61.14
90.159	1156.96	61.71
90.180	1157.35	61.71
90.200	1157.74	61.43
90.221	1158.13	60.71
90.241	1158.52	61.57
90.262	1158.91	60.71
90.282	1159.30	60.43
90.303	1159.69	60.57
90.323	1160.08	60.86
90.344	1160.47	61.00
90.365	1160.86	60.71
90.385	1161.24	61.14
90.406	1161.63	62.57
90.426	1162.02	61.14
90.447	1162.41	60.71
90.467	1162.80	59.29
90.488	1163.19	59.00
90.509	1163.58	58.14
90.529	1163.97	57.29
90.550	1164.36	56.57
90.570	1164.75	56.71
90.591	1165.14	56.86
90.611	1165.53	55.86
90.632	1165.92	54.43
90.652	1166.31	53.71
90.673	1166.70	53.71
90.694	1167.09	53.43
90.714	1167.48	53.00
90.735	1167.87	52.86
90.755	1168.26	53.00
90.776	1168.65	52.86
90.796	1169.04	51.86
90.817	1169.43	51.71
90.837	1169.82	50.57
90.858	1170.20	49.86
90.879	1170.59	48.57

90.899	1170.98	47.86
90.920	1171.37	46.71
90.940	1171.76	46.57
90.961	1172.15	45.86
90.981	1172.54	44.57
91.002	1172.93	45.00
91.023	1173.32	44.43
91.043	1173.71	42.86
91.064	1174.10	41.43
91.084	1174.49	40.43
91.105	1174.88	39.86
91.125	1175.27	40.00
91.146	1175.66	40.29
91.166	1176.05	40.29
91.187	1176.44	40.57
91.208	1176.83	40.14
91.228	1177.22	38.29
91.249	1177.61	37.86
91.269	1178.00	37.29
91.290	1178.39	37.00
91.310	1178.78	37.57
91.331	1179.17	38.00
91.351	1179.55	37.43
91.372	1179.94	37.00
91.393	1180.33	35.14
91.413	1180.72	35.71
91.434	1181.11	35.14
91.454	1181.50	35.86
91.475	1181.89	36.00
91.495	1182.28	36.71
91.516	1182.67	36.29
91.537	1183.06	35.29
91.557	1183.45	36.57
91.578	1183.84	37.14
91.598	1184.23	38.00
91.619	1184.62	38.29
91.639	1185.01	37.43
91.660	1185.40	35.86
91.680	1185.79	36.14
91.701	1186.18	36.00
91.722	1186.57	36.71

91.742	1186.96	37.14
91.763	1187.35	39.00
91.783	1187.74	40.57
91.804	1188.13	40.43
91.824	1188.51	39.43
91.845	1188.90	38.00
91.866	1189.29	37.29
91.886	1189.68	35.57
91.907	1190.07	36.14
91.927	1190.46	36.71
91.948	1190.85	39.00
91.968	1191.24	40.71
91.989	1191.63	40.57
92.009	1192.02	37.57

APPENDIX 2

ULTRAVIOLET-STIMULATED LUMINESCENCE DATA

Depth (mm)	Age (cal yr BP)	Grayscale Pixel Value
0.000	N/A	44.14
0.062	N/A	12.86
0.125	N/A	18.14
0.187	N/A	16.86
0.250	N/A	18.14
0.312	N/A	20.57
0.375	N/A	22.57
0.437	N/A	27.14
0.499	N/A	29.43
0.562	N/A	35.29
0.624	N/A	40.14
0.687	N/A	41.57
0.749	N/A	44.71
0.811	N/A	44.14
0.874	N/A	43.71
0.936	N/A	44.57
0.999	N/A	47.57
1.061	496.62	47.57
1.124	496.99	46.86
1.186	497.35	47.00
1.248	497.72	49.14
1.311	498.08	52.86
1.373	498.45	50.71
1.436	498.81	57.57
1.498	499.18	62.43
1.561	499.54	70.71
1.623	499.91	73.29
1.685	500.27	74.00
1.748	500.64	75.29
1.810	501.00	82.00
1.873	501.36	87.29
1.935	501.73	91.29
1.997	502.09	96.14
2.060	502.46	95.00

2.122	502.82	88.29
2.185	503.19	92.29
2.247	503.55	87.71
2.310	503.92	95.71
2.372	504.28	105.00
2.434	504.65	113.57
2.497	505.01	134.86
2.559	505.38	130.29
2.622	505.74	126.71
2.684	506.11	143.43
2.746	506.47	140.71
2.809	506.84	141.00
2.871	507.20	141.43
2.934	507.57	143.43
2.996	507.93	151.86
3.059	508.30	154.29
3.121	508.66	159.14
3.183	509.03	169.43
3.246	509.39	173.43
3.308	509.75	177.71
3.371	510.12	179.71
3.433	510.48	178.00
3.496	510.85	177.57
3.558	511.21	169.57
3.620	511.58	176.57
3.683	511.94	185.57
3.745	512.31	186.57
3.808	512.67	186.86
3.870	513.04	187.29
3.932	513.40	180.86
3.995	513.77	185.14
4.057	514.13	189.00
4.120	514.50	180.43
4.182	514.86	178.43
4.245	515.23	170.00
4.307	515.59	164.14
4.369	515.96	182.86
4.432	516.32	185.29
4.494	516.69	193.57
4.557	517.05	193.14
4.619	517.41	187.57

4.682	517.78	187.86
4.744	518.14	186.43
4.806	518.51	173.71
4.869	518.87	180.86
4.931	519.24	182.57
4.994	519.60	184.71
5.056	519.97	188.43
5.118	520.33	186.29
5.181	520.70	190.00
5.243	521.06	190.29
5.306	521.43	193.57
5.368	521.79	191.71
5.431	522.16	189.14
5.493	522.52	187.43
5.555	522.89	190.57
5.618	523.25	176.14
5.680	523.62	176.71
5.743	523.98	168.14
5.805	524.35	166.29
5.868	524.71	160.14
5.930	525.07	152.86
5.992	525.44	144.43
6.055	525.80	134.14
6.117	526.17	131.14
6.180	526.53	126.86
6.242	526.90	126.29
6.304	527.26	122.00
6.367	527.63	122.14
6.429	527.99	118.71
6.492	528.36	122.29
6.554	528.72	127.00
6.617	529.09	126.71
6.679	529.45	128.43
6.741	529.82	124.71
6.804	530.18	127.86
6.866	530.55	133.14
6.929	530.91	135.00
6.991	531.28	139.57
7.053	531.64	136.57
7.116	532.01	138.29
7.178	532.37	122.86

7.241	532.74	123.71
7.303	533.10	116.29
7.366	533.46	128.71
7.428	533.83	127.86
7.490	534.19	146.29
7.553	534.56	135.14
7.615	534.92	137.71
7.678	535.29	135.14
7.740	535.65	137.14
7.803	536.02	130.14
7.865	536.38	133.57
7.927	536.75	140.71
7.990	537.11	147.00
8.052	537.48	149.14
8.115	537.84	143.86
8.177	538.21	141.86
8.239	538.57	133.14
8.302	538.94	136.86
8.364	539.30	135.43
8.427	539.67	138.29
8.489	540.03	139.00
8.552	540.40	135.00
8.614	540.76	132.29
8.676	541.12	131.71
8.739	541.49	134.14
8.801	541.85	132.86
8.864	542.22	132.57
8.926	542.58	131.00
8.989	542.95	135.29
9.051	543.31	138.43
9.113	543.68	140.43
9.176	544.04	142.29
9.238	544.41	136.57
9.301	544.77	134.00
9.363	545.14	140.00
9.425	545.50	136.71
9.488	545.87	135.86
9.550	546.23	139.71
9.613	546.60	128.43
9.675	546.96	137.29
9.738	547.33	143.86

9.800	547.69	154.14
9.862	548.06	139.71
9.925	548.42	145.14
9.987	548.78	136.86
10.050	549.15	138.71
10.112	549.51	161.57
10.175	549.88	164.86
10.237	550.24	149.43
10.299	550.61	158.71
10.362	550.97	163.14
10.424	551.34	163.71
10.487	551.70	159.14
10.549	552.07	157.00
10.611	552.43	152.86
10.674	552.80	144.57
10.736	553.16	165.29
10.799	553.53	156.86
10.861	553.89	156.57
10.924	554.26	157.86
10.986	554.62	159.00
11.048	554.99	147.86
11.111	555.35	155.29
11.173	555.72	153.43
11.236	556.08	156.57
11.298	556.45	151.71
11.361	556.81	149.00
11.423	557.17	150.57
11.485	557.54	151.29
11.548	557.90	152.86
11.610	558.27	149.00
11.673	558.63	155.71
11.735	559.00	157.29
11.797	559.36	158.00
11.860	559.73	157.29
11.922	560.09	155.00
11.985	560.46	154.57
12.047	560.82	150.00
12.110	561.19	154.86
12.172	561.55	154.29
12.234	561.92	151.71
12.297	562.28	156.71

12.359	562.65	153.00
12.422	563.01	154.00
12.484	563.38	164.00
12.546	563.74	162.57
12.609	564.11	163.57
12.671	564.47	158.57
12.734	564.83	158.86
12.796	565.20	159.86
12.859	565.56	155.86
12.921	565.93	152.43
12.983	566.29	148.57
13.046	566.66	146.29
13.108	567.02	146.71
13.171	567.39	155.00
13.233	567.75	155.29
13.296	568.12	151.29
13.358	568.48	149.57
13.420	568.85	150.71
13.483	569.21	149.43
13.545	569.58	142.86
13.608	569.94	129.14
13.670	570.31	129.71
13.732	570.67	127.43
13.795	571.04	110.86
13.857	571.40	112.43
13.920	571.77	113.71
13.982	572.13	111.29
14.045	572.49	110.43
14.107	572.86	101.86
14.169	573.22	99.71
14.232	573.59	94.14
14.294	573.95	90.14
14.357	574.32	88.86
14.419	574.68	108.86
14.482	575.05	93.57
14.544	575.41	92.86
14.606	575.78	82.14
14.669	576.14	80.00
14.731	576.51	83.57
14.794	576.87	89.00
14.856	577.24	88.71

14.918	577.60	98.00
14.981	577.97	106.14
15.043	578.33	117.14
15.106	578.70	112.43
15.168	579.06	114.29
15.231	579.43	114.57
15.293	579.79	129.29
15.355	580.16	141.43
15.418	580.52	131.29
15.480	580.88	134.00
15.543	581.25	133.57
15.605	581.61	135.00
15.668	581.98	139.14
15.730	582.34	143.57
15.792	582.71	141.86
15.855	583.07	148.43
15.917	583.44	156.14
15.980	583.80	158.29
16.042	584.17	153.29
16.104	584.53	153.57
16.167	584.90	151.71
16.229	585.26	151.14
16.292	585.63	155.00
16.354	585.99	156.71
16.417	586.36	166.86
16.479	586.72	164.71
16.541	587.09	158.71
16.604	587.45	162.43
16.666	587.82	165.71
16.729	588.18	165.29
16.791	588.54	152.43
16.853	588.91	141.00
16.916	589.27	144.71
16.978	589.64	148.43
17.041	590.00	160.57
17.103	590.37	146.86
17.166	590.73	147.14
17.228	591.10	139.43
17.290	591.46	130.00
17.353	591.83	130.43
17.415	592.19	125.14

17.478	592.56	115.00
17.540	592.92	116.71
17.603	593.29	114.86
17.665	593.65	117.86
17.727	594.02	111.43
17.790	594.38	101.71
17.852	594.75	106.29
17.915	595.11	111.29
17.977	595.48	117.00
18.039	595.84	123.86
18.102	596.20	115.43
18.164	596.57	114.00
18.227	596.93	109.14
18.289	597.30	104.57
18.352	597.66	104.86
18.414	598.03	101.86
18.476	598.39	96.00
18.539	598.76	89.71
18.601	599.12	92.00
18.664	599.49	99.71
18.726	599.85	100.86
18.789	600.22	100.29
18.851	600.58	100.86
18.913	600.95	92.86
18.976	601.31	86.86
19.038	601.68	82.43
19.101	602.04	93.00
19.163	602.41	88.43
19.225	602.77	75.86
19.288	603.14	51.86
19.350	603.50	47.57
19.413	603.86	45.57
19.475	604.23	41.29
19.538	604.59	54.86
19.600	604.96	44.71
19.662	605.32	47.43
19.725	605.69	47.71
19.787	606.05	47.29
19.850	606.42	44.29
19.912	606.78	44.14
19.975	607.15	45.71

20.037	607.51	45.00
20.099	607.88	47.14
20.162	608.24	44.57
20.224	608.61	46.29
20.287	608.97	49.71
20.349	609.34	55.29
20.411	609.70	64.14
20.474	610.07	75.43
20.536	610.43	95.86
20.599	610.80	114.71
20.661	611.16	141.57
20.724	611.53	150.00
20.786	611.89	161.57
20.848	612.25	171.43
20.911	612.62	179.29
20.973	612.98	184.14
21.036	613.35	193.29
21.098	613.71	197.29
21.160	614.08	196.43
21.223	614.44	195.86
21.285	614.81	195.29
21.348	615.17	198.57
21.410	615.54	197.14
21.473	615.90	193.14
21.535	616.27	191.00
21.597	616.63	184.14
21.660	617.00	175.71
21.722	617.36	168.14
21.785	617.73	156.71
21.847	618.09	152.57
21.910	618.46	138.43
21.972	618.82	137.00
22.034	619.19	132.14
22.097	619.55	127.00
22.159	619.91	121.00
22.222	620.28	113.57
22.284	620.64	113.71
22.346	621.01	117.14
22.409	621.37	115.57
22.471	621.74	126.29
22.534	622.10	130.86

22.596	622.47	135.29
22.659	622.83	130.14
22.721	623.20	130.57
22.783	623.56	116.00
22.846	623.93	121.00
22.908	624.29	127.71
22.971	624.66	127.29
23.033	625.02	135.29
23.096	625.39	122.86
23.158	625.75	120.57
23.220	626.12	119.71
23.283	626.48	132.14
23.345	626.85	134.00
23.408	627.21	140.00
23.470	627.57	137.86
23.532	627.94	150.14
23.595	628.30	136.29
23.657	628.67	136.29
23.720	629.03	132.43
23.782	629.40	136.43
23.845	629.76	140.43
23.907	630.13	138.86
23.969	630.49	143.14
24.032	630.86	150.29
24.094	631.22	153.43
24.157	631.59	150.86
24.219	631.95	144.29
24.282	632.32	157.57
24.344	632.68	145.29
24.406	633.05	148.71
24.469	633.41	140.14
24.531	633.78	130.86
24.594	634.14	142.43
24.656	634.51	139.00
24.718	634.87	129.57
24.781	635.24	132.43
24.843	635.60	129.14
24.906	635.96	129.00
24.968	636.33	131.57
25.031	636.69	142.86
25.093	637.06	141.29

25.155	637.42	144.86
25.218	637.79	131.86
25.280	638.15	146.29
25.343	638.52	145.57
25.405	638.88	151.43
25.467	639.25	139.00
25.530	639.61	142.86
25.592	639.98	138.43
25.655	640.34	132.00
25.717	640.71	137.86
25.780	641.07	139.86
25.842	641.44	150.14
25.904	641.80	146.00
25.967	642.17	137.71
26.029	642.53	129.57
26.092	642.90	138.86
26.154	643.26	145.43
26.217	643.62	148.00
26.279	643.99	135.43
26.341	644.35	153.29
26.404	644.72	167.00
26.466	645.08	183.86
26.529	645.45	197.29
26.591	645.81	191.71
26.653	646.18	195.00
26.716	646.54	199.00
26.778	646.91	200.29
26.841	647.27	196.86
26.903	647.64	200.00
26.966	648.00	198.29
27.028	648.37	200.29
27.090	648.73	199.71
27.153	649.10	199.14
27.215	649.46	197.29
27.278	649.83	187.71
27.340	650.19	201.86
27.403	650.56	203.71
27.465	650.92	199.86
27.527	651.28	191.14
27.590	651.65	198.57
27.652	652.01	198.86

27.715	652.38	197.71
27.777	652.74	198.43
27.839	653.11	191.71
27.902	653.47	192.43
27.964	653.84	188.00
28.027	654.20	191.29
28.089	654.57	189.57
28.152	654.93	197.57
28.214	655.30	183.71
28.276	655.66	173.29
28.339	656.03	162.71
28.401	656.39	163.29
28.464	656.76	160.71
28.526	657.12	161.43
28.589	657.49	166.29
28.651	657.85	162.14
28.713	658.22	166.29
28.776	658.58	156.86
28.838	658.95	138.57
28.901	659.31	165.14
28.963	659.67	175.57
29.025	660.04	180.86
29.088	660.40	166.57
29.150	660.77	161.71
29.213	661.13	156.43
29.275	661.50	154.71
29.338	661.86	150.71
29.400	662.23	156.71
29.462	662.59	168.14
29.525	662.96	169.71
29.587	663.32	164.14
29.650	663.69	178.86
29.712	664.05	179.29
29.775	664.42	190.00
29.837	664.78	199.00
29.899	665.15	176.14
29.962	665.51	175.00
30.024	665.88	181.57
30.087	666.24	183.86
30.149	666.61	179.86
30.211	666.97	199.43

30.274	667.33	197.86
30.336	667.70	202.14
30.399	668.06	190.43
30.461	668.43	163.71
30.524	668.79	156.29
30.586	669.16	156.86
30.648	669.52	180.14
30.711	669.89	147.29
30.773	670.25	193.71
30.836	670.62	188.57
30.898	670.98	177.71
30.960	671.35	171.43
31.023	671.71	168.71
31.085	672.08	186.43
31.148	672.44	172.71
31.210	672.81	161.00
31.273	673.17	169.14
31.335	673.54	166.43
31.397	673.90	162.14
31.460	674.27	182.29
31.522	674.63	176.57
31.585	674.99	173.14
31.647	675.36	165.71
31.710	675.72	168.14
31.772	676.09	157.14
31.834	676.45	164.71
31.897	676.82	162.43
31.959	677.18	159.71
32.022	677.55	155.86
32.084	677.91	165.29
32.146	678.28	167.71
32.209	678.64	169.43
32.271	679.01	168.71
32.334	679.37	166.57
32.396	679.74	172.71
32.459	680.10	157.71
32.521	680.47	153.71
32.583	680.83	155.00
32.646	681.20	160.86
32.708	681.56	162.14
32.771	681.93	159.86

32.833	682.29	158.43
32.896	682.66	157.00
32.958	683.02	165.43
33.020	683.38	175.29
33.083	683.75	180.14
33.145	684.11	184.43
33.208	684.48	180.86
33.270	684.84	174.57
33.332	685.21	171.57
33.395	685.57	167.57
33.457	685.94	158.57
33.520	686.30	156.14
33.582	686.67	141.29
33.645	687.03	148.71
33.707	687.40	152.43
33.769	687.76	159.57
33.832	688.13	171.14
33.894	688.49	187.71
33.957	688.86	199.14
34.019	689.22	218.29
34.082	689.59	225.00
34.144	689.95	234.00
34.206	690.32	235.71
34.269	690.68	242.43
34.331	691.04	245.71
34.394	691.41	244.57
34.456	691.77	242.86
34.518	692.14	238.86
34.581	692.50	236.00
34.643	692.87	233.57
34.706	693.23	229.86
34.768	693.60	229.43
34.831	693.96	220.43
34.893	694.33	224.43
34.955	694.69	230.14
35.018	695.06	230.57
35.080	695.42	233.00
35.143	695.79	230.86
35.205	696.15	235.00
35.267	696.52	227.43
35.330	696.88	224.57

35.392	697.25	226.14
35.455	697.61	225.86
35.517	697.98	223.43
35.580	698.34	220.57
35.642	698.70	216.00
35.704	699.07	220.86
35.767	699.43	219.71
35.829	699.80	222.86
35.892	700.16	222.43
35.954	700.53	224.00
36.017	700.89	227.29
36.079	701.26	233.00
36.141	701.62	214.86
36.204	701.99	209.86
36.266	702.35	204.43
36.329	702.72	205.14
36.391	703.08	212.57
36.453	703.45	212.86
36.516	703.81	211.71
36.578	704.18	208.86
36.641	704.54	207.14
36.703	704.91	200.43
36.766	705.27	192.71
36.828	705.64	201.43
36.890	706.00	203.14
36.953	706.37	203.29
37.015	706.73	207.14
37.078	707.09	207.43
37.140	707.46	192.43
37.203	707.82	209.29
37.265	708.19	189.43
37.327	708.55	190.86
37.390	708.92	192.29
37.452	709.28	201.29
37.515	709.65	204.43
37.577	710.01	206.00
37.639	710.38	213.71
37.702	710.74	214.29
37.764	711.11	216.00
37.827	711.47	212.29
37.889	711.84	208.71

37.952	712.20	198.86
38.014	712.57	192.57
38.076	712.93	184.57
38.139	713.30	176.57
38.201	713.66	177.71
38.264	714.03	185.14
38.326	714.39	191.29
38.389	714.75	183.43
38.451	715.12	184.86
38.513	715.48	201.00
38.576	715.85	205.86
38.638	716.21	210.57
38.701	716.58	216.86
38.763	716.94	220.14
38.825	717.31	216.00
38.888	717.67	221.14
38.950	718.04	222.43
39.013	718.40	204.86
39.075	718.77	223.71
39.138	719.13	217.29
39.200	719.50	222.57
39.262	719.86	223.57
39.325	720.23	220.86
39.387	720.59	218.57
39.450	720.96	227.00
39.512	721.32	220.86
39.574	721.69	230.43
39.637	722.05	222.00
39.699	722.41	231.29
39.762	722.78	229.00
39.824	723.14	233.00
39.887	723.51	219.57
39.949	723.87	220.86
40.011	724.24	226.43
40.074	724.60	234.00
40.136	724.97	226.86
40.199	725.33	225.29
40.261	725.70	212.43
40.324	726.06	209.71
40.386	726.43	211.14
40.448	726.79	213.00

40.511	727.16	220.57
40.573	727.52	222.29
40.636	727.89	224.57
40.698	728.25	217.14
40.760	728.62	217.00
40.823	728.98	211.71
40.885	729.35	199.71
40.948	729.71	206.14
41.010	730.08	206.71
41.073	730.44	213.57
41.135	730.80	210.14
41.197	731.17	209.43
41.260	731.53	208.29
41.322	731.90	207.29
41.385	732.26	204.29
41.447	732.63	204.14
41.510	732.99	197.00
41.572	733.36	206.57
41.634	733.72	202.29
41.697	734.09	188.43
41.759	734.45	185.86
41.822	734.82	217.71
41.884	735.18	172.43
41.946	735.55	204.71
42.009	735.91	186.43
42.071	736.28	191.14
42.134	736.64	194.43
42.196	737.01	177.86
42.259	737.37	181.29
42.321	737.74	185.57
42.383	738.10	188.14
42.446	738.46	199.14
42.508	738.83	190.57
42.571	739.19	205.86
42.633	739.56	190.00
42.696	739.92	177.86
42.758	740.29	180.71
42.820	740.65	183.71
42.883	741.02	179.00
42.945	741.38	182.57
43.008	741.75	174.43

43.070	742.11	174.00
43.132	742.48	161.86
43.195	742.84	159.14
43.257	743.21	165.43
43.320	743.57	173.86
43.382	743.94	164.00
43.445	744.30	166.57
43.507	744.67	158.57
43.569	745.03	169.29
43.632	745.40	174.43
43.694	745.76	183.43
43.757	746.12	181.71
43.819	746.49	193.29
43.881	746.85	199.71
43.944	747.22	197.71
44.006	747.58	198.71
44.069	747.95	193.86
44.131	748.31	199.14
44.194	748.68	203.57
44.256	749.04	203.86
44.318	749.41	204.00
44.381	749.77	212.00
44.443	750.14	217.86
44.506	750.50	219.43
44.568	750.87	218.14
44.631	751.23	211.29
44.693	751.60	201.14
44.755	751.96	199.00
44.818	752.33	207.43
44.880	752.69	210.57
44.943	753.06	214.57
45.005	753.42	221.86
45.067	753.78	223.14
45.130	754.15	231.00
45.192	754.51	221.43
45.255	754.88	221.57
45.317	755.24	221.14
45.380	755.61	211.43
45.442	755.97	211.43
45.504	756.34	206.86
45.567	756.70	203.00

45.629	757.07	204.57
45.692	757.43	201.71
45.754	757.80	210.57
45.817	758.16	207.14
45.879	758.53	209.14
45.941	758.89	198.57
46.004	759.26	206.14
46.066	759.62	211.43
46.129	759.99	212.86
46.191	760.35	216.71
46.253	760.72	210.00
46.316	761.08	215.14
46.378	761.45	214.29
46.441	761.81	212.29
46.503	762.17	207.00
46.566	762.54	205.43
46.628	762.90	211.57
46.690	763.27	213.29
46.753	763.63	214.57
46.815	764.00	210.57
46.878	764.36	207.71
46.940	764.73	204.29
47.003	765.09	204.57
47.065	765.46	195.43
47.127	765.82	193.57
47.190	766.19	195.43
47.252	766.55	180.43
47.315	766.92	179.57
47.377	767.28	170.43
47.439	767.65	179.00
47.502	768.01	172.86
47.564	768.38	177.00
47.627	768.74	180.43
47.689	769.11	191.43
47.752	769.47	196.71
47.814	769.83	196.86
47.876	770.20	202.71
47.939	770.56	206.14
48.001	770.93	214.00
48.064	771.29	208.29
48.126	771.66	207.14

48.189	772.02	198.29
48.251	772.39	195.14
48.313	772.75	188.71
48.376	773.12	193.43
48.438	773.48	193.43
48.501	773.85	192.57
48.563	774.21	189.43
48.625	774.58	185.43
48.688	774.94	182.43
48.750	775.31	179.43
48.813	775.67	164.57
48.875	776.04	154.71
48.938	776.40	156.57
49.000	776.77	157.71
49.062	777.13	162.71
49.125	777.49	164.71
49.187	777.86	146.43
49.250	778.22	158.57
49.312	778.59	154.43
49.374	778.95	149.43
49.437	779.32	153.14
49.499	779.68	145.00
49.562	780.05	138.14
49.624	780.41	139.86
49.687	780.78	143.71
49.749	781.14	145.57
49.811	781.51	143.14
49.874	781.87	154.86
49.936	782.24	158.14
49.999	782.60	162.57
50.061	782.97	157.86
50.124	783.33	149.71
50.186	783.70	151.43
50.248	784.06	137.00
50.311	784.43	143.43
50.373	784.79	140.71
50.436	785.16	135.86
50.498	785.52	136.86
50.560	785.88	126.71
50.623	786.25	139.57
50.685	786.61	134.86

50.748	786.98	120.14
50.810	787.34	121.29
50.873	787.71	138.29
50.935	788.07	138.43
50.997	788.44	145.57
51.060	788.80	149.29
51.122	789.17	159.29
51.185	789.53	153.86
51.247	789.90	150.57
51.310	790.26	150.00
51.372	790.63	147.57
51.434	790.99	146.57
51.497	791.36	143.57
51.559	791.72	146.71
51.622	792.09	142.57
51.684	792.45	148.86
51.746	792.82	152.29
51.809	793.18	152.29
51.871	793.54	153.29
51.934	793.91	159.71
51.996	794.27	189.29
52.059	794.64	169.57
52.121	795.00	150.86
52.183	795.37	164.57
52.246	795.73	184.29
52.308	796.10	165.43
52.371	796.46	169.00
52.433	796.83	168.86
52.496	797.19	148.43
52.558	797.56	176.00
52.620	797.92	169.14
52.683	798.29	173.43
52.745	798.65	177.14
52.808	799.02	176.57
52.870	799.38	177.86
52.932	799.75	192.00
52.995	800.11	185.57
53.057	800.48	185.29
53.120	800.84	193.57
53.182	801.20	197.29
53.245	801.57	196.43

53.307	801.93	197.43
53.369	802.30	198.00
53.432	802.66	203.71
53.494	803.03	210.71
53.557	803.39	199.43
53.619	803.76	194.86
53.681	804.12	192.29
53.744	804.49	189.43
53.806	804.85	195.29
53.869	805.22	214.29
53.931	805.58	187.00
53.994	805.95	200.43
54.056	806.31	182.71
54.118	806.68	189.86
54.181	807.04	195.00
54.243	807.41	208.57
54.306	807.77	199.00
54.368	808.14	196.00
54.431	808.50	188.29
54.493	808.87	187.86
54.555	809.23	189.29
54.618	809.59	211.43
54.680	809.96	213.14
54.743	810.32	213.14
54.805	810.69	210.00
54.867	811.05	207.71
54.930	811.42	203.29
54.992	811.78	197.57
55.055	812.15	198.14
55.117	812.51	195.00
55.180	812.88	194.57
55.242	813.24	181.14
55.304	813.61	187.43
55.367	813.97	186.43
55.429	814.34	189.14
55.492	814.70	189.57
55.554	815.07	186.86
55.617	815.43	185.86
55.679	815.80	185.00
55.741	816.16	169.71
55.804	816.53	165.57

55.866	816.89	168.86
55.929	817.25	164.57
55.991	817.62	166.43
56.053	817.98	163.57
56.116	818.35	157.29
56.178	818.71	164.57
56.241	819.08	168.71
56.303	819.44	167.43
56.366	819.81	169.29
56.428	820.17	163.29
56.490	820.54	167.43
56.553	820.90	168.86
56.615	821.27	150.00
56.678	821.63	150.00
56.740	822.00	141.00
56.803	822.36	133.29
56.865	822.73	141.00
56.927	823.09	152.43
56.990	823.46	163.86
57.052	823.82	150.29
57.115	824.19	149.14
57.177	824.55	143.29
57.239	824.91	151.29
57.302	825.28	124.14
57.364	825.64	132.57
57.427	826.01	124.00
57.489	826.37	125.43
57.552	826.74	134.57
57.614	827.10	137.00
57.676	827.47	133.86
57.739	827.83	135.57
57.801	828.20	121.86
57.864	828.56	119.57
57.926	828.93	120.86
57.988	829.29	130.14
58.051	829.66	127.43
58.113	830.02	137.71
58.176	830.39	131.43
58.238	830.75	105.71
58.301	831.12	91.71
58.363	831.48	145.86

58.425	831.85	142.71
58.488	832.21	174.00
58.550	832.58	153.00
58.613	832.94	175.71
58.675	833.30	141.57
58.738	833.67	158.14
58.800	834.03	173.86
58.862	834.40	182.43
58.925	834.76	190.86
58.987	835.13	195.43
59.050	835.49	182.29
59.112	835.86	189.57
59.174	836.22	172.43
59.237	836.59	176.71
59.299	836.95	182.43
59.362	837.32	188.29
59.424	837.68	181.29
59.487	838.05	172.14
59.549	838.41	174.71
59.611	838.78	178.86
59.674	839.14	170.57
59.736	839.51	152.29
59.799	839.87	134.86
59.861	840.24	128.43
59.924	840.60	127.57
59.986	840.96	135.43
60.048	841.33	129.00
60.111	841.69	148.86
60.173	842.06	133.57
60.236	842.42	140.00
60.298	842.79	139.43
60.360	843.15	127.57
60.423	843.52	117.43
60.485	843.88	142.14
60.548	844.25	138.00
60.610	844.61	127.43
60.673	844.98	145.14
60.735	845.34	155.71
60.797	845.71	160.57
60.860	846.07	152.86
60.922	846.44	159.57

60.985	846.80	163.29
61.047	847.17	159.86
61.110	847.53	160.43
61.172	847.90	160.71
61.234	848.26	174.14
61.297	848.62	174.29
61.359	848.99	171.29
61.422	849.35	172.71
61.484	849.72	172.86
61.546	850.08	176.43
61.609	850.45	175.00
61.671	850.81	168.14
61.734	851.18	162.29
61.796	851.54	165.14
61.859	851.91	161.29
61.921	852.27	168.29
61.983	852.64	176.14
62.046	853.00	177.00
62.108	853.37	173.57
62.171	853.73	188.86
62.233	854.10	198.57
62.295	854.46	185.00
62.358	854.83	188.71
62.420	855.19	184.57
62.483	855.56	185.29
62.545	855.92	192.00
62.608	856.29	206.57
62.670	856.65	199.57
62.732	857.01	199.71
62.795	857.38	193.71
62.857	857.74	197.14
62.920	858.11	199.00
62.982	858.47	195.29
63.045	858.84	189.43
63.107	859.20	186.00
63.169	859.57	187.29
63.232	859.93	193.29
63.294	860.30	194.29
63.357	860.66	197.71
63.419	861.03	200.29
63.481	861.39	205.71

63.544	861.76	198.00
63.606	862.12	194.29
63.669	862.49	192.00
63.731	862.85	194.57
63.794	863.22	193.57
63.856	863.58	190.29
63.918	863.95	185.14
63.981	864.31	185.71
64.043	864.67	182.29
64.106	865.04	182.71
64.168	865.40	184.00
64.231	865.77	186.29
64.293	866.13	188.00
64.355	866.50	195.00
64.418	866.86	200.71
64.480	867.23	207.71
64.543	867.59	203.43
64.605	867.96	203.57
64.667	868.32	204.57
64.730	868.69	198.43
64.792	869.05	201.29
64.855	869.42	193.86
64.917	869.78	172.00
64.980	870.15	165.86
65.042	870.51	189.57
65.104	870.88	196.00
65.167	871.24	194.14
65.229	871.61	198.43
65.292	871.97	199.43
65.354	872.33	193.71
65.417	872.70	202.00
65.479	873.06	207.43
65.541	873.43	211.71
65.604	873.79	210.57
65.666	874.16	210.00
65.729	874.52	212.00
65.791	874.89	216.00
65.853	875.25	216.00
65.916	875.62	216.86
65.978	875.98	219.14
66.041	876.35	208.29

66.103	876.71	199.86
66.166	877.08	194.86
66.228	877.44	199.00
66.290	877.81	197.43
66.353	878.17	188.86
66.415	878.54	186.57
66.478	878.90	187.57
66.540	879.27	180.86
66.603	879.63	185.29
66.665	880.00	186.86
66.727	880.36	176.14
66.790	880.72	184.00
66.852	881.09	179.71
66.915	881.45	181.29
66.977	881.82	170.14
67.039	882.18	176.00
67.102	882.55	174.43
67.164	882.91	172.43
67.227	883.28	174.43
67.289	883.64	174.29
67.352	884.01	174.86
67.414	884.37	167.00
67.476	884.74	156.43
67.539	885.10	149.00
67.601	885.47	142.14
67.664	885.83	154.71
67.726	886.20	147.43
67.788	886.56	149.43
67.851	886.93	150.57
67.913	887.29	146.43
67.976	887.66	146.86
68.038	888.02	150.00
68.101	888.38	154.86
68.163	888.75	158.00
68.225	889.11	160.43
68.288	889.48	154.57
68.350	889.84	156.14
68.413	890.21	159.14
68.475	890.57	149.57
68.538	890.94	143.86
68.600	891.30	132.00

68.662	891.67	139.43
68.725	892.03	160.29
68.787	892.40	165.57
68.850	892.76	179.14
68.912	893.13	184.29
68.974	893.49	152.57
69.037	893.86	158.00
69.099	894.22	174.57
69.162	894.59	177.00
69.224	894.95	179.86
69.287	895.32	172.86
69.349	895.68	171.14
69.411	896.04	172.14
69.474	896.41	173.29
69.536	896.77	173.43
69.599	897.14	169.29
69.661	897.50	171.86
69.724	897.87	171.29
69.786	898.23	170.43
69.848	898.60	165.86
69.911	898.96	169.00
69.973	899.33	163.86
70.036	899.69	163.00
70.098	900.06	162.43
70.160	900.42	161.00
70.223	900.79	158.43
70.285	901.15	159.43
70.348	901.52	153.29
70.410	901.88	139.00
70.473	902.25	143.86
70.535	902.61	139.29
70.597	902.98	137.00
70.660	903.34	137.86
70.722	903.70	138.00
70.785	904.07	137.86
70.847	904.43	161.00
70.910	904.80	161.29
70.972	905.16	164.86
71.034	905.53	166.29
71.097	905.89	171.71
71.159	906.26	192.71

71.222	906.62	189.71
71.284	906.99	197.86
71.346	907.35	195.86
71.409	907.72	189.14
71.471	908.08	172.14
71.534	908.45	159.29
71.596	908.81	158.00
71.659	909.18	165.29
71.721	909.54	173.86
71.783	909.91	174.57
71.846	910.27	165.14
71.908	910.64	161.00
71.971	911.00	150.86
72.033	911.37	154.86
72.095	911.73	160.71
72.158	912.09	160.00
72.220	912.46	163.71
72.283	912.82	172.43
72.345	913.19	162.57
72.408	913.55	161.43
72.470	913.92	162.29
72.532	914.28	172.29
72.595	914.65	171.29
72.657	915.01	166.57
72.720	915.38	169.43
72.782	915.74	163.43
72.845	916.11	152.86
72.907	916.47	156.57
72.969	916.84	159.71
73.032	917.20	163.29
73.094	917.57	162.00
73.157	917.93	153.43
73.219	918.30	152.14
73.281	918.66	164.14
73.344	919.03	159.00
73.406	919.39	158.43
73.469	919.75	159.71
73.531	920.12	163.43
73.594	920.48	157.29
73.656	920.85	154.29
73.718	921.21	157.00

73.781	921.58	152.14
73.843	921.94	148.86
73.906	922.31	151.57
73.968	922.67	144.57
74.031	923.04	152.57
74.093	923.40	145.43
74.155	923.77	135.57
74.218	924.13	121.71
74.280	924.50	125.29
74.343	924.86	118.29
74.405	925.23	113.86
74.467	925.59	106.43
74.530	925.96	103.71
74.592	926.32	96.43
74.655	926.69	108.43
74.717	927.05	111.00
74.780	927.41	110.00
74.842	927.78	108.57
74.904	928.14	117.00
74.967	928.51	117.71
75.029	928.87	120.00
75.092	929.24	118.29
75.154	929.60	126.43
75.217	929.97	126.71
75.279	930.33	125.57
75.341	930.70	121.29
75.404	931.06	120.29
75.466	931.43	123.86
75.529	931.79	121.86
75.591	932.16	120.86
75.653	932.52	122.71
75.716	932.89	122.71
75.778	933.25	125.43
75.841	933.62	118.29
75.903	933.98	113.71
75.966	934.35	108.86
76.028	934.71	119.86
76.090	935.08	128.00
76.153	935.44	128.14
76.215	935.80	120.86
76.278	936.17	118.57

76.340	936.53	115.86
76.402	936.90	122.86
76.465	937.26	121.43
76.527	937.63	128.29
76.590	937.99	127.14
76.652	938.36	133.57
76.715	938.72	131.29
76.777	939.09	128.00
76.839	939.45	130.43
76.902	939.82	130.29
76.964	940.18	123.43
77.027	940.55	121.71
77.089	940.91	113.57
77.152	941.28	115.14
77.214	941.64	120.00
77.276	942.01	118.29
77.339	942.37	116.00
77.401	942.74	112.14
77.464	943.10	111.29
77.526	943.46	108.86
77.588	943.83	101.71
77.651	944.19	104.86
77.713	944.56	101.00
77.776	944.92	109.43
77.838	945.29	103.43
77.901	945.65	102.29
77.963	946.02	97.86
78.025	946.38	88.29
78.088	946.75	81.71
78.150	947.11	77.29
78.213	947.48	74.86
78.275	947.84	75.14
78.338	948.21	76.43
78.400	948.57	77.29
78.462	948.94	74.86
78.525	949.30	68.14
78.587	949.67	75.00
78.650	950.03	74.86
78.712	950.40	76.43
78.774	950.76	78.00
78.837	951.12	77.14

78.899	951.49	81.86
78.962	951.85	80.86
79.024	952.22	81.14
79.087	952.58	78.86
79.149	952.95	78.00
79.211	953.31	72.43
79.274	953.68	77.86
79.336	954.04	79.71
79.399	954.41	79.57
79.461	954.77	81.14
79.524	955.45	85.71
79.586	956.63	86.57
79.648	957.81	91.86
79.711	958.99	90.71
79.773	960.18	89.43
79.836	961.36	93.14
79.898	962.54	93.57
79.960	963.72	89.86
80.023	964.91	95.00
80.085	966.09	90.71
80.148	967.27	89.86
80.210	968.46	91.71
80.273	969.64	88.29
80.335	970.82	87.14
80.397	972.00	86.71
80.460	973.19	88.14
80.522	974.37	85.29
80.585	975.55	86.29
80.647	976.73	85.00
80.709	977.92	84.14
80.772	979.10	89.71
80.834	980.28	97.43
80.897	981.46	97.00
80.959	982.65	97.14
81.022	983.83	99.86
81.084	985.01	95.71
81.146	986.20	100.29
81.209	987.38	97.71
81.271	988.56	99.43
81.334	989.74	98.86
81.396	990.93	100.86

81.459	992.11	103.14
81.521	993.29	99.71
81.583	994.47	104.57
81.646	995.66	106.00
81.708	996.84	104.86
81.771	998.02	98.86
81.833	999.21	102.00
81.895	1000.39	105.29
81.958	1001.57	107.71
82.020	1002.75	104.86
82.083	1003.94	103.14
82.145	1005.12	101.00
82.208	1006.30	100.29
82.270	1007.48	102.14
82.332	1008.67	100.43
82.395	1009.85	101.29
82.457	1011.03	99.71
82.520	1012.22	104.29
82.582	1013.40	103.29
82.645	1014.58	104.00
82.707	1015.76	102.29
82.769	1016.95	105.43
82.832	1018.13	106.14
82.894	1019.31	103.71
82.957	1020.49	104.29
83.019	1021.68	100.86
83.081	1022.86	104.29
83.144	1024.04	100.14
83.206	1025.22	96.43
83.269	1026.41	98.14
83.331	1027.59	97.14
83.394	1028.77	96.86
83.456	1029.96	93.00
83.518	1031.14	96.29
83.581	1032.32	96.00
83.643	1033.50	96.29
83.706	1034.69	95.43
83.768	1035.87	91.14
83.831	1037.05	92.43
83.893	1038.23	95.00
83.955	1039.42	92.43

84.018	1040.60	95.86
84.080	1041.78	98.57
84.143	1042.97	101.71
84.205	1044.15	99.14
84.267	1045.33	101.43
84.330	1046.51	102.43
84.392	1047.70	103.29
84.455	1048.88	103.86
84.517	1050.06	108.00
84.580	1051.24	108.57
84.642	1052.43	105.29
84.704	1053.61	107.14
84.767	1054.79	108.57
84.829	1055.98	107.71
84.892	1057.16	103.86
84.954	1058.34	107.00
85.017	1059.52	109.14
85.079	1060.71	109.29
85.141	1061.89	110.14
85.204	1063.07	112.29
85.266	1064.25	109.29
85.329	1065.44	109.57
85.391	1066.62	111.57
85.453	1067.80	111.71
85.516	1068.98	108.57
85.578	1070.17	101.00
85.641	1071.35	95.00
85.703	1072.53	99.00
85.766	1073.72	103.14
85.828	1074.90	98.86
85.890	1076.08	100.14
85.953	1077.26	99.43
86.015	1078.45	96.86
86.078	1079.63	93.29
86.140	1080.81	97.14
86.202	1081.99	102.86
86.265	1083.18	110.43
86.327	1084.36	109.14
86.390	1085.54	107.71
86.452	1086.73	109.71
86.515	1087.91	106.71

86.577	1089.09	107.57
86.639	1090.27	113.29
86.702	1091.46	112.00
86.764	1092.64	110.14
86.827	1093.82	111.00
86.889	1095.00	106.71
86.952	1096.19	102.71
87.014	1097.37	108.86
87.076	1098.55	110.29
87.139	1099.74	108.29
87.201	1100.92	106.29
87.264	1102.10	110.00
87.326	1103.28	110.14
87.388	1104.47	125.86
87.451	1105.65	123.00
87.513	1106.83	124.86
87.576	1108.01	124.43
87.638	1109.20	125.29
87.701	1110.38	126.14
87.763	1111.56	125.43
87.825	1112.74	132.29
87.888	1113.93	131.86
87.950	1115.11	135.57
88.013	1116.29	140.00
88.075	1117.48	134.43
88.138	1118.66	137.43
88.200	1119.84	140.14
88.262	1121.02	135.43
88.325	1122.21	134.00
88.387	1123.39	137.14
88.450	1124.57	137.00
88.512	1125.75	137.00
88.574	1126.94	133.14
88.637	1128.12	139.57
88.699	1129.30	138.43
88.762	1130.49	135.29
88.824	1131.67	126.71
88.887	1132.85	123.86
88.949	1134.03	120.57
89.011	1135.22	118.43
89.074	1136.40	120.14

89.136	1137.58	111.00
89.199	1138.76	107.86
89.261	1139.95	112.57
89.324	1141.13	113.71
89.386	1142.31	111.57
89.448	1143.49	109.57
89.511	1144.68	112.29
89.573	1145.86	109.57
89.636	1147.04	118.57
89.698	1148.23	115.29
89.760	1149.41	116.43
89.823	1150.59	106.00
89.885	1151.77	104.43
89.948	1152.96	105.29
90.010	1154.14	110.29
90.073	1155.32	103.29
90.135	1156.50	98.14
90.197	1157.69	105.57
90.260	1158.87	102.29
90.322	1160.05	102.29
90.385	1161.24	101.00
90.447	1162.42	102.14
90.509	1163.60	101.57
90.572	1164.78	101.71
90.634	1165.97	101.14
90.697	1167.15	101.14
90.759	1168.33	101.57
90.822	1169.51	99.00
90.884	1170.70	99.43
90.946	1171.88	96.43
91.009	1173.06	95.57
91.071	1174.25	95.86
91.134	1175.43	95.00
91.196	1176.61	97.43
91.259	1177.79	88.86
91.321	1178.98	82.86
91.383	1180.16	80.29
91.446	1181.34	77.43
91.508	1182.52	72.57
91.571	1183.71	70.57
91.633	1184.89	69.14

91.695	1186.07	67.00
91.758	1187.25	65.57
91.820	1188.44	62.43
91.883	1189.62	56.00
91.945	1190.80	52.29
92.008	1191.99	68.14

APPENDIX 3

TRACE ELEMENT DATA

			Trace Element (Wt%)					
Sample Name	**Depth (mm)**	**Age (cal yr BP)**	**Al**	**Cu**	**Fe**	**Mg**	**P**	**Pb**
BT1-T39	0.50	N/A	0.01797	0.00000	0.00121	0.02153	0.00000	0.00000
BT1-T38	2.91	507.4	0.00287	0.00000	0.00076	0.02130	0.00000	0.00000
BT1-T37	5.32	521.5	0.00000	0.00000	0.00000	0.02080	0.00000	0.00000
BT1-T36	7.72	535.6	0.00000	0.00000	0.00450	0.01696	0.00056	0.00000
BT1-T35	10.13	549.6	0.00000	0.00000	0.00633	0.01721	0.00351	0.00000
BT1-T34	12.54	563.7	0.01175	0.00000	0.01121	0.01659	0.00726	0.00000
BT1-T33	14.95	577.8	0.00000	0.00000	0.00249	0.01313	0.00058	0.00000
BT1-T32	17.36	591.8	0.00000	0.00000	0.00074	0.01214	0.00000	0.00000
BT1-T31	19.76	605.9	0.00000	0.00000	0.00142	0.01372	0.00000	0.00000
BT1-T30	22.17	620.0	0.00000	0.00000	0.00265	0.02406	0.01053	0.00082
BT1-T29	24.58	634.1	0.00000	0.00000	0.00059	0.01361	0.00330	0.00000
BT1-T28	26.99	648.1	0.00000	0.00000	0.00116	0.01748	0.00932	0.00000
BT1-T27	29.39	662.2	0.00000	0.00000	0.00170	0.01449	0.00000	0.00000
BT1-T26	31.80	676.3	0.02237	0.00000	0.00167	0.01988	0.00000	0.00084
BT1-T25	34.21	690.3	0.01005	0.00000	0.00236	0.02207	0.00000	0.00000
BT1-T24	36.62	704.4	0.00000	0.00000	0.00154	0.01437	0.00682	0.00000
BT1-T23	39.03	718.5	0.01517	0.00000	0.00266	0.01973	0.00222	0.00000
BT1-T22	41.43	732.6	0.00000	0.00000	0.00409	0.00916	0.00217	0.00000
BT1-T21	43.84	746.6	0.00000	0.00000	0.00091	0.01592	0.00179	0.00117

BT1-T20	46.25	760.7	0.00000	0.00000	0.00078	0.01545	0.00000	0.00000
BT1-T19	48.66	774.8	0.00893	0.00000	0.00000	0.01719	0.00083	0.00155
BT1-T18	51.07	788.8	0.00000	0.00000	0.00000	0.01937	0.00108	0.00123
BT1-T17	53.47	802.9	0.00000	0.00000	0.00119	0.01673	0.00000	0.00000
BT1-T16	55.88	817.0	0.00000	0.00000	0.00086	0.02260	0.00000	0.00117
BT1-T15	58.29	831.1	0.00000	0.00000	0.00173	0.02170	0.00000	0.00000
BT1-T14	60.70	845.1	0.01724	0.00000	0.00066	0.01765	0.00000	0.00000
BT1-T13	63.11	859.2	0.00000	0.00000	0.00119	0.01818	0.00000	0.00126
BT1-T12	65.51	873.3	0.00000	0.00000	0.00091	0.01881	0.00879	0.00000
BT1-T11	67.92	887.3	0.00000	0.00000	0.00122	0.02003	0.00342	0.00000
BT1-T10	70.33	901.4	0.00000	0.00000	0.00157	0.02443	0.00061	0.00108
BT1-T9	72.74	915.5	0.00252	0.00000	0.00000	0.02471	0.00000	0.00295
BT1-T8	75.14	929.5	0.02136	0.00000	0.00093	0.02896	0.00000	0.00240
BT1-T7	77.55	943.6	0.00000	0.00000	0.00000	0.02331	0.00000	0.00188
BT1-T6	79.96	963.7	0.00000	0.00017	0.00145	0.03769	0.01629	0.00293
BT1-T5	82.37	1009.3	0.00000	0.00000	0.00000	0.02478	0.00784	0.00318
BT1-T4	84.78	1055.0	0.01148	0.00000	0.00166	0.02909	0.01525	0.00525
BT1-T3	87.18	1100.6	0.02867	0.00062	0.00000	0.02176	0.01298	0.00488
BT1-T2	89.59	1146.2	0.00000	0.00000	0.00000	0.02204	0.00534	0.00832
BT1-T1	92.00	1191.8	0.01456	0.00137	0.00495	0.02869	0.02497	0.00534

APPENDIX 4

STABLE ISOTOPE DATA

Sample Name	Depth (mm)	Age (cal yr BP)	d^{18}O (‰ V-PDB)	d^{13}C (‰ V-PDB)
BTI-188	0.00	N/A	-2.1	-2.0
BTI-187	0.49	N/A	-2.5	-5.9
BTI-186	0.98	496.2	-2.2	-7.1
BTI-185	1.48	499.0	-2.3	-6.4
BTI-184	1.97	501.9	-3.1	-7.5
BTI-183	2.46	504.8	-2.8	-7.8
BTI-182	2.95	507.7	-2.9	-8.2
BTI-181	3.44	510.5	-2.7	-8.1
BTI-180	3.94	513.4	-3.3	-7.4
BTI-179	4.43	516.3	-3.0	-7.5
BTI-178	4.92	519.2	-2.7	-7.9
BTI-177	5.41	522.0	-2.3	-7.4
BTI-176	5.90	524.9	-2.4	-5.7
BTI-175	6.40	527.8	-2.0	-5.7
BTI-174	6.89	530.7	-3.2	-6.6
BTI-173	7.38	533.5	-3.4	-8.6
BTI-172	7.87	536.4	-2.8	-6.2
BTI-171	8.36	539.3	-3.3	-7.0
BTI-170	8.86	542.2	-3.0	-7.0
BTI-169	9.35	545.0	-2.6	-6.1
BTI-168	9.84	547.9	-2.6	-7.3
BTI-167	10.33	550.8	-2.7	-8.3
BTI-166	10.82	553.7	-3.2	-9.2
BTI-165	11.32	556.5	-3.3	-9.3
BTI-164	11.81	559.4	-3.4	-9.4
BTI-163	12.30	562.3	-3.5	-9.0
BTI-162	12.79	565.2	-3.3	-8.9
BTI-161	13.28	568.0	-3.5	-9.0
BT1-160	13.78	570.9	-3.6	-9.9
BT1-159	14.27	573.8	-3.7	-10.1
BT1-158	14.76	576.7	-3.7	-10.0
BT1-157	15.25	579.5	-3.4	-8.2
BT1-156	15.74	582.4	-3.5	-8.5

BT1-155	16.24	585.3	-3.5	-9.3
BT1-154	16.73	588.2	-3.9	-9.5
BT1-153	17.22	591.0	-3.8	-9.2
BT1-152	17.71	593.9	-3.6	-9.1
BT1-151	18.20	596.8	-3.7	-9.3
BT1-150	18.70	599.7	-4.2	-9.5
BT1-149	19.19	602.5	-4.2	-9.5
BT1-148	19.68	605.4	-4.1	-9.9
BT1-147	20.17	608.3	-3.8	-10.2
BT1-146	20.66	611.2	-4.4	-10.8
BT1-145	21.16	614.0	-3.6	-8.9
BT1-144	21.65	616.9	-2.9	-7.6
BT1-143	22.14	619.8	-3.2	-7.6
BT1-142	22.63	622.7	-2.6	-5.6
BT1-141	23.12	625.5	-2.0	-5.9
BT1-140	23.61	628.4	-3.0	-7.7
BT1-139	24.11	631.3	-4.2	-11.0
BT1-138	24.60	634.2	-4.3	-11.3
BT1-137	25.09	637.0	-4.1	-11.2
BT1-136	25.58	639.9	-3.7	-10.8
BT1-135	26.07	642.8	-4.1	-12.0
BT1-134	26.57	645.7	-3.7	-10.5
BT1-133	27.06	648.5	-2.8	-9.2
BT1-132	27.55	651.4	-3.2	-7.3
BT1-131	28.04	654.3	-4.6	-8.9
BT1-130	28.53	657.2	-5.6	-10.6
BT1-129	29.03	660.0	-6.2	-10.6
BT1-128	29.52	662.9	-6.6	-10.5
BT1-127	30.01	665.8	-5.9	-10.3
BT1-126	30.50	668.7	-5.5	-10.0
BT1-125	30.99	671.5	-5.4	-10.0
BT1-124	31.49	674.4	-3.8	-10.4
BT1-123	31.98	677.3	-3.9	-10.9
BT1-122	32.47	680.2	-4.3	-11.2
BT1-121	32.96	683.0	-4.3	-11.0
BT1-120	33.45	685.9	-4.4	-11.0
BT1-119	33.95	688.8	-4.9	-10.7
BT1-118	34.44	691.7	-4.8	-10.6
BT1-117	34.93	694.5	-4.9	-11.3
BT1-116	35.42	697.4	-4.8	-11.4
BT1-115	35.91	700.3	-4.3	-10.7

BT1-114	36.41	703.2	-5.1	-11.7
BT1-113	36.90	706.0	-5.3	-11.5
BT1-112	37.39	708.9	-5.5	-11.9
BT1-111	37.88	711.8	-5.8	-12.3
BT1-110	38.37	714.7	-4.5	-11.7
BT1-109	38.87	717.5	-3.6	-10.4
BT1-108	39.36	720.4	-4.5	-10.0
BT1-107	39.85	723.3	-4.9	-11.0
BT1-106	40.34	726.2	-4.9	-10.9
BT1-105	40.83	729.0	-4.8	-11.1
BT1-104	41.33	731.9	-3.3	-10.6
BT1-103	41.82	734.8	-3.3	-10.8
BT1-102	42.31	737.7	-3.9	-10.5
BT1-101	42.80	740.5	-3.7	-10.5
BT1-100	43.29	743.4	-3.5	-10.0
BT1-99	43.79	746.3	-2.8	-10.7
BT1-98	44.28	749.2	-2.7	-10.6
BT1-97	44.77	752.0	-2.9	-9.8
BT1-96	45.26	754.9	-4.0	-10.0
BT1-95	45.75	757.8	-4.2	-10.8
BT1-94	46.25	760.7	-3.6	-11.1
BT1-93	46.74	763.5	-3.3	-10.5
BT1-92	47.23	766.4	-2.9	-10.1
BT1-91	47.72	769.3	-2.9	-8.8
BT1-90	48.21	772.2	-3.2	-9.5
BT1-89	48.71	775.0	-3.2	-9.9
BT1-88	49.20	777.9	-2.4	-8.8
BT1-87	49.69	780.8	-4.0	-9.7
BT1-86	50.18	783.7	-4.3	-10.2
BT1-85	50.67	786.5	-4.6	-10.5
BT1-84	51.17	789.4	-3.9	-10.5
BT1-83	51.66	792.3	-3.9	-10.5
BT1-82	52.15	795.2	-3.7	-10.4
BT1-81	52.64	798.0	-3.4	-9.9
BT1-80	53.13	800.9	-3.3	-10.3
BT1-79	53.63	803.8	-3.6	-10.3
BT1-78	54.12	806.7	-2.4	-10.4
BT1-77	54.61	809.5	-3.5	-10.4
BT1-76	55.10	812.4	-4.5	-11.2
BT1-75	55.59	815.3	-4.3	-10.9
BT1-74	56.09	818.2	-4.0	-10.5

BT1-73	56.58	821.0	-3.4	-10.0
BT1-72	57.07	823.9	-3.1	-10.5
BT1-71	57.56	826.8	-3.6	-10.2
BT1-70	58.05	829.7	-3.7	-10.1
BT1-69	58.55	832.5	-3.5	-9.7
BT1-68	59.04	835.4	-2.9	-9.8
BT1-67	59.53	838.3	-3.3	-10.2
BT1-66	60.02	841.2	-3.1	-10.2
BT1-65	60.51	844.0	-3.9	-10.0
BT1-64	61.01	846.9	-4.5	-10.8
BT1-63	61.50	849.8	-4.1	-10.9
BT1-62	61.99	852.7	-4.4	-11.0
BT1-61	62.48	855.5	-3.9	-10.5
BT1-60	62.97	858.4	-4.3	-11.0
BT1-59	63.47	861.3	-4.7	-11.1
BT1-58	63.96	864.2	-4.7	-11.3
BT1-57	64.45	867.0	-4.3	-11.2
BT1-56	64.94	869.9	-4.1	-9.6
BT1-55	65.43	872.8	-4.2	-9.7
BT1-54	65.93	875.7	-3.6	-9.0
BT1-53	66.42	878.5	-4.1	-10.4
BT1-52	66.91	881.4	-4.4	-10.6
BT1-51	67.40	884.3	-4.0	-10.6
BT1-50	67.89	887.2	-3.7	-10.6
BT1-49	68.39	890.0	-4.4	-10.8
BT1-48	68.88	892.9	-4.0	-10.8
BT1-47	69.37	895.8	-3.5	-10.4
BT1-46	69.86	898.7	-3.4	-9.1
BT1-45	70.35	901.5	-4.0	-10.7
BT1-44	70.84	904.4	-4.0	-10.2
BT1-43	71.34	907.3	-4.6	-11.1
BT1-42	71.83	910.2	-4.2	-10.6
BT1-41	72.32	913.0	-4.0	-10.6
BT1-40	72.81	915.9	-4.4	-11.2
BT1-39	73.30	918.8	-4.2	-11.4
BT1-38	73.80	921.7	-3.9	-11.0
BT1-37	74.29	924.5	-4.3	-10.9
BT1-36	74.78	927.4	-3.9	-10.4
BT1-35	75.27	930.3	-3.6	-10.1
BT1-34	75.76	933.2	-3.1	-9.1
BT1-33	76.26	936.0	-3.3	-9.8

BT1-32	76.75	938.9	-3.0	-9.6
BT1-31	77.24	941.8	-3.2	-9.8
BT1-30	77.73	944.7	-3.4	-10.6
BT1-29	78.22	947.5	-3.9	-10.7
BT1-28	78.72	950.4	-4.1	-10.2
BT1-27	79.21	953.3	-3.7	-9.6
BT1-26	79.70	958.8	-2.2	-3.0
BT1-25	80.19	968.1	-2.2	-2.9
BT1-24	80.68	977.4	-2.5	-4.4
BT1-23	81.18	986.8	-2.5	-4.7
BT1-22	81.67	996.1	-2.4	-4.2
BT1-21	82.16	1005.4	-2.1	-3.6
BT1-20	82.65	1014.7	-2.8	-6.9
BT1-19	83.14	1024.1	-2.8	-6.8
BT1-18	83.64	1033.4	-2.7	-5.6
BT1-17	84.13	1042.7	-2.5	-5.0
BT1-16	84.62	1052.0	-2.5	-5.4
BT1-15	85.11	1061.3	-2.5	-5.1
BT1-14	85.60	1070.7	-2.3	-4.3
BT1-13	86.10	1080.0	-1.9	-3.4
BT1-12	86.59	1089.3	-3.3	-10.1
BT1-11	87.08	1098.6	-3.5	-9.7
BT1-10	87.57	1107.9	-3.4	-8.0
BT1-9	88.06	1117.3	-3.2	-7.4
BT1-8	88.56	1126.6	-3.9	-8.0
BT1-7	89.05	1135.9	-4.6	-9.0
BT1-6	89.54	1145.2	-3.8	-8.2
BT1-5	90.03	1154.6	-3.4	-8.2
BT1-4	90.52	1163.9	-3.8	-8.4
BT1-3	91.02	1173.2	-4.0	-7.0
BT1-2	91.51	1182.5	-4.0	-8.2
BT1-1	92.00	1191.8	-3.7	-7.7